and sticks represent an extended zeolitic framework of a realistic 120T quantum cluster.

	Isolated	ADS	TS1	INT1	TS2	INT2
Distance						
Al-V	2.781	2.774	2.926	2.963	2.967	2.931
V-O1	1.586	1.587	1.684	1.769	2.011	2.225
V-O2	1.591	1.592	1.583	1.577	1.570	1.582
Al-Oa	1.766	1.768	1.765	1.742	1.753	1.758
Al-Ob	1.766	1.768	1.735	1.747	1.732	1.727
V-Oa	1.980	1.974	1.997	2.203	2.148	2.093
V-Ob	1.980	1.973	2.214	2.056	2.134	2.146
C1-C2	1.519	1.518	1.527	1.509	1.466	1.425
C1-H1	1.094	1.097	1.093	1.095	1.368	2.973
C2-H2	1.097	1.096	1.452	3.267	3.739	3.930
Angle						
O1-V-O2	110.4	110.5	108.0	103.2	97.3	86.9
Oa-Al-Ob	90.2	90.1	90.4	90.0	90.4	91.2
C1-C2-C3	112.6	112.7	114.9	115.3	119.5	121.2

Results and Discussion

The optimized M06L/6-31G(d,p) structure of VO$_2$-MCM-22 whose molecular oxide specie acts as an active site embedded in the intersection cavity at the 12T membered ring of the supercage is illustrated in Figure 2. The active model is similar to that used in our previous study on isolated metal oxide on zeolite.[45]

The [VO$_2$]$^+$ ionic group lies between the two bridging oxygen atoms of the zeolite framework forming the tetrahedral arrangement at the vanadium atom which is the most stable configuration. The optimized V-O bond lengths are 1.586, 1.591, 1.980 and 1.980 Å for V-O1, V-O2, V-Oa and V-Ob, respectively (See Table 1). The distance between the V and Al atoms is 2.781 Å.

In the propane oxidative dehydrogenation reaction mechanism, the propane molecule is first adsorbed on VO$_2$-MCM-22 with a hydrogen bond between protons of propane (H1 and H2) and oxygen atoms (O1 and O2). The V-O1 bond was barely changed (1.586 to 1.587 Å)The computed adsorption energy -6.3 kcal/mol is obtained from the 14T quantum cluster. In order to see the effect of zeolitic framework on the reaction mechanism, the extended 120T quantum cluster calculation was performed on the structure optimized from the 14T quantum cluster. The extended framework enhances the adsorption energy to be -7.0 kcal/mol, which is about 10% higher than that from the 14T quantum cluster calculation. The computed adsorption energy is in the range of the experimentally observed values for heat of adsorption (~ -8 kcal/mol).[46]
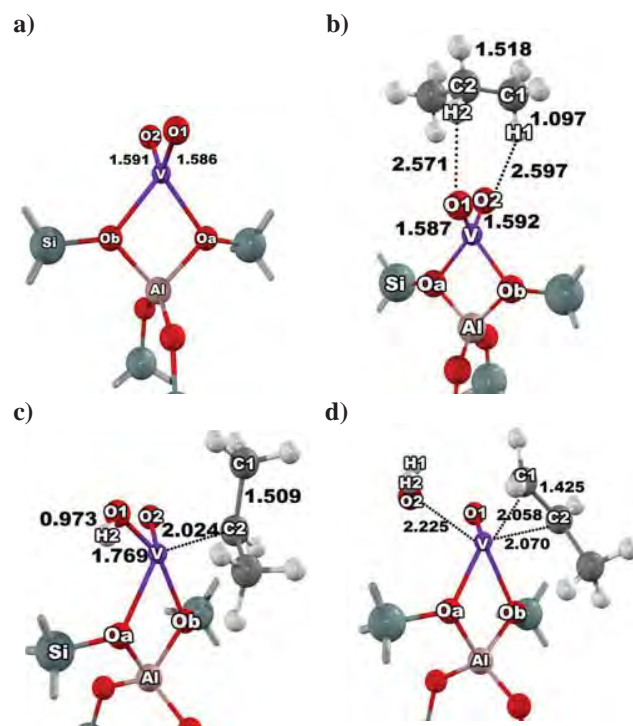

Figure 2. Optimized structures of VO$_2$-MCM-22 complexes **a)** bare model of VO$_2$-MCM-22 **b)** adsorption complex of VO$_2$-MCM-22 and propane (ADS) **c)** their corresponding intermediate (INT1) and **d)** the reaction products (INT2).
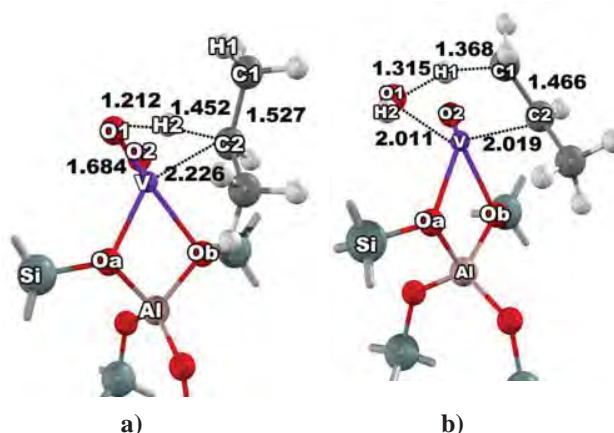

Figure 3. The transition structures of the propane oxidative dehydrogenation reaction, **a)** TS1 and **b)** TS2.
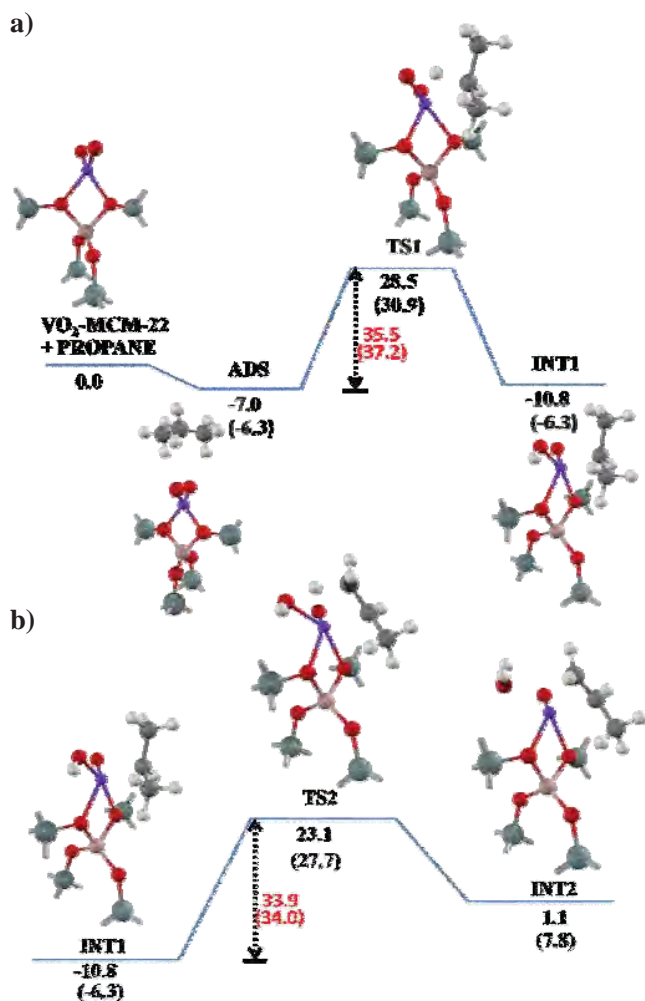
a)

b)

Figure 4. 120T M06-L/6-31G(d,p) energy profile (kcal/mol) for a) the hydrogen abstraction step and b) the propene formation step of the propane oxidative dehydrogenation reaction over VO$_2$-MCM-22. The values in parenthesis are calculated at the 14T M06-L/6-31G(d,p) level of theory.

In the next step, the hydrogen atom was abstracted from propane to an α-oxygen of VO$_2$-MCM-22 zeolite. Configuration of the transition structure was distorted from the tetrahedral structure (Figure 3). The O1-H2 and C2-H2 distances were found to be 1.212 and 1.452Å, respectively, while the V-O1 distance is longer than those of the bare catalyst (1.586 to 1.684 Å). The imaginary frequency of 1372i cm^{-1} of the transition state corresponds to the moving of the H2 atom toward and backward between the O1 and C2 atoms. We found that the framework reduces the energy barrier whose the required actual activation barrier is 35.5 kcal/mol, while the apparent activation barrier is 28.5 kcal/mol (see Figure 4). This is in the range of experimental information of

propane oxidative dehydrogenation over supported vanadia catalysts (20-30 kcal/mol).[12,47,48] The isopropyl radical intermediate [INT1] was found to be the product of this step with relative energy of -10.8 kcal/mol. The isopropyl radical intermediate is closely coordinated on the vanadium atom at the active site with a V-C2 distance of 2.024 Å.

In the last step, the isopropyl radical intermediate can be converted to propene via the second hydrogen abstraction from C1 to the O1H hydroxyl group on the vanadium atom yielding an adsorbed water molecule. At the transition state, the C1-H1 bond of the propyl radical is elongated from 1.093 to 1.368 Å, corresponding with the forming of H1---O1 which is decreased from 2.740 to 1.315 Å. The calculated actual activation barrier and apparent activation barrier are 33.9 and 23.1 kcal/mol, respectively. The barrier height for this step [TS2] is lower than that for the first hydrogen abstraction step [TS1]. Therefore, the first hydrogen abstraction can be considered as a rate determining step.

The water and propene products are strongly adsorbed to the vanadium atom [INT2]. To remove water and propene, it requires the energy of 27.0 and 57.2 kcal/mol, respectively. The energy profile is shown in the Figure 4. With the M06L functional, the adsorption and activation energies for oxidative dehydrogenation reaction of propane on VO$_2$-MCM-22 agree well with the range of experiment data.

Conclusions

Reaction mechanisms of propane oxidative dehydrogenation over a 14T VO$_2$-exchanged MCM-22 model were investigated by a newly developed density functional theory (DFT), M06-L, with the effective core potential Stuttgart and Born, for the V atom, and 6-31G(d,p), for the rest, were employed for all calculations. To take the extended framework effect into account, 120T structures were used for single-point calculations at the same level of theory. The reaction began with a hydrogen abstraction on the VO$_2$ group, and acquired the HO-V-O intermediate. This was the rate determining step in which the activation energy was 35.5 kcal/mol. In the propene formation step, the hydroxyl group reacted with the isopropyl radical which required energy of 33.9 kcal/mol. The apparent activation energy was 28.5 kcal/mol, which was in good agreement with experimental results of propane oxidative dehydrogenation over other silica supports.

References

(1) G. Centi, F. C., F. Trifiro` *Selective Oxidation by Heterogeneous Catalysis,*; Kluwer Academic, New York, 2001.

(2) Blasco, T.; Lopez Nieto, J. M. *Appl. Catal. A* **1997**, *157*, 117-142.

(3) Mamedov, E. A.; Cortés Corberán, V. *Appl. Catal. A* **1995**, *127*, 1-40.

(4) Chaar, M. A.; Patel, D.; Kung, H. H. *J. Catal.* **1988**, *109*, 463-467.

(5) Corma, A.; Nieto, J. M. L.; Paredes, N. *J. Catal.* **1993**, *144*, 425-438.

(6) Hardcastle, F. D.; Wachs, I. E. *J. Mol. Catal.* **1988**, *46*, 173-186.

(7) Wachs, I. E.; Weckhuysen, B. M. *Appl. Catal. A* **1997**, *157*, 67-90.

(8) Eon, J. G.; Olier, R.; Volta, J. C. *J. Catal.* **1994**, *145*, 318-326.

(9) Khodakov, A.; Olthof, B.; Bell, A. T.; Iglesia, E. *J. Catal.* **1999**, *181*, 205-216.

(10) Khodakov, A.; Yang, J.; Su, S.; Iglesia, E.; Bell, A. T. *J. Catal.* **1998**, *177*, 343-351.

(11) Kondratenko, E. V.; Baerns, M. *Appl. Catal. A* **2001**, *222*, 133-143.

(12) Argyle, M. D.; Chen, K.; Bell, A. T.; Iglesia, E. *J. Catal.* **2002**, *208*, 139-149.

(13) Kondratenko, E. V.; Cherian, M.; Baerns, M. *Catal. Today* **2006**, *112*, 60-63.

(14) Cavani, F.; Ballarini, N.; Cericola, A. *Catal. Today* **2007**, *127*, 113-131.

(15) Julbe, A.; Farrusseng, D.; Jalibert, J. C.; Mirodatos, C.; Guizard, C. *Catal. Today* **2000**, *56*, 199-209.

(16) Karakoulia, S. A.; Triantafyllidis, K. S.; Tsilomelekis, G.; Boghosian, S.; Lemonidou, A. A. *Catal. Today* **2009**, *141*, 245-253.

(17) Teixeira-Neto, A. A.; Marchese, L.; Landi, G.; Lisi, L.; Pastore, H. O. *Catal. Today* **2008**, *133-135*, 1-6.

(18) Dinse, A.; Khennache, S.; Frank, B.; Hess, C.; Herbert, R.; Wrabetz, S.; Schlögl, R.; Schomäcker, R. *J. Mol. Catal. A: Chem.* **2009**, *307*, 43-50.

(19) Engeser, M.; Schlangen, M.; Schröder, D.; Schwarz, H.; Yumura, T.; Yoshizawa, K. *Organometallics* **2003**, *22*, 3933-3943.

(20) Feyel, S.; Schröder, D.; Rozanska, X.; Sauer, J.; Schwarz, H. *Angew. Chem., Int. Ed.* **2006**, *45*, 4677-4681.

(21) Cheng, M. J.; Chenoweth, K.; Oxgaard, J.; Van Duin, A.; Goddard III, W. A. *J. Phys. Chem. C* **2007**, *111*, 5115-5127.

(22) Rozanska, X.; Fortrie, R.; Sauer, J. *J. Phys. Chem. C* **2007**, *111*, 6041-6050.

(23) Rozanska, X.; Kondratenko, E. V.; Sauer, J. *J. Catal.* **2008**, *256*, 84-94.

(24) Redfern, P. C.; Zapol, P.; Sternberg, M.; Adiga, S. P.; Zygmunt, S. A.; Curtiss, L. A. *J. Phys. Chem. B* **2006**, *110*, 8363-8371.

(25) Fu, H.; Liu, Z. P.; Li, Z. H.; Wang, W. N.; Fan, K. N. *J. Am. Chem. Soc.* **2006**, *128*, 11114-11123.

(26) Maihom, T.; Namuangruk, S.; Nanok, T.; Limtrakul, J. *J. Phys. Chem. C* **2008**, *112*, 12914-12920.

(27) Jansang, B.; Nanok, T.; Limtrakul, J. *J. Phys. Chem. C* **2008**, *112*, 540-547.

(28) Choomwattana, S.; Maihom, T.; Khongpracha, P.; Probst, M.; Limtrakul, J. *J. Phys. Chem. C* **2008**, *112*, 10855-10861.

(29) Jansang, B.; Nanok, T.; Limtrakul, J. *J. Mol. Catal. A: Chem.* **2007**, *264*, 33-39.

(30) Namuangruk, S.; Tantanak, D.; Limtrakul, J. *J. Mol. Catal. A: Chem.* **2006**, *256*, 113-121.

(31) Namuangruk, S.; Khongpracha, P.; Pantu, P.; Limtrakul, J. *J. Phys. Chem. B* **2006**, *110*, 25950-25957.

(32) Lomratsiri, J.; Probst, M.; Limtrakul, J. *Journal of Molecular Graphics and Modelling* **2006**, *25*, 219-225.

(33) Kasuriya, S.; Namuangruk, S.; Treesukol, P.; Tirtowidjojo, M.; Limtrakul, J. *J. Catal.* **2003**, *219*, 320-328.

(34) Bobuatong, K.; Limtrakul, J. *Appl. Catal. A* **2003**, *253*, 49-64.

(35) Zhao, Y.; Truhlar, D. G. *Theor. Chem. Acc.* **2008**, *120*, 215-241.

(36) Zhao, Y.; Truhlar, D. G. *Acc. Chem. Res.* **2008**, *41*, 157-167.

(37) Maihom, T.; Boekfa, B.; Sirijaraensre, J.; Nanok, T.; Probst, M.; Limtrakul, J. *J. Phys. Chem. C* **2009**, *113*, 6654-6662.

(38) Boekfa, B.; Choomwattana, S.; Khongpracha, P.; Limtrakul, J. *Langmuir* **2009** DOI:10.1021/la901841w.

(39) Kumsapaya, C.; Bobuatong, K.; Khongpracha, P.; Tantirungrotechai, Y.; Limtrakul, J. *J. Phys. Chem. C* **2009**, *113*, 16128-16137.

(40) Chen, K.; Iglesia, E.; Bell, A. T. *J. Catal.* **2000**, *192*, 197-203.

(41) Leonowicz, M. E.; Lawton, J. A.; Lawton, S. L.; Rubin, M. K. *Science* **1994**, *264*, 1910-1913.

(42) Zhou, D.; Bao, Y.; Yang, M.; He, N.; Yang, G. *J. Mol. Catal. A: Chem.* **2006**, *244*, 11-19.

(43) Dolg, M.; Wedig, U.; Stoll, H.; Preuss, H. *J. Chem. Phys.* **1986**, *86*, 866-872.

(44) Frisch, M. J. , Trucks, G. W.; Schlegel, H. B.; Scuseria, G. E.; Robb, M. A.; Cheeseman, J. R.; Montgomery, Jr., J. A.; Vreven, T.; Kudin, K. N.; Burant, J. C.; Millam, J. M.; Iyengar, S. S.; Tomasi, J.; Barone, V.; Mennucci, B.; Cossi, M.; Scalmani, G.; Rega, N.; Petersson, G. A.; Nakatsuji, H.; Hada, M.; Ehara, M.; Toyota, K.; Fukuda, R.; Hasegawa, J.; Ishida, M.; Nakajima, T.; Honda, Y.; Kitao, O.; Nakai, H.; Klene, M.; Li, X.; Knox, J. E.; Hratchian, H. P.; Cross, J. B.; Bakken, V.; Adamo, C.; Jaramillo, J.; Gomperts, R.; Stratmann, R. E.; Yazyev, O.; Austin, A. J.; Cammi, R.; Pomelli, C.; Ochterski, J. W.; Ayala, P. Y.; Morokuma, K.; Voth, G. A.; Salvador, P.; Dannenberg, J. J.; Zakrzewski, V. G.; Dapprich, S.; Daniels, A. D.; Strain, M. C.; Farkas, O.; Malick, D. K.; Rabuck, A. D.; Raghavachari, K.; Foresman, J. B.; Ortiz, J. V.; Cui, Q.; Baboul, A. G.; Clifford, S.; Cioslowski, J.; Stefanov, B. B.; Liu, G.; Liashenko, A.; Piskorz, P.; Komaromi, I.; Martin, R. L.; Fox, D. J.; Keith, T.; Al-Laham, M. A.; Peng, C. Y.; Nanayakkara, A.; Challacombe, M.; Gill, P. M. W.; Johnson, B.; Chen, W.; Wong, M. W.; Gonzalez, C.; and Pople, J. A.; Gaussian, Inc., Wallingford CT, **2004.**

(45) Pantu, P.; Pabchanda, S.; Limtrakul, J. *ChemPhysChem* **2004**, *5*, 1901-1906.

(46) Kamper, A.; Auroux, A.; Baerns, M. *Phys. Chem. Chem. Phys.* **2000**, *2*, 1069-1075.

(47) Chen, K.; Bell, A. T.; Iglesia, E. *J. Phys. Chem. B* **2000**, *104*, 1292-1299.

(48) Heracleous, E.; Machli, M.; Lemonidou, A. A.; Vasalos, I. A. *J. Mol. Catal. A: Chem.* **2005**, *232*, 29-39.

ADSORPTION AND CRACKING REACTION OF *N*-HEXANE OVER H-ZSM-5: A M06-2X STUDY

Thana Maihom[a,b,c], Piboon Pantu[a, b, c], Chaiwat Tachakritikul[d], and Jumras Limtrakul[a,b,c]*

[a]Laboratory for Computational and Applied Chemistry, Physical Chemistry Division, Department of Chemistry, Faculty of Science, Kasetsart University, Bangkok 10900, Thailand
[b]Center of Nanotechnology, Kasetsart University Research and Development Institute, Bangkok 10900, Thailand
[c]NANOTEC Center of Excellence, National Nanotechnology Center, Kasetsart University, Bangkok 10900, Thailand
[d]PTT Research and Technology Institute, PTT Public Company Limited, Thailand

Introduction

The catalytic cracking of hydrocarbons is an important reaction in the petrochemical industry. It is used to break down large hydrocarbons in crude oil into light hydrocarbons for the production of fuels. Zeolite catalysts, especially Y and ZSM-5, are widely used in cracking processes due to their advantages of high catalytic activity and selectivity.

The catalytic cracking of hydrocarbons is proposed to occur via a bimolecular and a monomolecular mechanism.[1-4] The bimolecular mechanism involves hydride-transfer between an alkane and an adsorbed carbenium ion followed by isomerization and β-scission. This mechanism prevails under high partial pressure of hydrocarbons and, especially, in large pore zeolites. A monomolecular cracking is believed to be an important mechanism for the cracking reaction of hydrocarbons in medium pore zeolites such as ZSM-5. In this mechanism, a carbonium-like ionic intermediate is formed through the direct protonation of Brønsted acid to the C–C bond.[3-9] It then leads to the scission of the C–C bond to produce alkane and alkene products. This mechanism is expected to be very sensitive to the acid strength of the Brønsted proton.

A number of theoretical studies have been carried out to investigate the cracking reaction of alkane over the zeolite catalysts.[6-10] Recently, Boronat et al.[9] have proposed that protolytic cracking of *n*-butane occurred in two steps. The first step is protonation to the C-C bond to form a carbonium ion intermediate having a two-electron three-centre C–H–C bridge adsorbed on the zeolite surface. The subsequent step is the decomposition of the carbonium ion to form an alkane and an alkene.

To understand hydrocarbon reactions, it is of particular interest to study the reactivity and stability of the carbonium ion intermediate on the zeolite surface. It is expected that the zeolite framework should have profound effects on reactive intermediates and the reaction mechanism for catalytic reactions over zeolite catalysts.[11-13] Therefore, it is suggested that it is essential to use relatively large clusters for investigations of reaction mechanisms in zeolites.

Recently, the new density functional M06-2X method has been found to successfully account for the effect of the zeolite framework on the adsorption and reaction of hydrocarbons over large quantum clusters of zeolites.[14-16] In this report, full quantum calculations on a large 34T cluster model of H-ZSM-5 using the M06-2X method are performed to investigate the mechanism of *n*-hexane protolytic cracking. The structures and energetics of reaction intermediates and transition states and the reaction mechanism are discussed.

Models and Method

The structure of the 34T cluster model is used for representing the lattice of ZSM-5 zeolite,[17] which covers the intersection region of the straight and zigzag channels, as shown in Figure 1. One of the silicon atoms at the T12 site is replaced with an aluminium atom to generate the Brønsted acid site. This T12 site is found to be the most stable Al substitution site and has been generally used to model the active site of H-ZSM-5 zeolite. In our previous studies, this model had been employed for studying the adsorption and reactions of hydrogen exchange on unsaturated aliphatic, aromatic and heterocyclic compounds and gave reasonable results for adsorption and activation energies, compared with experimental values.[14,15]
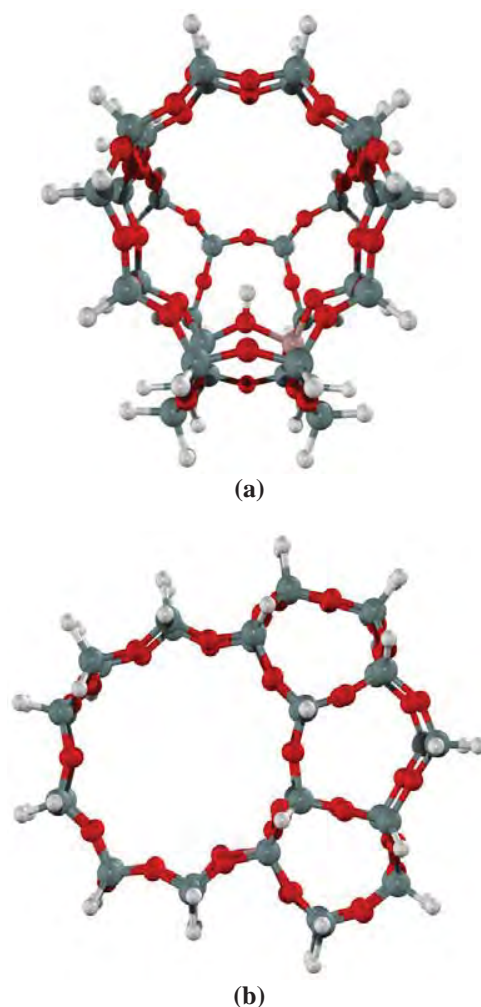

(a)

(b)

Figure 1. 34T cluster model of H-ZSM-5 zeolite: (a) sinusoidal channel view and (b) straight channel view.

All structure optimizations were performed with the M06-2X density functional[18-21] and the 6-31G (d,p) basis set. During optimization, only the 5T cluster of the active region, [(≡SiO)$_3$Al(OH)Si≡] and the probe molecules are allowed to relax, while the remaining atoms are fixed at the crystallographic coordinates. Verification that the optimized transition state connects the intended reactant and product was made by normal mode analysis. All calculations were performed using the Gaussian 03 code[22] modified to incorporate the Minnesota Density Functional module 3.1 by Zhao and Truhlar.

Results and Discussion

Adsorption of *n*-Hexane. Optimized adsorption structures of *n*-hexane on H-ZSM-5 zeolites obtained from the M06-2X method and the 6-31G(d,p) basis set are shown in Figure 2. It can be seen that the *n*-hexane molecule is weakly adsorbed on H-ZSM-5 zeolite through the interaction between two carbon atoms (C–C) and the Brønsted acid site (O1–H1). Four possible configurations of weak adsorption complexes were found. The calculated adsorption energies are –18.0, –17.6, –19.7 and –17.6 kcal/mol for the Ads1, Ads2, Ads3 and Ads4 geometries, respectively, with internuclear H1···C distances in the range of 2.71–3.66 Å. In this zeolite, the adsorption via the central C-C unit (Ads3) is slightly more stable (by 2 kcal/mol) than other structures. These predicted adsorption energies are in agreement with the experimental estimates of –19.6 kcal/mol.[23] These results suggest that the M06-2X/6-31G(d,p) method is suitable for studying the interactions of *n*-hexane in zeolites and should also be suitable for studying the *n*-hexane cracking.
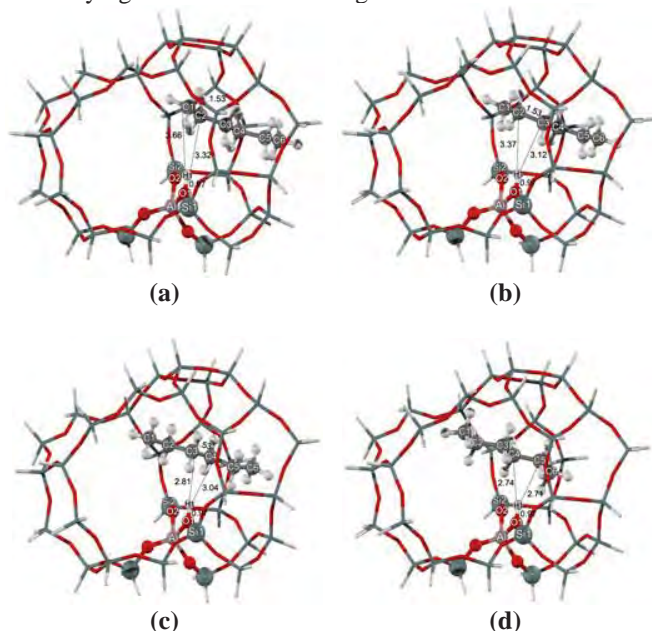

Figure 2. Optimized structures of *n*-hexane adsorbed over H-ZSM-5 zeolite (a) Ads1, (b) Ads2, (c) Ads3 and (d) Ads4.

Reaction Mechanism of *n*-Hexane Cracking. It has been reported that propane (C$_3$H$_8$) and propene (C$_3$H$_6$) are the major products of monomolecular *n*-hexane cracking on numerous zeolites.[24,25] Therefore, we concentrate on the protolytic cracking of the central C3–C4 bond only. The reaction profile and structures of intermediates and transition states are shown in Figure 3.

In the first step, the adsorbed *n*-hexane molecule is protonated by the acidic proton at the central C-C bond to form the adsorbed 3-C-hexonium intermediates via the three-center/two-electron bonds cationic transition state TS1. In this transition state, the C3–C4 bond of *n*-hexane is ruptured by the acidic proton. The O1–H1 bond distance is elongated from 0.98 to 1.74 Å while the C3–C4 bond distance is increased to 1.76 Å. The 3-C-hexonium intermediate having the C–H–C bridge adsorbed on the zeolite surface by forming hydrogen bond interactions with the basic oxygen atom of the zeolite. The C3–H1–C4 bridge angle is 101.4°. The bond distances of C3-H1 and C4-H1 are almost equal. The activation energy of this step is 44.5 kcal/mol. The adsorbed 3-C-hexonium intermediate is less stable than the adsorbed *n*-hexane by 43.1 kcal/mol. Boronat et al.[9] have also reported that the adsorbed 2-C-butonium intermediate is much less stable than the adsorbed *n*-butane.

The second step is the decomposition of the 3-C-hexonium intermediate to form the products of propane and propene via transition state TS2. At the transition state, the C3–H1–C4 bridge is broken. The C3–H1 distance increases to 1.88 Å while the H1–C4 bond is contracted to 1.11 Å. The adjacent C2–H2 bond is broken and the H2 proton is back-transferred to the oxygen of the zeolite framework. The hybridization of C2 changes from tetrahedral (sp^3) to planar (sp^2). The activation energy of this step is 11.9 kcal/mol. The products are propane and propene adsorbed on the acidic site through a π-bond interaction.

From the energy profile, the first step, which is the protonation of adsorbed *n*-hexane, is found to be the rate determining step with the activation energy of 44.5 kcal/mol. The 3-C-hexonium is found to be a true intermediate. This result is in agreement with the computational result of Boronat et al.[9] on *n*-butane cracking. Subsequently, the decomposition of the 3-C-hexonium to form a propane and a propene molecule is facile with an activation energy of 11.9 kcal/mol. The apparent activation energy is found to be 35.3 kcal/mol. This value is higher than the previous experimental reports of about 25 kcal/mol.[26,27] However, it is in good agreement with a recent report[26,27] in which an apparent activation energy of 35±2 kcal/mol was observed. In those works, the authors used purified *n*-hexane at very low partial pressures and relatively high reaction temperatures to ensure the monomolecular cracking mechanism. Lónyi et al.[28] have suggested that the activation energy of monomolecular cracking should be higher than that of the bimolecular cracking which supports the result of Babitz et al.[26] and van Bokhoven et al.[27] and agrees with our computed result.
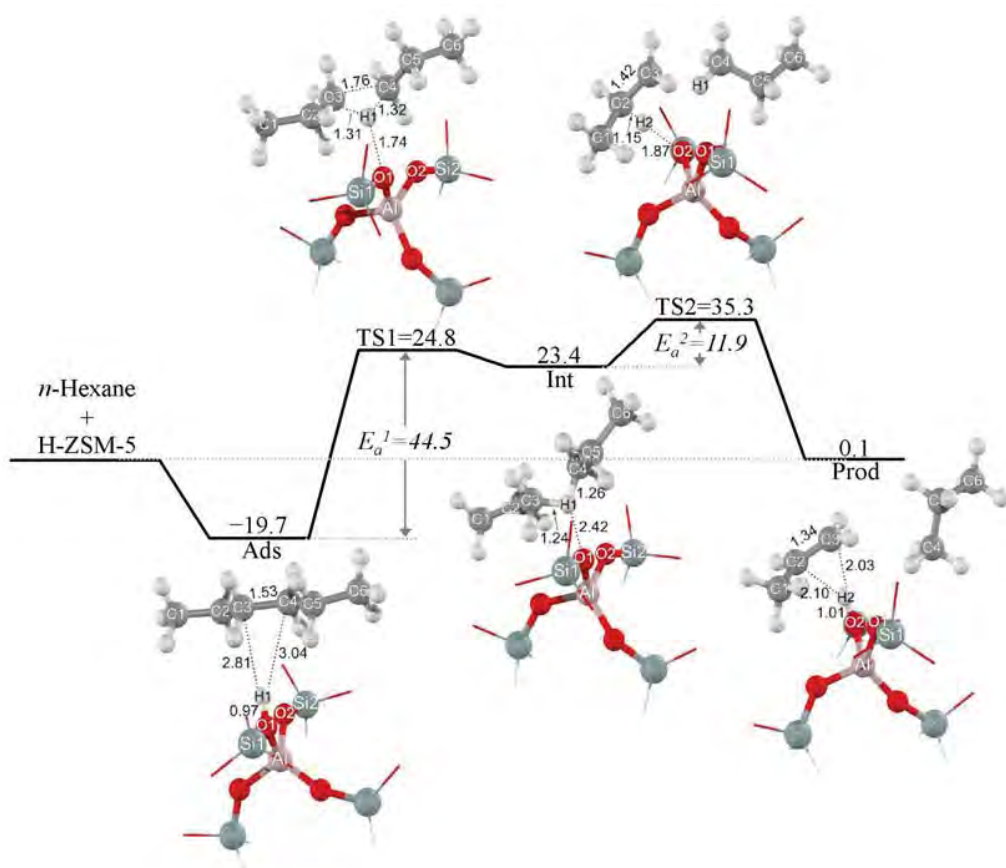
Figure 3. Energies and geometries of molecules and transition states involved in the *n*-hexane cracking mechanisms over H-ZSM-5 zeolite (energies are in kcal/mol).

Conclusions

The monomolecular cracking reaction of *n*-hexane have been investigated by using the 34T H-ZSM-5 cluster model calculated at the M06-2X/6-31G(d,p) level of theory. This calculation provides reasonable adsorption energies of *n*-hexane in H-ZSM-5 that are in good agreement with the experimental measurements. In the first step of the reaction, the *n*-hexane C–C bond is protonated to form a 3-C-surface hexonium intermediate. Then, the 3-C-hexonium intermediate is decomposed to produce propane and propene products. The activation energies are 44.5 and 11.9 kcal/mol for the first and second step, respectively. The apparent activation energy is 35.3 kcal/mol which is in agreement with the experimental result of monomolecular cracking of n-hexane. These results also confirm that relatively large quantum clusters are needed for the study of hydrocarbon reactions in zeolites and the M06-2X method is one of the well-suited methods for this case.

References

(1) Corma, A.; Planelles, J.; Sánchez-Marín, J.; Thomás, F. J. *Catal.* **1985**, *93*, 30.

(2) Krannila, H.; Haag, W. O.; Gates, B. C. *J. Catal.* **1992**, *135*, 115.

(3) Sie, S.T. *Ind. Eng. Chem. Res.* **1992**, *31*, 1881.

(4) Lercher, J. A.; Santen, R. A. v.; Vinek, H. *Catal. Lett.* **1994**, *27*, 91.

(5) Olah, A. G.; Halpern, Y.; Shen, J.; Mo, K. Y. *J. Am. Chem. Soc.* **1973**, *95*, 4960.

(6) Kazansky, V. B.; Frash, M. V.; Santen, R. A. v. *Appl. Catal. A* **1996**, *146*, 225.

(7) Zygmunt, S. A.; Curtiss, L. A.; Zapol, P.; Iton, L. E. *J. Phys. Chem. B* **2000**, *104*, 1944.

(8) Zheng, X.; Blowers, P. *J. Phys. Chem. A* **2005**, *109*, 10734.

(9) Boronat, M.; Corma, A. *Appl. Catal. A: General* **2008**, *336*, 2.

(10) Milas, I.; Nascimento, M. A. C. *Chem. Phys. Lett.* **2006**, *418*, 368.
(11) Brändle, M.; Sauer, J. *J. Am. Chem. Soc. , ,* **1998**, *120(7)*, 1556.
(12) Sinclair, P. E.; de Vries, A. H.; Sherwood, P.; Catlow, C. R. A.; R.A., V. S. *J. Chem. Soc., Faraday Trans.* **1998**, *94*, 3401.
(13) Clark, L. A.; Sierka, M.; Sauer, J. *J. Am. Chem. Soc.* **2003**, *125*, 2136.
(14) Maihom, T.; Boekfa, B.; Sirijaraensre, J.; Nanok, T.; Probst, M.; Limtrakul, J. *J. Phys. Chem. C* **2009**, *113*, 6654.
(15) Boekfa, B.; Choomwattana, S.; Khongpracha, P.; Limtrakul, J. *Langmuir* **2009**, Articles ASAP.
(16) Kumsapaya, C.; Bobuatong, K.; Khongpracha, P.; Tantirungrotechai, Y.; Limtrakul, J. *J. Phys. Chem. C* **2009**, *113* 16128.
(17) van Koningsveld, H.; Bekkum, H. v.; Jansen, J. C. *Acta. Crystallogr. B* **1987**, *43*, 127.
(18) Zhao, Y.; Schultz, N. E.; Truhlar, D. G. **2006**, *2*, 364.
(19) Zhao, Y.; Truhlar, D. G. **2008**, *41*, 157.
(20) Zhao, Y.; Truhlar, D. G. *Theor. Chem. Acc.* **2008**, *120*, 215.
(21) Zhao, Y.; Truhlar, D. G. **2008**, *112*, 6860.
(22) Frisch, M. J.; Trucks, G. W.; Schlegel, H. B.; Scuseria, G. E.; Robb, M. A.; Cheeseman, J. R.; Montgomery, J. A.; Jr.; Vreven, T.; Kudin, K. N.; Burant, J. C.; Millam, J. M.; Iyengar, S. S.; Tomasi, J.; Barone, V.; Mennucci, B.; Cossi, M.; Scalmani, G.; Rega, N.; Petersson, G. A.; Nakatsuji, H.; Hada, M.; Ehara, M.; Toyota, K.; Fukuda, R.; Hasegawa, J.; Ishida, M.; Nakajima, T.; Honda, Y.; Kitao, O.; Nakai, H.; Klene, M.; Li, X.; Knox, J. E.; Hratchian, H. P.; Cross, J. B.; Adamo, C.; Jaramillo, J.; Gomperts, R.; Stratmann, R. E.; Yazyev, O.; Austin, A. J.; Cammi, R.; Pomelli, C.; Ochterski, J. W.; Ayala, P. Y.; Morokuma, K.; Voth, G. A.; Salvador, P.; Dannenberg, J. J.; Zakrzewski, V. G.; Dapprich, S.; Daniels, A. D.; Strain, M. C.; Farkas, O.; Malick, D. K.; Rabuck, A. D.; Raghavachari, K.; Foresman, J. B.; Ortiz, J. V.; Cui, Q.; Baboul, A. G.; Clifford, S.; Cioslowski, J.; Stefanov, B. B.; Liu, G.; Liashenko, A.; Piskorz, P.; Komaromi, I.; Martin, R. L.; Fox, D. J.; Keith, T.; Al-Laham, M. A.; Peng, C. Y.; Nanayakkara, A.; Challacombe, M.; Gill, P. M. W.; Johnson, B.; Chen, W.; Wong, M. W.; Gonzalez, C.; Pople, J. A. *Gaussian 03*, revision B.05, Gaussian, Inc, Wallingford, CT, 2004.
(23) Eder, F.; Stockenhuber, M.; Lercher, J. A. *J. Phys. Chem. B* **1997**, *101*, 5414.
(24) Kotrel, S.; Rosynek, M. P.; Lunsford, J. H. *J. Phys. Chem. B* **1999**, *103*, 818.
(25) Narbeshuber, T. F.; H. Vinek; Lercher, J. A. *J. Catal.* **1995**, *157*, 388.
(26) Babitz, S. M.; B.A.Williams; Miller, J. T.; Snurr, R. Q.; W.O. Haag; Kung, H. *Appl. Catal. A Gen.* **1999**, *179*, 71.
(27) van Bokhoven, J. A.; Williams, B. A.; Ji, W.; Koningsberger, D. C.; Kung, H. H.; Miller, J. T. *J. Catal.* **2004**, *224* 50.
(28) Lónyi, F.; Kovács , A.; Valyon, J. *J. Phys. Chem. B* **2006**, *110*, 1711.

394 - Density functional study of epoxide ring-opening reaction with methanol promoted by dicopper carboxylate in metal-organic framework

Sudarat Yadnum, Saowapak Choomwattana, Pipat Khongpracha, Dr. Jumras Limtrakul, Prof. Dr. . Department of Chemistry, Faculty of Science, Kasetsart University Laboratory for Computational & Applied Chemistry, Physical Chemistry Division Chatuchak Bangkok Thailand, Center of Nanotechnology, Kasetsart University Research and Development Institute Chatuchak Bangkok Thailand, NANOTEC Center of Nanotechnology, National Nanotechnology Center, Kasetsart University Chatuchak Bangkok Thailand

The ring-opening reaction mechanism of epoxide with methanol, an important process in alkoxy alcohol synthesis, was investigated with the new density-functional theory (M062X/6-31G(d,p)) for the systems of bare model and dicopper carboxylate "paddlewheels" with a metal-organic framework (MOF) as a catalyst. The concerted transition state concerning the C-O bond formation, C-O and O-H bond dissociation, and hydrogen transfer was proposed. For the bare system, the coadsorption energy is -8.1 kcal/mol and its reaction energy is -32.3 kcal/mol. In the catalyzed mechanism, epoxide is initially adsorbed over the dicopper carboxylate with an adsorption energy of -21.1 kcal/mol. Coadsorption energy between the epoxide and methanol is -28.7 kcal/mol. This catalyzed reaction is exothermic by -55.7 kcal/mol. The Cu-MOF was found to be an efficient catalyst in ring-opening reactions of epoxides with alcohols leading to a lower energy barrier (48.0 kcal/mol) as compared to that of the bare model system (60.1 kcal/mol).

Sunday, March 21, 2010 07:00 PM

Chemistry of Materials (07:00 PM - 09:00 PM)

Close Window

1301 - Molecular dynamics simulation of *ortho-*, *para-* and *meta*-xylenes diffusion in MOF-5 with a model potential of Zn-O bonds for MOF materials

Chadchalerm Raksakoon, *Saowapak Choomwattana*, *Jumras Limtrakul, Prof. Dr. . Department of Chemistry, Faculty of Science, Kasetsart University Laboratory for Computational & Applied Chemistry, Physical Chemistry Division Chatuchak Bangkok Thailand, Center of Nanotechnology, Kasetsart University Research and Development Institute Chatuchak Bangkok Thailand, NANOTEC Center of Nanotechnology, National Nanotechnology Center, Kasetsart University Chatuchak Bangkok Thailand*

We present a Zn-O bonds potential for Metal-Organic Framework in which the potential parameters are fitted to density functional theory data of B3LYP/6-31G(d,p) and ONIOM(B3LYP/6-31G(d,p):UFF) calculations on Zn_4O and $Zn_4O(O_2C-C(CH)_2)_6$ models, respectively. To verify its accuracy, molecular dynamics (MD) simulations of *ortho-*, *para-* and *meta*-xylenes in MOF-5 at 300 K were performed with the combination of novel in-house potential energy surfaces (PES) and existing potentials to determine the maximum loading. The lattice dynamics is found at a loading of 58 molecules per unit cell and keeps increasing at higher loadings. Moreover, xylene isomers could be differentiated from their self-diffusion coefficients (D_{self}) in the framework. At the same loading, *p*-xylene is found to expand the lattice the most. Unlike in zeolites, where the pore window hindrance is the key difficulty, the diffusion in the open MOF-5 has to overcome p-p attraction of xylenes in the binding pockets.

Thursday, March 25, 2010 03:30 PM

Computational Chemistry (01:30 PM - 04:30 PM)

Close Window

685 - Decomposition of nitrous oxide on transition metal-doped carbon nanotubes

Panvika Pannopard, *Pipat Khongpracha*, *Dr. Chompunuch Warakulwit, Dr. Jumras Limtrakul, Prof. Dr. . Department of Chemistry, Faculty of Science, Kasetsart University Laboratory for Computational & Applied Chemistry, Physical Chemistry Division Chatuchak Bangkok Thailand, Center of Nanotechnology, Kasetsart University Research and Development Institute Chatuchak Bangkok Thailand, NANOTEC Center of Nanotechnology, National Nanotechnology Center, Kasetsart University Chatuchak Bangkok Thailand*

The catalytic activity of Carbon Nanotubes (CNTs) for greenhouse gas removal, like N_2O, is fine-tuned by metal doping. We take advantage of the superb capability of Sc, Ti and V transition metals in converting N_2O to N_2 to improve the less reactive surfaces of CNTs. As such, the stable composite catalysts of Sc-, Ti- and V- doped on (5,5) Single-Walled Carbon Nanotubes (SWCNTs) along with the unmodified one were investigated by employing the practical tool $Dmol^3$ for periodic systems. Without metal doping, the concerted N_2O decomposition on the bare tube proceeds via a high energy barrier (54.3 kcal/mol). However, such barriers can be overcome with the presence of active metals, i.e. reduced to 3.6, 8.0 and 10.2 kcal/mol for V-, Ti- and Sc- (5,5)SWCNTs, respectively. This superior reactivity is the result of the cooperative effect of the metal and SWCNT which enhances the electron transfers from the tube to N_2O.

Tuesday, March 23, 2010 04:10 PM

Chemistry of Materials (01:30 PM - 04:30 PM)

Close Window

American Chemical Society National meeting & Exposition" ครั้งที่ 240

ณ ประเทศสหรัฐอเมริกา

ระหว่างวันที่ 22-26 สิงหาคม 2553

จำนวน 6 เรื่อง

441 - Structures and reaction mechanisms of propene oxide isomerization to propanal on H-FER zeolite: A theoretical study using the newly developed density functional theory

Dr. Bundet Boekfa, Thana Maihom, Sippakorn Wannakao, Karan Bobuatong, Prof. Jumras Limtrakul. Laboratory for Computational & Applied Chemistry, Physical Chemistry Division, Department of Chemistry, Faculty of Science, Kasetsart University, Bangkok, Thailand; Center of Nanotechnology, Kasetsart University Research and Development Institute, Kasetsart University, Bangkok, Thailand; NANOTEC Center of Nanotechnology, National Nanotechnology Center, Kasetsart University, Bangkok, Thailand; Chemistry Department, Faculty of Liberal Arts and Science, Kasetsart University Kamphaeng Saen Campus, Nakhon Pathom, Thailand

The isomerization mechanism of propene oxide over H-FER has been carried out via the utilization of 23T nanocluster models where T are Si or Al atoms, calculated by the newly developed Density Functional Theory, M08-HX. The calculated adsorption energy of propene oxide on H-FER is predicated to be -25.4 kcal/mol. The propene oxide isomerization to propanal is calculated to be an exothermic reaction with a reaction energy of 20.8 kcal/mol. The reaction mechanism is considered to proceed through a stepwise mechanism: (1) the epoxide ring protonation, and concurrently the ring-opening, and (2), the 1,2-hydride shift formatting the adsorbed carbonyl compound. The latter step is found to be the rate-determining step with the activation energies of 24 kcal/mol as compared with the former of 22 kcal/mol. The understanding gained of the adsorption and the reaction mechanism in the confinement of nanopore zeolite will be used to improve the catalytic performance.

Tuesday, August 24, 2010 03:10 PM
Inorganic Catalysts (01:30 PM - 05:10 PM)
Location: Boston Convention & Exhibition Center
Room: Room 257B

Close Window

460 - Catalytic dehydrogenation of ethylbenzene to styrene over Fe-ZSM-5 zeolite: A newly developed density functional theory (M06-L) in ONIOM scheme

Dr. Bundet Boekfa, Thana Maihom, Sippakorn Wannakao, Pailin Limtrakul, Prof. Jumras Limtrakul. Laboratory for Computational & Applied Chemistry, Physical Chemistry Division, Department of Chemistry, Faculty of Science, Kasetsart University, Bangkok, Thailand; Center of Nanotechnology, Kasetsart University Research and Development Institute, Kasetsart University, Bangkok, Thailand; NANOTEC Center of Nanotechnology, National Nanotechnology Center, Kasetsart University, Bangkok, Thailand; Chemistry Department, Faculty of Liberal Arts and Science, Kasetsart University Kamphaeng Saen Campus, Nakhon Pathom, Thailand

The dehydrogenation mechanism of ethylbenzene to styrene over Fe-ZSM-5 zeolite was investigated by M06L/6-31G(d,p) //ONIOM(M06L/6-31G(d,p):UFF) model cluster of 46T//5T:46T where T are Si or Al atoms. The adsorption energy is calculated to be -29.0 kcal/mol, which compares well with the experimental observation. A hydrogen abstraction on the O-Fe-O group starts the reaction, and yields the ethylbenzene radical over HO-Fe-O. This step is the rate determining step with an activation energy of 14.2 kcal/mol. This is followed by the hydroxyl reacting with the ethylbenzene radical and results in the styrene product with activation energy of 6.9 kcal/mol. The reaction is exothermic reaction with a reaction energy of 56.5 kcal/mol. The catalytic dehydrogenation of Ethylbenzene to Styrene over Fe-ZSM-5 has been clearly demonstrated by the "noncovalent interaction represented" M06-L method on the zeolite framework.

Wednesday, August 25, 2010 06:00 PM
Molecular Systems for Efficient Solar Energy Conversion and Storage (06:00 PM - 09:00 PM)
Location: Boston Convention & Exhibition Center
Room: Hall C

Close Window

455 - Structures and reaction pathways of methylation of 2-methylnaphthalene with methanol over H-BEA zeolite

Karan Bobuatong, Dr. Bundet Boekfa, Sippakorn Wannakao, Prof. Jumras Limtrakul. Laboratory for Computational and Applied Chemistry, Department of Chemistry, Faculty of Science, Kasetsart University, Bangkok, Thailand; Center of Nanotechnology, Kasetsart University Research and Development Institute, Kasetsart University, Bangkok, Thailand

The methylation of 2-methylnaphthalene (2-MN) with methanol to 2,6 dimethylnaphthalene (2,6-DMN) and 2,7-dimethylnaphthalene (2,7-DMN) catalyzed over H-BEA has been investigated using the M06-2X functional. Three different reaction pathways include, (1) the methylation of 2-MN to 2,6-DMN, (2) the methylation of 2-MN to 2-7-DMN, and (3) the intramolecular isomerization between 2,6-DMN and 2,7-DMN have been proposed. For the first two mechanisms, the methoxide formation from methanol is the initial step followed by the methyl migration to 2-MN leading to naphthalynic carbocations as the key intermediates, subsequently converted into 2,6-DMN and 2,7-DMN. The calculated reaction profiles of 2,6-DMN and 2,7-DMN formation are similar and in agreement with experimental observation that the selectivity to ratio of 2,6-DMN/2,7-DMN produced on H-BEA was almost 1. In the case of the competitive reaction, the intramolecular isomerization between these two isomers was found difficult to occur due to the unfavorable high-energy barrier required for the methyl migration.

Wednesday, August 25, 2010 06:00 PM
Molecular Systems for Efficient Solar Energy Conversion and Storage (06:00 PM - 09:00 PM)
Location: Boston Convention & Exhibition Center
Room: Hall C

Close Window

337 - DFT study of oxidative dehydrogenation of propane over a VO$_2$-exchanged MCM-22 and ZSM-5 zeolites

Sippakorn Wannakao, *Thana Maihom, Dr. Winyoo Sangthong, Dr. Bundet Boekfa, Dr. Pipat Khongpracha,* _Prof. Jumras Limtrakul_. *Laboratory for Computational & Applied Chemistry, Physical Chemistry Division, Department of Chemistry, Faculty of Science, Kasetsart University, Bangkok, Thailand; Center of Nanotechnology, Kasetsart University Research and Development Institute, Kasetsart University, Bangkok, Thailand; NANOTEC Center of Nanotechnology, National Nanotechnology Center, Kasetsart University, Bangkok, Thailand; Chemistry Department, Faculty of Liberal Arts and Science, Kasetsart University Kamphaeng Saen Campus, Nakhon Pathom, Thailand*

The adsorption and the mechanism of the oxidative dehydrogenation (ODP) of propane over VO$_2$-exchanged 14T MCM-22 and 12T ZSM-5 zeolites were investigated by density functional theory calculations at the M06-L/6-31G(d,p) level of theory. The adsorption energies of propane are comparable to the ones derived from computationally much more demanding MP2 calculations and to experimental results while, as expected, the values from the B3LYP functional are too small. The reaction begins with the abstraction of a methylene hydrogen to the oxygen atom of VO$_2$ group, leading to a HO-V-O intermediate. This step is the rate determining step with apparent activation energies of 30.9 and 32.3 kcal/mol for MCM-22 and ZSM-5, respectively. The subsequent step is the propene together with the water formation. Although the catalyst reoxidation step was not included in rate limiting step, it was found to be important for releasing the product at the end of the reaction.

Wednesday, August 25, 2010 06:00 PM
Challenges for Density Functional Theory (06:00 PM - 09:00 PM)
Location: Boston Convention & Exhibition Center
Room: Hall C

Close Window

442 - Reaction mechanisms of ethene formation via ethanol dehydration catalyzed by Fe-ZSM-5 zeolite: An ONIOM study with an M06-L functional

Thana Maihom, Dr. Bundet Boekfa, Sippakorn Wannakao, Prof. Jumras Limtrakul. Laboratory for Computational & Applied Chemistry, Physical Chemistry Division, Department of Chemistry, Faculty of Science, Kasetsart University, Bangkok, Thailand; Center of Nanotechnology, Kasetsart University Research and Development Institute, Kasetsart University, Bangkok, Thailand

Stepwise and concerted mechanisms of ethene formation through the ethanol dehydration over Fe-ZSM-5 zeolite have been investigated by the utilization of a nanocluster of a large 46T model where T are Si or Al atoms, calculated by the M06-L, incorporated into the ONIOM scheme (M06-L/6-31G(d,p):UFF). In the stepwise mechanism, the ethanol dehydration commences from the hydrogen abstraction of the ethanol OH group to form the ethoxide-hydroxide intermediate with a low activation energy of 19.2 kcal/mol. This is followed by the C-H bond of the methyl carbon of ethoxide intermediate being dissociated to produce the ethene-water product with activation barrier of 63.4 kcal/mol. For the concerted mechanism, the ethanol dehydration into ethene product occurs in a single step without the intermediate formation with the activation energy of 35.6 kcal/mol. These results suggested that the production of ethene from ethanol dehydration over Fe-ZSM-5 preferably occurs through the concerted mechanism.

Tuesday, August 24, 2010 03:30 PM
Inorganic Catalysts (01:30 PM - 05:10 PM)
Location: Boston Convention & Exhibition Center
Room: Room 257B

Close Window

457 - Quantum chemical calculation of the hydrogenation reaction of encapsulated formaldehyde in Na-FAU zeolite

Dr. Winyoo Sangthong, Sippakorn Wannakao, Saowapak Choomwattana, Thana Maihom, Dr. Bundet Boekfa, Prof. Jumras Limtrakul. Laboratory for Computational & Applied Chemistry, Physical Chemistry Division, Department of Chemistry, Faculty of Science, Kasetsart University, Bangkok, Thailand; Center of Nanotechnology, Kasetsart University Research and Development Institute, Kasetsart University, Bangkok, Thailand; NANOTEC Center of Nanotechnology, National Nanotechnology Center, Kasetsart University, Bangkok, Thailand; Chemistry Department, Faculty of Liberal Arts and Science, Kasetsart University Kamphaeng Saen Campus, Nakhon Pathom, Thailand

Structures of Na-exchanged zeolite-encapsulated formaldehyde (HCHO@Na-zeolite) and their interactions with hydrogen molecule to produce methanol have been investigated by the recently developed density functional theory (M06-2X/6-31G(d,p)). Three model systems were utilized to study the hydrogenation reaction of hydrogen and formaldehyde: (1) formaldehyde in Na-exchanged zeolite: HCHO@Na-zeolite/H_2; (2) naked Na(I) as the catalyst: Na(I)/HCHO/H_2; (3) a bare model where only the reactants are present: HCHO/H_2. It was found that inclusion of the large electrostatic field generated by the naked Na(I) cation leads to a lower energy barrier (53.78 kcal/mol) of the reaction as compared to the bare model system (69.25 kcal/mol). Surprisingly, the inclusion of the extended zeolite framework had an effect on the structure and energetics of the adsorption complexes. Furthermore, stabilizing the transition state complex led to the lowest energy barrier (32.83 kcal/mol).

Wednesday, August 25, 2010 06:00 PM
Molecular Systems for Efficient Solar Energy Conversion and Storage (06:00 PM - 09:00 PM)
Location: Boston Convention & Exhibition Center
Room: Hall C

Close Window

Nanothailand 2010: Nanotechnology for a Sustainable World

ณ โรงแรมรามา การ์เด้นส์ กรุงเทพฯ ประเทศไทย

ระหว่างวันที่ 18-20 พฤศจิกายน 2553

จำนวน 15 เรื่อง

Healing of a Vacancy Defect in a Single-Walled Carbon Nanotube by Carbon Monoxide Disproportionation

Teeranan Nongnual[1,2,3], Jumras Limtrakul[1,2,3*]

[1]*Laboratory for Computational and Applied Chemistry, Department of Chemistry, Faculty of Science and Center of Nanotechnology, Kasetsart University Research and Development Institute, Kasetsart University, Bangkok 10900, Thailand*
[2]*NANOTEC Center of Excellence, National Nanotechnology Center, Kasetsart University, Bangkok 10900, Thailand*
[3]*Center for Advanced Studies in Nanotechnology and Its Applications in Chemical, Food and Agricultural Industries, Kasetsart University, Bangkok 10900, Thailand*

*Corresponding author: Tel. +66 2562 5555 ext 2169, Fax: +66 2562 5555 ext 2176, E-mail address: jumras.l@ku.ac.th

Keywords Single-Walled Carbon Nanotube, Defect Healing, Carbon Monoxide Disproportionation

Abstract

We proposed a new method of bimolecular healing of the vacancy defect in single-walled carbon nanotubes (SWCNTs). The creation of a new method was of particular importance to avoid the errors often encountered in the electronic properties of carbon nanotubes. Using DFT calculations with the PBE functional, we investigated the reaction mechanism of the monatomic vacancy defect in the (8, 0) SWCNT healing process using carbon monoxide disproportionation. Successful healing of the vacancy defect will enable numerous advantages: **(1)** The activation energy is relatively low, 9.37 kcal mol^{-1}, at the 4-membered-ring opening step under a high CO concentration condition; **(2)** no catalyst is needed, thus no purification step is needed to remove the catalyst; **(3)** only the CO ambient is used as a reactant; **(4)** no oxygen byproduct was found; and **(5)**, there was high selectivity of CO to vacancy defect sites. Our finding established that a CNT with a vacancy defect, which was generally obtained from the syntheses or other uses as a nanomaterial device, can be healed completely to resume its function as a perfect CNT holding the original electronic properties.
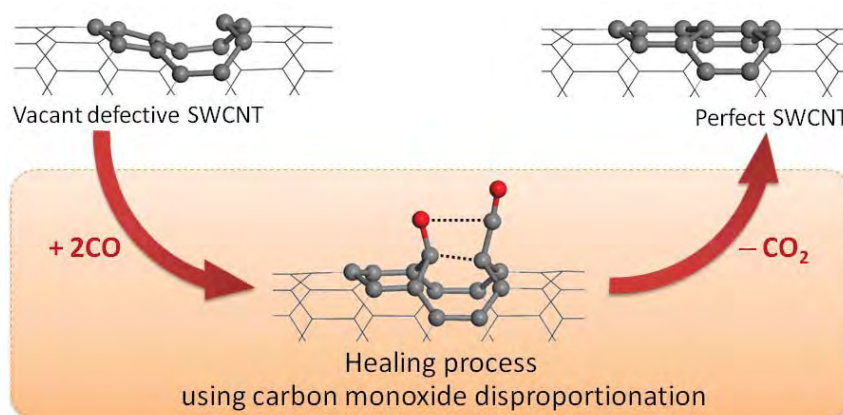
Fig. 1 Structures and reaction mechanisms of bimolecular healing of the monatomic vacancy defect in single-walled carbon nanotubes (SWCNTs).
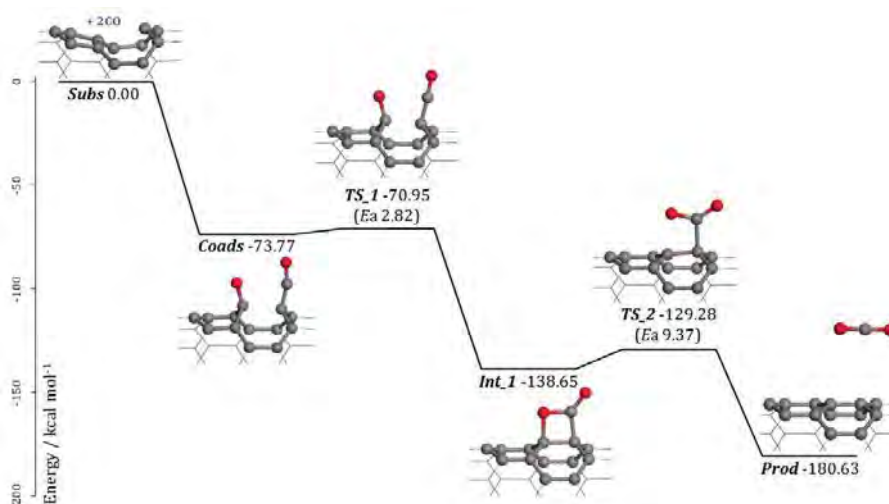
Fig. 2 The Associative-Coadsorption Pathway (ACP) energy profile of the healing process of the monatomic vacancy defect in the (8, 0) SWCNT using carbon monoxide disproportionation was proposed under the high CO concentration.
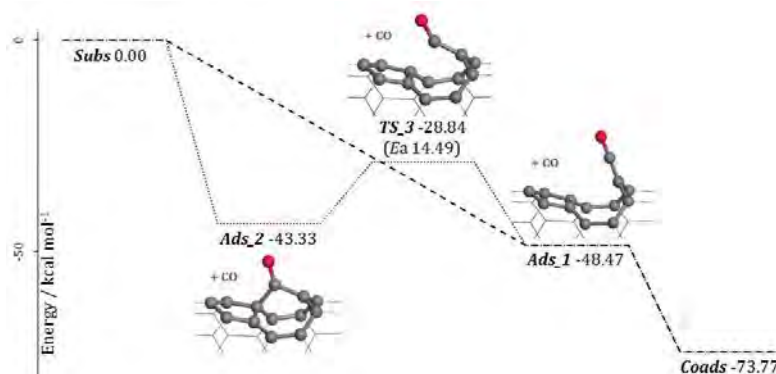

Fig. 3 The Consecutive-Coadsorption Pathway (CCP) energy profile of the healing process of the monatomic vacancy defect in the (8, 0) SWCNT using carbon monoxide disproportionation was proposed under the low CO concentration. (Dashed line is the CCP-1; Dotted line is the CCP-2.)

References

Page A. J., Y. Ohta, Y. Okamoto, S. Irle and K. Morokuma; "Defect Healing During Single-Walled Carbon Nanotube Growth: A Density-Functional Tight-Binding Molecular Dynamics Investigation." The Journal of Physical Chemistry C, 113, 20198–20207 (2009).

Nikolaev P., M. J. Bronikowski, R. K. Bradley, F. Rohmund, D. T. Colbert, K. A. Smith and R. E. Smalley; "Gas-Phase Catalytic Growth of Single-Walled Carbon Nanotubes from Carbon Monoxide." Chemical Physics Letters, 313, 91–97 (1999).

Carbonyl-ene Reaction of Encapsulated Formaldehyde in Cu(I), Ag(I) and Au(I) Exchanged FAU Zeolites

Sippakorn Wannakao[1,2,3], Pipat Khongpracha[1,2,3], Jumras Limtrakul[1,2,3*]

[1]Laboratory for Computational and Applied Chemistry, Department of Chemistry, Faculty of Science and Center of Nanotechnology, Kasetsart University Research and Development Institute, Kasetsart University, Bangkok 10900, Thailand
[2]NANOTEC Center of Excellence, National Nanotechnology Center, Kasetsart University, Bangkok 10900, Thailand
[3]Center for Advanced Studies in Nanotechnology and Its Applications in Chemical, Food and Agricultural Industries, Kasetsart University, Bangkok 10900, Thailand

*Corresponding author: Tel. +66 2562 5555 ext 2169, Fax: +66 2562 5555 ext 2176,
E-mail address: jumras.l@ku.ac.th

Keywords Zeolite, Transition metal exchange, Formaldehyde, Chemical reaction, Density functional theory

Abstract

Carbonyl-ene reaction is one of the common and very powerful tools for organic synthesis. In this work, we investigated the reaction mechanism of propene interacting with an encapsulated formaldehyde in Cu, Ag and Au-exchanged faujasite zeolites by means of the density functional theory using the newly developed and more accurate M06-L/6-31G(d,p) level of theory. Formaldehyde bound to the metal site provided adsorption energies of -15.8, -18.3 and -20.9 kcal/mol for Cu, Ag and Au-FAU, respectively. From NBO calculation, a high ionicity bonding characteristic between Au and O formed by 6s orbital of the Au atom and 2p orbital of the O atom was clearly observed. Moreover, Au-FAU was also the most active for the reaction which required 15.0 kcal/mol for the activation barrier while the rest were around 18.0 kcal/mol. These results provide significant information for utilizing these novel transition metal exchanged materials for organic synthesis processes.
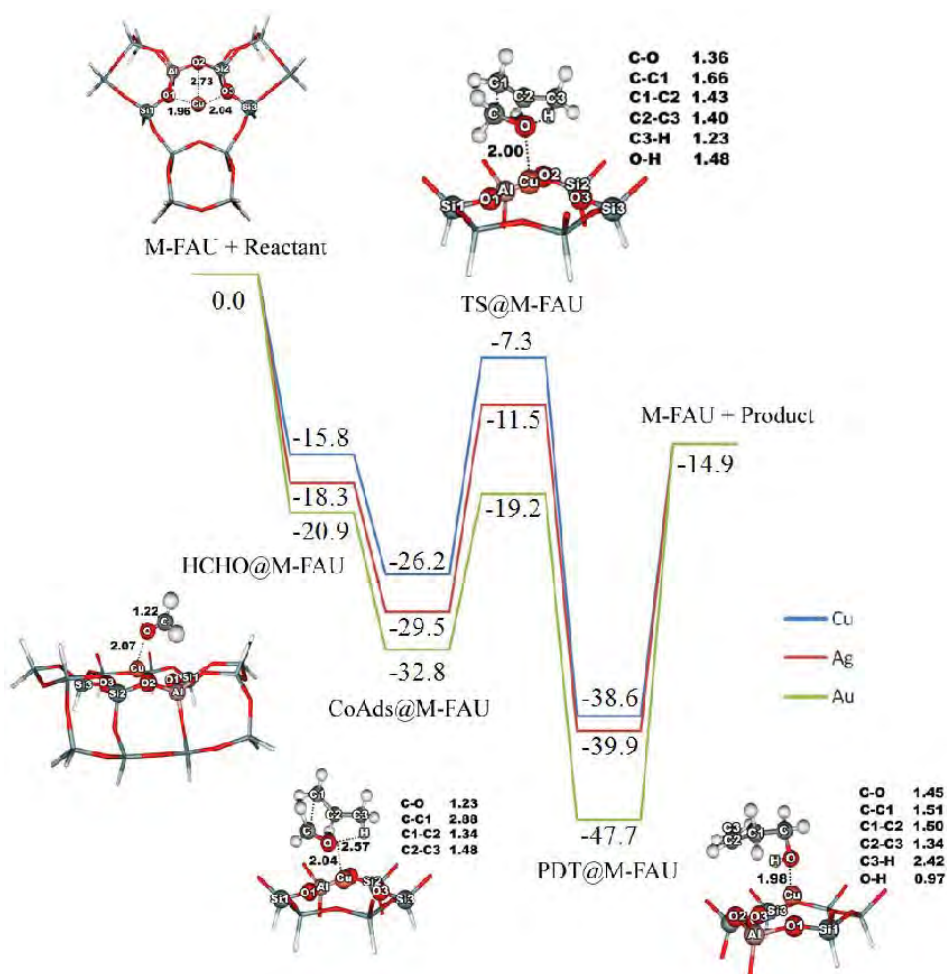
Fig. 1 Reaction profile of the formaldehyde-propene carbonyl-ene reaction over Cu, Ag and Au-FAU zeolites. Energies are in kcal/mol units.

Acknowledgements

References

Sangthong W., M. Probst and J. Limtrakul; "Computational Study of the Carbonyl-ene Reaction of Encapsulated Formaldehyde in Na-FAU Zeolite", J. Mol. Struct., 748(1-3), 119-127 (2005).

Choomwattana S., T. Maihom, P. Khongpracha, M. Probst and J. Limtrakul; "Structures and Mechanisms of the Carbonyl-ene Reaction between MOF-11 Encapsulated Formaldehyde and Propylene: An ONIOM Study", J. Phys. Chem. C, 112 (29), 10855–10861 (2008).

Zhao Y. and D.G. Truhlar; "Density Functionals with Broad Applicability in Chemistry", Acc. Chem. Res., 41(2), 157-167 (2008).

Theoretical Investigation of the Effect of the Zeolite Acidic Strength on the Reaction Mechanism of *n*-Hexane Cracking

Thana Maihom[1,2,3], Jumras Limtrakul[1,2,3*]

[1]*Laboratory for Computational and Applied Chemistry, Department of Chemistry, Faculty of Science and Center of Nanotechnology, Kasetsart University Research and Development Institute, Kasetsart University, Bangkok 10900, Thailand*
[2]*NANOTEC Center of Excellence, National Nanotechnology Center, Kasetsart University, Bangkok 10900, Thailand*
[3]*Center for Advanced Studies in Nanotechnology and Its Applications in Chemical, Food and Agricultural Industries, Kasetsart University, Bangkok 10900, Thailand*

*Corresponding author: Tel. +66 2562 5555 ext 2169, Fax: +66 2562 5555 ext 2176,
E-mail address: jumras.l@ku.ac.th

Abstract

The catalytic cracking of hydrocarbons is one of the important reactions in the petrochemical industry. It is used to break down large hydrocarbons in crude oil into light hydrocarbons for the production of fuels. It is generally accepted that the activity of this reaction is related to the acid strength of the zeolite. Therefore, it is of interest to study what role the zeolite's acid strength plays in the cracking reaction.

In this work, the effects of the acid strength on the cracking reaction have been investigated using the isomorphously substituted MFI zeolites: the H-[Al]-MFI and the H-[B]-MFI zeolites as catalysts at the M06-2X/6-311+G(2df,2p)//M06-2X/6-31G(d,p) level of theory. The calculated adsorption energies of n-hexane are –18.2 and –17.2 kcal/mol for H-[Al]-MFI and H-[B]-MFI, respectively. The former estimated adsorption energy is in excellent agreement with experimental measurement. The reaction mechanism of n-hexane cracking consists of two steps. In the first step, the acidic proton of the zeolites is protonated to the n-hexane C-C bond to form the highly unstable 3-C-hexonium intermediate in the nanocavity. For the second step, the 3-C-hexonium intermediate is decomposed to generate the propane and propene products. The first step is found to be the rate-determining step with activation energies of 45.8 and 54.2 kcal/mol for H-[Al]-MFI and H-[B]-MFI, respectively. The apparent and overall reaction energies are calculated to be 36.8 and 55.0 kcal/mol for H-[Al]-MFI zeolite and 45.3 and 62.5 kcal/mol for H-[B]-MFI zeolite. The activation energies in H-[Al]-MFI zeolite are lower due to their more acidic than H-[B]-MFI zeolite. The results verified that the intrinsic catalytic activity of n-hexane cracking is more sensitive to the acid strength of zeolites.
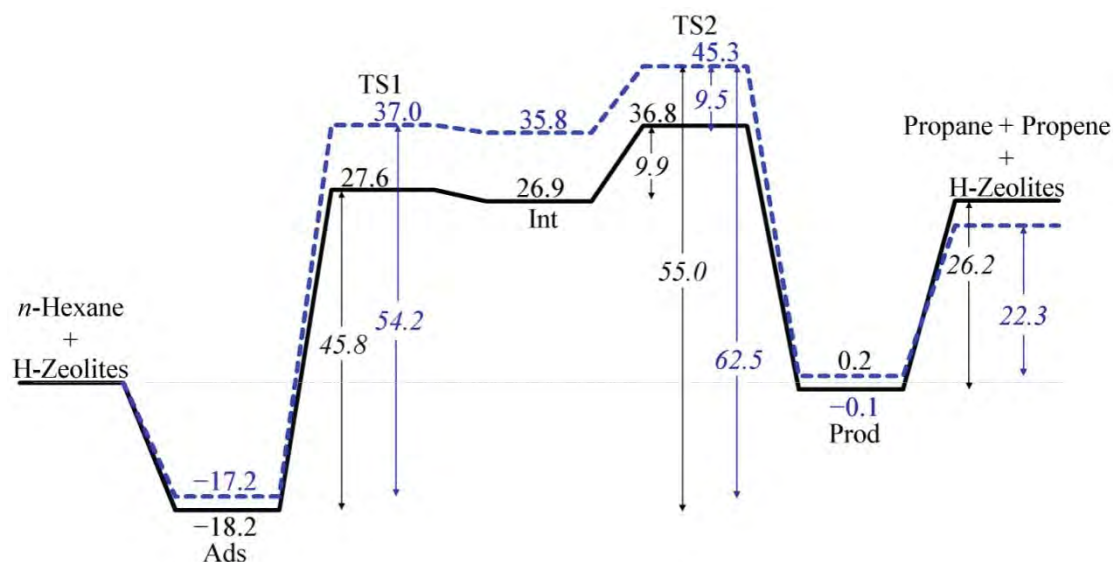
Fig. 1 Energy profile for the n-hexane cracking mechanisms for both zeolites: H-[Al]-MFI zeolite (solid line) and H-[B]-MFI (dashed line) zeolite (energies are in kcal/mol).

References

Maihom T., P. Pantu, C. Tachakritikul, M. Probst and J. Limtrakul; "Effect of the Zeolite Nanocavity on the Reaction Mechanism of n-Hexane Cracking: A Density Functional Theory Study" J. Phys. Chem. C , 114, 7850-7856 (2010).

Sirijaraensre J. and J. Limtrakul; "Effect of the Acidic Strength on the Vapor Phase Beckmann Rearrangement of Cyclohexanone Oxime over the MFI Zeolite: an Embedded ONIOM Study". Phys Chem Chem Phys 11 (3), 578-585 (2009).

Zhao Y. and D. G. Truhlar; "Benchmark Data for Interactions in Zeolite Model Complexes and Their Use for Assessment and Validation of Electronic Structure Methods" J. Phys. Chem. C. 112, 6860-6868 (2008).

Williams B. A., S. M. Babitz, J. T. Miller, R. Q. Snurr and H. H. Kung; "The Roles of Acid Strength and Pore Diffusion in the Enhanced Cracking Activity of Steamed Y Zeolites" Appl. Catal. A 177, 161-175 (1999).

H-Bond Formation Assisted by a Single Au Atom and an Au$_{13}$ Cluster: A DFT Study

Anawat Thivasasith[1,2,3], Panvika Pannopard[1,2,3], Pipat Khongpracha[1,2,3], Chompunuch Warakulwit[1,2,3], Jumras Limtrakul[1,2,3*]

[1]*Laboratory for Computational and Applied Chemistry, Department of Chemistry, Faculty of Science and Center of Nanotechnology, Kasetsart University Research and Development Institute, Kasetsart University, Bangkok 10900, Thailand*
[2]*NANOTEC Center of Excellence, National Nanotechnology Center, Kasetsart University, Bangkok 10900, Thailand*
[3]*Center for Advanced Studies in Nanotechnology and Its Applications in Chemical, Food and Agricultural Industries, Kasetsart University, Bangkok 10900, Thailand*

*Corresponding author: Tel. +66 2562 5555 ext 2169, Fax: +66 2562 5555 ext 2176, E-mail address: jumras.l@ku.ac.th

Abstract

An "Au$_{13}$-cysteine-formic acid" system was used as a simple model for a high sensitive biosensor. In this model, an Au$_{13}$ cluster linked with a cysteine molecule via a metal-thiolate (M-S) bond was chosen to represent a unit of Au clusters or Au nanostructures-based biosensor. The interaction between cysteine and formic acid was selected to be used as a very simple model representing an H-bond interaction that might be utilized in a biosensor. The geometries and electronic properties of the bare Au$_{13}$ cluster, cysteine (Cys), formic acid (HCO$_2$H) and their hybrid system were investigated by using density functional theory (DFT) calculations with the B3LYP functional. The calculations were performed by using the 6-31G** basis set for all the atoms except Au, for which the LANL2DZ was used. The calculations showed that the cysteine has high affinity to the single Au atom and the Au$_{13}$ cluster via the metal-thiolate bond with interaction energies of 46.04 kcal/mol and 63.27 kcal/mol, respectively. In the presence of the Au atom and the Au$_{13}$ cluster, the interaction energies between the Cys/HCO$_2$H molecules were found to be higher (17.30 kcal/mol and 17.58 kcal/mol, respectively) than that of the bare complex (14.67 kcal/mol). Thus, the Au atom or the Au$_{13}$ cluster slightly affected the interaction energy between cysteine and formic acid. However, the modulation of the energy gap between the highest occupied molecular orbital (HOMO) and the lowest unoccupied molecular orbital (LUMO) of the system revealed that the presence of the Au atom and the Au$_{13}$ cluster increase the conductivity of the system by lowering the HOMO-LUMO gap (4.28 eV and 4.30 eV for the Au/Cys/HCO$_2$H and the Au$_{13}$/Cys/HCO$_2$H hybrid systems vs. 6.28 eV for the bare Cys/HCO$_2$H complex).

Acknowledgements

References

Tiwari S. and P.C Mishra; "Vibrational Spectra of Cysteine Zwitterion and Mechanism of Its formation: Bulk and Specific Solvent Effects and Geometry Optimization in Aqueous Media" Spectrochimica Acta Part A: Molecular and Biomolecular Spectroscopy, 73, 719–729 (2009).

Larsson J. A., M. Nolan and J.C. Greer; "Interactions between Thiol Molecular Linkers and the Au_{13}.Nanopaticle" The Journal of Physical Chemistry B, 106, 5931-5931 (2002).

Pannopard P., P. Khongpracha, M. Probst and J. Limtrakul; "Structure and Electronic Properties of ''DNA–Gold–Nanotube'' Systems: A Quantum Chemical Analysis" Journal of Molecular Graphics and Modelling, 26, 1066-1075 (2007).

Theoretical Studies of Nitrous Oxide Decomposition Reaction in Transition Metals (TM) Ion Exchanged ZSM-5 Zeolite

Boonruen Sunpetch[1,2,4], Bundet Boekfa[2,3,4], Piboon Pantu[1,2,4],
Jumras Limtrakul[1,2,4*]

[1]*Laboratory for Computational and Applied Chemistry, Department of Chemistry, Faculty of Science and Center of Nanotechnology, Kasetsart University Research and Development Institute, Kasetsart University, Bangkok 10900, Thailand*
[2]*NANOTEC Center of Excellence, National Nanotechnology Center, Kasetsart University, Bangkok 10900, Thailand*
[3]*Chemistry Department, Faculty of Liberal Art and Science, Kasetsart University Kamphaeng Saen Campus, Nakhon Pathom 73140, Thailand*
[4]*Center for Advanced Studies in Nanotechnology and Its Applications in Chemical, Food and Agricultural Industries, Kasetsart University, Bangkok 10900, Thailand*

*Corresponding author: Tel. +66 2562 5555 ext 2169, Fax: +66 2562 5555 ext 2176,
E-mail address: jumras.l@ku.ac.th

Keywords Heterogeneous Catalysis, Metal-Exchanged Zeolite, nitrous oxide decomposition, ONIOM approach, M06 functional

Introduction

Zeolites are used in a variety of applications such as petrochemical cracking, ion-exchange, and as a reducing toxic agent. Due to their excellent environmental catalyst, the transition metal (TM) loaded zeolites are used for the nitrous oxide (N_2O) decomposition reaction. In experiment, the nitrous oxide decomposition over transition metal ion exchanged zeolites has been studied extensively, but the detailed mechanism and reactivity are still being debated. Fe-ZSM-5 is one of the most widely studied transition metal-exchanged zeolites for nitrous oxide decomposition due to its high activity. The quantum calculation has been used to study the reaction of nitrous oxide decomposition. These works lead us to understand the reaction mechanism, however, the quantum models are quite small and the effects of the zeolite framework are not included. More recently the effects of the zeolite framework have been successfully studied with the newly developed density functional theory, M06 functional. The aim of this work is then: 1) to study the nitrous oxide decomposition on the nanostructure of ZSM-5 zeolite by including the confinement effect via the ONIOM (M06-2X:UFF) approach, and 2) to investigate the activity of different transition metal-exchanged zeolites.

Computational Details

The nitrous oxide decomposition over transition metal exchanged zeolite has been studied via the ONIOM approach. The inner layer 12T active region was treated with the new density function theory. The outer layer model is extended up to a 96T quantum cluster to realistically represent the confinement effect of the zeolite framework, performed with the UFF force field. The structures of reactants, intermediates, transition states, and products were optimized at the M06 level of theory. The Effective Core Potentials (ECP) of Stuttgart and Born basis sets were assigned to metal center atoms (Ni and Fe) and the 6-31G(d,p) basis sets were applied for other remaining atoms. The total spin of the systems are

kept constant at high spin as sextet and quartet for Fe- and Ni-ZSM-5, respectively. In order to improve the accuracy of reaction energies, single point calculations at M06-2X/6-311+G(df,2p):UFF level of theory were carried out for optimized structures. All calculations were performed with the Gaussian 03 code modified to incorporate the Minnesota Density Functional module 3.1 by Zhao and Truhlar.

Results and Discussion

The reaction mechanism of nitrous oxide decomposition over TM-ZSM-5 is summarized in Fig. 1. The initial active site is metal oxo species (I) which was reported as the active site for isolated Fe monodentate in ZSM-5. The first step is the adsorption of the first N_2O molecule over the active site ([TMO]+, metal oxo species) through its O-end which is defined as structure II. The adsorbed N_2O is decomposed through the transition state structure (III). The generated N_2 molecule adsorbed on the metal dioxo species (([OTMO]+, IV) was desorbed and the extremely active species (V) was generated. Then, the second N_2O comes to adsorb on the metal dioxo isolated site and form the adsorption complex (VI). This complex was changed through the transition state structure (VII) to be the second N_2 molecule and 3 O-atoms bound about the TM atom (VIII). Finally, 2 O-atoms adsorbed in the form of an O_2 molecule (IX) were desorbed and regenerated the starting active oxo species (I). The decomposition of N_2O through this reaction mechanism was applied to all metal species to make comparable reaction structures.
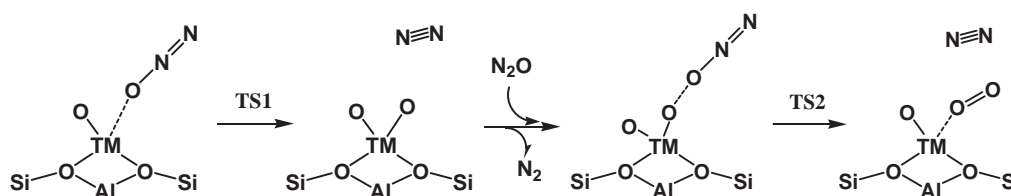

Fig. 1 The proposed mechanism for N_2O decompositions over TM-ZSM-5 (TM = Fe or Ni).

The nitrous oxide decomposition over Fe- and Ni-ZSM-5 is calculated with the ONIOM 12T:96T (M06-2X/6-311+G(df,2p):UFF//M06/6-31G(d,p):UFF) approach. The reaction of the nitrous oxide molecule locates in the intersection of ZSM-5, as shown in Fig. 2. The adsorption energies of nitrous oxide ([TMO]+, metal oxo species) are -19.6 and -13.3 kcal/mol for Fe-ZSM-5 and Ni-ZSM-5, respectively. The optimized adsorption energies agree well with the experiment of -16 kcal/mol. Nitrous oxide decompositions in transition metal ion exchanged zeolitess are shown in Fig. 3.

The reaction energy profile of nitrous oxide decomposition over Fe-ZSM-5 and Ni-ZSM-5 are shown in Fig. 4. The apparent activation energies of N_2O decomposition are calculated to be 36.5 and 51.6 kcal/mol for Fe- and Ni-ZSM-5, respectively. These results were in the same range as the work of Ryder that calculated the activation energy of N_2O over FeO-ZSM-5 as 37.6 kcal/mol. The produced N_2 molecule was desorbed with the desorption energy 5.5 and 1.3 kcal/mol for Fe-, and Ni-ZSM-5, respectively.

2 N₂O

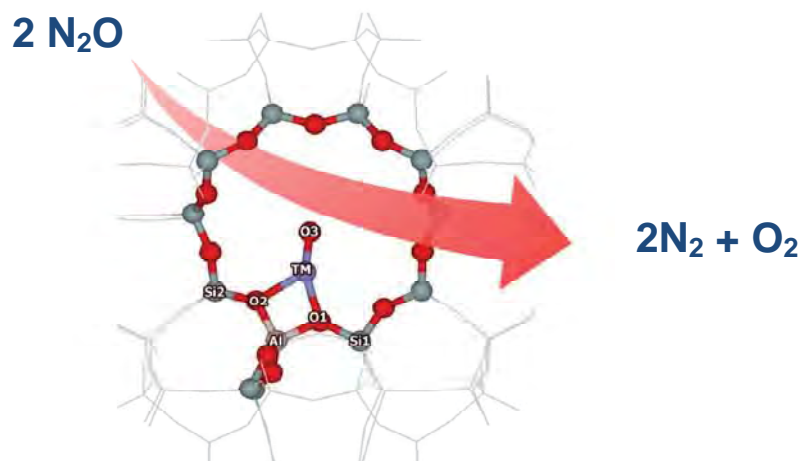**2N₂ + O₂**

Fig. 2 The structure of the nitrous oxide molecule on the 12T:96T model of Fe-ZSM-5.

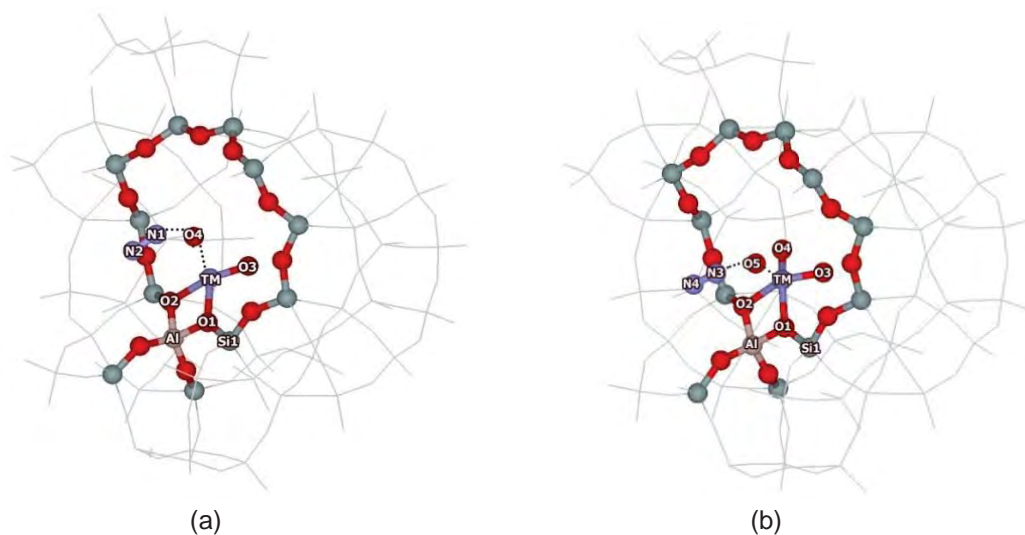(a)   (b)

Fig. 3 Transition Structure of first (a) and second (b) nitrous oxide decomposition on TM-ZSM-5.
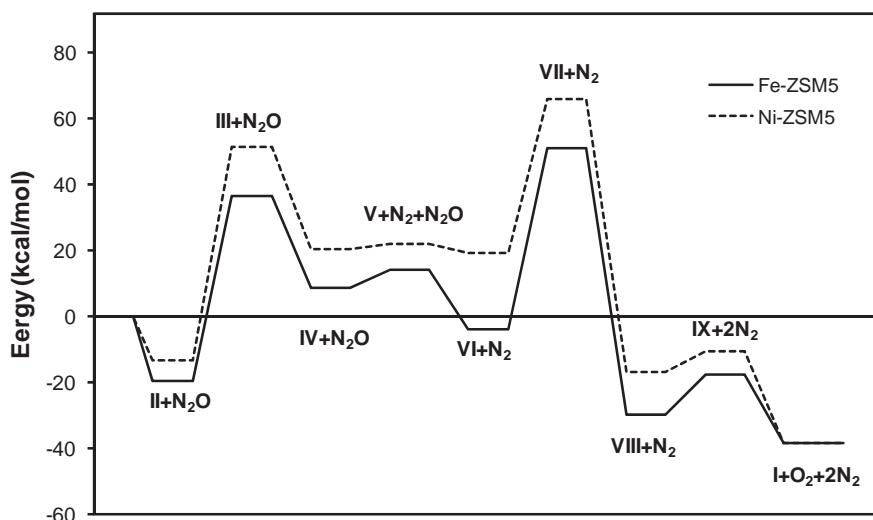
Fig. 4 Energy profile of N_2O decomposition over TMOx-ZSM-5.

The second N_2O came to adsorb over the metal dioxo ZSM-5 through the oxygen atom (VI) with adsorption energies of -17.8 and 0.1 kcal/mol for Fe- and Ni-ZSM-5, respectively. The adsorption formed over metal dioxo ZSM-5 is less exothermic than the adsorption over metal oxo ZSM-5. This adsorbed N_2O was decomposed through the transition structure (VII). The apparent activation energies for the second N_2O decomposition are 37.0 and 46.8 kcal/mol for Fe- and Ni-ZSM-5, respectively. The product of this stage was the N_2 molecule adsorbed on TMO_3-ZSM-5 (VIII). The activation energies in this calculation are also close to the experimental results.

Finally, the O_2 molecule was released from the TM-ZSM-5 and reproduced the initial active oxo species (I). To eliminate this O_2 molecule from TMO-ZSM-5 required the energies of only 12.0 and 6.6 kcal/mol for Fe- and Ni-ZSM-5, respectively. Hence, the rate limiting step of N_2O decomposition over TM-ZSM-5 in this study was the decomposition of first N_2O for both Fe- and Ni-ZSM-5. The decomposition of N_2O over Ni-ZSM-5 requires higher energy than Fe-ZSM-5. This activity trend agrees well with the trend of N_2O decomposition on TM-ZSM-5 reported by Abu-Zied and coworkers that Fe-ZSM-5 is more active than Ni-ZSM-5.

Conclusion

The catalytic cycle of nitrous oxide decomposition over transition-metal exchanged ZSM-5 zeolite is studied with the ONIOM 12T:96T approach. The models are calculated with the M06-2X:UFF//M06:UFF level of theory. The adsorption energies of nitrous oxide are calculated to be -19.6 and -13.3 kcal/mol for Fe-ZSM-5 and Ni-ZSM-5 zeolite, respectively. The nitrous oxide decomposed reactions are considered to proceed via two steps of mechanism: (1) the decomposition of the first nitrous oxide molecule on metal oxo species to produce nitrogen gas and the metal dioxo species, after that (2) the decomposition of the second nitrous oxide molecule to produce nitrogen gas, oxygen gas and metal oxo species. The reaction mechanisms are proposed to be exothermic. The first step of the reaction is calculated to be the rate of the reaction mechanism. The calculated apparent activation energies are 36.5 and 51.6 kcal/mol for Fe- and Ni-ZSM-5 zeolite, respectively. For the second step of the reaction the apparent activation energies are 37.0 and 46.8 kcal/mol, respectively. This calculation shows that Fe-ZSM-5 is more active than Ni-ZSM-5 for the reaction of nitrous oxide decomposition and agree well with experiment data. The ONIOM (M06:UFF) model, which includes the zeolite framework effect, can be used to calculate more reliable results.

Acknowledgements

References

Boekfa B., S. Choomwattana, P. Khongpracha, and J. Limtrakul; "Effects of the Zeolite Framework on the Adsorptions and Hydrogen-Exchange Reactions of Unsaturated Aliphatic, Aromatic, and Heterocyclic Compounds in ZSM-5 Zeolite: A Combination of Perturbation Theory (MP2) and a Newly Developed Density Functional Theory (M06-2X) in ONIOM Scheme" Langmuir. 25(22), 12990–12999 (2009).

Choi S. H., B. R.Wood, J. A. Ryder and A. T. Bell; "X-ray Absorption Fine Structure characterization of the local structure of Fe in Fe-ZSM-5" J. Phys. Chem. B 107, 11843-11851 (2003).

Fellah M. F. and I. Onal; "N_2O decomposition on Fe- and Co-ZSM-5: A density functional study." Catal. Today. 137, 410-417 (2008).

Heyden A., B. Peters, A. T. Bell and F. J. Keli; "Comprehensive DFT study of nitrous oxide decomposition over Fe-ZSM5" J. Phys. Chem. B. 109(5), 1857-1873 (2005).

Maihom T., P. Pantu, C. Tachakritikul, M. Probst and J. Limtrakul; "Effect of the Zeolite Nanocavity on the Reaction Mechanism of n-Hexane Cracking: A Density Functional Theory Study" J. Phys. Chem. C. 114 (17), 7850-7856 (2010).

Pantu P., S. Pabchanda and J. Limtrakul; "Theoretical investigation of the selective oxidation of methane to methanol on nanostructured Fe-ZSM-5 by the ONIOM method" Chem. Phys. Chem. 5, 1901-1906 (2004).

Ryder J., A. K. Chakraborty and A. T. Bell; "Density Functional Theory study of nitrous decomposition over Fe- and Co- ZSM5" J. Phys. Chem. B. 106, 7059-7064 (2002)

Wood B. R., J. A. Reimer and A.T. Bell; "Studies of N_2O Adsorption and Decomposition on Fe–ZSM-5" J. Catal. 209, 151- 158 (2002).

Zhao Y. and D. G. Truhlar; "Benchmark Data for Interactions in Zeolite Model Complexes and Their Use for Assessment and Validation of Electronic Structure Methods" J. Phys. Chem. C. 112, 6860-6868 (2008).

Corporative Effect of Zeolite Framework and Cation on Dehydrogenation of Methanol over Na-Exchanged Faujasite Zeolite: A Newly Developed Density Functional (M06-2X)

Winyoo Sangthong[1,2,3], Jumras Limtrakul[1,2,3*]

[1]Laboratory for Computational and Applied Chemistry, Department of Chemistry, Faculty of Science and Center of Nanotechnology, Kasetsart University Research and Development Institute, Kasetsart University, Bangkok 10900, Thailand
[2]NANOTEC Center of Excellence, National Nanotechnology Center, Kasetsart University, Bangkok 10900, Thailand
[3]Center for Advanced Studies in Nanotechnology and Its Applications in Chemical, Food and Agricultural Industries, Kasetsart University, Bangkok 10900, Thailand

*Corresponding author: Tel. +66 2562 5555 ext 2169, Fax: +66 2562 5555 ext 2176,
E-mail address: jumras.l@ku.ac.th

Abstract

Methanol interacting with cluster models of Na-exchanged Faujasite zeolite (CH_3OH@Na-FAU) together with its dehydrogenation mechanisms to produce formaldehyde have been investigated by the recently developed and more accurate density functional theory (M06-2X/6-311+G(2df,p)//M06-2X/6-31G(d,p)). In order to be able to make a comparison, the dehydrogenation was also investigated for the uncatalyzed system and the bare Na(I). We propose two reaction mechanisms. The initial step of the stepwise mechanism comprises the proton transfer from the hydroxyl group to the zeolite framework as well as the formation of the methoxide species. This step requires an activation energy (ΔE_{act}) of 52.8 kcal/mol, and is considered to be the rate determining step. The step following, the second step, is the formation of hydrogen from the proton of the zeolite framework and the hydrogen atom from the methoxy species. This requires an activation energy of 15.6 kcal/mol. For the concerted mechanism, the mechanism consists of the movement of the hydroxyl proton to simultaneously form a bond with the methyl hydrogen atom. The energy barriers are predicted to be 89.0, 96.7, and 81.7 kcal/mol for Na-exchanged faujasite, uncatalyzed system, and bare Na(I), respectively. The reason for this is that the electrostatic field generated by the naked Na(I) ion and the destabilizing role of the oxygen atom in the zeolite lattice surrounding the cation. The results are indicative of the stepwise pathway being favored over the concerted one and demonstrates that the inclusion of the extended zeolite framework has an effect on the structure and energetic of the reaction system. Furthermore, the zeolite framework has a corporative effect on the stabilizing of the transition state complex and the intermediate leading to the lowest energy barrier.
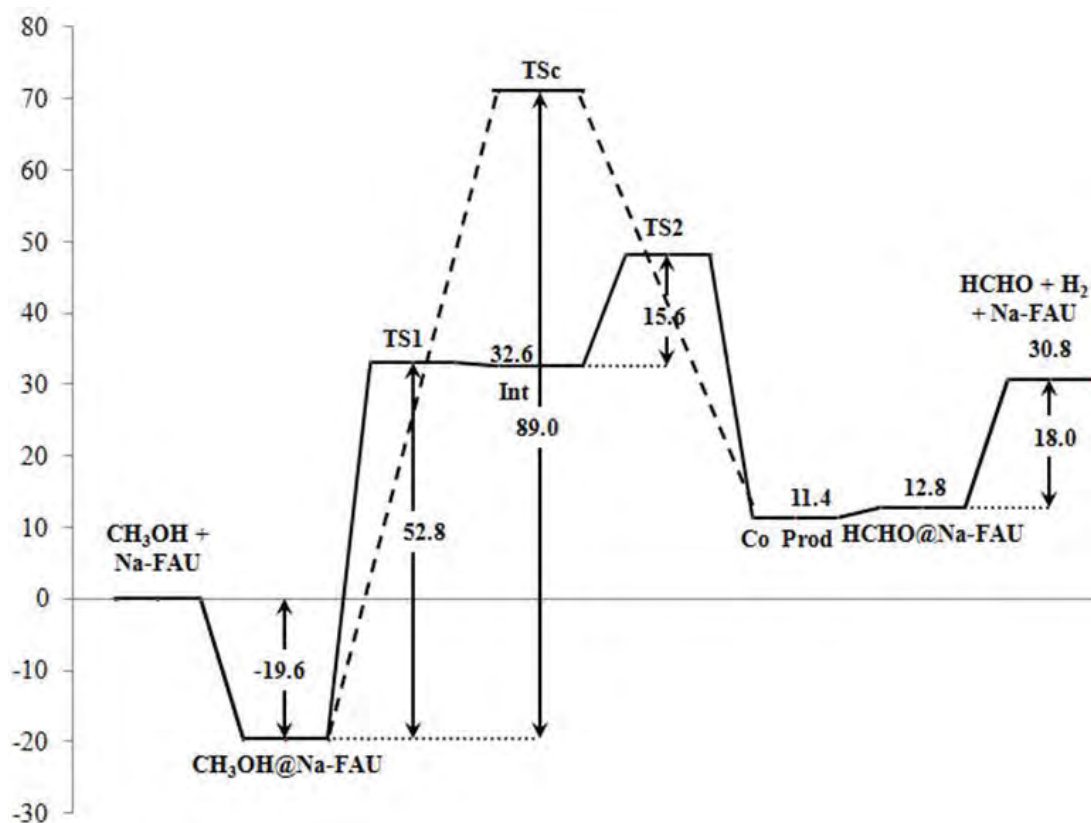
Fig. 1 Energy profiles for the dehydrogenation reaction of methanol on the 30T quantum cluster of Na-FAU calculated with M06-2X/6-311+G(2df,2p) method: stepwise mechanism (solid line) and concerted mechanism zeolite (dashed line) (energies are in kcal/mol).

References

Plant D. F., A. Simperler and R. G. Bell; "Adsorption of Methanol on Zeolites X and Y. An Atomistic and Quantum Chemical Study." J. Phys. Chem. B, 110, 6170-6178 (2006).

Kang L. and K. Han; "Adsorption and Dehydrogenation of Methanol on Alkali-Cation-Exchanged Zeolite: A First-Principles Density Functional Study." Microporous and Mesoporous Materials, 127, 90-95 (2010).

Boekfa B., S. Choomwattana, P. Khongpracha, and J. Limtrakul; "Effects of the Zeolite Framework on the Adsorptions and Hydrogen-Exchange Reactions of Unsaturated Aliphatic, Aromatic, and Heterocyclic Compounds in ZSM-5 Zeolite: A Combination of Perturbation Theory (MP2) and a Newly Developed Density Functional Theory (M06-2X) in ONIOM Scheme." Langmuir, 25(22), 12990-12999 (2009).

The Confinement Effect of the Zeolite Framework on the Isomerization Reaction of Propene Oxide over Nanostructured H-FER Zeolite Catalyst Using a Newly Developed "Embedded MP2:M06" Method

Bundet Boekfa[1,2,3], Jumras Limtrakul[1,3,4*]

[1]NANOTEC Center of Excellence, National Nanotechnology Center, Kasetsart University, Bangkok 10900, Thailand
[2]Chemistry Department, Faculty of Liberal Arts and Science, Kasetsart University Kamphaeng Saen Campus, Nakhon Pathom 73140, Thailand
[3]Center for Advanced Studies in Nanotechnology and Its Applications in Chemical, Food and Agricultural Industries, Kasetsart University, Bangkok 10900, Thailand
[4]Laboratory for Computational and Applied Chemistry, Department of Chemistry, Faculty of Science and Center of Nanotechnology, Kasetsart University Research and Development Institute, Kasetsart University, Bangkok 10900, Thailand

*Corresponding author: Tel. +66 2562 5555 ext 2169, Fax: +66 2562 5555 ext 2176, E-mail address: jumras.l@ku.ac.th

Keywords Heterogeneous Catalysis, Zeolite, Isomerization reaction, embedded ONIOM, Confinement effect

Abstract

The confinement effect of the zeolite framework on the adsorption and reaction mechanism has been studied with various methods: quantum cluster, ONIOM (Our own N-layered Integrated molecular Orbital + Molecular mechanics) and a newly developed embedded ONIOM method. The pore structure of H-FER is represented by models from 5T clusters up to realistic 34T clusters. The models are calculated with the newly developed and much accurate computational methods MP2/6-311+G(2df,2p):M06-2X/6-311+G(2df,2p), with the periodic charge from the infinite zeolite lattice included. To begin, the adsorption of propene oxide, propanal and propanone on H-FER zeolite are calculated and found to be -25.5, -24.5 and -26.0 kcal/mol, which agree well with experimental data for the propanone interacted with zeolite (-31.1 kcal/mol). The contributions of the confinement effect from the extended framework are 36, 38 and 67 % of adsorption energies for propene oxide, propanal and propanone over H-FER, respectively. In order to be able to account for the framework lattice, the more accurate "embedded MP2/6-311+G(2df,2p):M06-2X/6-311+G(2df,2p)" method is applied to study the reaction mechanism of propene oxide. The isomerization reaction mechanism of propene oxide is considered to proceed through a stepwise mechanism: (1) the epoxide ring protonation, and, concurrently, the ring-opening, and (2), the 1,2-hydride shift formatting the adsorbed carbonyl compound. Two different types of product, propanal and propanone, were observed. Exothermic reactions were detected with the heat of reaction -20.1 and -29.3 kcal/mol for propene oxide to propanal and propanone, respectively. The transition state complexes are stabilized by the framework. Consequently, it decreases the activation barrier by about 16 – 50%. For the propanal product, the ring opening step is found to be the rate-determining step with an activation barrier of 31.6 kcal/mol, whereas for the propanone product, the hydride shift formatting step is found to be the rate-determining step with a higher activation barrier of 48.9 kcal/mol. The results suggest that the "embedded MP2:M06" is a suitable tool for evaluating the adsorption and reaction mechanism in the nanoconfinement of zeolite.
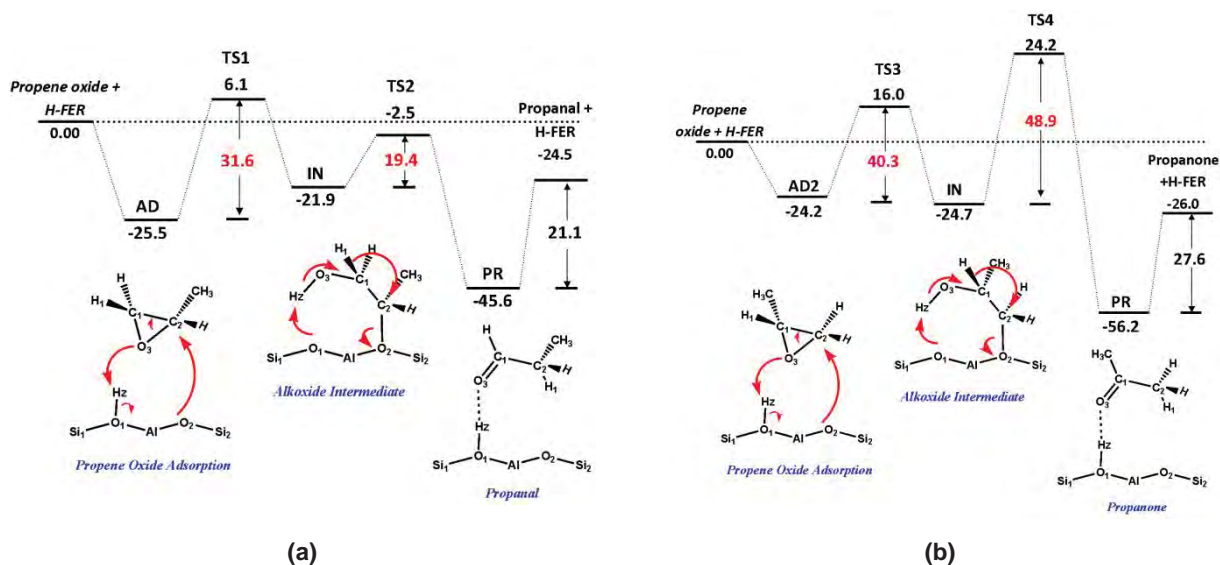
Fig. 1 Potential energy diagram of the propene oxide isomerization to (a) propanal and (b) propanone on the 5T:34T ONIOM cluster of H-FER, calculated with the embedded MP2/6-311+G(2df,2p):M06-2X/6-311+G(2df,2p)//MP2/6-31G(d,p):M06-2X/6-31G(d,p) method. (kcal/mol).

Acknowledgements

References

Boekfa B., S. Choomwattana, P. Khongpracha, and J. Limtrakul; "Effects of the Zeolite Framework on the Adsorptions and Hydrogen-Exchange Reactions of Unsaturated Aliphatic, Aromatic, and Heterocyclic Compounds in ZSM-5 Zeolite: A Combination of Perturbation Theory (MP2) and a Newly Developed Density Functional Theory (M06-2X) in ONIOM Scheme" Langmuir 25(22), 12990–12999 (2009).

Derouane G. E. and C. D. Chang; "Confinement effects in the adsorption of simple bases by zeolites" Micropor. Mesopor. Mat. 35–36, 425–433 (2000).

Maihom T., B. Boekfa, J. Sirijaraensre, T. Nanok, M. Probst and J. Limtrakul; "Reaction Mechanisms of the Methylation of Ethylene with Methanol and Dimethyl Ether over H-ZSM-5: An ONIOM Study" J. Phys. Chem. C 113, 6654-6662 (2009).

Namuangruk S., P. Khongpracha, P. Pantu, and J. Limtrakul; "Structures and Reaction Mechanisms of Propene Oxide Isomerization on H-ZSM-5: An ONIOM Study". J. Phys. Chem. B 110, 25950-25957 (2006).

Pantu P., B. Boekfa and J. Limtrakul; "The adsorption of saturated and unsaturated hydrocarbon on nanostructured zeolite (H-MOR and H-FAU): An ONIOM study." J. Mol. Cat. A 277,171-179 (2007).

Zhao Y. and D. G. Truhlar; "Benchmark Data for Interactions in Zeolite Model Complexes and Their Use for Assessment and Validation of Electronic Structure Methods" J. Phys. Chem. C 112, 6860-6868 (2008).

Structures and Reaction Mechanisms of Skeletal Isomerization of 1-Butene over Ferrierite Zeolite:
An Embeded Nanocluster Approach

Chularat Wattanakit[1,2,4], Somkiat Nokbin[1,2,4], Bundet Boekfa[2,3,4],
Piboon Pantu[1,2,4], Jumras Limtrakul[1,2,4*]

[1]Laboratory for Computational and Applied Chemistry, Department of Chemistry, Faculty of Science
and Center of Nanotechnology, Kasetsart University Research and Development Institute, Kasetsart University,
Bangkok 10900, Thailand
[2]NANOTEC Center of Excellence, National Nanotechnology Center, Kasetsart University, Bangkok 10900,
Thailand
[3]Chemistry Department, Faculty of Liberal Art and Science, Kasetsart University Kamphaeng Saen Campus,
Nakhon Pathom 73140, Thailand
[4]Center for Advanced Studies in Nanotechnology and Its Applications in Chemical, Food and Agricultural
Industries, Kasetsart University, Bangkok 10900, Thailand

*Corresponding author: Tel. +66 2562 5555 ext. 2169, Fax: +66 2562 5555 ext. 2176,
E-mail address: jumras.l@ku.ac.th

Introduction

The skeletal isomerization of linear butenes to isobutene has emerged as one of the most interesting topics with concentrated research in both the academic and industry fields. This intense interest has arisen because isobutene can be used in the preparation of intermediates for many productions, including fuel additives and antioxidants, e.g., ethyl tert-butyl ether (ETBE), isooctane and butylated hydroxyanisole (BHA). In general, the skeletal isomerization mechanisms of n-butene to isobutene on zeoites have been proposed in three pathways: the monomolecular mechanism, bimolecular mechanism and pseudomonomolecular mechanism (autocatalytic processes). Although many reaction mechanisms have been studied, the monomolecular mechanism still remains the most suitable one with medium pore zeolites, such as FER, TON and AEL to study the high selectivity of isobutene. Since the isobutoxide, secondary butoxide, the tert-butoxide and the tert-butyl cabenium species have been expected to be the intermediates for the skeletal isomerization of butene isomers. In both the experimental and theoretical studies, it has not been clearly reported whether the tert-butyl carbenium ion is a transition state or a stable intermediate, nor have the stabilities among these species been clearly reported. To address these unclear issues, the complete monomolecular mechanism and the stabilities of related intermediates for the skeletal isomerization of 1-butene to isobutene, including the formation of isobutoxide, 2-butoxide and tert-butyl species as intermediates, will be discussed by means of the DFT approach.

Methodology

A 37T quantum cluster of the ferrierite zeolite (FER), consisting of 136 atoms ($Si_{37}O_{49}H_{50}$) (Fig. 1a), covering a two-dimensional pore system consisting of 10-membered ring (4.2 Å × 5.4 Å) channels intersected by 8-membered ring (3.5 Å × 4.8 Å) channels in which the isomerization of 1-butene takes place, was selected. All calculations were carried out by means of the density functional theory (DFT) at M08-HX/6-31G(d,p) level of theory. Furthermore, the confinement effects of the

zeolite framework were also demonstrated by the single point calculations at the M08-HX/6-31G(d,p) level of theory using the 114T and 5T models in which the framework effects were considered and neglected, respectively (Fig.s 1b and 1c). In order to be able to cover long range electrostatic interactions of the zeolitic framework beyond the largest model of 144T, the SCREEP model has been employed.
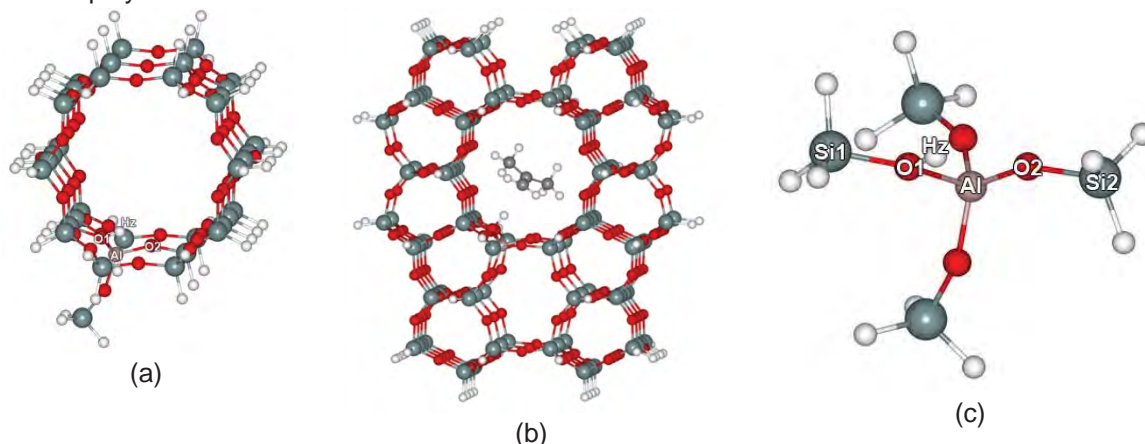

(a)

(b)

(c)

Fig. 1 The different models used in the skeletal isomerization of 1-butene to isobutene in H-FER: (a) 37T, (b) 114T and (c) 5T models.

Results and Discussion

Adsorption of 1-Butene and Isobutene Over H-Fer

The adsorption energies of 1-butene and isobutene adsorption complexes, at the O1 position, on the 37T H-FER cluster are calculated to be -19.4 and -16.8 kcal/mol, respectively. The isobutene adsorption complex was reported to be less stable than the 1-butene adsorption complex by 2.6 kcal/mol due to steric repulsion between the zeolite frameworks and the methyl groups in the more bulky isobutene molecule. The significance of the confinement effects of the zeolite pore was also investigated by the single point calculations on the 5T, 114T and 114T+SCREEP clusters. For the 5T model, the adsorption energies for the 1-butene and isobutene were -10.2 and -9.6 kcal/mol, respectively, while increasing the cluster sizes to 114T (and 114T including the infinite lattice framework of zeolite) the corresponding adsorption energies were evaluated to be -20.0 (-20.8) and -16.9 (-17.8) kcal/mol, respectively. Our results suggest that the adsorption complexes can be significantly stabilized in the zeolite framework.

Monomolecular Mechanism of The Skeletal Isomerization of 1-Butene To Isobutene

The reaction mechanism was proposed via four elementary steps as demonstrated in Fig. 2. The mechanism starts with the protonation of the adsorbed 1-butene (I) on the acidic site to provide the 2-butoxide intermediate (III) with an activation energy of 14.1 kcal/mol for the 37T model. The 2-butoxide was subsequently transformed into isobutoxide via the cyclic transition state (IV) which required an activation energy of 26.6 kcal/mol. Subsequently, the transformation of isobutoxide to tert-butyl cation existed through 1,2-hydride transfer with the activation energy of 35.0 kcal/mol and this step was determined to be the rate-determining step. The tert-butyl cation was less stable than isobutoxide and 2-butoxide by about 10.4 and 8.4 kcal/mol, respectively and was easily altered to be an isobutene product by activation energy of only 6.0 kcal/mol. Increasing the framework effect in the 114T cluster, SCREEP charges included, demonstrates that the tert-butyl cation is energetically favorable, similar to those of the isobutoxide and 2-butoxide. The effect of the framework shows significantly different stabilities of alkoxides and carbenium ion as well as the reaction energies. All the alkoxides were destabilized in the zeolite framework, whereas the carbenium ion in the framework effect was more stable than that without the framework effect. Therefore, this work confirms that the existence of tert-butyl cation in the pore of ferrierite was a true intermediate on the potential energy surface (PES) in the realistic system.
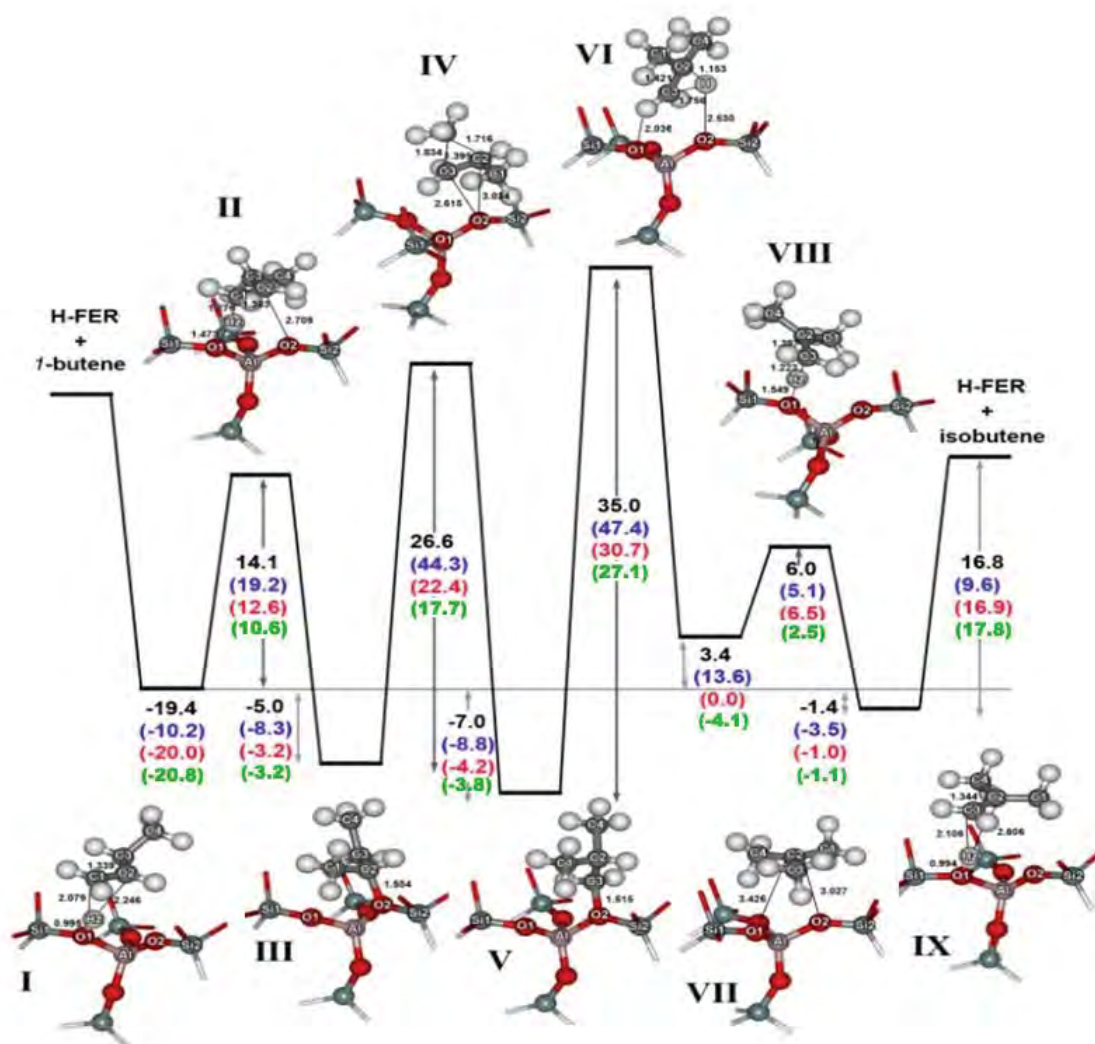
Fig. 2 The reaction energy profile of 1-butene skeletal isomerization over 5T, 37T, 114T and 114T+SCREEP H-FER zeolite models. Energy values (kcal/mol) for 5T, 37T, 114T and 114T+SCREEP systems are written in blue, black, red and green, respectively.

Conclusion

The complete reaction mechanisms of skeletal isomerization of 1-butene over ferrierite zeolite have been theoretically investigated using a newly developed density functional theory, M08-HX method with 6-31G(d,p) basis set. The reaction mechanisms of the skeletal isomerization of 1-butene to isobutene are proposed by the monomolecular reaction followed by four elementary steps. The rate-determining step related to the 1,2-hydride shift transition state (VI) in the conversion of isobutoxide to the tert-butyl cation intermediate with the corresponding apparent activation barriers of 38.6, 28.0, 26.5 and 23.3 kcal/mol, for the 5T over the 37T, and up to the more realistic models of 114T and 114T+SCREEP, respectively.

Acknowledgements

References

Boekfa B., S. Choomwattana, P. Khongpracha and J. Limtrakul; "Effects of the zeolite framework on the adsorptions and hydrogen-exchange reactions of unsaturated aliphatic, aromatic, and heterocyclic compounds in ZSM-5 zeolite: a combination of perturbation theory (MP2) and a newly developed density functional theory (M06-2X) in ONIOM scheme", Langmuir 25, 12990-12999 (2009).

Boronat M. and A. Corma; "Are carbenium and carbonium ions reaction intermediates in zeolite-catalyzed reactions?", Appl. Catal. A 336, 2-10 (2008).

Namuangruk S., D. Tantanak and J. Limtrakul; "Application of ONIOM calculations in the study of the effect of the zeolite framework on the adsorption of alkenes to ZSM-5", J. Mol. Catal. A 256, 113-121 (2006).

DFT Analysis of the MOF Catalyzed Ring-Opening Reaction of Epoxides: An Important Process in Alkoxy Alcohol Synthesis

Sudarat Yadnum[1,2,3], Saowapak Choomwattana[1,2,3], Pipat Khongpracha[1,2,3], Chompunuch Warakulwit[1,2,3],Jumras Limtrakul[1,2,3*]

[1]*Laboratory for Computational and Applied Chemistry, Department of Chemistry, Faculty of Science and Center of Nanotechnology, Kasetsart University Research and Development Institute, Kasetsart University, Bangkok 10900, Thailand*
[2]*NANOTEC Center of Excellence, National Nanotechnology Center, Kasetsart University, Bangkok 10900, Thailand*
[3]*Center for Advanced Studies in Nanotechnology and Its Applications in Chemical, Food and Agricultural Industries, Kasetsart University, Bangkok 10900, Thailand*

*Corresponding author: Tel. +66 2562 5555 ext 2169, Fax: +66 2562 5555 ext 2176, E-mail address: jumras.l@ku.ac.th

Keywords Metal-Organic Framework, M06L, ONIOM, Ring-Opening, Catalyst

Abstract

The MOF-catalyzed ring-opening reactions of epoxides by methanol, an important route for alkoxy alcohol production, were investigated by using the density functional theory, a recently developed DFT "M06L" with 6-31G(d,p) basis set. The dicopper carboxylate "paddlewheels unit" model was used to represent an active site of MOF-505 catalyst. The interaction of the epoxide ring with methanol was found to take place in a single concerted reaction step. The transition state involving the forming of the C-O bond and the breaking of the C-O and O-H bonds, and hydrogen transfer was proposed. In the dicopper carboxylate catalyzed mechanism, the epoxide initially adsorbed over the dicopper carboxylate with an energy of -16.6 kcal/mol. Subsequently, the interaction energy of the co-adsorption of epoxide and methanol was observed to be -27.9 kcal/mol. This catalyzed reaction was calculated to be exothermic by -47.0 kcal/mol. The dicopper carboxylate, acting as a catalyst, is able to stabilize the "transition state complex" and hence leads to a lower energy barrier (ΔE_{act}) (43.4 kcal/mol) as compared to that of the uncatalyzed reaction (52.0 kcal/mol). To take the framework effect into account, the ONIOM (our-Own-N-layered Integrated molecular Orbital + Molecular Mechanics) (M06L/6-31G(d,p): UFF) calculation was also carried out. The confinement effect of the extended MOF-505 framework was shown to stabilize the adsorption complexes (-27.9 kcal/mol to -32.3 kcal/mol) where the activation energy was not decreased.
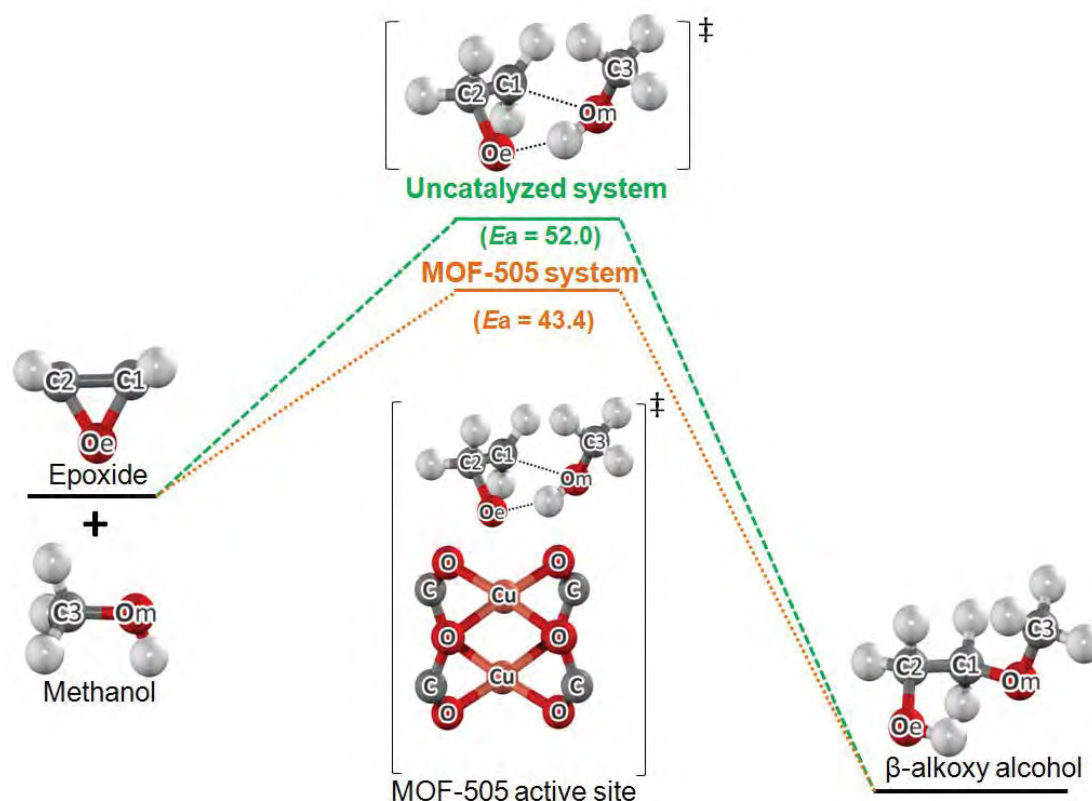
Fig. 1 Structures and energy profile (kcal/mol) for the epoxide ring-opening in the dicopper carboxylate system (orange line) and the uncatalyzed system (green line).

References

Jiang D., T. Mallat, F. Krumeich, A. Baiker; "Copper-Based Metal-Organic Framework for the Facile Ring-Opening of Epoxides." J. Catal., 257, 390-395 (2008).

Choomwattana S., T. Maihom, P. Khongpracha, M. Probst, J. Limtrakul; "Structures and Mechanisms of the Carbonyl-ene Reaction between MOF-11 Encapsulated Formaldehyde and Propylene: An ONIOM study." J. Phys. Chem. C, 112, 10855-10861 (2008).

First-Principle-Derived Potential Energy Function for Zn$_4$O Tetrahedron-Based Metal-Organic Frameworks

Chadchalerm Raksakoon[1,2,3], Saowapak Choomwattana[1,2,3], Jumras Limtrakul[1,2,3*]

[1]*Laboratory for Computational and Applied Chemistry, Department of Chemistry, Faculty of Science and Center of Nanotechnology, Kasetsart University Research and Development Institute, Kasetsart University, Bangkok 10900, Thailand*
[2]*NANOTEC Center of Excellence, National Nanotechnology Center, Kasetsart University, Bangkok 10900, Thailand*
[3]*Center for Advanced Studies in Nanotechnology and Its Applications in Chemical, Food and Agricultural Industries, Kasetsart University, Bangkok 10900, Thailand*

*Corresponding author: Tel. +66 2562 5555 ext 2169, Fax: +66 2562 5555 ext 2176,
E-mail address: jumras.l@ku.ac.th

Keywords Metal-Organic Framework, Force Field, Zn-O bond, Molecular Dynamics, Diffusion

Abstract

　　The Zn-O intermolecular potential functions were newly developed for investigating the adsorption and diffusion of *o*-, *m*- and *p*- xylene isomers in metal-organic framework. We constructed the LJ potential for Zn-O by fitting the parameters of the functions of the intermolecular distances to energies derived from B3LYP/6-31G(d,p) calculations. Zn coordinates are generated along lines tetrahedrally coordinated to the O atom according to the vibrational modes taken from the more realistic model of Zn$_4$O(O$_2$C-C(CH)$_2$)$_6$ evaluated at the ONIOM (B3LYP/6-31G(d,p):UFF) level of theory.

Lennard-Jones equation:
$$U_{12-6}(r) = (A/r^{12}) - (B/r^6)$$

　　The parameters of the equation employed describing the Zn-O potential energy surfaces were obtained by minimizing the least-square deviation between the energies from the LJ formula and their density functional theory calculated counterparts. Meanwhile, the atomic interactions of the rest of the framework are treated with Morse and harmonic potentials.

Morse potential:
$$U_{Morse}(r) = E_0\left[\{1 - \exp(-k(r - r_0))\}^2 - 1\right]$$

Harmonic potential:
$$U_{harmonic}(r) = \frac{1}{2}k(r - r_0)^2$$
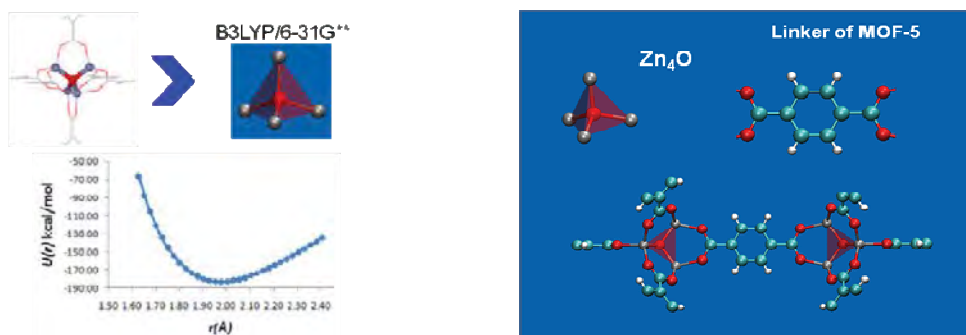
Fig. 1 (Left) The potential energy surface of Zn$_4$O in which the Zn-O is tetrahedrally, symmetrically stretched was calculated by B3LYP/6-31G (d,p) method. (Right) MOF-5 components: Zn$_4$O inorganic node and 1,4-benzenedicarboxylate organic linker and its connectivity. (Zn = grey, O = red, C = cyan, H = white)

Table 1 Comparison of the calculated lattice using our combined parameterized functions in various conditions and the X-ray crystallographic data

Parameter	NVT				NPT				X-ray*
	258	300	350	400	258	300	350	400	
Zn-Oc	1.951	1.953	1.953	1.951	1.951	1.950	1.952	1.953	1.941
Zn-O	1.929	1.928	1.929	1.927	1.928	1.928	1.927	1.927	1.922
Zn-Zn	3.191	3.191	3.191	3.189	3.190	3.189	3.179	3.198	
O-C1	1.303	1.302	1.301	1.299	1.301	1.299	1.299	1.299	1.301
C1-C2	1.492	1.495	1.493	1.494	1.489	1.491	1.491	1.490	1.486
C2-C3	1.404	1.405	1.405	1.404	1.403	1.404	1.403	1.404	1.392
C3-C3	1.401	1.401	1.401	1.402	1.397	1.404	1.401	1.398	1.388
C3-H	1.083	1.081	1.082	1.082	1.082	1.081	1.078	1.084	
Lattice	25.832				25.755	25.738	25.727	25.718	

* Jesse L. C. Rowsell et al. Science 309(5739), 1350 – 1354 (2005).

Our combined parameterized functions are found to reproduce the lattice parameter of MOF-5 when compared to the experimental data. To verify its accuracy, molecular dynamics (MD) simulations of ortho-, para- and meta-xylenes in MOF-5 at the temperature of 300 K were performed with the combination of novel in-house potential energy surfaces (PES) and existing potentials to determine the maximum loading. Our calculation reveals that the lattice parameter decreases upon the loading amount increase. At a loading of 56 molecules per unit cell for o-xylene and 54 molecules per unit cell for m- and p-isomers, the lattice parameter begins to increase. This indicates that our derived force field can reproduce the breathing effect in MOF. Moreover, xylene isomers can be differentiated by their self-diffusion coefficients (D_{self}) in the framework of MOF-5. At the same loading, p-xylene is found to expand the lattice the most. Unlike in zeolites, where the pore window hindrance is the key difficulty, the diffusion in the open MOF-5 has to overcome π-π attraction of xylenes in the binding pockets. Our original potentials combination could, therefore, give an accurate prediction for other MOF-5 properties.
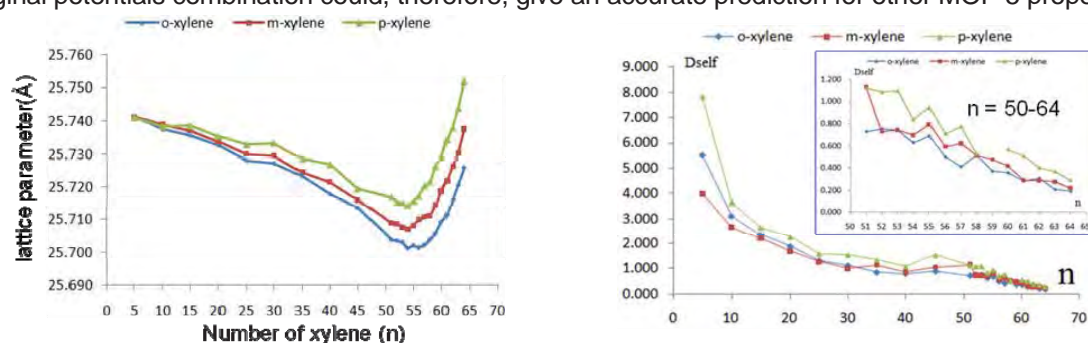
Fig. 2 Loading amount-dependent variation of the simulated lattice constant of MOF-5 (Left) and self-diffusion coefficient of xylenes (Right) at T = 300 K.

References

Li H., M. Eddaoudi, M. O'Keeffe, O. M. Yaghi; "Design and Synthesis of an Exceptionally Stable and Highly Porous Metal-Organic Framework" Nature, 402, 276-279 (1999).

Tafipolsky M., S. Amirjalayer, R. Schmid; "Ab Initio Parametrized MM3 Force Field for the Metal-Organic Framework MOF-5." J. Comp. Chem. 28(7), 1169–1176 (2007).

Density Functional Analysis of the Confinement Effect in Nanoporous MCM-22 Petrochemical Catalyst: Nanocluster Model Approach

Pemikar Srifa[1,2,4], Somkiat Nokbin[1,2,4], Bundet Boekfa[2,3,4], Jumras Limtrakul[1,2,4*]

[1]Laboratory for Computational and Applied Chemistry, Department of Chemistry, Faculty of Science and Center of Nanotechnology, Kasetsart University Research and Development Institute, Kasetsart University, Bangkok 10900, Thailand
[2]NANOTEC Center of Excellence, National Nanotechnology Center, Kasetsart University, Bangkok 10900, Thailand
[3]Chemistry Department, Faculty of Liberal Art and Science, Kasetsart University Kamphaeng Saen Campus, Nakhon Pathom 73140, Thailand
[4]Center for Advanced Studies in Nanotechnology and Its Applications in Chemical, Food and Agricultural Industries, Kasetsart University, Bangkok 10900, Thailand

*Corresponding author: Tel. +66 2562 5555 ext 2169, Fax: +66 2562 5555 ext 2176, E-mail address: jumras.l@ku.ac.th

Keywords Pyridine adsorption, MCM-22 zeolite, Acidity, Brønsted site, DFT, M06-2X

Introduction

Acidic MCM-22 (H-MCM-22) is one of the porous aluminosilicate zeolites used as the acid catalyst for petrochemical processes. Basically, the catalytic properties of this material can be investigated by the adsorption of basic probe molecules such a pyridine on its Brønsted acidic site. Inside this adsorption process, the confinement effect of all physical interactions between adsorbed substrate and the zeolitic framework has played an important role on adsorption enthalpies. The confinement effect from the zeolite framework on the adsorption of pyridine has been recently investigated via QM:MM calculations named "B3LYP:UFF". The calculated adsorption energies of pyridine over two types of zeolites, H-ZSM-5 and H-FAU agree well with experimental data. However, it is due to a larger extent from the fact that the overestimation of "van der Waals interactions" generated by the force field, UFF coupled nicely with the systemical compensation of the interactions from a small quantum cluster treated by the density functional, B3LYP method. However, one might expect somewhat underestimated adsorption energy derived from this hybrid model (B3LYP:UFF) when increasing the size of the quantum cluster, and especially when absorbing species are quite large organic molecules such as large aliphatic and aromatic hydrocarbons. Recently, the newly developed density functional theory, M06 functional, has been successfully applied to address and understand the confinement contributed from nanoporous materials. In this study the effect of zeolite confinement on the adsorption properties of pyridine interacted with nanoporous H-MCM-22 will be investigated and their results will be compared with experimental data. Thus, it can to some extent be employed to fine tune the acidity of zeolites and, hence, be useful for the zeolite's community and for them to systemically select the right candidates for their reaction.

Computational Details

Protonic H-MCM-22 zeolite was selected to study the pyridine adsorption reaction in order to examine the confinement effect of the H-MCM-22 zeolite. Five different cluster sizes, i.e., 5T, 14T, 38T, 54T and 120T clusters (T represents the tetrahedral of Si or Al atoms) were employed in this work, as shown in Fig. 1. In all models, one Si atom at the T1 position was replaced by an Al atom,

leading to the generation of the Brønsted acid site. All geometry optimizations of pyridine adsorption over the 5T, 14T and 38T models were calculated at the M06-2X/6-31G(d,p) level of theory. In order to get more accurate adsorption energies due to the confinement effect of H-MCM-22, single-point energy calculations of the optimized structures of the 38T systems embedded in the 54T and 120T systems were also carried out at the same level. All calculations were carried out using the Gaussian 03 code incorporated with the Minnesota Density Functionals module 3.1 by Zhao and Truhlar.
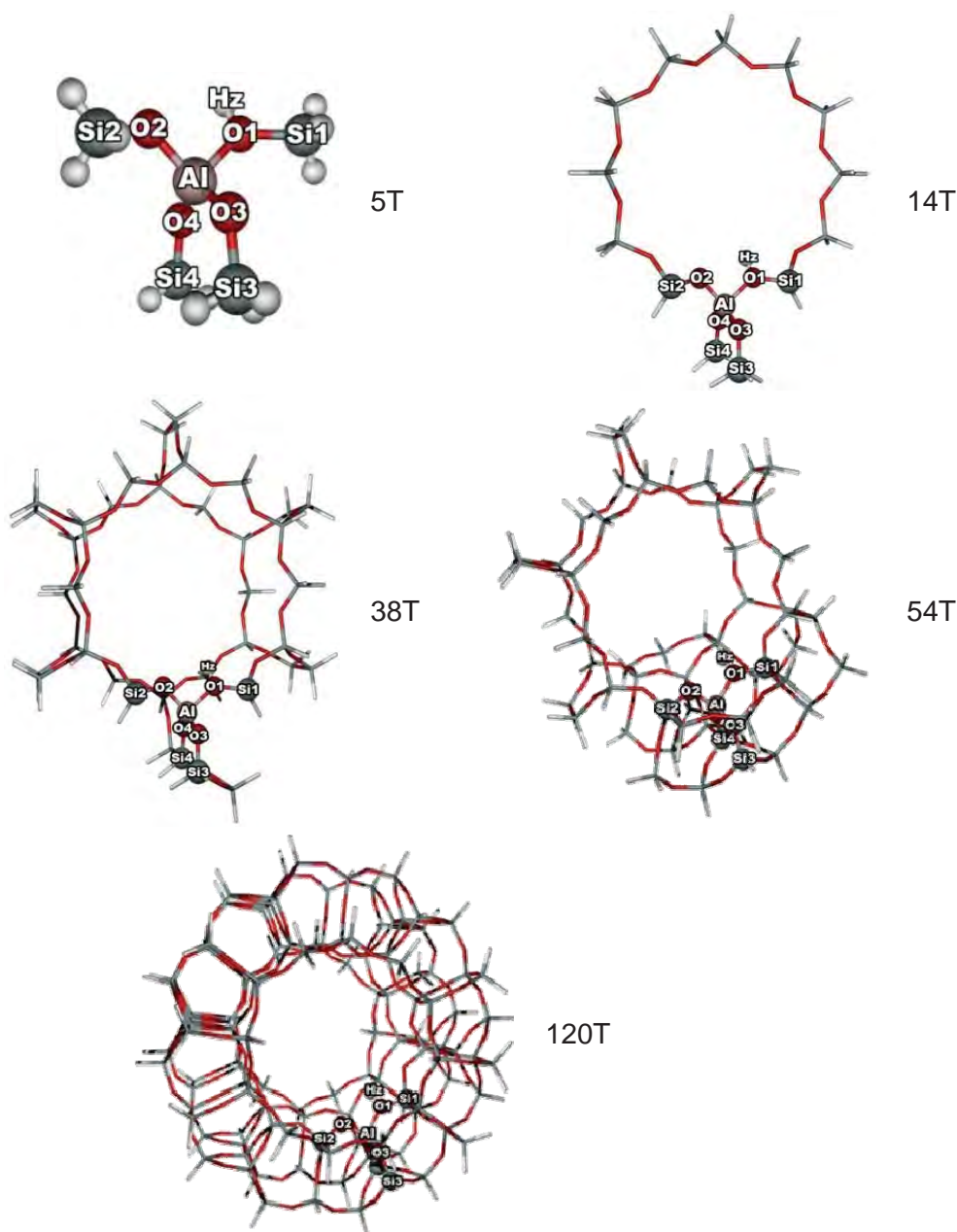
Fig. 1 Presentation of H-MCM-22 models in different sizes generated from the finite lattice framework.

Results and Discussion

Table 1 documents the selected geometries parameters of the 5T, 14T and 38T models. The calculated adsorption energies of pyridine on the zeolitic models are -20.9, -41.3, -46.1, -50.8 and -54.0 kcal/mol for 5T, 14T, 38T, 54T and 120T, respectively. Our results show that the adsorption energy of the 120T model is in very good agreement with the experimental value of -55.0 kcal/mol. This suggests that the confinement effect as well as the environmental framework of the zeolite play

vital roles in the pyridine adsorption energies which are related to the prediction of the acidity of zeolite.

(a)   (b)
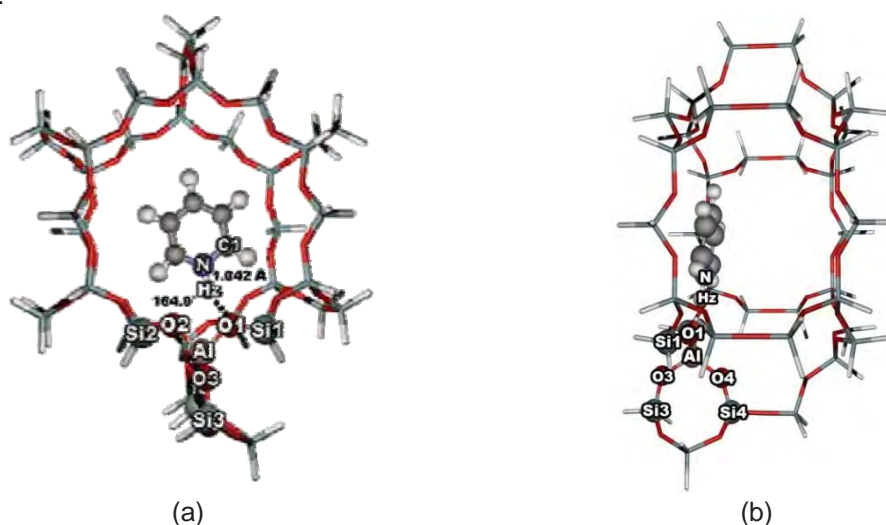
Fig. 2 Presentation of the pyridine adsorption on the 38T model of H-MCM-22 viewed through the 12 MR (a) and through the 10 MR, which is perpendicular to 12 MR (b). The bond lengths are in angstroms.

Table 1 Geometrical parameters of pyridine adsorbed on three sizes of H-MCM-22 models. (Distances are in angstroms and angles are in degrees.)

Parameter	System					
	5T		14T		38T	
	Isolated	Complex	Isolated	Complex	Isolated	Complex
O1-Hz	0.969	1.345	0.969	1.822	0.970	1.804
O2-Hz	2.347	2.631	2.565	2.138	2.567	2.226
O2-H1	-	2.050	-	2.430	-	2.338
Al-O1	1.841	1.754	1.815	1.720	1.813	1.716
Al-O2	1.692	1.708	1.675	1.713	1.671	1.707
Al-O3	1.708	1.721	1.708	1.726	1.704	1.725
Al-O4	1.683	1.697	1.676	1.689	1.681	1.697
Al-Hz	2.314	2.553	2.408	2.651	2.397	2.686
N-O1	-	2.496	-	2.783	-	2.795
N-Hz	-	1.153	-	1.042	-	1.042
< Al-O1-Si1	127.7	124.1	125.1	123.3	126.9	125.1
<Al-O1-Hz	106.8	175.6	116.5	96.9	115.6	99.5
<Al-O2-H1	-	123.6	-	146.7	-	145.2
< N-Hz-O1	-	110.3	-	151.7	-	157.5

Conclusion

The effect of the zeolitic nanocage on the adsorption properties of the important heterocyclic base, pyridine, of different sizes of H-MCM-22 has been investigated. The results demonstrate that the hybrid density functional M06-2X is able to encompass important weak interactions describing the nano-confinement effect from the zeolite framework, especially the van der Waals interaction. The nano-confinement effect of the extended zeolite framework has been clearly demonstrated not only to stabilize the pyridine/zeolite complexes but also to improve the corresponding adsorption energies to approach the experimental benchmark.

Acknowledgements

References

Boekfa B., S. Choomwattana, P. Khongpracha and J. Limtrakul; "Effects of the zeolite framework on the adsorptions and hydrogen-exchange reactions of unsaturated aliphatic, aromatic, and heterocyclic compounds in ZSM-5 zeolite: A combination of perturbation theory (MP2) and a newly developed density functional theory (M06-2X) in ONIOM scheme", Langmuir, 25(22), 12990-12999 (2009).

Derouane G. E. and C. D. Chang; "Confinement effects in the adsorption of simple bases by zeolites" Micropor. Mesopor. Mat. 35–36, 425–433 (2000).

Injan N., N. Pannorad, M. Probst and J. Limtrakul; "Pyridine adsorbed on H-faujasite zeolite: Electrostatic effect of the infinite crystal lattice calculated from a point charge representation", Int. J. Quantum Chem., 105(6), 898-905 (2005).

Maihom T., P. Pantu, C. Tachakritikul, M. Probst, and J. Limtrakul; "Effect of the Zeolite Nanocavity on the Reaction Mechanism of n-Hexane Cracking: A Density Functional Theory Study" J. Phys. Chem. C, 114, 7850–7856 (2010).

Parrillo J. D. and R. J. Gorte; "Characterization of Acidity in H-ZSM-5, H-ZSM-12, H-Mordenite, and H-Y Using Microcalorimetry" J. Phys. Chem. 97, 8786-8792 (1993)[1]

Zhao Y. and D. G. Truhlar; "Density functionals with broad applicability in chemistry", Accounts Chem. Res., 41(2), 157-167 (2008).

Reaction Mechanisms for ETBE Production Catalyzed by H-BEA as Nanoporous Zeolite

Panida Singra[1,2,3], Pipat Khongpracha[1,2,3], Jumras Limtrakul[1,2,3*]

[1]Laboratory for Computational and Applied Chemistry, Department of Chemistry, Faculty of Science and Center of Nanotechnology, Kasetsart University Research and Development Institute, Kasetsart University, Bangkok 10900, Thailand
[2]NANOTEC Center of Excellence, National Nanotechnology Center, Kasetsart University, Bangkok 10900, Thailand
[3]Center for Advanced Studies in Nanotechnology and Its Applications in Chemical, Food and Agricultural Industries, Kasetsart University, Bangkok 10900, Thailand

*Corresponding author: Tel. +66 2562 5555 ext 2169, Fax: +66 2562 5555 ext 2176,
E-mail address: jumras.l@ku.ac.th

Keywords Zeolite, Etherification reaction, Octane booster, Ethyl tert-butyl ether (ETBE)

Introduction

Ethyl tert-butyl ether (ETBE) can be considered a prime candidate to be a high-octane additive for its remarkably friendly environmental properties. ETBE easily mixes with gasoline, to make gasoline burn cleanly and completely, and reduce the vehicle's greenhouse gas emission from the exhaust.

ETBE is readily synthesized by the etherification reaction of isobutene with ethanol. Conventionally, sulfonated acidic ion-exchange resin catalysts, such as Amberlyst-15 and Lewatit K2631 were used to catalyze the reaction for synthesis of the ETBE. Although these catalysts are very efficient, they have some disadvantages, such as low thermal stability and corrosion problems in the reactor. Hence, zeolites become more advantageous because of high thermal and chemical stability, and their ability to be recycled result in there being many investigations on zeolite catalysts. From a previous experimental study on the vapor phase synthesis of MTBE and ETBE, it was found that H-BEA is as active as Amberlyst-15. The order for the activity of commonly used zeolites decreases as follow: H-BEA > H-Y ≥ H-mordenite > H-ZSM-5.

Quantum chemical calculation is a useful tool in this work to investigate and analyze the reaction mechanisms for ETBE production via the etherification reaction of isobutene and ethanol, and compares uncatalyzed and catalyzed reactions by H-BEA, nanostructured zeolite.

Methodology

The uncatalyzed reaction, the bare model system, is investigated with M06-2X/6-311+G(2df,2p) //M06-2X/6-31G(d,p) calculations.

For the catalyzed reaction, the 54T nanocluster is used as the model of the Brønsted acid site in the H-BEA zeolite framework. This model is taken from the BEA zeolite crystal lattice structures. For computational efficiency, the 54T nanocluster model is subdivided into two layers according to the Our-own-N-layered-integrated molecular orbital + molecular mechanics (ONIOM) scheme. An inner layer, high level, consists of a 14T cluster including the 12-membered ring and the other two Si atoms around the Al atom, as the active site region, is treated with the density function, namely M06-2X with the 6-31G(d,p) basis set. An outer layer, low level, consists of the rest of the extended framework, is treated with the universal force field (UFF). This force field has been found to provide a good description of the long-range van der Waals (vdW) interactions. In the structure

optimization, only the 5T cluster of the active site region, [($\equiv$SiO)$_3$ Al(OH)Si$\equiv$], and the probe molecule are allowed to relax while the rest is fixed at the crystallographic coordinates. Frequency calculation at the same level of the active site region was carried out to verify transition states structure with only one imaginary frequency. In order to make the results more reliable, single point calculations are performed using M06-2X method, 6-311+G(2df,2p) basis set for the active site region, and 6-31G(d,p) basis set for the rest of the extended framework. All calculations were performed using the Gaussian 03 code.

(a) (b)
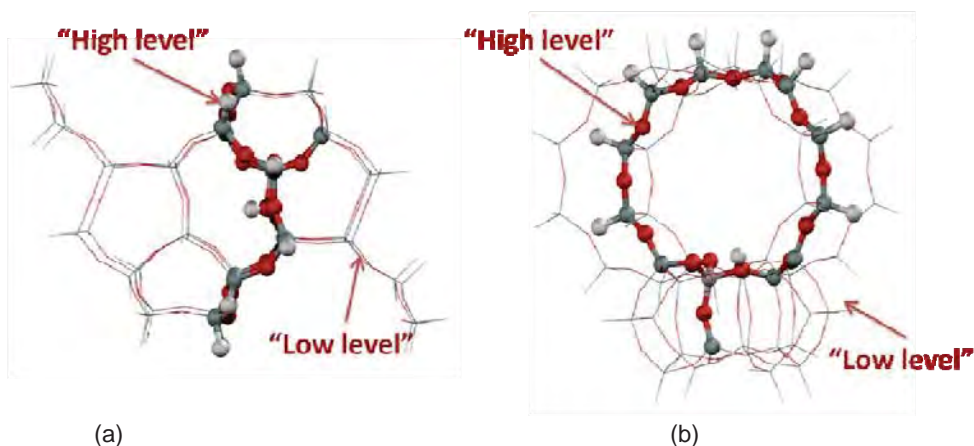
Fig. 1 Extended 54T cluster model of H- BEA (a) An intersection of two perpendicular 12-membered ring channel systems which serve as a nanoreactor (b) View along the main channel.

Results and Discussion

The etherification reaction of isobutene and ethanol to ETBE catalyzed by H-BEA. The reaction is initiated by the coadsorption between isobutene and ethanol over the Brønsted acid site of BEA, the coadsorption complex (B_Ads_1), was stabilized by orbital interaction between the π bonding orbital of the C1=C2 bond of isobutene with the σ*-antibonding orbital of O1-Hz bond zeolite and interaction between H atom of ethanol with the O atom of zeolite. This was followed by the concerted transition state (B_TS_1), a protonation of the adsorbed isobutene and an ethanol molecule attraction to isobutene occurs simultaneously, resulting in adsorbed ETBE (B_Ads_2), which is desorbed in the final step.   The uncatalyzed reaction is from the bare model system. The transition state concerns the O-H bond dissociation, O-C and H-C bond formation. The optimized geometric parameters of all species involved in the etherification of isobutene with ethanol are showed in Tables1 and 2.

Table 1 Optimized geometric parameters of all species involved in the ETBE formation of the uncatalyzed reaction, the bare model system.

Parameter	Ads_1	TS_1	Ads_2
Distance (Å)			
C1-H	2.57	1.40	1.09
C2-H	2.35	1.74	2.16
H-O	0.97	1.24	2.64
C1-C2	1.34	1.42	1.53
Angle (°)			
C2-C1-H	65.1	76.3	109.7
C1-C2-H	83.8	51.2	28.4
C1-H-O	155.5	130.2	67.0
C1-C2-O	99.2	90.4	110.6

Table 2 Optimized geometric parameters of all species involved in the ETBE formation of the catalyzed reaction by H-BEA zeolite.

Parameter	zeolite	B_Ads_1	B_TS_1	B_Ads_2
Distance (Å)				
O1-Hz	0.97	1.01	1.34	2.35
C1-Hz	-	1.97	1.35	1.09
C2-Hz	-	2.28	2.12	2.16
C1-C2	-	1.35	1.38	1.52
O3-C2	-	3.67	2.66	1.50
O3-C3	-	1.42	1.42	1.46
O3-H1	-	0.97	0.97	1.10
H1-O2	-	2.20	1.97	1.38
Angle (°)				
Al-O1-Si	131.8	130.2	129.2	130.0
Al-O2-Si	129.8	130.5	133.4	129.8
O1-Hz-C1	-	172.4	156.2	161.6
Hz-C1-C2	-	163.9	102.0	110.5

The H-BEA zeolite, as the catalyst changes the reaction path by lowering the energy barrier from 53.3 kcal/mol to 8.3 kcal/mol, which leads to increasing the rate of the reaction. The reaction for the ETBE production was exothermic and this study provides the calculated reaction energy of −18.4 kcal/mol. This result is reasonable and compares well with the experimental study of the enthalpy of reaction by −14.9±0.5 kcal/mol. The calculated relative energies of all reaction coordinates are summarized in Fig. 2.

(a)   (b)
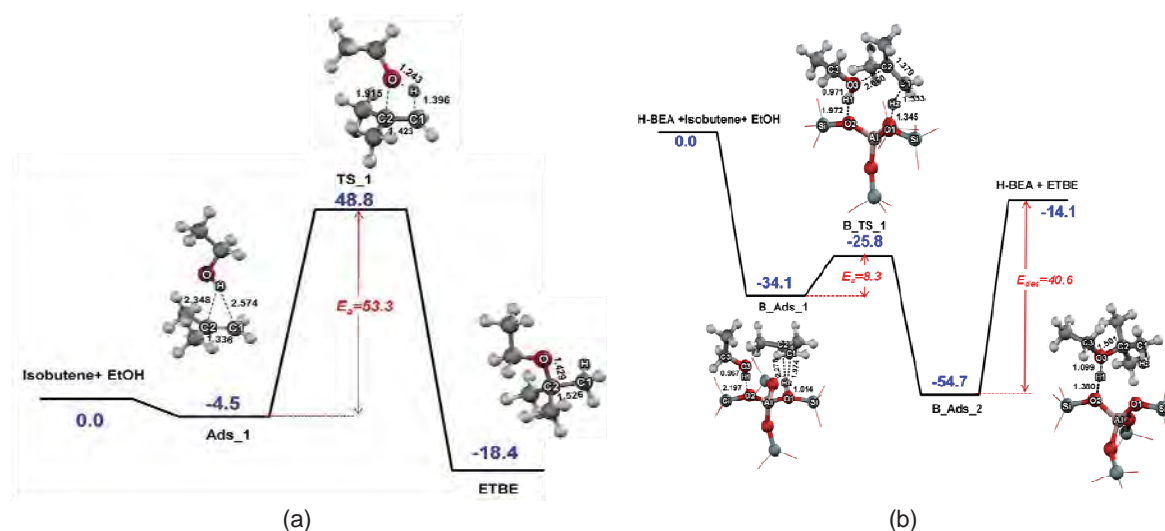
Fig. 2 Relative energies (kcal/mol) of all reaction coordinates in the etherification reaction of isobutene with ethanol to ETBE. (a) Uncatalyzed reaction, the bare model system, (b) Catalyzed reaction by H-BEA zeolite.

Conclusion

The reaction mechanisms for ETBE production via the etherification reaction of isobutene and ethanol catalyzed reactions by H-BEA is investigated by using the ONIOM(M06-2X/6-31G(d,p):UFF) method. Single point calculations are performed using the M06-2X method, 6-311+G(2df,2p) basis set for the active site region, and 6-31G(d,p) basis set for the rest of the extended framework. For the uncatalyzed reaction, the bare model system is investigated with M06-2X/6-311+G(2df,2p)//M06-2X/6-31G(d,p) method. The overall reaction was estimated to be the exothermic of −18.4 kcal/mol. The H-BEA as a nanostructured zeolite was found to be an efficient catalyst in the etherification of isobutene with ethanol, culminating in a lower energy barrier (8.3 kcal/mol) as compared to that of the bare model system (53.3 kcal/mol).

Acknowledgements

References

Collignon F. and G. Poncelet; "Comparative vapor phase synthesis of ETBE from ethanol and isobutene over different acid zeolites", J. Catal., 202(1):68-77 (2001).

Collignon F., M. Mariani, S. Moreno, M. Remy and G. Poncelet; "Gas phase synthesis of MTBE from methanol and isobutene over dealuminated zeolites". J. Catal., 166(1):53-66 (1997).

Doğu T., N. Boz, E. Aydın, Nuray Oktar, K. Murtezaoğlu and G. Doğu; "DRIFT studies for the reaction and adsorption of alcohols and isobutylene on acidic resin catalysts and the mechanism of ETBE and MTBE synthesis". Ind. Eng. Chem. Res., 40(23):5044-5051 (2001).

Iborra M., J. F. Izquierdo, J. Tejero and F. Cunili; "Equilibrium Constant for Ethyl tert-Butyl Ether Vapor-Phase Synthesis", J. Chem. Eng. Data, 34:1-5 (1989).

Jansang B., T. Nanok and J. Limtrakul; "Structure and Reaction Mechanism of Alkylation of Phenol with Methanol over H-FAU Zeolite: An ONIOM Study". J. Phys. Chem. C, 112: 540-547 (2008).

Kumsapaya C., K. Bobuatong, P. Khongpracha, Y. Tantirungrotechai and J. Limtrakul; "Mechanistic Investigation on 1,5- to 2,6-Dimethylnaphthalene Isomerization Catalyzed by Acidic β Zeolite: ONIOM Study with an M06-L Functional". J. Phys. Chem. C, 113:16128-16137 (2009).

Maihom T., B. Boekfa, J. Sirijaraensre, T. Nanok, M. Probst and J. Limtrakul; "Reaction Mechanisms of the Methylation of Ethene with Methanol and Dimethyl Ether over H-ZSM-5: An ONIOM Study". J. Phys. Chem. C, 113:6654-6662 (2009).

Zhao Y. and D.G. Truhlar; "Density functionals with broad applicability in chemistry", Accounts Chem. Res., 41(2), 157-167 (2008).

Adsorption of a Basic Probe Molecule over Nanoporous Catalysts (H-FAU and H-MOR): an Embedded Nanocluster Approach

Supalak Khueanphet[1,2,4], Bundet Boekfa[2,3,4], Tanin Nanok[1,2,4], Jumras Limtrakul[1,2,4*]

[1]Laboratory for Computational and Applied Chemistry, Department of Chemistry, Faculty of Science and Center of Nanotechnology, Kasetsart University Research and Development Institute, Kasetsart University, Bangkok 10900, Thailand
[2]NANOTEC Center of Excellence, National Nanotechnology Center, Kasetsart University, Bangkok 10900, Thailand
[3]Chemistry Department, Faculty of Liberal Art and Science, Kasetsart University Kamphaeng Saen Campus, Nakhon Pathom 73140, Thailand
[4]Center for Advanced Studies in Nanotechnology and Its Applications in Chemical, Food and Agricultural Industries, Kasetsart University, Bangkok 10900, Thailand

*Corresponding author: Tel. +66 2562 5555 ext 2169, Fax: +66 2562 5555 ext 2176,
E-mail address: jumras.l@ku.ac.th

Introduction

An acid site in zeolites acting with probe molecules has generated considerable interest because it represents the initial step of chemical reactions resulting from catalyzation by acidic zeolites. The heat of adsorption complexes that is created when a basic probe molecule is adsorbed on the nanostructure zeolitic pores is the sum of two significant terms, the chemisorption and the physisorption. The latter term relates to a large degree to the confinement effect arising from the van der Waals interaction, which is a main factor for the determination of selective adsorption and catalytic activity in the acid-catalyzed reaction of zeolites.

Derouane *et al.* investigated the confinement effect of ammonia adsorption on various silicalites and zeolites. This report led to some important studies on the adsorption of ammonia in zeolites using quantum cluster calculations that have since been reported. These works guide us to elucidate on the influence of zeolitic confinement on structure and mechanisms. However, most of the investigations lack inclusion of the effect of zeolite frameworks that include an important contribution of dispersion energy. Recently, the newly developed density functional theory coupled with accurate long range electrostatic interactions called "embedded M06-2X functional" has been successfully employed to describe the confinement effect of the zeolite framework. The goal of our work is to systemically investigate the confinement effect of ammonia adsorption on the different types of zeolite, namely H-FAU and H-MOR zeolites.

Methodology

The cluster models, 5T, 14T, and 38T, were optimized by the M06-2X functional with the 6-31G(d,p) level of theory. During the optimization, the Brønsted acid site of H-FAU and H-MOR, for the 5T, $\equiv(SiO)_3Al(OH)Si\equiv$, and ammonia were allowed to relax while the other atoms were kept fixed to their crystallographic coordinates. The long-range electrostatic potential was carried out by single-point calculations with the electronic embedding approach. The electrostatic potential from the extended lattice is generated by optimized point charges which enclose around the realistic quantum cluster of 38T. The adsorption energy is evaluated as:

$$\Delta E_{ads} = E_{H-Z} + E_{NH3} - E_{NH4-Z}$$

where E_{H-Z}, E_{NH3}, and E_{NH4-Z} refer to the total energy of each structure.

In order to be able to derive more accurate results, all ΔE_{ads} were corrected for the basis set superposition error (BSSE) via the counterpoise correction. All calculations were performed by using the Gaussian 03 code modified M06 functional by Zhao Y. and D. G. Truhlar.

Results and Discussion

Comparisons of geometrical structures of different quantum cluster models

The adsorption of the ammonia on H-FAU and H-MOR zeolites was investigated with the M06-2X functional. The ammonia molecules are located at the 12T supercage of H-FAU and the 12T straight channel of H-MOR. The adsorption process of ammonia on the Brønsted acid site of zeolites is as follow: the proton (Hz) of the acid site was transferred to ammonia, and hence generates the ammonium ion adsorbed to the acid site of zeolites in the form of an ion-pair complex, $Z^- NH_4^+$. The geometrical structures of cluster models are illustrated in Fig. 1.
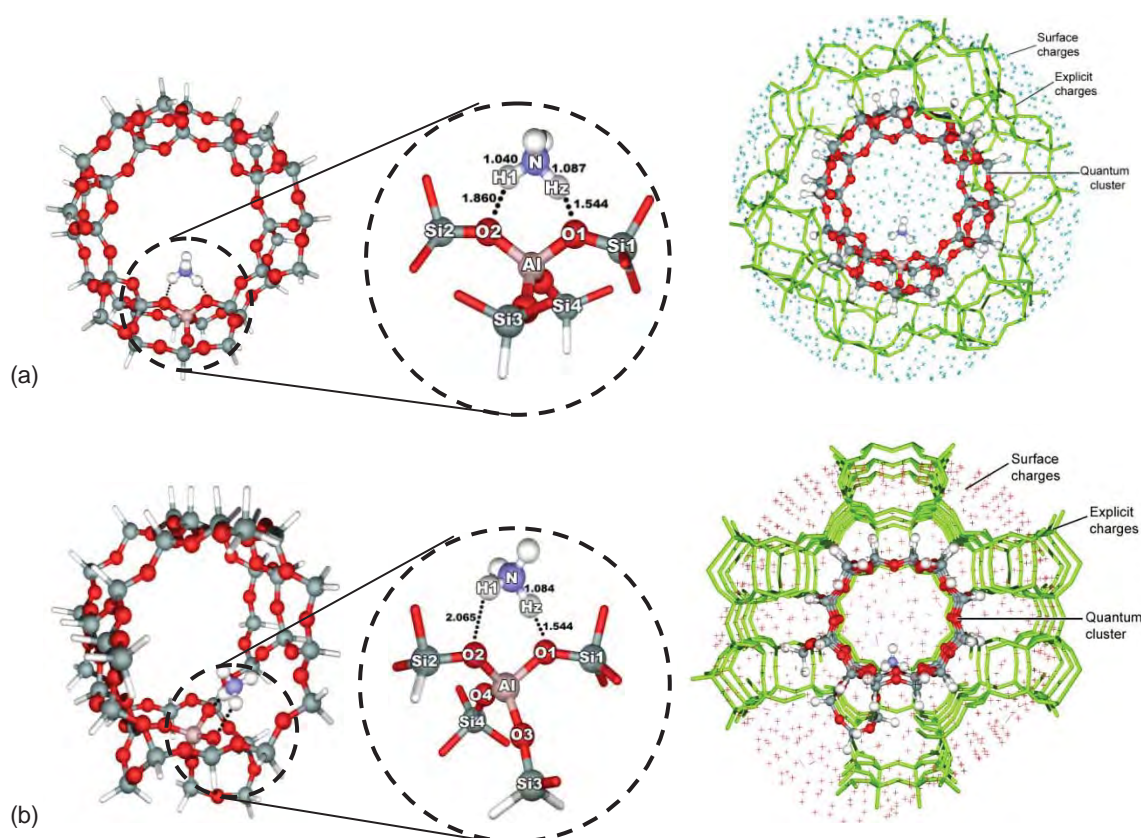
Fig. 1 Adsorption complex of NH_3 in the 38T and embedded cluster models of H-FAU (a) and H-MOR (b), respectively. (Distances are in Å.)

The geometrical parameters of the optimized structures of H-FAU and H-MOR are documented in Tables 1 and 2, respectively. Without the confinement effect, the ammonia is adsorbed on the small quantum 5T cluster by forming a strong hydrogen bond between the nitrogen atom of ammonia and the proton Brønsted acid of zeolites. Increasing the models to 14T and 38T quantum clusters, the formation of the ion-pair of ammonia on the deprotonated zeolites can be observed. The shortening Al-O1 and a lengthening of Al-O2 bond distances are in accordance with Gutmann's rules. The O1-Hz bond distances are 1.109, 1.484 and 1.544 Å for the 5T, 14T, respectively, and 38T clusters of H-FAU, and are 1.130, 1.399 and 1.544 Å for the 5T, 14T and 38T

clusters, respectively of H-MOR. Therefore, it indicates that for the small quantum 5T cluster, hydrogen bonded complexes are found and for the larger 38T cluster the ion-pair is favored.

Another important evidence that can be used to be able to calibrate our models is the Al···Hz distances. Klinowski *et al.* used H-NMR to observe these distances and compiled an experimental range of 2.340 to 2.520 Å. Our predicted Al···Hz distances are in the range of 2.35 to 2.53 Å, that agree well with their experimental observation.

Table 1 Selected geometric parameters of the adsorption complex of ammonia on H-FAU (Distances are in Å and angles are in degrees).

Parameters	Models					
	5T		14T		38T	
	Isolated	Complex	Isolated	Complex	Isolated	Complex
O1-Hz	0.967	1.109	0.971	1.484	0.971	1.544
O2-H1	-	2.023	-	1.856	-	1.860
Al-O1	1.962	1.886	1.972	1.835	1.968	1.828
Al-O2	1.721	1.757	1.719	1.792	1.724	1.800
Al-O3	1.715	1.721	1.715	1.726	1.719	1.728
Al-O4	1.707	1.719	1.709	1.725	1.710	1.723
Al-O$_{avg}$	1.776	1.770	1.779	1.769	1.780	1.770
Al···Hz	2.481	2.471	2.511	2.651	2.532	2.669
Si-O1	1.730	1.692	1.720	1.652	1.719	1.641
N-O1	-	2.493	-	2.552	-	2.589
N-Hz	-	1.403	-	1.104	-	1.087
N-H1	-	1.026	-	1.040	-	1.040
<Al-O1-Si1	131.0	130.7	130.8	130.6	132.3	131.8
<N-Hz-O1	-	165.8	-	160.6	-	159.0
<N-H1-O2	-	137.4	-	139.9	-	141.2
<H1-N-Hz	-	98.3	-	102.0	-	103.3
<O2-Al-O1	100.5	102.2	102.2	103.4	106.3	106.5

Table 2 Selected geometric parameters of the adsorption complex of ammonia on H-MOR (Distances are in Å and angles are in degrees).

Parameters	Models					
	5T		14T		38T	
	Isolated	Complex	Isolated	Complex	Isolated	Complex
O1-Hz	0.969	1.130	0.970	1.399	0.971	1.544
O2-H1	-	2.023	-	2.026	-	2.065
O4-H2	-	4.128	-	4.109	-	4.186
Al-O1	1.868	1.809	1.848	1.758	1.834	1.737
Al-O2	1.702	1.726	1.694	1.736	1.685	1.723
Al-O3	1.685	1.690	1.683	1.685	1.673	1.682
Al-O4	1.682	1.694	1.676	1.689	1.673	1.688
Al-O$_{avg}$	1.734	1.730	1.725	1.717	1.716	1.708
Al···Hz	2.345	2.429	2.405	2.552	2.398	2.662
Si-O1	1.705	1.664	1.692	1.621	1.679	1.600
N-O1	-	2.480	-	2.503	-	2.604
N-Hz	-	1.364	-	1.128	-	1.084
N-H1	-	1.025	-	1.030	-	1.030
<Al-O1-Si1	130.1	129.7	130.3	131.8	132.7	133.1
<N-Hz-O1	-	167.5	-	164.3	-	164.2
<N-H1-O2	-	131.8	-	129.7	-	123.3
<H1-N-Hz	-	97.4	-	101.1	-	103.9
<O2-Al-O1	94.5	97.6	97.6	100.5	96.2	97.6

Adsorption energies of ammonia on the acidic site of H-FAU and H-MOR zeolites

Table 3 shows calculated and adsorption energies (kcal/mol) on different types of zeolite of various cluster sizes. The models range from the small cluster of 5T up to the more realistic cluster models of 38T. Overall, it can be seen that ΔE_{ads} for the 5T model of all types of zeolites are virtually the same and there is only a slight change for the 14T cluster models. The significant alternations in ΔE_{ads} are observed at the larger cluster of 38T. The effect of the long range interactions is also included via optimized point charges added to the realistic nanocluster 38T, which we called "embedded nanocluster". Inclusion of the extended zeolitic framework covering the nanocluster has an effect on the adsorption properties and yields the adsorption energies which agree well with the available experimental data, -35.6 vs -35.8 kcal/mol for H-FAU and   -39.5 vs -38.2 kcal/mol for H-MOR, respectively. Thus, it can to some extent be used to fine tune the acidity of zeolites and hence be useful for zeolite chemists to systemically select their right candidates for their reaction.

Table 3 Calculated adsorption energies of ammonia on various cluster models of zeolites[a] (kcal/mol).

Zeolite	ΔE_{ads}^{BSSE}				Exp.[c]
	5T[a]	14T[a]	38T[a]	Embedded 38T[b]	
H-FAU	-24.6	-28.7	-30.3	-35.6	-35.8±1.2
H-MOR	-24.1	-27.1	-35.1	-39.5	-38.2±1.2

[a]Cluster models of 5T up to 38T are optimized for full QM calculation.
[b]Single-point calculations on embedded 38T.
[c]Experimental values from the Microcalorimetric method.

Conclusion

The confinement effect for the adsorption of ammonia over different zeoiltes, H-FAU and H-MOR zeolites, has been clearly demonstrated with the newly developed Density Functional Theory, embedded M06-2X, with 6-31G(d,p) basis set. By increasing the cluster size of H-FAU and H-MOR, the adsorption energies of ammonia are slightly increased until close to the embedded cluster models. The adsorption energies for ammonia are calculated to be -35.6 and -39.5 kcal/mol, respectively, which agree well with experiment data. The nature of the local active site and surrounding framework of different zeolites are the main factors leading to the variation in the ammonia adsorption energy. Our findings suggest that the "embedded M06-2X" is a practical and accurate model to examine the confinement effects on the adsorption and reaction mechanisms.

References

Boekfa B., S. Choomwattana, P. Khongpracha, and J. Limtrakul; "Effects of the Zeolite Framework on the Adsorptions and Hydrogen-Exchange Reactions of Unsaturated Aliphatic, Aromatic, and Heterocyclic Compounds in ZSM-5 Zeolite: A Combination of Perturbation Theory (MP2) and a Newly Developed Density Functional Theory (M06-2X) in ONIOM Scheme" Langmuir. 25(22), 12990–12999 (2009).

Derouane G. E. and C. D. Chang; "Confinement effects in the adsorption of simple bases by zeolites" Micropor. Mesopor. Mat. 35–36, 425–433 (2000).

Injan N., N. Pannorad, M. Probst, and J. Limtrakul; "Pyridine Adsorbed on H-Faujasite Zeolite: Electrostatic Effect of the Infinite Crystal Lattice Calculated From a Point Charge Representation" Int. J. Quantum. Chem. 105, 898–905 (2005).

Maihom T., P. Pantu, C. Tachakritikul, M. Probst, and J. Limtrakul; "Effect of the Zeolite Nanocavity on the Reaction Mechanism of n-Hexane Cracking: A Density Functional Theory Study" J. Phys. Chem. C, 114, 7850–7856 (2010).

Pantu P., B. Boekfa, and J. Limtrakul; "The adsorption of saturated and unsaturated hydrocarbons on nanostructured zeolites (H-MOR and H-FAU): An ONIOM study" J. Mol. Catal. A: Chem. 277, 171–179 (2007).

Parrillo J. D. and R. J. Gorte; "Characterization of Acidity in H-ZSM-5, H-ZSM-12, H-Mordenite, and H-Y Using Microcalorimetry" J. Phys. Chem. 97, 8786-8792 (1993)

Zhao Y. and D. G. Truhlar; "Density Functionals with Broad Applicability in Chemistry" Accounts. Chem. Res. 41, 157-167 (2007).

Catalytic Dehydrogenation of Ethylbenzene to Styrene over a Tetrahedral Platinum Nanocluster: A DFT Study

Patanachai Janthon[1,2,3], Teeranan Nongnual[1,2,3], Piboon Pantu[1,2,3], Jumras Limtrakul[1,2,3*]

[1]Laboratory for Computational and Applied Chemistry, Department of Chemistry, Faculty of Science and Center of Nanotechnology, Kasetsart University Research and Development Institute, Kasetsart University, Bangkok 10900, Thailand
[2]NANOTEC Center of Excellence, National Nanotechnology Center, Kasetsart University, Bangkok 10900, Thailand
[3]Center for Advanced Studies in Nanotechnology and Its Applications in Chemical, Food and Agricultural Industries, Kasetsart University, Bangkok 10900, Thailand

*Corresponding author: Tel. (+66)02-562-5555 ext 2169, Fax: (+66)02-562-5555 ext 2176, E-mail address: jumras.l@ku.ac.th

Keywords Dehydrogenation, Ethylbenzene, Styrene, Tetrahedral Platinum, Density-Functional Theory

Introduction

Styrene (C_8H_8) has been one of the highly significant chemicals used widely in the synthetic polymer industry[1]. The dehydrogenation of ethylbenzene over a potassium promoted iron (III) oxide catalyst at high temperature was mainly used for the production of commercial styrene. However, there were disadvantages in this process - endothermic reaction and rapid deactivation, but many researchers have developed new catalysts, adsorbents and catalyst supports to overcome these. Among the developments, the Pt(111) surface was a candidate catalyst for the dehydrogenation of ethylbenzene to styrene concerning the dissociation of ethylbenzene at low temperature on the surface forming styrene and hydrogen products[2]. But, this again had the disadvantage that the styrene desorption step was quenched by its strong binding to the surface, resulting in the polymerization of glued styrene molecules under an annealing temperature condition. The activity of unsupported Pt nanoclusters was studied by determining an activation of the small hydrocarbons such as methane[3-5]. This brought about the small Pt nanoclusters (Pt_n) which were more reactive than monatomic Pt by at least one order of magnitude. The tetrahedral Pt nanocluster (Pt_4) was also found to improve the oxidative dehydrogenation of propane[4].

In this work, we introduce the tetrahedral Pt nanocluster as a novel candidate catalyst for the dehydrogenation of ethylbenzene to styrene.

Computational Details

Neutral Pt_4 with C_2 symmetry in a triplet state was used in our model. Full geometry optimizations for all pathways were performed using the B3LYP method including 6d functions and unrestricted spin polarization, implemented in the Gaussian 03 program. We have employed the LANL2DZ basis set for all Pt atoms, which uses 18-electron relativistic effective core potentials (ECP) to reduce the number of electrons explicitly. The 6-31G (d, p) basis set for all H and C atoms was added in the calculation, increasing the accuracy of the dehydrogenation processes.

Results and Discussion

The dehydrogenation of ethylbenzene over the Pt_4 catalyst was categorized by the number of catalytic Pt atoms into three mechanistic pathways: single-site catalytic Pt_4 (SCP), double-site

catalytic Pt$_4$ (DCP), and triple-site catalytic Pt$_4$ (TCP) as shown in Fig. 1. The DCP pathway has been separated into two sub pathways, DCP_i and DCP_ii, which are dealing with the Int4 and Int5, respectively. Due to the same single-site, the SCP pathway was investigated by comparing the results with activation of the monatomic Pt catalyst. The dehydrogenation was investigated by dealing with the H' and H" dissociations.

Fig. 1 The mechanism scheme for the dehydrogenation of ethylbenzene to styrene over Pt$_4$ catalyst: single-site catalytic Pt$_4$ (SCP, black solid line), double-site catalytic Pt$_4$ (DCP_i, red dash line and DCP_ii, blue dot line) and triple-site catalytic Pt$_4$ (TCP, purple dash-dot line)
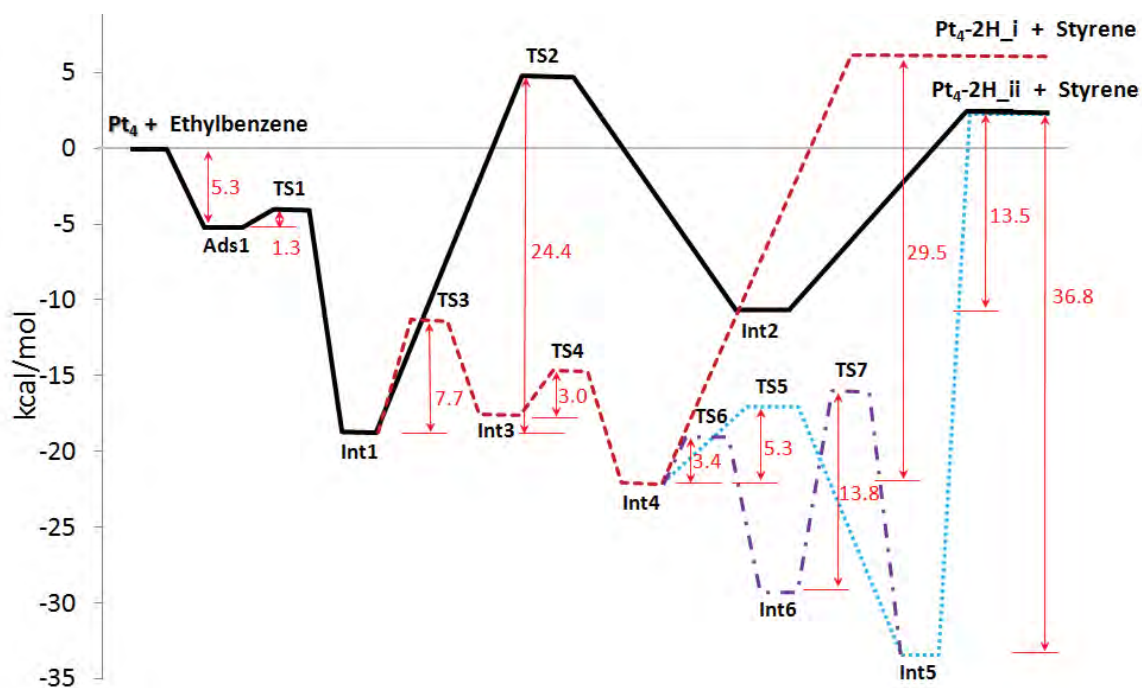

Fig. 2 Energy profiles for the dehydrogenation of ethylbenzene to styrene over Pt$_4$ catalyst: SCP (black solid line), DCP_i (red dash line), DCP_ii (blue dot line) and TCP (purple dash-dot line).

For all catalytic Pt_4 pathways as shown in Fig. 2, the dehydrogenation started from the adsorption of ethylbenzene on the first catalytic site of the Pt_4 (Ads1) with the adsorption energy of -5.3 Kcal/Mol. The C-H' bond was then dissociated with the activation energy of 1.3 kcal/mol (TS1) forming the intermediate Int1. After that, the three main pathways were considered.

For the SCP pathway, the C-H" bond was broken, moving the H" to the same catalytic site with the activation energy of 24.4 kcal/mol (TS2) forming an unstable intermediate with the adsorbed styrene product (Int2). This is the rate determining step caused by an increasing steric effect of seven coordinates on the single platinum site. Surprisingly, the styrene and Pt_4-2H_ii were then easily desorbed with the desorption energy of 13.5 kcal/mol due to the high steric effect.

For the DCP pathway, the H' migrated to the second catalytic site with the activation energy of 7.7 kcal/mol (TS3) forming the intermediate Int3. The C-H" bond was then broken with the activation energy of 3.0 kcal/mol (TS4), moving the H" onto the first catalytic site (Int4) with the absorbed styrene product. Focusing on the DCP_I pathway, the styrene was desorbed with the desorption energy of 29.5 kcal/mol leaving the Pt_4-2H_I. On the other hand, the DCP_ii pathway forwarded by the H" moving to join with the H' on the second catalytic site with the activation energy of 5.3 kcal/mol (TS5) stabilizing the intermediate Int5. Thus, the desorption energy was increased to 36.8 kcal/mol leaving the Pt_4-2H_ii.

For the TCP pathway, the H" of the Int4 moved to the third catalytic site with the activation energy of 3.4 kcal/mol (TS6) forming the intermediate Int6. Next, the H" moved to join with the H' with the activation energy of 13.8 kcal/mol (TS7), merging to the Int5 as in the DCP_ii pathway.

The hydrogen migrations on the catalytic sites, using low activation energy in the range of 3.4 to 13.8 kcal/mol, can stabilize an intermediate. This led to the higher desorption energy for the styrene product. Therefore, the rate determining step of the DCP and the TCP pathways were associated with the styrene desorption step. In contrast, this H-moving step was not considered in the SCP pathway, therefore, the stabilization of an intermediate was not observed. Thus, its non-stabilized intermediate (Int2) can assist the styrene desorption more easily with lower desorption energy.
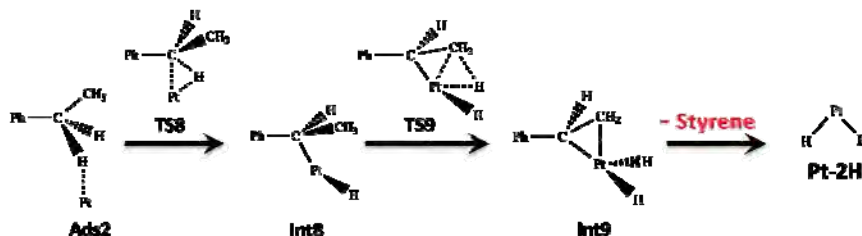

Fig. 3 The mechanism scheme for the dehydrogenation of ethylbenzene to styrene over monatomic Pt catalyst.

Fig. 4 Energy profile for the dehydrogenation of ethylbenzene to styrene over monatomic Pt catalyst.

Although the overall activation energy of the SCP pathway was the smallest, the DCP and TCP pathways were kinetically favorable. Therefore, the dehydrogenation was terminated at the Int5 and Int6 steps with styrene products attached to the catalytic site. To avoid this problem, the SCP pathway must be chosen, thus, the single site catalytic must be favorably controlled.

The dehydrogenation of ethylbenzene over the monatomic Pt catalyst was shown in Fig. 3 with the energy profile in Fig. 4. The C-H' bond was broken with the activation energy of 12.9 kcal/mol (TS8). The C-H" bond was then dissociated with the activation energy of 25.5 kcal/mol (TS9). This was the same as that of the SCP pathway. The styrene was then desorbed with the activation energy of 35.0 kcal/mol, which was the rate determining step. This activation energy is higher than that of the SCP pathway due to its lower steric effect to push the styrene out. It can be suggested that three vacant sites of the Pt_4 can assist the dehydrogenation of the H' and can increase the steric effect to the active site.

Conclusion

We report here the first theoretical study of the dehydrogenation of ethylbenzene over the Pt_4 catalyst. Although the overall activation energy of the SCP pathway was the smallest, the DCP and TCP pathways were kinetically favorable without desorption of the styrene product. To avoid this problem, the SCP pathway must be chosen, thus, the single site catalytic must be favorably controlled. The H-migration step was not considered in the SCP pathway. For this reason, the stabilization of an intermediate was not observed. Therefore, the non-stabilized intermediate of SCP pathway (Int2) can assist the styrene desorption more easily with the lower desorption energy. This caused the overall activation energy of 24.4 kcal/mol that belonged to the C-H" to dissociate. In addition, we suggest the control for the SCP pathway by the assistance of an adsorbent blocking three sites with remaining one active site of the Pt_4 catalyst. Moreover, in order to recover the Pt_4 catalyst, the oxidative dehydrogenation should be introduced to eliminate the two adsorbed-H atoms remaining on the catalyst. This understanding can be applied for an alternative styrene synthesis.

References

1. Lee W. J. and G. F. Froment; "Ethylbenzene Dehydrogenation into Styrene: Kinetic Modeling and Reactor Simulation." Industrial & Engineering Chemistry Research. **47**(23), 9183-9194 (2008).
2. Ranke W. and W. Weiss; "Adsorption and thermal decomposition of ethylbenzene and styrene on Pt(111) studied by UPS and XPS." Surface Science. **465**(3), 317-330 (2000).
3. Xiao L. and L. Wang; "Methane Activation on Pt and Pt_4: A Density Functional Theory Study." The Journal of Physical Chemistry B. **111**(7), 1657-1663 (2007).
4. Trevor D. J., D. M. Cox, A. Kaldor; "Methane activation on unsupported platinum clusters." Journal of the American Chemical Society. **112**(10), 3742-3749 (1990).
5. Vajda S., M. J. Pellin, J. P. Greeley, C. L. Marshall, L. A. Curtiss, G. A. Ballentine, J. W. Elam, S. Catillon-Mucherie, P. C. Redfern, F. Mehmood, P. Zapol; "Subnanometre platinum clusters as highly active and selective catalysts for the oxidative dehydrogenation of propane." Nature Materials. **8**(3), 213-216 (2009).

DFT Study on the Effect of Phosphate Ionic Core on Basicity of $PW_{12}O_{40}^{3-}$ Polyoxometalate

Saowapak Choomwattana[1,2,3], Jakkapan Sirijaraensre[1,2,3], Jumras Limtrakul[1,2,3*]

[1]Laboratory for Computational and Applied Chemistry, Department of Chemistry, Faculty of Science and Center of Nanotechnology, Kasetsart University Research and Development Institute, Kasetsart University, Bangkok 10900, Thailand
[2]NANOTEC Center of Excellence, National Nanotechnology Center, Kasetsart University, Bangkok 10900, Thailand
[3]Center for Advanced Studies in Nanotechnology and Its Applications in Chemical, Food and Agricultural Industries, Kasetsart University, Bangkok 10900, Thailand

*Corresponding author: Tel. +66 2562 5555 ext 2169, Fax: +66 2562 5555 ext 2176, E-mail address: jumras.l@ku.ac.th

Abstract

The surface oxygen sites of α-Keggin phosphotungstate (PT) anion ($PW_{12}O_{40}^{3-}$) and neutral $W_{12}O_{36}$ cage were differentiated with pyrrole using the density-functional theory (DFT-GGA-PW91/DNP). It was found that the ionic core plays a dominant role on the intermolecular interaction as the adsorption energy of the two cases are about 10 kcal mol^{-1} different. However, the preferred trend adsorption site of corner-sharing oxygen < terminal oxygen < edge-sharing oxygen is preserved even when the ionic core is removed. The strongest adsorption at the edge-sharing oxygen atom in $[PW_{12}O_{40}]^{3-}$ can be explained by the electron donation from the *p* orbital of POM O to the *p* vacant orbital of pyrrole H. From PDOS analyses, the phosphate anionic core induces the formation of intermolecular hydrogen bonding between the POM and pyrrole. The understanding can be applied for advanced studies on tailor-made polyoxometalate and catalytic mechanism with the POM.
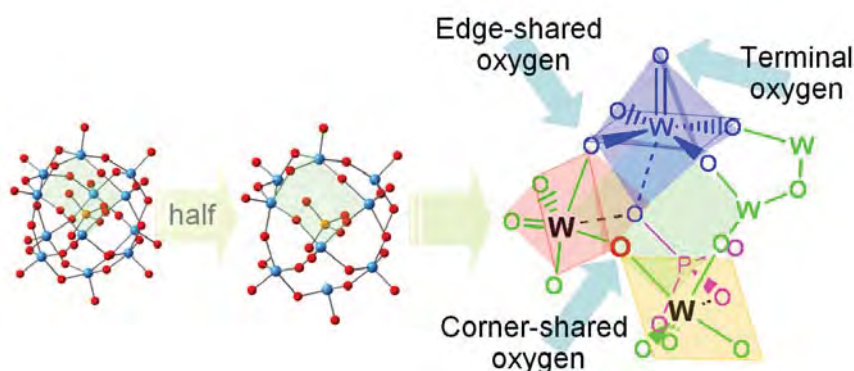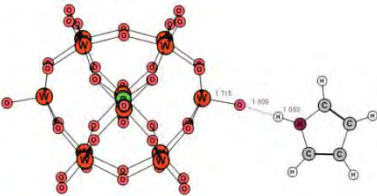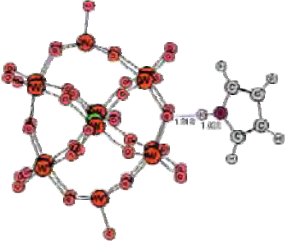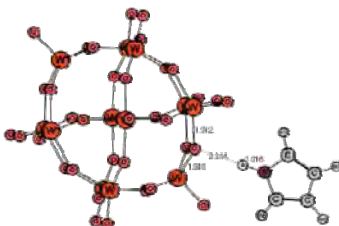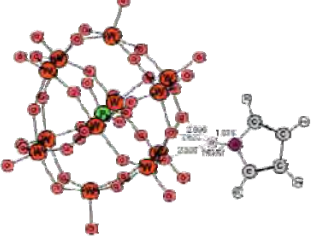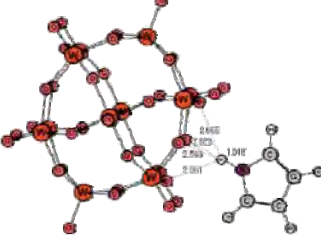
Fig. 1 Three types of surface oxygen in PT anion: terminal, edge-shared and corner-shared.

Table 1 Orientations and their adsorption energy (kcal mol^{-1}) of pyrrole complexes with $PW_{12}O_{40}^{3-}$ and $W_{12}O_{36}$.

Oxygen site	System	
	$PW_{12}O_{40}^{3-}$	$W_{12}O_{36}$
Terminal	-17.08	-9.90
Edge-shared	-18.61	-10.24
Corner-shared	-15.17	-8.85

References

Lavalley J. C.; "Infrared spectrometric studies of the surface basicity of metal oxides and zeolites using adsorbed probe molecules", Catal. Today 27(3-4), 377-401 (1996).

Nongnual T., S. Nokbin, P. Khongpracha, P. A. Bopp and J. Limtrakul; "Density functional theory evidence for an electron hopping process in single-walled carbon nanotube-mediated redox reactions", Carbon 48(5):1524-1530 (2010).

Soares-Santos P. C. R., L. Cunha-Silva, F. L. Sousa, L. Mafra, J. Rocha, A. M. V. Cavaleiro, T. Trindade, F. A. A. Paz, J. Klinowski and H. I. S. Nogueira; "Two novel supramolecular organic-inorganic adducts containing dibenzo-30-crown-10 and $H_3PM_{12}O_{40}$ (M = W or Mo)", J. Molec. Struct., 888(1-3), 99-106 (2008).

Zhang F. Q., X. M. Zhang, H. S. Wu and H. Jiao; "Structural and Electronic Properties of Hetero-Transition-Metal Keggin Anions: A DFT Study of α/β-$[XW_{12}O_{40}]^{n-}$ (X = Cr^{VI}, V^{V}, Ti^{IV}, Fe^{III}, Co^{III}, Ni^{III}, Co^{II}, and Zn^{II}) Relative Stability", J. Phys. Chem. A, 111(1):159-166, (2006).

American Chemical Society National meeting & Exposition" ครั้งที่ 241

ณ ประเทศสหรัฐอเมริกา

ระหว่างวันที่ 27-31 มีนาคม 2554

จำนวน 12 เรื่อง

SKELETAL ISOMERIZATION OF 1-BUTENE TO ISOBUTENE ON H-ZSM-5 ZEOLITE: A NEWLY DEVELOPED DENSITY FUNCTIONAL THEORY STUDY

Bundet Boekfa[a,c,d], Kanokwan Kongpatpanich[b,c,d],
Pailin Limtrakul[b,c,d] and Jumras Limtrakul[b,c,d]*

[a] Chemistry Department, Faculty of Liberal Arts and Science, Kasetsart University Kamphaeng Saen Campus, Nakhon Pathom 73140, Thailand
[b] Laboratory for Computational and Applied Chemistry, Department of Chemistry, Faculty of Science and Center of Nanotechnology, Kasetsart University Research and Development Institute, Kasetsart University, Bangkok 10900, Thailand
[c] NANOTEC Center of Excellence, National Nanotechnology Center, Kasetsart University, Bangkok 10900, Thailand
[d] Center for Advanced Studies in Nanotechnology and Its Applications in Chemical, Food and Agricultural Industries, Kasetsart University, Bangkok 10900, Thailand

Introduction

Isobutene is a raw material for the production of methyl *tert*-butyl ether (MTBE) and ethyl *tert*-butyl ether (ETBE), which is used as a potential additive in lead-free gasoline. Isobutene can be rearranged from the more abundant butene isomers, such as 1-butene and 2-butene, via the skeletal isomerization catalyzed by nanoporous catalysts[1-14].

Zeolites are considered to be one of the most promising catalysts due to their active and selective properties.[15-20] A survey of literature suggests that suitable catalysts of this reaction are the zeolites with a pore diameter between 4 and 5.5 Å, which are in the range of the 8- to 10-membered ring channels such as Ferrierite, Theta-1 and ZSM-5[3,9-10]. Among the various zeolites that were tested, ZSM-5 showed satisfsctory results with the isobutene conversion of nearly 90%. The general mechanisms proposed are based on either a bimolecular mechanism or a monomolecular mechanism. At a low number of acid sites and high temperature, it is reported that the skeletal isomerization of 1-butene toward isobutene is the monomolecular mechanism rather than dimerization, followed by cracking into light hydrocarbons[21].

The dimerization process was proposed to be an auto catalytic pathway via the active species of *tert*-butyl carbenium ions and trans-2-butene as input reactants[13]. For the monomolecular, a theoretical study was used to study this reaction on theta-1 zeolite[22]. These studies are helpful in predicting the reaction activity, however, the quantum cluster is small and the method does not take into account the van der Waals interaction.

The reaction mechanism of the skeletal isomerization of 1-butene provides useful knowledge to improve the catalytic performances of zeolite and increase the selectivity to the desired product. Unfortunately, 1-butene is very reactive and rapidly isomerizes or dimerizes even at room temperature. Therefore, the reaction mechanism of this reaction has so far been difficult to obtain from experiment.

Where a unit cell of zeolite contains hundreds of atoms, sophisticated methods of calculation, such as periodic ab initio, are computationally too expensive and even impractical. However, recently developed hybrid methods, such as the embedded cluster or the combined quantum mechanics/molecular mechanics (QM/MM) methods now make it possible to calculate larger zeolite systems with much greater accuracy. [23-28] The adsorption of butene was studied on various zeolites via QM/MM calculations[25-26,29]. These results show the importance of the confinement effect from the zeolite framework on the studies of the adsorption process and reaction mechanism. Recently the adsorption and reaction mechanism of hydrocarbon with a large quantum cluster has been successfully studied with the new density functional theory, M06-2X[30-32].

In this work the reaction mechanism of skeletal isomerization of 1-butene over H-ZSM-5 is explored by using a large quantum cluster, 120T, with the new density functional theory, M08-HX. In addition, the results are compared with the second-order Møller-Plesset perturbation theory, MP2.

Methodology

The cluster models were taken from the lattice structure of ZSM-5 Zeolite[33]. The 23T (T being Si or Al tetrahedral atoms) cluster is modeled to cover the intersection channel of H-ZSM-5 zeolite where the probe molecules occur as shown in Figure 1. The Al atom is selected to substitute at the most favored position T12[34]. An additional single point calculation on the extended 128T cluster is performed to account for the framework effect. The Brønsted acid site (Si_4O_4AlH) and the adsorbate are allowed to relax while the rest is kept fixed at the crystallographic coordinate. All models were treated with the M08-HX/6-31G(d,p) level of theory. In order to validate the energies from the M08-HX functional, the single point calculations at MP2/6-31G(d,p) have been used as benchmarks. All calculations were performed using the Gaussian 03 code[35] incorporated with the Minnesota Density Functional module 3.1 by Zhao and Truhlar[36-37].

(a)

(b)
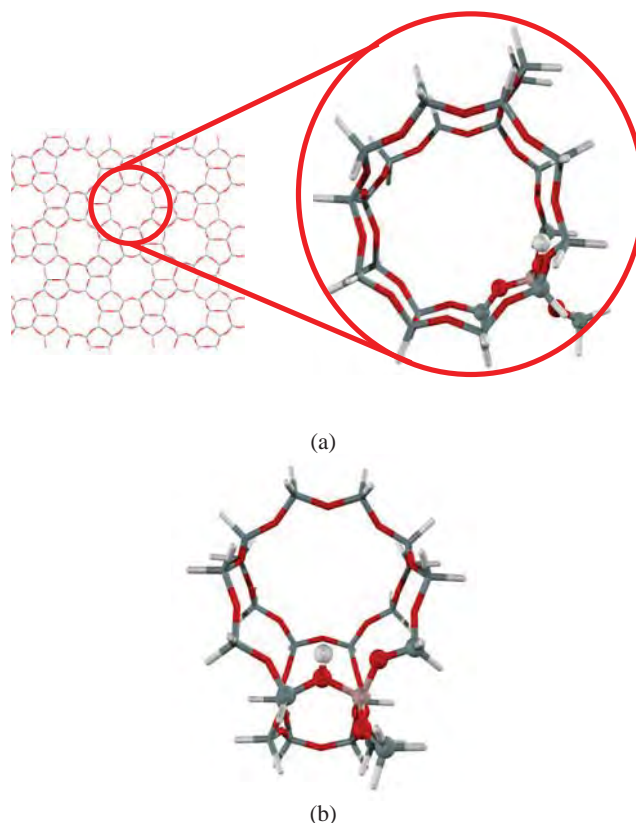
Figure 1. Presentation of the 23T cluster of H-ZSM-5 zeolite, (a) view from the straight channel and (b) view from the zigzag channel.

Results and Discussion

Model of H-ZSM-5 zeolite catalyst. The 23T quantum is modeled to cover the intersection cavity where the reactions normally take place, as shown in Figure 1. The model was then calculated with the new density functional, M08-HX with the 6-31G(d,p) basis set. The O1-Hz bond distance is about 0.97 Å. While the Al···Hz distance is about 2.36 Å, which agrees well with the experimental observation (2.38-2.48 Å) [38].
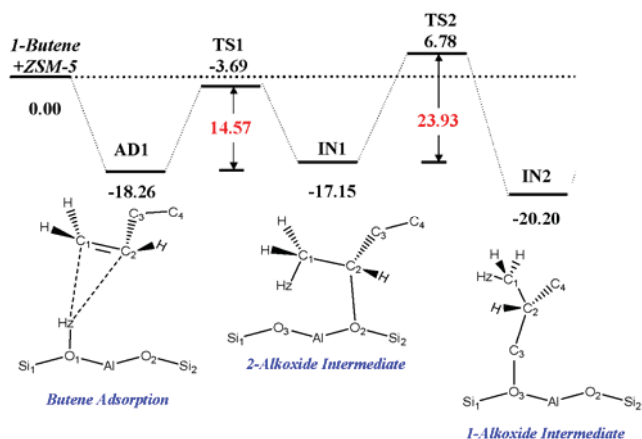
Figure 2. Potential energy diagram of the 1-butene to 1-alkoxide intermediate on the 120T//23T quantum cluster of H-ZSM-5, calculated with the M08-HX/6-31G(d,p) method (kcal/mol).
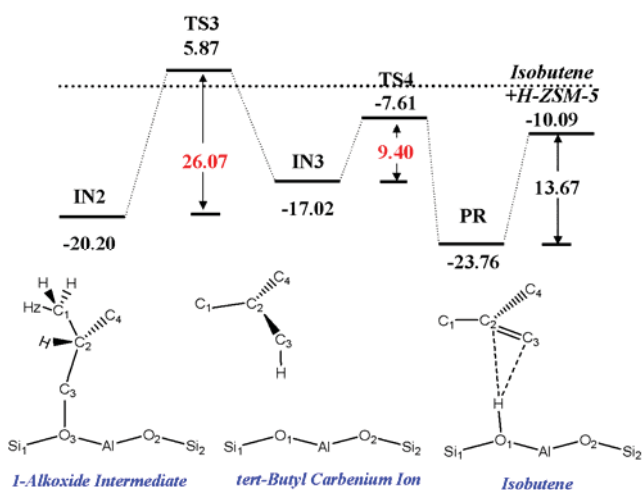
Figure 3. Potential energy diagram of the 1-alkoxide intermediate to isobutene on the 120T//23T quantum cluster of H-ZSM-5, calculated with the M08-HX/6-31G(d,p) method (kcal/mol).

Reaction mechanism for 1-butene isomerization to isobutene. The 1-butene molecule is located in the 10T membered ring at the intersection of H-ZSM-5 zeolite. It adsorbs on the Brønsted acid via a π-interaction, as shown in Figure 4(a). The slight increase of the Brønsted acid O1-Hz is observed to be about 0.02 Å corresponding with the slight elongation of the C-C double bond by about 0.01 Å. The intermolecular distance between the Brønsted acid and the carbon of the double bond are 2.18 and 2.22 Å for Hz···C1

and Hz···C2, respectively. The adsorption energy of 1-butene on the H-ZSM-5 model 120T//23T is computed to be -18.26 kcal/mol. To the best of our knowledge there is no experimental data available for the adsorption of butane on the protonic zeolites due to the oligomerization reaction. Only the heat of adsorption of n-butane on H-ZSM-5, which is reported to be -13.9 kcal/mol[39]. From our calculation, the adsorption of butane on H-ZSM-5 is calculated to be –11.5 kcal/mol with M08-HX/6-31G(d,p), which compared well with the experiment.

The isomerization mechanism of 1-butene to isobutene on H-FER is proposed as a stepwise reaction mechanism. The energy profile is shown in Figures 2 and 3. The mechanism consists of four steps: 1) protonation of the adsorbed 1-butene and form the secondary alkoxide intermediate, 2) the methyl shift via the cyclic transition state and form the primary alokoxide intermediate, 3) proton transfer and form the *tert*-carbenium cation and 4) protonation back to zeolite and desorption of isobutene.
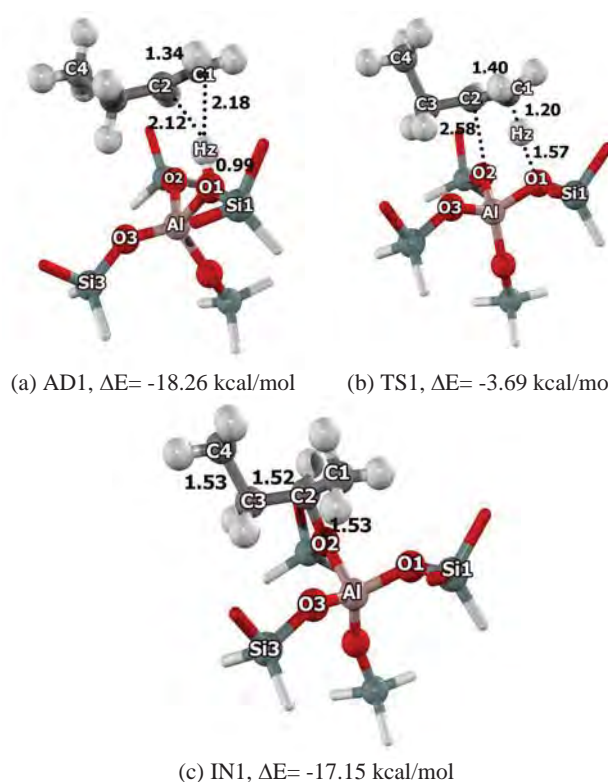
(a) AD1, ΔE= -18.26 kcal/mol   (b) TS1, ΔE= -3.69 kcal/mol

(c) IN1, ΔE= -17.15 kcal/mol

Figure 4. Optimized structures of 1-butene isomerization to isobutene on H-ZSM-5 zeolite: (a) the adsorption complex of 1-butene (AD1), (b) the transition structures (TS1), and (c) the secondary alkoxide intermediate (IN1). Distances are in Ås.

After adsorption of the 1-butene molecule, the secondary alkoxide intermediate [IN1, Figure 4(c)] is formed via the first step of the reaction [TS1, Figure 4(b)]. The O1-Hz bond is broken and the O2-C2 bond is formed. The C1-C2 double bond is elongated to become a single bond. The hybridization of C1 is changed from planar (sp²) to tetrahedral (sp³). The transition state is confirmed to be only one imaginary frequency at -217.4 cm⁻¹ related with the moving of the proton Hz form the zeolite to the carbon (C1) of the double bond of the 1-butene and forming of the bond between the carbon (C2) of the 1-butene and oxygen (O2) of the zeolite. The

activation energy is about 14.57 kcal/mol. The activation energy is in agreement with the experiment estimates of the activation energy for the isotope exchange of ethylene in zeolites of 15-20 kcal/mol[40]. The intermediate is the secondary alkoxide of the 1-butene. The strong covalent bond of C2-O2 is formed while the C1-C2 is elongated to become a single bond. The relative energy is -17.15 kcal/mol.
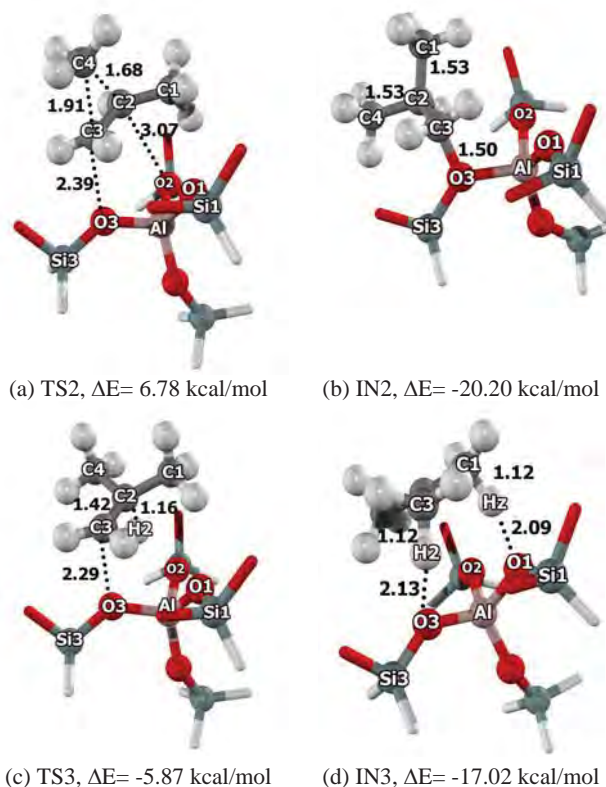
(a) TS2, ΔE= 6.78 kcal/mol   (b) IN2, ΔE= -20.20 kcal/mol

(c) TS3, ΔE= -5.87 kcal/mol   (d) IN3, ΔE= -17.02 kcal/mol

Figure 5. Optimized structures of 1-butene isomerization to isobutene on H-ZSM-5 zeolite: (a) the transition state (TS2), (b) the primary alkoxide intermediate (IN2), (c) the transition state (TS3), and (d) *tert*-butyl carbenium cation (IN3). Distances are in Ås.

The next step is the methyl shift via the cyclic transition state. The transition state [Figure 5(a)], the breaking of the C3-C4 and the O2-C2 bond corresponds with the formation of the C2-C4 and C3-O3 bond. One imaginary frequency is found at -101.3 cm⁻¹. The reaction is via the cyclic transition state, the C4 methyl group is breaking the bond from the C3 atom and is forming the bond with the C2 atom and breaking the C2-O2 bond and forming the C3-O3 bond. This step required the activation energy of 23.93 kcal/mol. The apparent activation energy is 6.78 kcal/mol. The product is the primary alkoxide intermediate as shown in Figure 5(b). The primary alkoxide intermediate is formed with the relative energy -20.20 kcal/mol. This shows that the IN2 is slightly stronger than IN1 because the bond of the primary alkoxide intermediate (C3-O3 1.50 Å) is shorter than the bond of the secondary alkoxide intermediate (C2-O2 1.53 Å).

The third step is the proton transfer and formation of the *tert*-carbenium cation [IN3, Figure 5(d)]. At this step, the covalent C3-O3 bond is breaking and one proton is moving from the C2 to the C3 atom. From a frequency calculation of the transition state geometry [TS3, Figure 5(c)], the imaginary frequency of -482.4 cm⁻¹ corresponds to the transition state. For the transition state it shows the hydrogen atom H2 is breaking the bond from the C2 atom to form the bond with the C3 atom and simultaneously breaking the C3-O3

bond. The activation energy is 26.07 kcal/mol. The *tert*-carbenium ion is found to be the intermediate with the relative energy of -17.02 kcal/mol. The symmetrical distances between C1-C2, C3-C2 and C4-C2 is about 1.42 Å. However, the *tert*-butyl carbenium ion does not have lower energy than the alkoxide intermediate and easily transfers to the isobutene via the proton shift back to the zeolite. The isobutene is the product as shown in Figure 6(b) with the activation barrier for this step of only 9.40 kcal/mol.

Table 1. Comparison of Model Size and Computational Approach on the Adsorption and Activation Energies of 1-butene Isomerization to Isobutene on H-ZSM-5 Zeolite. Intrinsic Activation Energies are in Parenthesis. Energies are in kcal/mol.

Model	23T	128T//23T	23T
Method	M08HX	M08HX	MP2 //M08HX
AD1	-16.99	-18.26	-16.35
TS1	1.28 (18.26)	-3.69 (14.57)	2.69 (19.05)
IN1	-17.63	-17.15	-16.14
TS2	10.76 (29.85)	6.78 (23.93)	9.81 (25.94)
IN2	-21.51	-20.2	-18.82
TS3	8.3 (29.81)	5.87 (26.07)	9.51(28.34)
IN3	-12.61	-17.02	-8.32
TS4	-0.52 (12.06)	-7.61 (9.40)	3.52 (11.85)
PR	-22.64	-23.76	-14.24

(a) TS4, ΔE= -7.61 kcal/mol   (b) PR, ΔE= -23.76 kcal/mol
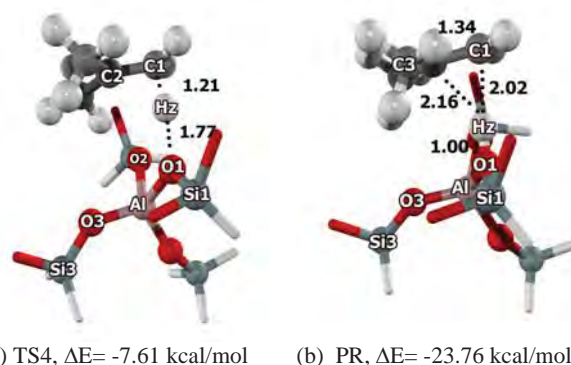
Figure 6. Optimized structures of 1-butene isomerization to isobutene on H-ZSM-5 zeolite: (a) transition state (TS4), and (b) product isobutene adsorption (PR). Distances are in Ås.

The 1-butene to iso-butene reaction is an exothermic reaction. The rate determining step is the third step which shows the breaking of the bond formation of the primary alkoxide intermediate and the proton shift. To verify the accuracy of this method, the single point at MP2 is used to perform the energy of the density functional theory (see Table 1). The adsorption energies of 1-butene on H-ZSM-5 are calculated to be -16.99 and -16.35 kcal/mol with M08-HX/6-31G(d,p) and MP2/6-31G(d,p)//M08-HX/6-31G(d,p) methods, respectively. The activation energies of 1-butene isomerization are computed to be 18.26, 29.85, 29.81 and 12.10 kcal/mol with M08-HX. With the MP2//M08-HX, the activation energies are computed to be 19.05, 25.94, 28.34 and 11.85 kcal/mol. This suggests that the

M08-HX is a suitable method to study the reaction mechanism in the zeolite system.

Conclusions

The adsorption and skeletal isomerization of 1-butene to isobutene on the nanostructured H-ZSM-5 catalyst has been studied by the newly developed Density Functional Theory, M08-HX. The 128T quantum cluster model covers the intersection cavity of ZSM-5 zeolite. The adsorption energy of 1-butene is calculated to be -18.26 kcal/mol. The reaction mechanism of the skeletal isomerization of 1-butene is proposed to be four steps: 1) the protonation of adsorbed 1-butene to a secondary alkoxide intermediate, 2) the methyl shift between adjacent carbon-carbon atoms of the secondary alkoxide to form the primary alkoxide, 3) the proton transfer to form the *tert*-butyl carbenium ion, and 4) the deprotonation of the carbenium intermediate leading to isobutene as the product of the reaction. From the calculated results, the third step of the reaction is the rate determining step with an activation energy of 26.07 kcal/mol, which agrees well with the experimental value of 30.0 kcal/mol.

References

(1) Andy, P.; Gnep, N. S.; Guisnet, M.; Benazzi, E.; Travers, C. *J. Catal.* **1998**, *173*, 322.
(2) Asensi, M. A.; Corma, A.; Martíez, A. *J. Catal.* **1996**, *158*, 561.
(3) Guisnet, M.; Andy, P.; Boucheffa, Y.; Gnep, N. S.; Travers, C.; Benazzi, E. *Catal. Lett.* **1998**, *50*, 159.
(4) Guisnet, M.; Andy, P.; Gnep, N. S.; Benazzi, E.; Travers, C. *J. Catal.* **1996**, *158*, 551.
(5) Houžvička, J.; Hansildaar, S.; Ponec, V. *J. Catal.* **1997**, *167*, 273.
(6) Jousse, F.; Leherte, L.; Vercauteren, D. P. *Mol. Simul.* **1996**, *17*, 175.
(7) Jousse, F.; Leherte, L.; Vercauteren, D. P. *J. Mol. Catal. A: Chem.* **1997**, *119*, 165.
(8) Meriaudeau, P.; Bacaud, R.; Ngoc Hung, L.; Vu, A. T. *J. Mol. Catal. A: Chem.* **1996**, *110*.
(9) Mériaudeau, P.; Tuan, V. A.; Le, N. H.; Szabo, G. *J. Catal.* **1997**, *169*, 397.
(10) Seo, G.; Jeong, H. S.; Lee, J. M.; Ahn, B. J. *Stud. Surf. Sci. Catal.* **1997**, *105 B*, 1431.
(11) Trombetta, M.; Busca, G.; Rossini, S.; Piccoli, V.; Cornaro, U. *J. Catal.* **1997**, *168*, 349.
(12) De Ménorval, B.; Ayrault, P.; Gnep, N. S.; Guisnet, M. *Catal. Lett.* **2004**, *98*, 211.
(13) De Ménorval, B.; Ayrault, P.; Gnep, N. S.; Guisnet, M. *J. Catal.* **2005**, *230*, 38.
(14) de Ménorval, B.; Ayrault, P.; Gnep, N. S.; Guisnet, M. *Appl Catal A Gen* **2006**, *304*, 1.
(15) Bhan, A.; Iglesia, E. *Acc. Chem. Res.* **2008**, *41*, 559.

(16) Chen, C. S. H.; Bridger, R. F. *J. Catal.* **1996**, *161*, 687.
(17) Corma, A. *J. Catal.* **2003**, *216*, 298.
(18) Smit, B.; Maesen, T. L. M. *Nature (London, U. K.)* **2008**, *451*, 671.
(19) Venuto, P. B. *Microporous Mater.* **1994**, *2*, 297.
(20) Yaluris, G.; Rekoske, J. E.; Aparicio, L. M.; Madon, R. J.; Dumesic, J. A. *J. Catal.* **1995**, *153*, 65.
(21) Rutenbeck, D.; Papp, H.; Ernst, H.; Schwieger, W. *Appl Catal A Gen* **2001**, *208*, 153.
(22) Boronat, M.; Viruela, P.; Corma, A. *Phys. Chem. Chem. Phys.* **2001**, *3*, 3235.
(23) Namuangruk, S.; Pantu, P.; Limtrakul, J. *J. Catal.* **2004**, *225*, 523.
(24) Namuangruk, S.; Pantu, P.; Limtrakul, J. *ChemPhysChem* **2005**, *6*, 1333.
(25) Namuangruk, S.; Khongpracha, P.; Pantu, P.; Limtrakul, J. *J. Phys. Chem. B* **2006**, *110*, 25950.
(26) Pantu, P.; Boekfa, B.; Limtrakul, J. *J. Mol. Catal. A: Chem.* **2007**, *277*, 171.
(27) Boekfa, B.; Pantu, P.; Limtrakul, J. *J. Mol. Struct.* **2008**, *889*, 81.
(28) Pantu, P.; Boekfa, B.; Sunpetch, B.; Limtrakul, J. *Chem. Eng. Commun.* **2008**, *195*, 1477.
(29) Nieminen, V.; Sierka, M.; Murzin, D. Y.; Sauer, J. *J. Catal.* **2005**, *231*, 393.
(30) Boekfa, B.; Choomwattana, S.; Khongpracha, P.; Limtrakul, J. *Langmuir* **2009**, *25*, 12990.
(31) Boekfa, B.; Pantu, P.; Probst, M.; Limtrakul, J. *J. Phys. Chem. C* **2010**, *114*, 15061.
(32) Maihom, T.; Boekfa, B.; Sirijaraensre, J.; Nanok, T.; Probst, M.; Limtrakul, J. *J. Phys. Chem. C* **2009**, *113*, 6654.
(33) Van Koningsveld, H.; Van Bekkum, H.; Jansen, J. C. *Acta Crystallogr., Sect. B: Struct. Sci.* **1987**, *B43*, 127.
(34) Lonsinger, S. R.; Chakraborty, A. K.; Theodorou, D. N.; Bell, A. T. *Catal. Lett.* **1991**, *11*, 209.
(35) Frisch, M. J.; Trucks, G. W.; Schlegel, H. B.; Scuseria, G. E.; Robb, M. A.; Cheeseman, J. R.; Montgomery, J. A., Jr.; Vreven, T.; Kudin, K. N.; Burant, J. C.; Millam, J. M.; Iyengar, S. S.; Tomasi, J.; Barone, V.; Mennucci, B.; Cossi, M.; Scalmani, G.; Rega, N.; Petersson, G. A.; Nakatsuji, H.; Hada, M.; Ehara, M.; Toyota, K.; Fukuda, R.; Hasegawa, J.; Ishida, M.; Nakajima, T.; Honda, Y.; Kitao, O.; Nakai, H.; Klene, M.; Li, X.; Knox, J. E.; Hratchian, H. P.; Cross, J. B.; Adamo, C.; Jaramillo, J.; Gomperts, R.; Stratmann, R. E.; Yazyev, O.; Austin, A. J.; Cammi, R.; Pomelli, C.; Ochterski, J. W.; Ayala, P. Y.; Morokuma, K.; Voth, G. A.; Salvador, P.; Dannenberg, J. J.; Zakrzewski, V. G.; Dapprich, S.; Daniels, A. D.; Strain, M. C.; Farkas, O.; Malick, D. K.; Rabuck, A. D.; Raghavachari, K.; Foresman, J. B.; Ortiz, J. V.; Cui, Q.; Baboul, A. G.; Clifford, S.; Cioslowski, J.; Stefanov, B. B.; Liu, G.; Liashenko, A.; Piskorz, P.; Komaromi, I.; Martin, R. L.; Fox, D. J.; Keith, T.; Al-Laham, M. A.; Peng, C. Y.; Nanayakkara, A.; Challacombe, M.; Gill, P. M. W.; Johnson, B.; Chen, W.; Wong, M. W.; Gonzalez, C.; Pople, J. A. *Gaussian 03, revision B.05; Gaussian, Inc.: Pittsburgh, PA*, 2003.
(36) Zhao, Y.; Truhlar, D. G. *J. Phys. Chem. C* **2008**, *112*, 6860.
(37) Zhao, Y.; Truhlar, D. G. *Acc. Chem. Res.* **2008**, *41*, 157.
(38) Klinowski, J. *Chem. Rev.* **1991**, *91*, 1459.
(39) Yoda, E.; Kondo, J. N.; Domen, K. *J. Phys. Chem. B* **2005**, *109*, 1464.
(40) Cant, N. W.; Hall, W. K. *J. Catal.* **1972**, *25*, 161.

STRUCTURES AND REACTION MECHANISMS OF n-BUTYL ALCOHOL CONVERSION TO iso-BUTYLENE OVER THETA-1 ZEOLITE: A DFT STUDY

Jitwadee Wiangngean[a,b,c], _Kanokwan Kongpatpanich_[a,b,c], _Sippakorn Wannakao_[a,b,c], _Bundet Boekfa_[b,c,d], and _Jumras Limtrakul_[a,b,c]*.

[a] Laboratory for Computational and Applied Chemistry, Department of Chemistry, Faculty of Science and Center of Nanotechnology, Kasetsart University Research and Development Institute, Kasetsart University, Bangkok 10900, Thailand
[b] Center for Advanced Studies in Nanotechnology and Its Applications in Chemical, Food and Agricultural Industries, Kasetsart University, Bangkok 10900, Thailand
[c] NANOTEC Center of Excellence, National Nanotechnology Center, Kasetsart University, Bangkok 10900, Thailand
[d] Chemistry Department, Faculty of Liberal Arts and Science, Kasetsart University Kamphaeng Saen Campus, Nakhon Pathom73140, Thailand

Introduction

isobutylene is an important raw material for the production of oxygenated species such as methyl _tert_-butyl ether (MTBE) and ethyl _tert_-butyl ether (ETBE), which are currently used as octane enhancer additives of gasolines. In addition, isobutylene is a potential intermediate for petroleum and chemical industries. When taking into consideration environmental concerns, production of isobutylene from sustainable resources, such as biomass, is of tremendous interest. Bio-butyl alcohol is produced from biomass fermentation to be a clean fuel[1-2] as well as an industrially important intermediate to produce higher value chemicals.

Butyl alcohol dehydration was studied in many solid acid catalysts including acidic zeolites[3-4]. Furthermore, skeletal isomerization of linear butylenes has also been widely studied[5-8], but only a few studies describe the conversion of n-butyl alcohol to isobutylene[9-10]. The general mechanisms of linear butylene isomerization can be considered either monomolecular or bimolecular mechanisms. When a low number of acid sites appeared on the catalyst surface or at low temperatures, the isomerization mechanism typically favored the monomolecular mechanism[11-12]. Moreover, small pore zeolites such as theta-1 and FER lead to a high selectivity of the isomerization products over that of oligomerization. Recently, Zhang et al. have successfully studied the one-step dehydration and isomerization of n-butyl alcohol to iso-butylene over various types of zeolites. They found that both dehydration and isomerization occurred over acid sites and concluded that the theta-1 zeolite provides a high conversion of butyl alcohol together with a high selectivity of isobutylene product. Although many theoretical studies of dehydration and isomerization have been conducted, to the best of our knowledge, information of the direct conversion of n-butyl alcohol to isobutylene over zeolite systems has not been reported.

Theta-1 is a synthetic zeolite with a one dimensional channel[13]. The medium-pore size (4.4x5.5 Å) of theta-1 zeolite with a high silica ratio exhibits valuable properties and yields many important reactions such as isomerization, oligomerization.[14-16]. It is accepted that, the confinement effect from the zeolite framework is important to describe a reaction mechanism in the nanopore size of the zeolite[17-20]. Recently, the confinement effect of the zeolite framework on the adsorption and reaction mechanism have been successfully studied with M06 functional[21-24].

The aim of this study is to describe the reaction mechanism of the conversion of n-butyl alcohol to isobutylene over theta-1 zeolite which can occur in complicated stepwise and concerted ways using the dispersion included functional, M06-2X.

Methodology

The quantum cluster structure was taken from the lattice structure of theta-1 zeolite. The 12T cluster model which represents its one direction pore character covering the straight channel of Theta-1 zeolite is shown in Figure 1. One Al atom was substituted in the T1 position and one H atom was attached to the neighboring oxygen, O11 to create a Brønsted acid site[25-26]. The Brønsted acid site (Si_4O_4AlH) and the probe molecule are allowed to relax while the rest is kept fixed at the crystallographic structure. The geometries of all the structures considered in this study have been optimized using the density functional, M06-2X, with the 6-31G(d,p) basis set. A normal-mode analysis of the transition state shows only one imaginary frequency that corresponds to the reaction mechansim. All calculations were performed with the Gaussian 03 code modified to incorporate the Minnesota Density Functional module 3.1 by Zhao and Truhlar[27].
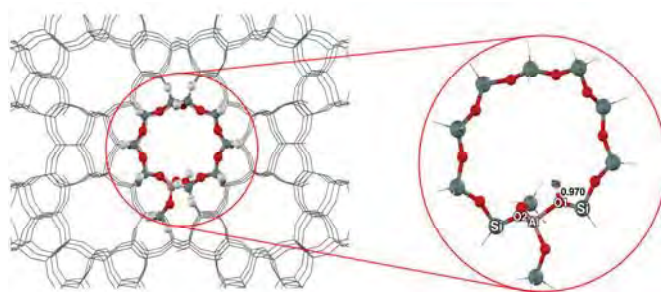
Figure 1. The 12T quantum cluster of the Theta-1 zeolite.

Results and Discussion

The structures and reaction mechanisms of n-butyl alcohol dehydration and isomerization were investigated using the M06-2X/6-31G(d,p) level of theory. The butyl alcohol adsorbed on the Brønsted acid with a hydrogen bond in the straight channel of theta-1 zeolite is shown in Figure 2 (a, b). There are two stable forms of n-butyl alcohol on zeolite: end-on and site-on structures. The end-on structure (Ads1_endon) is adsorbed with the two hydrogen bonds; 1) The oxygen atom at the hydroxyl group of n-butyl alcohol and Brønsted acid site (O3 ⋯ Hz-O1) and 2) the hydrogen atom at the hydroxyl group of n-butyl alcohol and the oxygen of zeolite (O3-H⋯O2). Whereas only one strong hydrogen bond (O3 ⋯ Hz-O1) occurs in the side-on adsorption structure (Ads2_sideon). The O3…Hz distances are 1.403 and 1.407 Å for the end-on and the side-on structures, respectively. This distance corresponds with the calculated adsorption energies for the end-on and the side-on structures to be -31.5 and -29.1 kcal/mol, respectively. With this small difference of the adsorption energies, the n-butyl alcohol can possibly change its adsorption form without a significant energy change.

The conversion of n-butyl alcohol to isobutylene is achieved via the consecutive dehydration and skeletal isomerization. The dehydration of n-butyl alcohol over theta-1 zeolite can be considered as either a stepwise or a concerted mechanism. While skeletal isomerization is proposed in two pathways depending on the existence of the carbenium ion intermediate.
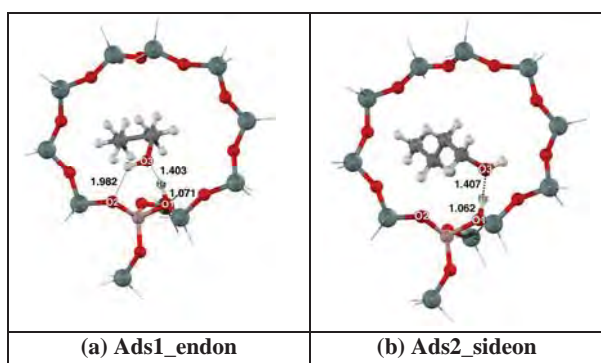
Figure 2. The optimized structures of the adsorption complexes on the 12T cluster model of Theta-1: (a) endon n-butyl alcohol adsorption b) sideon n-butyl alcohol adsorption

1. Dehydration of n-butyl alcohol on Theta-1 zeolite

The dehydration of n-butyl alcohol on the theta-1 zeolite is proposed to be a stepwise mechanism. After the first step of adsorption, the Brønsted proton of zeolite interacts with the end-on n-butyl alcohol adsorption to form the alkoxide intermediate through the transition state (TS1_dehy). The transition state, the breaking of the C1-O3 **bond and forming the C1-O2 bond occur with one imaginary frequency at 401i cm^{-1}. This step requires the activation energy of 42.9 kcal/mol. The primary alkoxide intermediate is formed (Int_butox+H$_2$O) with the energy of -9.8 kcal/mol. The *desorption water of the alkoxide intermediate (Int2_butox) requires 1.7 kcal/mol. The next step is the primary alkoxide intermediate (Int2_butox) which changes to butylene via the transition state (TS_form). The breaking of the C1-O2 bond, the C2-H bond and forming the H-O1 bond of transition state require the activation energy of 33.4 kcal/mol. The n- butylene product occurs with the relative energy of 6.0 kcal/mol.

2. Skeletal isomerization of butylene on Theta-1 zeolite

After the dehydration occurs, the n-butylene can be converted to isobutylene via skeletal isomerization. The reaction mechanism is proposed to be four steps: 1) the protonation of adsorbed butylene to give the secondary butoxide intermediate (Int4_2-butox), 2) the conversion of the secondary alkoxide intermediate to a branched primary compound via a cyclic transition state (Int5_iso_butox), 3) the proton transfer to form the *tert*-butyl carbenium ion (Int6_tert) and 4) the deprotonation of the carbenium intermediate leading to the isobutylene product (Pro_isobut).

The first step, the transition state (TS_but_pro) proceeds via the forming of the C2-O2 bond and breaking of the C1-Hz bond. The C1-C2 bond changes from a double to a single bond. This step requires the activation energy of 19.9 kcal/mol. The secondary alkoxide intermediate (Int4_2-butox) is formed with a relative energy of 0.8 kcal/mol. The second step is the conversion of the secondary alkoxide intermediate to a branched primary compound via a cyclic transition state (TS_conver), the methy group transferring, with the activation energy of 32.1 kcal/mol. The primary butoxide intermediate (Int5_iso_butox) is the product of this step with the energy of -3.7 kcal/mol.(see Figure 6 for the structural information)
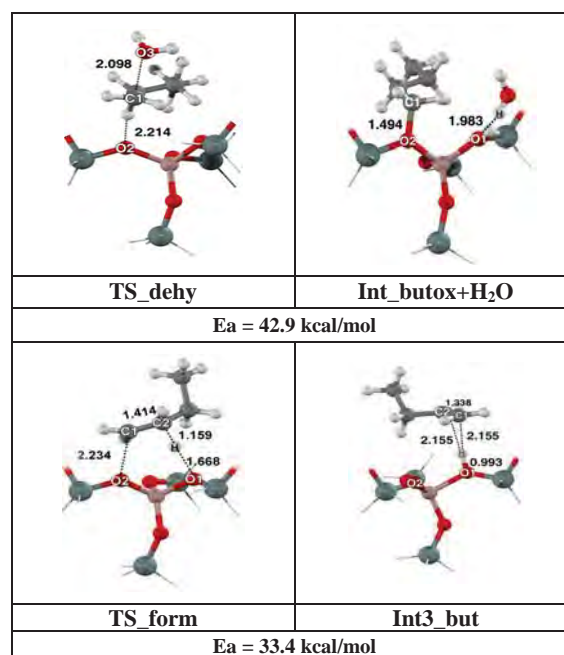
Figure 3. The optimized structures of the n-butyl alcohol dehydration step (stepwise mechanism) on the 12T cluster model of Theta-1

Next, the third step (The structures are shown in Figure 6) is the proton transfer to form the carbenium ion via the transition state (TS_cat). At this step, the C3-O1 bond breaks and one hydrogen atom transfers from the C2 to the C3 atom with the activation energy of 32.4 kcal/mol. The carbenium ion (Int6_tert) is not stable and can easily transform to isobutylene via the transition state (TS_H_shf) with the activation energy of only 0.5 kcal/mol. The final product is isobutylene (Prod_isobut) which interacted with the zeolite via the hydrogen bond between the π bond of butylene and the Brønsted acid of zeolite. The desorption energy of isobutylene on theta-1 is calculated to be 17.1 kcal/mol.

The concerted mechanism from the primary butoxide intermediate to isobutylene is proposed via the transition state (TS_decom) which is shown in Figure 7. The activation energy is 34.1 kcal/mol. These results show whether the mechanism from butylene to isobutylene should proceed via the carbenium ion or not, because of a very small amount of energy difference in the high temperature reaction process.

The overall reaction is calculated to be an endothermic reaction with the reaction energy of 16.9 kcal/mol. The first step of dehydrogenation of the butyl alcohol to the n-butylene is proposed to be the rate determining step of this reaction. This study will be beneficial for the further reaction mechanism to produce biomass to chemicals with zeolite catalysis.

Ea = 19.9 kcal/mol

Ea = 32.1 kcal/mol
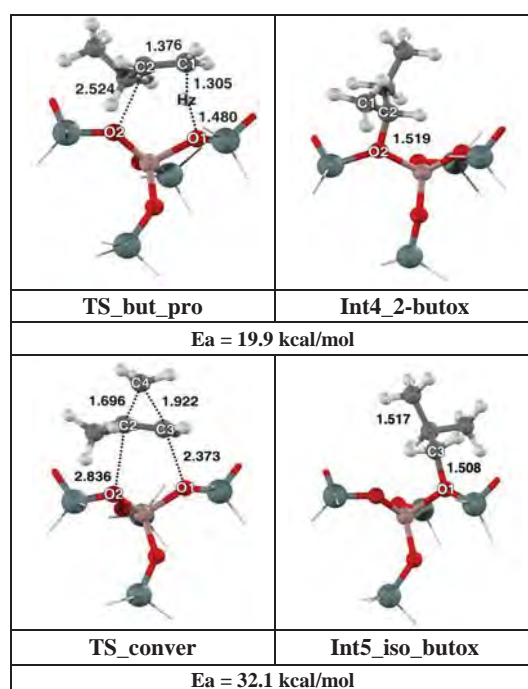
Figure 5. The optimized structures of protonation of the butylene step and conversion of the secondary to branched primary alkoxide intermediate step on the 12 cluster model of Theta-1.

Ea = 32.4 kcal/mol

Ea = 0.5 kcal/mol
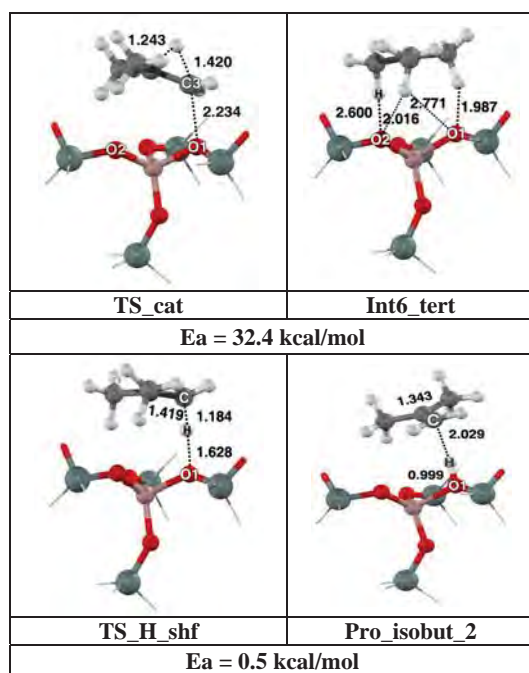
Figure 6. The optimized structures of the transition state and the intermediate complex on the isomerization mechanism proceeding via the carbenium ion.

Ea = 34.1 kcal/mol
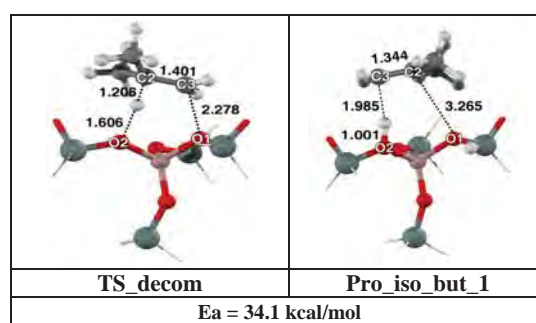
Figure 7. The optimized structures of the decomposition of the branched primary alkoxide intermediate to the isobutylene step (concerted mechanism) on the 12 cluster model of Theta-1.

Conclusions

Conversion of a bundle of biomass derived butyl alcohol to isobutylene over theta-1 zeolite has been a subject of great industrial significance. We investigated this by the M06-2X/6-31G(d,p) level of theory. The isobutylene production can proceed the stepwise mechanism of dehydration of butyl alcohol to produce butylene resulting in an isomerisation reaction to form isobutylene. First, the reaction began with the dehydration of butyl alcohol resulting from the butoxide intermediate forming 1-butylene with the activation barrier of 42.9 and 33.4 kcal/mol, respectively. The butoxide intermediate formation step is the rate determining step for the overall reaction. Next, the skeletal isomerization occurred through the carbenium ions. The four steps from butylene to isobutylene are proposed with activation energies of 19.9, 32.1, 32.4 and 0.5 kcal/mol, respectively. The obtained results suggest that the reaction mechanisms of direct conversion of n-butyl alcohol to isobutylene preferably proceeds via the concerted reaction pathway.

References

(1) Vane, L. M. *J. Chem. Technol. Biotechnol.* **2005**, *80*, 603-629.
(2) Qureshi, N.; Ezeji, T. C. *Biofuels, Bioproducts and Biorefining* **2008**, *2*, 319-330.
(3) Mashkina, A. V.; Khairulina, L. N. *Kinet. Catal.* **2002**, *43*, 684-690.
(4) West, R. M.; Braden, D. J.; Dumesic, J. A. *J. Catal.* **2009**, *262*, 134-143.
(5) Boronat, M.; Viruela, P.; Corma, A. *J. Phys. Chem. A* **1998**, *102*, 982-989.
(6) Onyestyak, G.; Valyon, J.; Pal-Borbely, G.; Rees, L. V. C. *Appl. Surf. Sci.* **2002**, *196*, 401-407.
(7) Namuangruk, S.; Tantanak, D.; Limtrakul, J. *J. Mol. Catal. A:Chem* **2006**, *256*, 113-121.
(8) Boronat, M.; Viruela, P.; Corma, A. *Phys. Chem. Chem. Phys.* **2001**, *3*, 3235-3239.

(9)   Zhang, D. Z.; Al-Hajri, R.; Barri, S. A. I.; Chadwick, D. *Chem. Commun. (Cambridge, U. K.)* **2010**, *46*, 4088-4090.
(10) Macho, V.; Kralik, M.; Jurecekova, E.; Hudec, J.; Jurecek, L. *Appl. Catal., A* **2001**, *214*, 251-257.
(11) Seo, G.; Kim, N. H.; Lee, Y. H.; Kim, J. H. *Catal. Lett.* **1999**, *57*, 209-215.
(12) Čejka, J.; Wichterlová, B.; Sarv, P. *Appl. Catal., A* **1999**, *179*, 217-222.
(13) Barri, S. A. I.; Smith, G. W.; White, D.; Young, D. *Nature* **1984**, *312*, 533-534.
(14) Guisnet, M.; Andy, P.; Gnep, N. S.; Benazzi, E.; Travers, C. *Revue de l'Institute Francais du Petrole* **1999**, *54*, 23-28.
(15) Pirngruber, G. D.; Seshan, K.; Lercher, J. A. *Microporous Mesoporous Mater.* **2000**, *38*, 221-237.
(16) Fang, X.; Tong, G.; Liao, S.; Liu, Q.; Liu, P.; Yao, C.; Xie, L. *Petroleum Refinery Engineering* **2004**, *34*, 1-4.
(17) Kasuriya, S.; Namuangruk, S.; Treesukol, P.; Tirtowidjojo, M.; Limtrakul, J. *J. Catal.* **2003**, *219*, 320-328.
(18) Injan, N.; Pannorad, N.; Probst, M.; Limtrakul, J. *Int. J. Quantum Chem.* **2005**, *105*, 898-905.
(19) Namuangruk, S.; Tantanak, D.; Limtrakul, J. *J. Mol. Catal. A: Chem.* **2006**, *256*, 113-121.
(20) Pantu, P.; Boekfa, B.; Limtrakul, J. *J. Mol. Catal. A: Chem.* **2007**, *277*, 171-179.
(21) Wannakao, S.; Boekfa, B.; Khongpracha, P.; Probst, M.; Limtrakul, J. *ChemPhysChem* **2010**, *11*, 3432 – 3438.
(22) Boekfa, B.; Choomwattana, S.; Khongpracha, P.; Limtrakul, J. *Langmuir* **2009**, *25*, 12990-12999.
(23) Maihom, T.; Boekfa, B.; Sirijaraensre, J.; Nanok, T.; Probst, M.; Limtrakul, J. *J. Phys. Chem. C* **2009**, *113*, 6654-6662.
(24) Kumsapaya, C.; Bobuatong, K.; Khongpracha, P.; Tantirungrotechai, Y.; Limtrakul, J. *J. Phys. Chem. C* **2009**, *113*, 16128-16137.
(25) Boronat, M.; Zicovich-Wilson, C. M.; Viruela, P.; Corma, A. *J. Phys. Chem. B* **2001**, *105*, 11169-11177.
(26) Boronat, M.; Zicovich-Wilson, C. M.; Viruela, P.; Corma, A. *Chem.-Eur. J.* **2001**, *7*, 1295-1303.
(27) Frisch, M. J. T., G. W.; Schlegel, H. B.; Scuseria, G. E.; Robb, M. A.; Cheeseman, J. R.; Montgomery, J. A., Jr.; Vreven, T.; Kudin, K. N.; Burant, J. C.; Millam, J. M.; Iyengar, S. S.; Tomasi, J.; Barone, V.; Mennucci, B.; Cossi, M.; Scalmani, G.; Rega, N.; Petersson, G. A.; Nakatsuji, H.; Hada, M.; Ehara, M.; Toyota, K.; Fukuda, R.; Hasegawa, J.; Ishida, M.; Nakajima, T.; Honda, Y.; Kitao, O.; Nakai, H.; Klene, M.; Li, X.; Knox, J. E.; Hratchian, H. P.; Cross, J. B.; Adamo, C.; Jaramillo, J.; Gomperts, R.; Stratmann, R. E.; Yazyev, O.; Austin, A. J.; Cammi, R.; Pomelli, C.; Ochterski, J. W.; Ayala, P. Y.; Morokuma, K.; Voth, G. A.; Salvador, P.; Dannenberg, J. J.; Zakrzewski, V. G.; Dapprich, S.; Daniels, A. D.; Strain, M. C.; Farkas, O.; Malick, D. K.; Rabuck, A. D.; Raghavachari, K.; Foresman, J. B.; Ortiz, J. V.; Cui, Q.; Baboul, A. G.; Clifford, S.; Cioslowski, J.; Stefanov, B. B.; Liu, G.; Liashenko, A.; Piskorz, P.; Komaromi, I.; Martin, R. L.; Fox, D. J.; Keith, T.; Al-Laham, M. A.; Peng, C. Y.; Nanayakkara, A.; Challacombe, M.; Gill, P. M. W.; Johnson, B.; Chen, W.; Wong, M. W.; Gonzalez, C.; Pople, J. A. Gaussian 03, revision B.05; Gaussian, Inc.: Pittsburgh, PA, **2003**.

Quantum Effect on the Reaction Mechanism of Propene Oxide Isomerization in H-ITQ-22: A DFT Investigation

Kulwadee Theanngern[a,b,c], *Bundet Boekfa*[b,c,d],
Pipat Khongpracha[a,b,c] *and* *Jumras Limtrakul*[a,b,c*]

[a] Laboratory for Computational and Applied Chemistry, Department of Chemistry, Faculty of Science and Center of Nanotechnology, Kasetsart University Research and Development Institute, Kasetsart University, Bangkok 10900, Thailand
[b] NANOTEC Center of Excellence, National Nanotechnology Center, Kasetsart University, Bangkok 10900, Thailand
[c] Center for Advanced Studies in Nanotechnology and Its Applications in Chemical, Food and Agricultural Industries, Kasetsart University, Bangkok 10900, Thailand
[d] Chemistry Department, Faculty of Liberal Arts and Science, Kasetsart University Kamphaeng Saen Campus, Nakhon Pathom73140, Thailand

Introduction

The reactive epoxide, driven from the constraint of the three-membered ring, makes it suitable to be a building block in the synthesis of organic compounds and polymers. The use of epoxide as a chemical starting material is of great current interest from both academic and industrial viewpoints. Propene oxide is one of the most important epoxides with a huge application in polymer industries[1-4]. The reaction of propene oxide that is attracting attention is the "ring-opening isomerization" to various oxygenated products, especially propanal and propanone[5-7]. This process can be catalyzed by either homogeneous or heterogeneous catalysts such as Al_2O_3, Al_2O_3-SiO_2, ZnO[8], Nafion-H, and zeolites[9-10]. The most current catalysts for this process are deficient in the versatility to be selective for the desired products. It is desirable to develop a catalytic process which is able to handle and give a beneficial selectivity.

Zeolite is an aluminosilicate porous material widely used in petroleum refineries and petrochemical industries[11-18]. Owing to its shape selectivity, intrinsic acidity and simple separation system, this material is one of the candidates for this process. Recently, Andras Fasi and co-workers studied the ring-opening isomerization of epoxide in various zeolites, including H-ZSM-5[9-10]. Their results showed that the reaction of epoxide in zeolite lead to the carbonyl compounds and propanal was the major product when H-ZSM-5 was employed as a catalyst. The comprehensive mechanistic study of this reaction in zeolite was initiated with the quantum chemical calculation[19]. Propene oxide isomerization over H-ZSM-5 zeolite was proposed in two mechanisms based on the reaction products, propanal and propanone. The ring-opening step was found to be the rate-determining step with activation barriers of 38.5 kcal/mol and 42.4 kcal/mol for propanal and propanone, respectively.

ITQ-22 (IWR) is the synthetic multipore zeolite with the dimension 8 x 10 x 12 membered ring pore structure[20]. Conventionally, this novel zeolite is applied for the isomerization of m-xylene, the disproportionation of m-xylene and the alkylation of benzene with isopropanol or propylene. The catalytic selectivity toward these reactions has proved to be better than ZSM-5 zeolite.

The exchange functional is required to realistically describe the interaction of ITQ-22 and the probing species. Therefore, the periodic calculation seems not to take into account some effects such as the van de Waals interaction, while the small quantum cluster is not able to represent the confinement effect of the zeolite framework.[21-23] The M06-2X functional recently developed by Zhao and Thrular[24-25] has been successfully applied to study the adsorption and reaction mechanisms of non-polar and aromatic molecules on zeolites.[26-29]

The aim of this work is to study the propene oxide isomerization over the multipore ITQ-22 zeolite using the density functional theory. The detailed reaction mechanism of propene oxide to propanal and propanone have been discussed.

Methods

The geometry of the ITQ-22 zeolite was obtained from the crystallographic structure[20]. The 14T quantum cluster where T means the tetrahedral unit of Si or Al atoms was used for representing the active site of ITQ-22 zeolite. The cluster covers the 12-membered ring at the intersection cavity. One Si atom was replaced with an Al atom at the most appropriate T1 position and subsequently one proton was added to the system yielding a Brønsted acid site. All geometries were optimized with the M06-2X functional using the 6-31G(d,p) basis set. Only the active region, $\equiv SiO(H)Al(OSi)_4\equiv$, and the probe molecule were allowed to relax while the rest was kept fixed with the crystallographic structure. Only one imaginary frequency with its vibration corresponding to the transition structure was confirmed by frequency calculation. In order to examine the effect of the extended framework, single point calculations were performed on a 58T quantum cluster covered intersection and 8-, 10- and 12-MR windows of ITQ-22 as shown in Fig 1. All calculations were carried out by the Gaussian 03 package[30] incorporated with the Minnesota Density Functionals module 3.1 by Zhao and Truhlar.
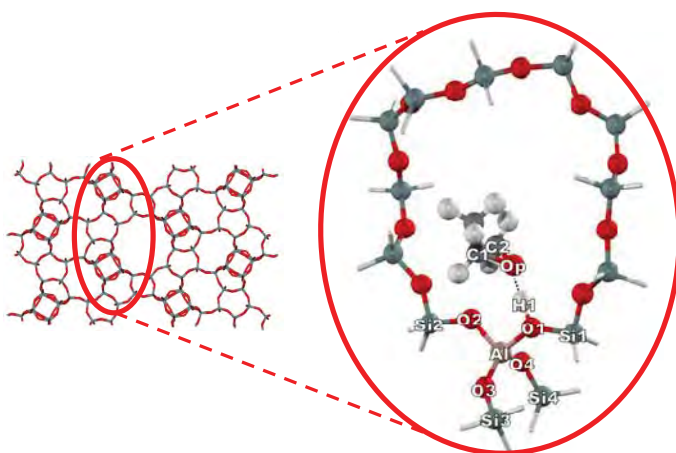
Figure 1. The selected structure of the 14T cluster of H-ITQ-22 zeolite.

Results and Discussion

The Zeolite Model and Adsorption Complexes. The active site of ITQ-22 zeolite calculated by the 14T quantum cluster is shown in Figure 1. The optimized geometric parameters from the 14T quantum cluster are tabulated in Table 1. The Brønsted acid O1-Hz bond distance is 0.97 Å. The Al···Hz distance is 2.35 Å, which compared well with the experimental value (2.38-2.48 Å).

The propene oxide adsorbed on the Brønsted acid site with the hydrogen bond at the intersection of ITQ-22 is shown in Figure 2. Two optimum adsorption configurations are found, namely ADS_A and ADS_B with comparable adsorption energies of -24.09 and -24.51 kcal/mol, respectively. On both adsorption complexes, most of the geometric parameters are the same (see Table 1 and Table 2). The Brønsted acid O1-Hz bond distance is significantly increased from 0.97 to 1.06 Å. Strong hydrogen bond interactions in both configurations are confirmed by high adsorption energy; a short

intermolecular distance between the propene oxide and the Brønsted acid of zeolite H1···Op (1.42 and 1.41 Å) and the nearly linear arrangement of O1-H1-Op angle (174.69 and 175.49 degrees). The shorter H1···Op distance of ADS_B refers to the higher interaction with the zeolite. The calculated adsorption energies are in the range of the experimental data of acetone adsorbed on H-ZSM-5 zeolite (-31.1 kcal/mol). [31]

a) ADS_A
ΔE = -24.09 kcal/mol

b) ADS_B
ΔE = -24.51 kcal/mol
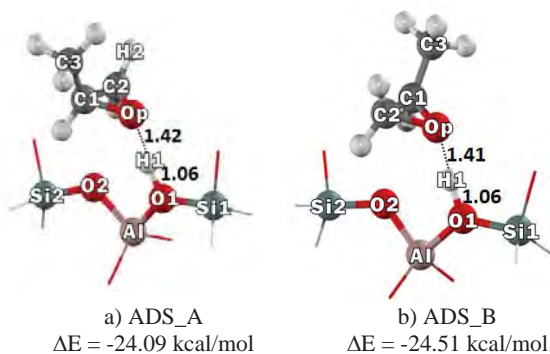
Figure2. Optimized structure of propene oxide on H-ITQ-22 zeolite: a) ADS_A and b) ADS_B. Distances are in Ås.

The Reaction Mechanism of Isomerization of Propene Oxide. The isomerization reaction of propene oxide occur via the C-O bond breaking in the propene oxide. Two different types of products, propanal and propanone, are produced from the breaking of the C-O bond at the tertiary carbon (C1-Op) and the other carbon atom (C2-Op). The energy profiles of both competitive routes are shown in Figure 3 and Figure 5.
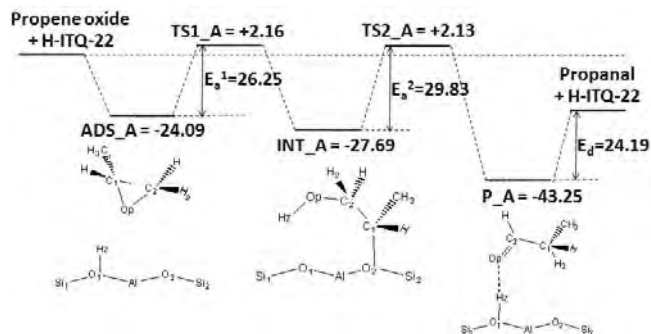
Figure3. The calculated energy profile for the isomerization of propene oxide to propanal over 14T clusters.

For a reaction that gives a propanal product, the reaction mechanism is proposed to be a stepwise mechanism. The optimized structures of all reaction intermediates are tabulated in Table 1. After the adsorption, ADS_A, the C1-Op bond is broken to produce a secondary alkoxide intermediate, INT_A. At the transition state structure, the C1-Op bond is broken and the coordination of C1 is changed from tetrahedral to the planar form. Only one imaginary frequency from the transition structure is observed at –497.41 cm^{-1} corresponding with the moving of O1-H1 bond and the breaking of the C1-Op bond. The calculated activation barrier is 26.25 kcal/mol. The intermediate, INT_A, is formed subsequently to this step and has a relative energy -27.69 kcal/mol with respect to the starting reagent.

a) TS1_A
ΔE = 2.16 kcal/mol

b) INT_A
ΔE = -27.69 kcal/mol

c) TS2_A
ΔE = 2.13 kcal/mol

d) P_A
ΔE = -43.25 kcal/mol

Figure 4. Optimized structure of propene oxide to propanal on H-ITQ-22 zeolite: a) TS1_A, b) INT_A, c) TS2_A and d) P_A. Distances are in Ås.

Table 1. Optimized Structural Parameters of the Adsorption and Reaction Complexes of Propene oxide to Propanal on H-ITQ-22 Zeolite. Distances are in Ås and Angles are in Degrees.

parameter	Bare	ADS_A	TS1_A	INT_A	TS2_A	P_A
Distances						
O1-H1	0.97	1.06	1.85	2.56	1.78	1.08
Al-H1	2.35	2.20	3.04	3.79	2.67	2.43
Al-O1	1.89	1.83	1.74	1.71	1.75	1.84
Al-O2	1.70	1.71	1.76	1.85	1.74	1.70
O1-Si1	1.69	1.67	1.61	1.60	1.61	1.66
O2-Si2	1.62	1.61	1.62	1.70	1.61	1.61
H1-Op		1.42	0.98	0.97	0.99	1.38
Op-C1	1.42	1.44	2.39	2.45	2.41	2.39
Op-C2	1.42	1.44	1.38	1.40	1.34	1.23
C1-C2	1.47	1.47	1.48	1.55	1.41	1.49
C1-H2	1.09	2.23	2.02	2.15	1.49	1.10
C2-H2	2.20	1.09	1.11	1.09	1.23	2.09
O2-C1		3.04	2.63	1.52	2.34	3.48
O2-C2		2.95	3.27	2.53	2.52	2.64
Angles						
Si1-O1-Al	135.8	133.8	135.7	138.1	140.2	133.8

The next step is the 1,2 hydride shift where H transfers from the C2 atom to the C1 atom and concurrently the proton H1 moves back

to the zeolite. The transition state, TS2_A, is confirmed by one imaginary frequency at –709.25 cm^{-1} where the vibration shows consecutive movement between the intermediate INT_A and the product. The activation barrier is calculated to be 29.83 kcal/mol. Therefore, this step is the rate-determining step of this pathway. The propanal product, P_A has a relative energy of -43.25 kcal/mol. The desorption energy of propanol from the ITQ-22 is calculated to be 24.19 kcal/mol. The propene oxide isomerization to propanal is exothermic reaction with the heat of reaction -19.06 kcal/mol.
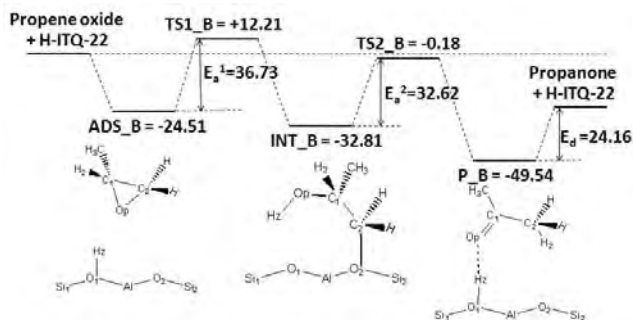
Figure5. The calculated energy profile for the isomerization of propene oxide to propanone over 14T clusters.

a) TS1_B
ΔE = 12.21 kcal/mol

b) INT_B
ΔE = -32.81 kcal/mol

c) TS2_B
ΔE = -0.18 kcal/mol

d) P_B
ΔE = -49.54 kcal/mol

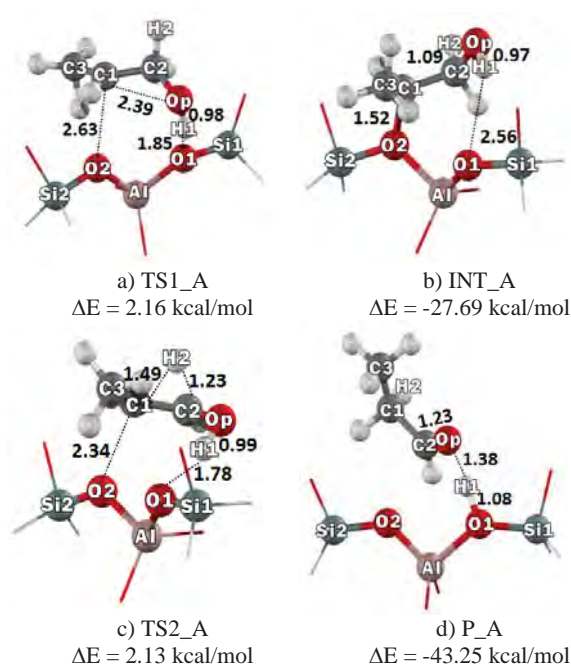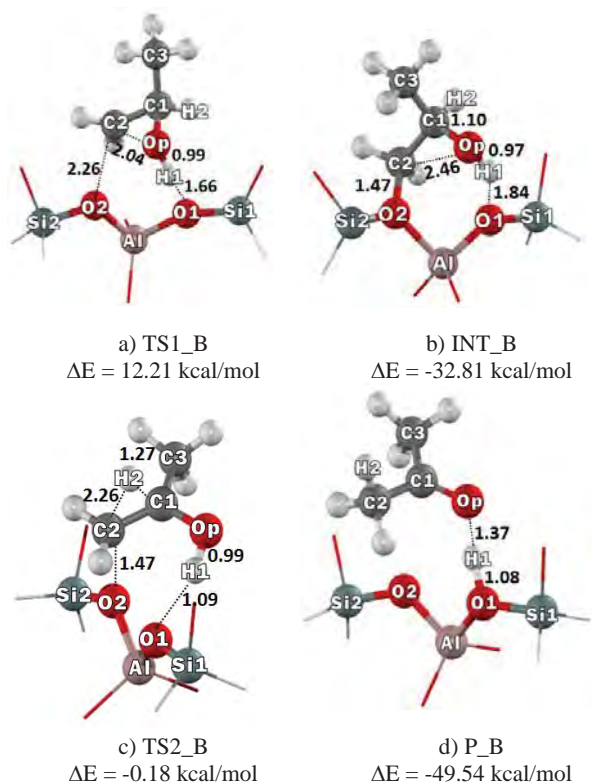**Figure 6**. Optimized structure of propene oxide to propanone on H-ITQ-22 zeolite: a) TS1_B, b) INT_B, c) TS2_B and d) P_B. Distances are in Ås.

For the propanone production route, the reaction mechanism is similar to with the propanal route. The reaction is proposed to be a stepwise mechanism as shown in Figure 5. The optimized geometric

parameters of all reaction intermediates are tabulated in Table 2. First, propene oxide adsorbed on the ITQ-22 zeolite forms the adsorption complex ADS_B. The propene oxide molecule is then protonated at the Op atom and the C2-Op bond is broken yielding the carbenium ion activated complex. For the transition state, TS1_B, requires the energy barrier of 36.73 kcal/mol, which is higher than that in the propanal step. This is due to the fact that a carbenium ion in the TS1_B is considered to be a primary carbenium ion that is less stable than a secondary carbenium ion, as in the TS1_A transition structure. The reaction generates the primary alkoxide intermediate, INT_B, with a relative energy of -32.81 kcal/mol. Next, the reaction goes through the transition state, TS2_B, which is a 1,2 hydride shift transfer from the C1 atom to the C2 atom and the return of the acidic proton H1. This step requires the energy barrier of 32.62 kcal/mol. The propanone product has a relative energy of -49.54 kcal/mol. The desorption energy of propanone from ITQ-22 is 24.16 kcal/mol. The propene oxide isomerization to propanone is an exothermic reaction with the heat of reaction -25.38 kcal/mol.

The isomerization of propene oxide to propanal and propanone on H-ITQ-22 has been successfully studied with the M06-2X functional. The rate determining step requires activation energies 29.83 and 36.73 kcal/mol for propanal and propanone, respectively. This leads to the conclusion that propanal is the major product from the propene oxide isomerization reaction. Our findings are also confirmed by the experiment data that higher selectivity of propanal over propanone is observed in propene oxide isomerization using zeolite as a catalyst[9].

Table2. Optimized Structural Parameters of the Adsorption and Reaction Complexes of Propene Oxide to Propanone on H-ITQ-22 zeolite. Distances are in Ås and Angles are in Degrees.

parameter	Bare	ADS_B	TS1_B	INT_B	TS2_B	P_B
Distances						
O1-H1	0.97	1.06	1.66	1.84	1.83	1.08
Al-H1	2.35	2.42	2.70	2.77	2.91	2.38
Al-O1	1.89	1.83	1.75	1.72	1.75	1.83
Al-O2	1.70	1.71	1.74	1.85	1.76	1.71
O1-Si1	1.69	1.67	1.62	1.61	1.61	1.67
O2-Si2	1.62	1.61	1.62	1.70	1.62	1.60
H1-Op		1.41	0.99	0.97	0.98	1.37
Op-C1	1.42	1.44	1.42	1.40	1.33	1.23
Op-C2	1.42	1.44	2.04	2.46	2.38	2.39
C1-C2	1.47	1.47	1.47	1.55	1.41	1.50
C1-H2	2.21	1.09	1.09	1.10	1.27	2.11
C2-H2	1.09	2.17	2.16	2.12	1.48	1.10
O2-C1		2.98	3.25	2.50	3.24	2.80
O2-C2		3.03	2.26	1.47	2.05	2.91
Angles						
Si1-O1-Al	135.8	134.2	136.3	139.8	136.3	133.5

Conclusion

The selective isomerization of propene oxide over multi-nanopore zeolite, H-ITQ-22, has been investigated with the

M06-2X/6-31G(d,p) method. A 14T quantum cluster covered the intersection 12 membered ring was used to represent the acid site, where T is Si or Al atoms. The reaction mechanisms were proposed through the ring opening and the 1,2 hydride rearrangement. Two different pathways were systematically examined leading to the targeted products, namely propanal and propanone. The rate determining step leading to propanal was observed to be the 1,2 hydride rearrangement with an activation barrier of 29.8 kcal/mol, whereas, the ring-opening step was found to be the rate-determining step for propanone with an activation barrier of 36.7 kcal/mol. With chemically realistic and well-calibrated models together with an accurate DFT method, our findings clearly demonstrate that H-ITQ-22 zeolite is one of the good catalysts for the selective isomerization of propene oxide for the production of propanal.

References
(1) Smith, J. G. *Synthesis* **1984**, 629.
(2) Katsuki, T.; Sharpless, K. B. *J. Am. Chem. Soc.* **1980**, *102*, 5974.
(3) Cheng, Z.; Zhu, X.; Fu, G. D.; Kang, E. T.; Neoh, K. G. *Macromolecules* **2005**, *38*, 7187.
(4) Carlier, P. R. *Angew. Chem., Int. Ed.* **2004**, *43*, 2602.
(5) Ranu, B. C.; Jana, U. *J. Org. Chem.* **1998**, *63*, 8212.
(6) Karamé, I.; Tommasino, M. L.; Lemaire, M. *Tetrahedron Lett.* **2003**, *44*, 7687.
(7) Procopio, A.; Dalpozzo, R.; De Nino, A.; Nardi, M.; Sindona, G.; Tagarelli, A. *Synlett* **2004**, 2633.
(8) Molnár, Á.; Bucsi, I.; Bartók, M.; Resofszki, G.; Gáti, G. *J. Catal.* **1991**, *129*, 303.
(9) Fási, A.; Gömöry, A.; Pálinkó, I.; Kiricsi, I. *J. Catal.* **2001**, *200*, 340.
(10) Fási, A.; Pálinkó, I.; Gömöry, A.; Kiricsi, I. *J. Mol. Catal. A: Chem.* **2004**, *208*, 307.
(11) Andy, P.; Gnep, N. S.; Guisnet, M.; Benazzi, E.; Travers, C. *J. Catal.* **1998**, *173*, 322.
(12) Bhan, A.; Iglesia, E. *Acc. Chem. Res.* **2008**, *41*, 559.
(13) Corma, A. *J. Catal.* **2003**, *216*, 298.
(14) Hsia Chen, C. S.; Bridger, R. F. *J. Catal.* **1996**, *161*, 687.
(15) Luzgin, M. V.; Rogov, V. A.; Arzumanov, S. S.; Toktarev, A. V.; Stepanov, A. G.; Parmon, V. N. *Angew. Chem., Int. Ed.* **2008**, *47*, 4559.
(16) Smit, B.; Maesen, T. L. M. *Nature* **2008**, *451*, 671.
(17) Venuto, P. B. *Microporous Materials* **1994**, *2*, 297.
(18) Yaluris, G.; Rekoske, J. E.; Aparicio, L. M.; Madon, R. J.; Dumesic, J. A. *J. Catal.* **1995**, *153*, 65.
(19) Namuangruk, S.; Khongpracha, P.; Pantu, P.; Limtrakul, J. *J. Phys. Chem. B* **2006**, *110*, 25950.
(20) Corma, A.; Rey, F.; Valencia, S.; Jordá, J. L.; Rius, J. *Nature Materials* **2003**, *2*, 493.
(21) Namuangruk, S.; Tantanak, D.; Limtrakul, J. *J. Mol. Catal. A: Chem.* **2006**, *256*, 113.
(22) Pantu, P.; Boekfa, B.; Limtrakul, J. *J. Mol. Catal. A: Chem.* **2007**, *277*, 171.
(23) Pantu, P.; Boekfa, B.; Sunpetch, B.; Limtrakul, J. *Chem. Eng. Commun.* **2008**, *195*, 1477.
(24) Zhao, Y.; Truhlar, D. G. *J. Phys. Chem. C* **2008**, *112*, 6860.
(25) Zhao, Y.; Truhlar, D. G. *Acc. Chem. Res.* **2008**, *41*, 157.
(26) Boekfa, B.; Choomwattana, S.; Khongpracha, P.; Limtrakul, J. *Langmuir* **2009**, *25*, 12990.
(27) Kumsapaya, C.; Bobuatong, K.; Khongpracha, P.; Tantirungrotechai, Y.; Limtrakul, J. *J. Phys. Chem. C* **2009**, *113*, 16128.
(28) Maihom, T.; Boekfa, B.; Sirijaraensre, J.; Nanok, T.; Probst, M.; Limtrakul, J. *J. Phys. Chem. C* **2009**, *113*, 6654.
(29) Maihom, T.; Pantu, P.; Tachakritikul, C.; Probst, M.; Limtrakul, J. *J. Phys. Chem. C* **2010**, *114*, 7850.
(30) Frisch, M. J.; Trucks, G. W.; Schlegel, H. B.; Scuseria, G. E.; Robb, M. A.; Cheeseman, J. R.; Montgomery, J. A.; Vreven, T.; Kudin, K. N.; Burant, J. C.; Millam, J. M.; Iyengar, S. S.; Tomasi, J.; Barone, V.; Mennucci, B.; Cossi, M.; Scalmani, G.; Rega, N.; Petersson, G. A.; Nakatsuji, H.; Hada, M.; Ehara, M.; Toyota, K.; Fukuda, R.; Hasegawa, J.; Ishida, M.; Nakajima, T.; Honda, Y.; Kitao, O.; Nakai, H.; Klene, M.; Li, X.; Knox, J. E.; Hratchian, H. P.; Cross, J. B.; Adamo, C.; Jaramillo, J.; Gomperts, R.; Stratmann, R. E.; Yazyev, O.; Austin, A. J.; Cammi, R.; Pomelli, C.; Ochterski, J. W.; Ayala, P. Y.; Morokuma, K.; Voth, G. A.; Salvador, P.; Dannenberg, J. J.; Zakrzewski, V. G.; Dapprich, S.; Daniels, A. D.; Strain, M. C.; Farkas, O.; Malick, D. K.; Rabuck, A. D.; Raghavachari, K.; Foresman, J. B.; Ortiz, J. V.; Cui, Q.; Baboul, A. G.; Clifford, S.; Cioslowski, J.; Stefanov, B. B.; Liu, G.; Liashenko, A.; Piskorz, P.; Komaromi, I.; Martin, R. L.; Fox, D. J.; Keith, T.; Al-Laham, M. A.; Peng, C. Y.; Nanayakkara, A.; Challacombe, M.; Gill, P. M. W.; Johnson, B.; Chen, W.; Wong, M. W.; Gonzalez, C.; Pople, J. A. *Gaussian 03, revision B.05*, 2003.
(31) Šepa, J.; Lee, C.; Gorte, R. J.; White, D.; Kassab, E.; Evleth, E. M.; Jessri, H.; Allavena, M. *Journal of Physical Chemistry* **1996**, *100*, 18515.

STRUCTURES AND REACTION MECHANISMS OF BUTADIENE CYCLOADDITION OVER METAL-EXCHANGED FAUJASITE

Thittaya Yutthalekha [a,b,c], *Kanokwan Kongpatpanich* [a,b,c],
Thana Maihom [a,b,c], *Bundet Boekfa* [b,c,d],
and Jumras Limtrakul [a,b,c]

[a] Laboratory for Computational and Applied Chemistry, Department of Chemistry, Faculty of Science and Center of Nanotechnology, Kasetsart University Research and Development Institute, Kasetsart University, Bangkok 10900, Thailand
[b] NANOTEC Center of Excellence, National Nanotechnology Center, Kasetsart University, Bangkok 10900, Thailand
[c] Center for Advanced Studies in Nanotechnology and Its Applications in Chemical, Food and Agricultural Industries, Kasetsart University, Bangkok 10900, Thailand
[d] Chemistry Department, Faculty of Liberal Arts and Science, Kasetsart University Kamphaeng Saen Campus, Nakhon Pathom 73140, Thailand

Introduction

4-vinylcyclohexene (4-VCH) is primary used as the important intermediate in the synthesis of polystyrene and other useful copolymers. Currently, styrene is manufactured largely from benzene through ethylbenzene. The dehydrogenation of 4-VCH is important as an alternative route for the manufacture of styrene[1]. 4-VCH is produced through Diels–Alder cycloaddition reaction of two 1,3-butadiene molecules. Several researchers have studied this reaction in various catalysts, such as the promoted ZrO_2 catalyst, Pd catalysts supported on alumina and polyoxometalate[2-7]. This route is potentially attractive because it does not require petroleum-based aromatic feedstock and it is a fairly clean process.

The Diels–Alder cycloaddition of 1,3-butadiene to 4-VCH is a well-known thermally-initiated cycloaddition reaction between two 1,3-butadiene molecules in which one serves as the a conjugated diene and the other as the dienophile. This cyclic adduct formation of butadiene molecules has an energy barrier of 24.7 kcal/mol. It is kinetically second-order in 1,3-butadiene[8]. The catalytic role of zeolites has been understood in term that zeolites being able to confine 1,3-butadiene within their pores due to their shape and size selective properties. Thus, by increasing the 1,3-butadiene concentration inside the zeolitic pores relative to that in the external gas phase, the zeolite can enhance the rates of bimolecular reactions. In theoretical investigations, several mechanisms have been proposed for this process; the most popular are the concerted (symmetry-allowed) mechanism and the stepwise mechanism, which the latter involves the formation of a bisallyl biradical intermediate. It has been shown that both mechanisms are similar in their energetics[9-10].

Zeolites consist of hundreds of atoms per unit cell where the use of such sophisticated methods as periodic calculation are too computationally demanding and expensive. The recently developed hybrid methods, for example the embedded cluster or combined quantum mechanics/molecular mechanics (QM/MM) methods, as well as the more general Our-own-N-layered Integrated molecular Orbital + molecular Mechanics (ONIOM) method has brought more economical methods to study the adsorptions and reactions on zeolites[11-17]. More recently, the newly developed method, M06 functional, is successfully applied to study the interaction and reactions of hydrocarbon on various zeolites.[18-20]

The cycloaddition reaction of 1,3-butadiene has been studied over a large-pore zeolites, such as NaX[21-22], NaZSM-20[23],

NaBeta[23] and CuY[21,24]. Instead of the targeted cycloaddition of 1,3-butadiene, the Brønsted acid character of zeolite catalyzes the oligomerization yielding oligomeric residues such as polyolefinic species and alkenyl carbocations[25]. In the same manner as NaX, even the high butadiene conversion can be obtained but the selective for the cycloaddition adduct is relatively poor (<30%). The main products over NaX are oligomeric ones such as polyalkenes[22]. Moreover, Cu^+ exchanged zeolites were also active catalysts in many reactions, such as the direct decomposition of NO into N_2 and O_2, as well as in the selective photocatalytic reduction of NO_x, butene isomerization[26-27] and alkene oxidation[28]. The Diels–Alder cycloaddition of 1,3-butadiene over a Cu^+ exchanged zeolite gives an excellent yield of 4-VCH[25,29].

The goal of this work is to investigate the reaction mechanisms of 1,3-butadiene cycloaddition over Cu-exchanged Faujasite zeolite (Cu-FAU).

Methods

The active region consists of the 8T (T=tetrahedral of Si or Al atoms) inside the supercage, which can be considered as the smallest unit required to represent the active site of Faujasite zeolite. This was taken from the zeolite crystal lattice structures. The Si atom at the most favored position, T2, is replaced with an Al atom and a transition metal ion was placed to compensate for the charge. In the present study, we have employed the M06-2X functional using the 6-31G(d,p) basis set for H, C, O, Al and Si atoms, while the Stuttgart RSC 1997 effective core potential (ECP) were used for the Cu atom. Normal mode analyses were carried out to verify the transition states to have one imaginary frequency whose mode corresponded to the reaction coordinate. The total spin was kept constant at the singlet ground states. The charge distribution in the complexes has been analyzed via the natural population analysis (NPA). The 49T extended framework was treated with the single point calculation to represent the confinement effect of the zeolite framework. All calculations in this work have been performed by using the Gaussian 03 program[30] incorporated with the Minnesota Density Functionals module 3.1 by Zhao and Truhlar[31-32].
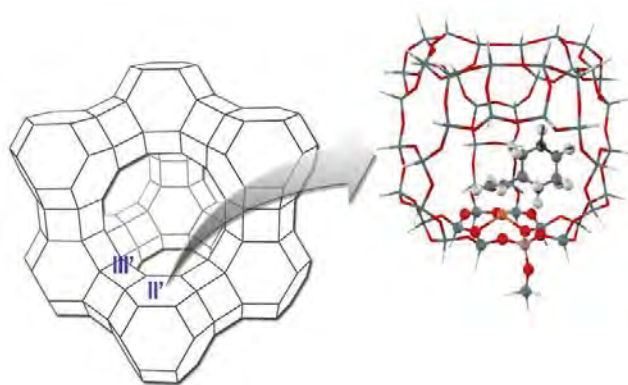

Figure 1. Model of the 49T cluster. The 8T quantum cluster is drawn as the bond and stick model.

Results and Discussion

The location of the copper cations in the zeolite framework are sites II' & III' which accessible to reactants and contribute to the activity of the catalyst[33]. The metal ion lies between the three bridging oxygen atoms of the zeolite framework. The Al-Cu bond is

3.06 Å, which agrees with experiment data[33]. Bond distances for the nearest-neighbor O and Cu atoms are shown in the Figure 1.
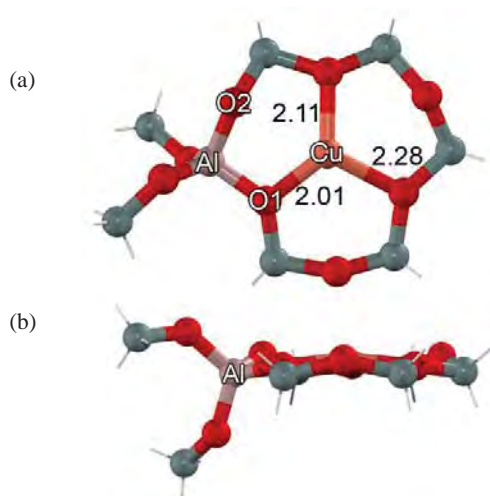

Figure 2. Optimized structure of the Cu-exchange faujasite complexes. (a) top view, (b) side view, Distances are in Å.

The optimized structures of Cu-FAU complexes and their reaction coordinates are shown in Figure 2 and the optimized geometrical parameters are tabulated in Table 1. The 1,3-butadiene adsorbs on Cu-FAU in the supercage over the 6T window of the FAU zeolite. The Al-Cu distance increases from 3.06 to 3.12 Å. The C1=C2 bond of the 1,3-butadiene was decreased to be 1.36 Å due to the π-back donation of electrons from the *d* orbitals of metal to the π* antibonding orbitals of 1,3-butadiene. The adsorption energy of 1,3-butadiene on the 8T cluster is -20.23 kcal/mol. To represent the confinement effect, the extended 49T quantum cluster gives the adsorption energy of -28.23 kcal/mol. There is no experimental data for the adsorption of butadiene on Cu-FAU. There is data only for the experiment of ethylene on Cu-FAU zeolite, which reports the adsorption energy to be -20.79 kcal/mol.

Table 1. Optimized structural parameters of reaction complexes during the cycloaddition of 1,3-butadiene over a Cu(I) faujasite which were obtained from M06-2X/6-31G(d,p) calculations.

Distance	Bare	Ads	Coads	TS	PR
Al-Cu	3.06	3.12	3.12	3.13	3.05
Si-O1	1.63	1.63	1.63	1.64	1.63
Si-O2	1.58	1.59	1.59	1.59	1.59
Al-O1	1.80	1.79	1.79	1.80	1.79
Al-O2	1.73	1.73	1.73	1.74	1.73
C1-Cu		2.25	2.24	2.57	3.55
C2-Cu		2.32	2.30	2.42	3.14
C1-C1'	-		3.36	2.02	1.53
C2-C4'	-		3.29	2.41	1.54
C1-C2	1.33	1.36	1.36	1.40	1.53
C2-C3	1.46	1.47	1.47	1.48	1.50
C3-C4	1.33	1.34	1.34	1.34	1.35
C1'-C2'	-		1.34	1.39	1.51
C2'-C3'	-		1.47	1.41	1.33
C3'-C4'	-		1.34	1.38	1.51

In the next step, another 1,3-butadiene diffuses over the adsorbed 1,3-butadiene on the metal-exchanged faujasite zeolite (Co-ads) as shown in Figure 2(b). The calculated energy on the 8T quantum cluster is -23.64 kcal/mol. The framework effect of the 49T quantum cluster increases the adsorption energy to -33.40 kcal/mol. The extended framework gives the coadsorption of the 1,3-butadiene and stabilizes the adsorption complex by 5.17 kcal/mol.
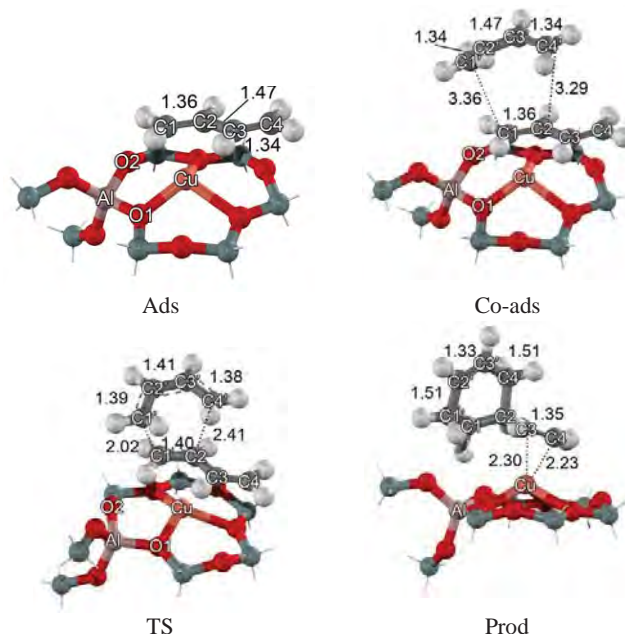
Figure 3. Optimized structures of the Cu-exchange faujasite complexes. Distances are in Å.

The cycloaddition reaction of two 1,3-butadiene give the 4-vinylcyclohexene product. The energy profile is shown in Figure 3. The transition state, the C1-C1' and C2-C4' bonds of the two 1,3-butadienes are decreased from 3.36 to 2.02 Å and 3.29 to 2.41 Å respectively. Only one imaginary frequency can be found at -559 cm^{-1} corresponding with the forming of the C1-C1' and C2-C4' bonds of the two 1,3-butadienes. This step requires activation barriers of 21.28 kcal/mol with the 8T quantum cluster. The extended framework reduces the apparent activation barrier by 8.90 kcal/mol.

In the last step, the 4-vinylcyclohexene product is strongly adsorbed to the metal atom via double of C3-C4 bond. The relative energies of the product are -71.34 and -79.07 kcal/mol for the 8T and 49T quantum cluster, respectively. The desorption energies are 20.76 and 28.49 kcal/mol for the 8T and the 49T quantum cluster, respectively.

The charge distribution in the complexes, which are analyzed by the natural population analysis (NPA), show the charge of metal ions in the Faujasite supercage to be 0.78, which is compensated by the surrounding oxygen atoms in the 6-ring inside the supercage. When 1,3-butadienes adsorbed on the metal, the charge of Cu$^+$ was decreased to 0.72, indicating that the Cu$^+$ makes 1,3-butadiene to be a better dienophile.

Table 2 Natural population analysis (NPA) parameters of reaction complexes during the cycloaddition of 1,3-butadiene over a Cu-FAU zeolite which were obtained from M06-2X/6-31G(d,p) calculations.

Atom	Bare	Ads	Coads	TS	PR
Cu	0.78	0.72	0.72	0.70	0.70
Al	2.08	2.09	2.09	2.10	2.10
O1	-1.36	-1.35	-1.36	-1.37	-1.37
O2	-1.31	-1.32	-1.32	-1.32	-1.32
C1		-0.49	-0.49	-0.49	-0.49
C2		-0.32	-0.33	-0.39	-0.39
C3		-0.26	-0.27	-0.27	-0.27
C4		-0.41	-0.41	-0.46	-0.46
C1'		-	-0.42	-0.45	-0.45
C2'		-	-0.26	-0.22	-0.22
C3'		-	-0.26	-0.28	-0.28
C4'		-	-0.42	-0.39	-0.39

The Diels–Alder cycloaddition of 1,3-butadiene on Cu-FAU is calculated with the M06-2X functional. The reaction is proposed via a concerted mechanism with an activation energy of 22.09 kcal/mol. The 4-vinylcyclohexene product is strongly adsorbed on Cu-FAU. The reaction is exothermic with a reaction energy – 50.58 kcal/mol. This calculation is useful to further produce styrene.

Figure 3. The energy profile (kcal/mol) for 8T (black line) and 49T (red line).

Conclusions

The Diels–Alder cycloaddition of 1,3-butadiene over Cu-exchange zeolite has been investigated theoretically by the M06-2X density functional. The 49T cluster is mod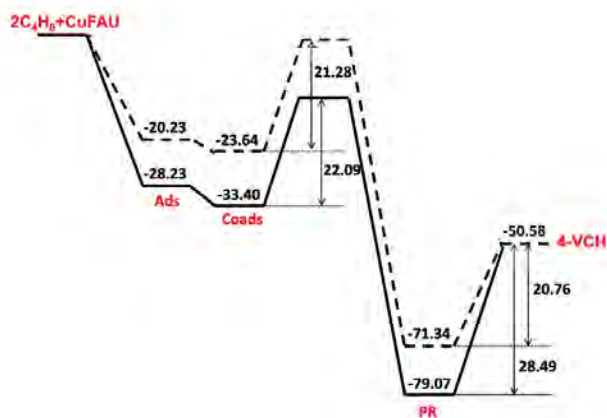eled to cover the supercage of Cu-FAU zeolite. The reaction occurs via a concerted mechanism without an intermediate. The adsorption energies are calculated to be -33.40 kcal/mol. The activation barriers are calculated to be 22.09 kcal/mol due to the metal making diene a better dienophile. The reaction is exothermic reaction with reaction energy of 50.58 kcal/mol. These results show that Cu-exchanged faujasite zeolite is active for the Diels–Alder cycloaddition of 1,3-butadiene and that it can stabilize all species in the reaction systems.

References
(1) Haggin, J. *Chemical and Engineering News* **1994**, *72*, 31.
(2) Thomas, M. L.; Fraga-Dubreuil, J.; Coote, A. S.; Poliakoff, M. *Green Chem.* **2008**, *10*, 197.
(3) Alimardanov, K. M.; Abdullayev, A. F. *Pet. Chem.* **1995**, *35*, 508.
(4) Neumann, R.; Dror, I. *Applied Catalysis A: General* **1998**, *172*, 67.
(5) De Bruyn, M.; Neumann, R. *Advanced Synthesis and Catalysis* **2007**, *349*, 1624.
(6) Choi, Y. S.; Park, Y. K.; Chang, J. S.; Park, S. E.; Cheetham, A. K. *Catal. Lett.* **2000**, *69*, 93.
(7) Castellan, A.; Tauszik, G. R. *J. Catal.* **1977**, *50*, 172.
(8) Vaughan, W. E. *J. Am. Chem. Soc.* **1932**, *54*, 3863.
(9) Li, Y.; Houk, K. N. *J. Am. Chem. Soc.* **1993**, *115*, 7478.
(10) Von Doering, W. E.; Franck-Neumann, M.; Hasselmann, D.; Kaye, R. L. *J. Am. Chem. Soc.* **1972**, *94*, 3833.
(11) Kasuriya, S.; Namuangruk, S.; Treesukol, P.; Tirtowidjojo, M.; Limtrakul, J. *J. Catal.* **2003**, *219*, 320.
(12) Pantu, P.; Pabchanda, S.; Limtrakul, J. *ChemPhysChem* **2004**, *5*, 1901.
(13) Namuangruk, S.; Pantu, P.; Limtrakul, J. *ChemPhysChem* **2005**, *6*, 1333.
(14) Sangthong, W.; Probst, M.; Limtrakul, J. *J. Mol. Struct.* **2005**, *748*, 119.
(15) Namuangruk, S.; Khongpracha, P.; Pantu, P.; Limtrakul, J. *J. Phys. Chem. B* **2006**, *110*, 25950.
(16) Namuangruk, S.; Tantanak, D.; Limtrakul, J. *J. Mol. Catal. A: Chem.* **2006**, *256*, 113.
(17) Pantu, P.; Boekfa, B.; Limtrakul, J. *J. Mol. Catal. A: Chem.* **2007**, *277*, 171.
(18) Boekfa, B.; Choomwattana, S.; Khongpracha, P.; Limtrakul, J. *Langmuir* **2009**, *25*, 12990.
(19) Kumsapaya, C.; Bobuatong, K.; Khongpracha, P.; Tantirungrotechai, Y.; Limtrakul, J. *J. Phys. Chem. C* **2009**, *113*, 16128.
(20) Maihom, T.; Pantu, P.; Tachakritikul, C.; Probst, M.; Limtrakul, J. *J. Phys. Chem. C* **2010**, *114*, 7850.
(21) Maxwell, I. E.; Downing, R. S.; Van Langen, S. A. J. *J. Catal.* **1980**, *61*, 485.
(22) Chang, J. S.; Park, S. E.; Gao, Q.; Férey, G.; Cheetham, A. K. *Chem. Commun. (Cambridge, U. K.)* **2001**, 859.
(23) Dessau, R. M. *J. Chem. Soc., Chem. Commun.* **1986**, 1167.
(24) Maxwell, I. E.; de Boer, J. J.; Downing, R. S. *J. Catal.* **1980**, *61*, 493.
(25) Voskoboinikov, T. V.; Coq, B.; Fajula, F.; Brown, R.; McDougall, G.; Luc Couturier, J. *Microporous Mesoporous Mater.* **1998**, *24*, 89.
(26) Dimitrov, C.; Leach, H. F. *J. Catal.* **1969**, *14*, 336.
(27) Nieminen, V.; Kumar, N.; Datka, J.; Päivärinta, J.; Hotokka, M.; Laine, E.; Salmi, T.; Murzin, D. Y. *Microporous Mesoporous Mater.* **2003**, *60*, 159.
(28) Espeel, P. H.; De Peuter, G.; Tielen, M. C.; Jacobs, P. A. *J. Phys. Chem.* **1994**, *98*, 11588.
(29) Kugel, V. Y.; Lakhman, L. I.; Abramova, A. V.; Matiyeva, Z. M.; Smirnov, V. K.; Irisova, K. N.; Livenbuk, M. I.; Slivinskii, Y. V. *Pet. Chem.* **1997**, *37*, 297.
(30) Frisch, M. J.; Trucks, G. W.; Schlegel, H. B.; Scuseria, G. E.; Robb, M. A.; Cheeseman, J. R.; Montgomery, J.; J. A.; Vreven, T.; Kudin, K. N.; Burant, J. C.; Millam, J. M.; Iyengar, S. S.; Tomasi, J.; Barone, V.;

Mennucci, B.; Cossi, M.; Scalmani, G.; Rega, N.; Petersson, G. A.; Nakatsuji, H.; Hada, M.; Ehara, M.; Toyota, K.; Fukuda, R.; Hasegawa, J.; Ishida, M.; Nakajima, T.; Honda, Y.; Kitao, O.; Nakai, H.; Klene, M.; Li, X.; Knox, J. E.; Hratchian, H. P.; Cross, J. B.; Bakken, V.; Adamo, C.; Jaramillo, J.; Gomperts, R.; Stratmann, R. E.; Yazyev, O.; Austin, A. J.; Cammi, R.; Pomelli, C.; Ochterski, J. W.; Ayala, P. Y.; Morokuma, K.; Voth, G. A.; Salvador, P.; Dannenberg, J. J.; Zakrzewski, V. G.; Dapprich, S.; Daniels, A. D.; Strain, M. C.; Farkas, O.; Malick, D. K.; Rabuck, A. D.; Raghavachari, K.; Foresman, J. B.; Ortiz, J. V.; Cui, Q.; Baboul, A. G.; Clifford, S.; Cioslowski, J.; Stefanov, B. B.; Liu, G.; Liashenko, A.; Piskorz, P.; Komaromi, I.; Martin, R. L.; Fox, D. J.; Keith, T.; Al-Laham, M. A.; Peng, C. Y.; Nanayakkara, A.; Challacombe, M.; Gill, P. M. W.; Johnson, B.; Chen, W.; Wong, M. W.; Gonzalez, C.; Pople, J. A.; Gaussian, Inc., Wallingford CT: 2004.

(31) Zhao, Y.; Schultz, N. E.; Truhlar, D. G. *Journal of Chemical Theory and Computation* **2006**, *2*, 364.

(32) Zhao, Y.; Truhlar, D. G. *Accounts of Chemical Research* **2008**, *41*, 157.

(33) Drake, I. J.; Zhang, Y.; Briggs, D.; Lim, B.; Chau, T.; Bell, A. T. *Journal of Physical Chemistry B* **2006**, *110*, 11654.

CATALYTIC DEHYDROGENATION OF ETHYLBENZENE TO STYRENE OVER A TETRAHEDRAL PLATINUM NANOCLUSTER: A DFT STUDY

Patanachai Janthon[1,2,3], Teeranan Nongnual[1,2,3], Piboon Pantu[1,2,3] and Jumras Limtrakul[1,2,3,*]

[1]Laboratory for Computational and Applied Chemistry, Department of Chemistry, Faculty of Science and Center of Nanotechnology, Kasetsart University Research and Development Institute, Kasetsart University, Bangkok 10900, Thailand
[2]NANOTEC Center of Excellence, National Nanotechnology Center, Kasetsart University, Bangkok 10900, Thailand
[3]Center for Advanced Studies in Nanotechnology and Its Applications in Chemical, Food and Agricultural Industries, Kasetsart University, Bangkok 10900, Thailand

Introduction

Styrene (C_8H_8) has been one of the highly significant chemicals used widely in the synthetic polymer industry.[1-2] The dehydrogenation of ethylbenzene over a potassium promoted iron (III) oxide catalyst at high temperature was mainly used for the production of commercial styrene. However, there were disadvantages in this process - endothermic reaction and rapid deactivation, but many researchers have developed new catalysts, adsorbents and catalyst supports to overcome these.[3-10] Among the developments, the Pt(111) surface was a candidate catalyst for the dehydrogenation of ethylbenzene to styrene concerning the dissociation of ethylbenzene at low temperature on the surface forming styrene and hydrogen products. But, this again had the disadvantage that the styrene desorption step was quenched by its strong binding to the surface, resulting in the polymerization of glued styrene molecules under an annealing temperature condition.[11] The activity of unsupported Pt nanoclusters was studied by determining an activation of the small hydrocarbons such as methane.[12-13] This brought about the small Pt nanoclusters (Pt_n) which were more reactive than monatomic Pt by at least one order of magnitude. The tetrahedral Pt nanocluster (Pt_4) was also found to improve the oxidative dehydrogenation of propane.[14]

In this work, we introduce the tetrahedral Pt nanocluster consisting of one dehydrogenating Pt site, withdrawing two H atoms, as a novel candidate catalyst for the dehydrogenation of ethylbenzene to styrene.

Methodology

Neutral Pt_4 with C_2 symmetry in a triplet state was used in our model. Full geometry optimizations for all pathways were performed using the B3LYP method including 6d functions and unrestricted spin polarization, implemented in the Gaussian 03 program.[15] We have employed the LanL2DZ basis set for all Pt atoms, which uses 18-electron relativistic effective core potentials (ECP) to reduce the number of electrons explicitly. The 6-31G(d,p) basis set for all H and C atoms was added in the calculation, increasing the accuracy of the dehydrogenation processes. In addition, neutral monatomic Pt in a triplet state was investigated using the same level of theory.

Results and Discussion

The dehydrogenation mechanism was investigated concerning with the H' and H'' dissociations over the Pt_4 catalyst. The dehydrogenation pathways were categorized by the number of Pt sites that these hydrogen atoms moving to. Three mechanistic pathways were proposed as shown in Figure 1. The DP pathway was separated into two sub pathways, DP_i and DP_ii, which are dealing with the *Int4* and *Int5*, respectively.

For all catalytic Pt_4 pathways, the dehydrogenation started from the adsorption of ethylbenzene on the dehydrogenating site of Pt_4
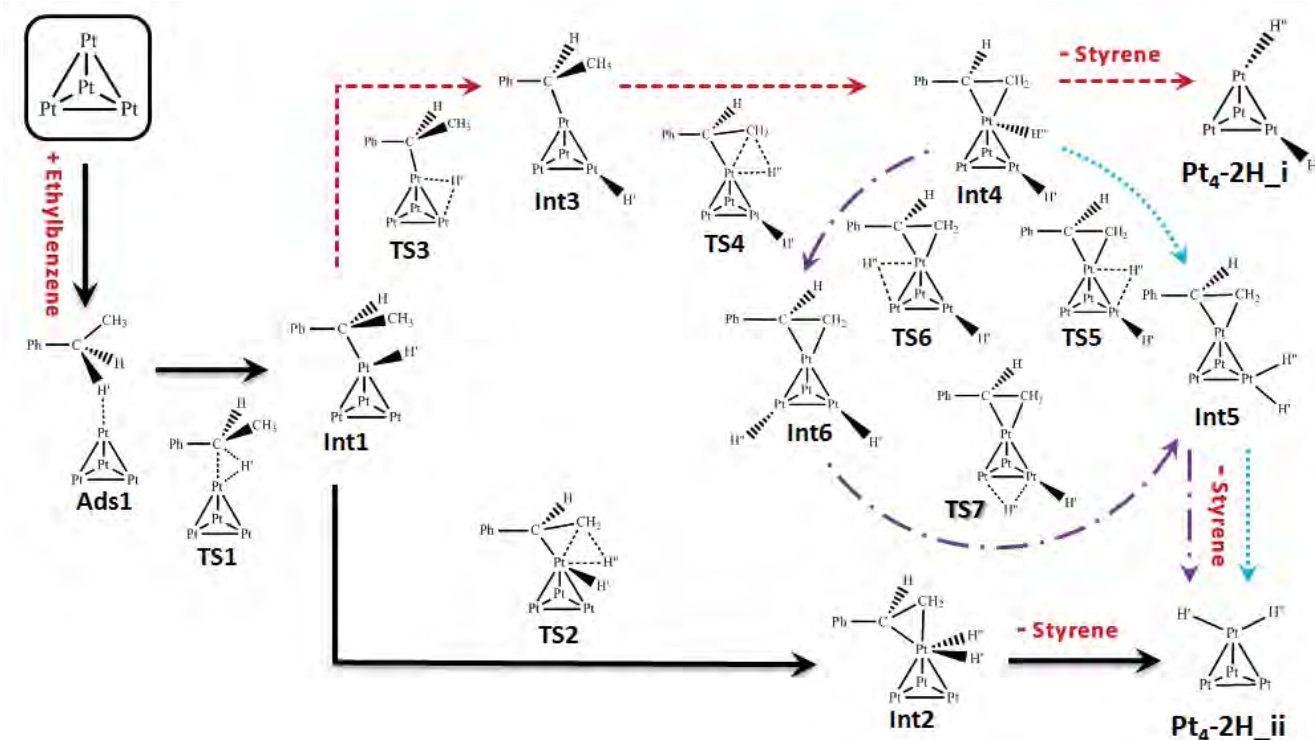

Figure 1. The mechanism pathways for the dehydrogenation of ethylbenzene to styrene over Pt_4 catalyst: single-catalytic-site Pt_4 (SP, black solid line), double-catalytic-site Pt_4 (DP_i, red dash line and DP_ii, blue dot line) and triple-catalytic-site Pt_4 (TP, purple dash-dot line)

(*Ads1*) with the adsorption energy of -5.3 kcal/mol. The C-H' bond was then dissociated with the activation energy of 1.3 kcal/mol (*TS1*) forming the intermediate *Int1*. After that, the three main pathways were considered.

For the SP pathway, the C-H" bond was broken, moving the H" to the first Pt_4 site - dehydrogenating site, with the activation energy of 24.4 kcal/mol (*TS2*) forming an unstable intermediate with the adsorbed styrene product (*Int2*). This is the rate determining step caused by an increasing steric effect of seven coordinates on the single platinum site. Surprisingly, the styrene and Pt_4-2H_ii were then easily desorbed with the desorption energy of 13.5 kcal/mol due to the high steric effect.

For the DP pathway, the H' migrated to the second Pt_4 site with the activation energy of 7.7 kcal/mol (*TS3*) forming the intermediate *Int3*. The C-H" bond was then broken with the activation energy of 3.0 kcal/mol (*TS4*), moving the H" onto the first Pt_4 site (*Int4*) with the absorbed styrene product. Focusing on the DP_i pathway, the styrene was desorbed with the desorption energy of 29.5 kcal/mol leaving the Pt_4-2H_i. On the other hand, the DP_ii pathway forwarded by the H" moving to join with the H' on the second Pt_4 site with the activation energy of 5.3 kcal/mol (*TS5*) stabilizing the intermediate *Int5*. Thus, the desorption energy was increased to 36.8 kcal/mol leaving the Pt_4-2H_ii.

For the TP pathway, the H" of the *Int4* moved to the third Pt_4 site with the activation energy of 3.4 kcal/mol (*TS6*) forming the intermediate *Int6*. Next, the H" moved to join with the H' on the second Pt_4 site with the activation energy of 13.8 kcal/mol (*TS7*), merging to the *Int5* as in the DP_ii pathway.

The hydrogen migrations on the Pt_4 sites (in the DP and the TP pathways) using low activation energy in the range of 3.4 to 13.8 kcal/mol, can stabilize an intermediate. This led the desorption energy for styrene product was higher. Therefore, the rate determining step of the DP and the TP pathways were associated with the styrene desorption step. In contrast, this H-moving step was not considered in the SP pathway, therefore, the stabilization of an intermediate was not observed. Moreover, this led the second dehydrogenation of the DP and the TP pathways (*TS4*) using less activation energy than the second dehydrogenation of the SP (*TS2*). Due to steric repulsion between adsorbed styrene and the hydrogen atoms that bonding to the same Pt_4 site, non-stabilized intermediate of SP (*Int2*) can assist the styrene desorption more easily with lower desorption energy.

Although the overall activation energy of the SP pathway was the smallest, the DP and TP pathways were kinetically favorable. Therefore, the dehydrogenation was terminated at the *Int5* and *Int6* steps with styrene products hardly attached to the catalytic site. To avoid this problem, the SP pathway must be chosen, thus, the single site catalytic must be favorably controlled.

The dehydrogenation of ethylbenzene over the monatomic Pt catalyst was shown in Figure 2. The C-H' bond was broken with the activation energy of 12.9 kcal/mol (*TS8*). The C-H" bond was then dissociated with the activation energy of 25.5 kcal/mol (*TS9*). This was the same as that of the SP pathway. The styrene was then desorbed with the activation energy of 35.0 kcal/mol, which was the rate determining step. This activation energy is higher than that of the SP pathway due to its lower steric effect to push the styrene out. It can be suggested that three vacant sites of the Pt_4 can assist the dehydrogenation of the H' and can increase the steric effect to the active site.

Figure 2. The mechanism for the dehydrogenation of ethylbenzene to styrene over monatomic Pt catalyst.

Conclusion

We report here the first theoretical study of the dehydrogenation of ethylbenzene over the Pt_4 catalyst. Although the overall activation energy of the SP pathway was the smallest, the DP and TP pathways were kinetically favorable without desorption of the styrene product. To avoid this problem, the SP pathway must be chosen, thus, the single site catalytic must be favorably controlled. The H-migration step was not considered in the SP pathway. For this reason, the stabilization of an intermediate was not observed. Therefore, the non-stabilized intermediate of SP pathway (*Int2*) can assist the styrene desorption more easily with the lower desorption energy. This caused the overall activation energy of 24.4 kcal/mol regarding to the C-H" dissociation. In addition, we suggest the control for the SP pathway by the assistance of an adsorbent blocking three sites with remaining one active site of the Pt_4 catalyst. Moreover, in order to recover the Pt_4 catalyst, the oxidative dehydrogenation should be introduced to eliminate the two adsorbed-H atoms remaining on the catalyst. This understanding can be applied for an alternative styrene synthesis.

References
(1) Lee, W. J.; and Froment, G. F. *Ind. & Eng. Chem. Res.* **2008**, *47(23)*, 9183-9194.
(2) Badstube, T.; Papp, H.; Kustrowski, P.; and Dziembaj, R. *Cat. Lett.* **1998**, *55*, 169–172.
(3) Morán, C.; González, E.; Sánchez, J.; Solano, R.; Carruyo, G.; Moronta, A. *J. Col. Interf. Sci.* **2007,** *315* (1), 164-169.
(4) Cavani, F.; Trifirò, F. *Appl. Cat. A: General* **1995,** *133* (2), 219-239.
(5) Yuichi, M.; Kazuyoshi, I.; Hiroshi, U.; Tadashi, H.; and Tomohiko, T. *App.Cat.***1982**, *2*, 67-74.
(6) Su, D. S.; Maksimova, N.; Delgado, J. J.; Keller, N.; Mestl, G.; Ledoux, M. J.; Schlögl, R. *Cat. Tod.* **2005**, *102–103*, 110–114.
(7) Su, D. S.; Delgado, J. J.; Liu, X.; Wang, D.; Schlögl, R.; Wang, L.; Zhang, Z.; Shan, Z.; and Xiao, F. S. *Chem. Asian J.* **2009**, *4*, 1108 – 1113.
(8) Keller, N.; Maksimova, N. I.; Roddatis, V. V.; Schur, M.; Mestl, G.; Butenko,Y. V.; Kuznetsov, V. L.; and Schlögl, R. *Angew. Chem. Int. Ed.* **2002**, *41(11)*, 1885-1888.
(9) Du, Y.; Li, J.; and Yang, X. *Cat. Com.* **2008**, *9*, 2331–2333.

(10) Sakurai, Y.; Suzaki, T.; Ikenaga, N.; and Suzuki, T. *Appl. Cat. A: General* **2000,** *192*, 281–288.

(11) Ranke, W.; and Weiss, W. *Surf Sci.* **2000**, *465(3)*, 317-330.

(12) Xiao, L.; and Wang, L. *J. Phys. Chem. B.* **2007**, *111(7),* 1657-1663.

(13) Trevor, D. J.; Cox, D. M.; and Kaldor, A. *J. Am. Chem. Soc.* **1990**, *112(10)*, 3742-3749.

(14) Vajda, S.; Pellin, M. J.; Greeley, J. P.; Marshall, C. L.; Curtiss, L. A.; Ballentine, G. A.; Elam, J. W.; Catillon-Mucherie, S.; Redfern, P. C.; Mehmood, F.; and Zapol, P. *Nat. Mat.* **2009**, *8(3)*, 213-216.

(15) Frisch, M. J.; Trucks, G. W.; Schlegel, H. B.; Scuseria, G. E.; Robb, M. A.; Cheeseman, J. R.; Montgomery, J. A.; Jr.; Vreven, T.; Kudin, K. N.; Burant, J. C.; Millam, J. M.; Iyengar, S. S.; Tomasi, J.; Barone, V.; Mennucci, B.; Cossi, M.; Scalmani, G.; Rega, N.; Petersson, G. A.; Nakatsuji, H.; Hada, M.; Ehara, M.; Toyota, K.; Fukuda, R.; Hasegawa, J.; Ishida, M.; Nakajima, T.; Honda, Y.; Kitao, O.; Nakai, H.; Klene, M.; Li, X.; Knox, J. E.; Hratchian, H. P.; Cross, J. B.; Adamo, C.; Jaramillo, J.; Gomperts, R.; Stratmann, R. E.; Yazyev, O.; Austin, A. J.; Cammi, R.; Pomelli, C.; Ochterski, J. W.; Ayala, P. Y.; Morokuma, K.; Voth, G. A.; Salvador, P.; Dannenberg, J. J.; Zakrzewski, V. G.; Dapprich, S.; Daniels, A. D.; Strain, M. C.; Farkas, O.; Malick, D. K.; Rabuck, A. D.; Raghavachari, K.; Foresman, J. B.; Ortiz, J. V.; Cui, Q.; Baboul, A. G.; Clifford, S.;Cioslowski, J.; Stefanov, B. B.; Liu, G.; Liashenko, A.; Piskorz, P.; Komaromi, I.; Martin, R. L.; Fox, D. J.; Keith, T.; Al-Laham, M. A.; Peng, C. Y.; Nanayakkara, A.; Challacombe, M.; Gill, P. M. W.; Johnson, B.; Chen, W.; Wong, M. W.; Gonzalez, C.; Pople, J. A.*Gaussian 03*, revision E.01, Gaussian, Inc, Wallingford, CT, 2004.

PETR   **Todd Gardner**   **Thursday, March 31, 2011**

113 - Density functional theory study of possible mechanisms of isooctene formation via isobutene dimerization over acidic beta zeolite

Panida Singra, *Kanokwan Kongpatpanich, Pipat Khongpracha PhD*, *Professor Jumras Limtrakul PhD*. *Laboratory for Computational and Applied Chemistry, Department of Chemistry, Faculty of Science and Center of Nanotechnology, Kasetsart University Research and Development Institute, Kasetsart University, Chatuchak, Bangkok, Thailand; NANOTEC Center of Excellence, National Nanotechnology Center, Kasetsart University, Chatuchak, Bangkok, Thailand; Center for Advanced Studies in Nanotechnology and Its Applications in Chemical, Food and Agricultural Industries, Kasetsart University, Chatuchak, Bangkok, Thailand*

Isobutene dimerization over beta zeolite has been investigated by using the recently developed and highly accurate M06-2X/6-31G(d,p) level of theory. The reaction starts with the protonation of isobutene by the Brønsted acid of zeolite and yields a "*tert*-butyl carbocation" intermediate. Subsequently, the C-C bond formation between the carbocation intermediate and the second isobutene molecule gives a "*tert*-octyl carbocation" intermediate and afterwhich it returns the proton back to the zeolite framework to give trimethylpentene isomers (isooctenes). The protonation of isobutene is observed to be the rate-determining step which requires an activation energy of 14.4 kcal/mol. Whereas the C-C bond formation more easily occurs with the activation energy of 4.0 kcal/mol and the sequential deprotonation requires activation energies of 1.2 and 5.4 kcal/mol for 2,4,4-trimethyl-1-pentene and 2,4,4-trimethyl-2-pentene,respectively. The calculated results found that 2,4,4-trimethyl-1-pentene was the kinetically primary product.

Thursday, March 31, 2011 08:30 AM
Chemistry of Petroleum and Emerging Technologies (08:30 AM - 11:20 AM)
Location: Anaheim Marriott
Room: Grand Blrm G

Close Window

241st ACS National Meeting, Anaheim, CA

Document ID: 19375

Program Area: INOR: Division of Inorganic Chemistry

Symposium Title: (INOR031) Inorganic Catalysts

INSTITUTIONS

1. Kasetsart University Kamphaeng Saen Campus, Chemistry Department, Faculty of Liberal Arts and Science, Nakhon Pathom, Nakhon Pathom, 73140, Thailand

2. Laboratory for Computational and Applied Chemistry, Faculty of Science and Center of Nanotechnology, Kasetsart University Research and Development Institute, Kasetsart University, Department of Chemistry, Jatujak, Bangkok, 10900, Thailand

3. NANOTEC Center of Excellence, National Nanotechnology Center, Kasetsart University, Jatujak, Bangkok, 10900, Thailand

4. Center for Advanced Studies in Nanotechnology and Its Applications in Chemical, Food and Agricultural Industries, Kasetsart University, Jatujak, Bangkok, 10900, Thailand

AUTHORS

1. Bundet Boekfa[1,3,4] , Dr., PhD, Kasetsart University Kamphaeng Saen Campus, Chemistry Department, Faculty of Liberal Arts and Science, Nakhon Pathom, Nakhon Pathom, 73140, Thailand , +66 2562 5555 ext 2169, bundet.b@ku.ac.th

2. Jumras Limtrakul[2,3,4] , Prof. Dr., PhD, Kasetsart University, Department of Chemistry, Laboratory for Computational and Applied Chemistry, Faculty of Science and Center of Nanotechnology, Kasetsart University Research and Development Institute, Kasetsart University, Jatujak, Bangkok, 10900, Thailand , +66 2562 5555 ext 2169, jumras.l@ku.ac.th

Reason for Abstract Submission: I am contributing this paper in response to the Call for Papers.

Invitation from: No response indicated

Email of Inviter: No response indicated

Criteria are met: Are met by at least one author

Presenting author will register: Yes

Abstract will be withdrawn if author cannot attend: Yes, I agree

Abstract submitted only once: Yes, I agree

Equipment Needs: No response indicated

Comments to Organizers: No response indicated

Preferred Presentation Method: Poster Preferred

Should this Paper be Considered for a SCI-MIX? No response indicated

Student Type No response indicated

Title: The Acid Location of the Brønsted Acid Site in ITQ-22 zeolite: A Newly Developed Density Functional Theory Study

Abstract Body: The location of Brønsted acid site, ≡Si-O(H)-Al≡, and the adsorption of pyridine on multipore zeolite H-ITQ-22 have been studied by the newly developed density functional theory, M08-HX. Different 44 Brønsted acid sites derived from the 16 different Al-substituted ITQ-22 zeolite were calculated with the 5T quantum cluster. Al1(O2H), Al14(O30H) and Al15(O33H) are the most favorable three positions for the Brønsted acid site. The extended 28T quantum cluster covered intersection cavity of ITQ-22 is used to study the adsorption of pyridine to determine the acid strength. The calculated adsorption energies are -46.5, -44.0 and -43.0 kcal/mol for Al1 (O2H), Al14(O30H) and Al15(O33H) positions, respectively compared well with the pyridine on H-ZSM-5 (-47.6 kcal/mol). The results of this study may be helpful for understanding the acidic of the zeolite for further applications.

PrePrint: No response indicated

Preview

Draft Preview of Document 19366

THIS COPY IS A DRAFT ONLY. YOUR FINAL PRINTOUT WILL BE AVAILABLE AT TIME OF SUBMISSION

Print document.

241st ACS National Meeting, Anaheim, CA

Document ID: 19366

Program Area: INOR: Division of Inorganic Chemistry

Symposium Title: (INOR013) Inorganic Catalysts

INSTITUTIONS

1. Kasetsart University Kamphaeng Saen Campus, Chemistry Department, Faculty of Liberal Arts and Science, Nakhon Pathom, 73140, Thailand

2. Laboratory for Computational and Applied Chemistry, Faculty of Science and Center of Nanotechnology, Kasetsart University Research and Development Institute, Kasetsart University, Department of Chemistry, Jatujak, Bangkok, 10900, Thailand

3. NANOTEC Center of Excellence, National Nanotechnology Center, Kasetsart University, Jatujak, Bangkok, 10900, Thailand

4. Center for Advanced Studies in Nanotechnology and Its Applications in Chemical, Food and Agricultural Industries, Kasetsart University, Jatujak, Bangkok, 10900, Thailand

AUTHORS

1. Bundet Boekfa[1,3,4] , Dr., PhD, Kasetsart University Kamphaeng Saen Campus, Chemistry Department, Faculty of Liberal Arts and Science, Nakhon Pathom, Nakhon Pathom, 73140, Thailand , +66 2562 5555 ext 2169, bundet.b@ku.ac.th

2. Jumras Limtrakul[2,3,4] , Prof. Dr., PhD, Kasetsart University, Department of Chemistry, Laboratory for Computational and Applied Chemistry, Faculty of Science and Center of Nanotechnology, Kasetsart University Research and Development Institute, Kasetsart University, Jatujak, Bangkok, 10900, Thailand , +66 2562 5555 ext 2169, jumras.l@ku.ac.th

Reason for Abstract Submission: I am contributing this paper in response to the Call for Papers.

Invitation from: No response indicated

Email of Inviter: No response indicated

Criteria are met: Are met by at least one author

Presenting author will register: Yes

Abstract will be withdrawn if author cannot attend: Yes, I agree

Abstract submitted only once: Yes, I agree

Equipment Needs: No response indicated

Comments to Organizers: No response indicated

Preferred Presentation Method: Oral Preferred

Should this Paper be Considered for a SCI-MIX? No response indicated

Student Type No response indicated

Title: Strength and Brønsted acid sites of ITQ-34/Pyridine Complexes: A Newly Developed Density Functional Theory Study

Abstract Body: The newly developed density functional theory, M08-HX, was applied to investigate the strength and location of Brønsted acid sites, $\equiv$Si-O(H)-Al$\equiv$, in the new ITQ-34 zeolite. The 25 Brønsted acid sites generated from the nine different Al-substitited ITQ-34 zeolite were calculated at the M08-HX/6-31G(d,p) level of theory. The 5T cluster model was employed for the acid site. The most favorable positions for the ITQ-34 were Al3(O4H), Al4 (O3H) and Al4(O13H). To determine the acid strength, the pyridine is selected to adsorb on the 28T quantum clusters. The calculated adsorption energies are -38.5, -41.4 and -42.3 kcal/mol for Al3(O4H), Al4(O3H) and Al4 (O13H) positions, respectively. The adsorption energies compared well with H-FAU zeolite (-43.1 kcal/mol). These important findings will be useful for applications of this new zeolite in areas of adsorption separation and catalysis adsorption.

PrePrint: No response indicated

Print document.

Preview

Draft Preview of Document 19358

THIS COPY IS A DRAFT ONLY. YOUR FINAL PRINTOUT WILL BE AVAILABLE AT TIME OF SUBMISSION

Print document.

241st ACS National Meeting, Anaheim, CA

Document ID: 19358

Program Area: INOR: Division of Inorganic Chemistry

Symposium Title: (INOR013) Inorganic Catalysts

INSTITUTIONS

1. Laboratory for Computational and Applied Chemistry, Faculty of Science and Center of Nanotechnology, Kasetsart University Research and Development Institute, Kasetsart University, Department of Chemistry, Jatujak, Bangkok, 10900, Thailand

2. NANOTEC Center of Excellence, National Nanotechnology Center, Kasetsart University, Jatujak, Bangkok, 10900, Thailand

3. Center for Advanced Studies in Nanotechnology and Its Applications in Chemical, Food and Agricultural Industries, Kasetsart University, Jatujak, Bangkok, 10900, Thailand

AUTHORS

1. Sippakorn Wannakao[1,2,3] , Kasetsart University, Department of Chemistry, Laboratory for Computational and Applied Chemistry, Faculty of Science and Center of Nanotechnology, Kasetsart University Research and Development Institute, Kasetsart University, Jatujak, Bangkok, 10900, Thailand , +66 2562 5555 ext 2169, jumras.l@ku.ac.th

2. Kanokwan Kongpatpanich[1,2,3] ,

3. Pipat Khongpracha[1,2,3] , Dr., PhD

4. Jumras Limtrakul[1,2,3] , Prof.Dr., PhD, Kasetsart University, Department of Chemistry, Laboratory for Computational and Applied Chemistry, Faculty of Science and Center of Nanotechnology, Kasetsart University Research and Development Institute, Kasetsart University, Jatujak, Bangkok, 10900, Thailand , +66 2562 5555 ext 2169, jumras.l@ku.ac.th

Reason for Abstract Submission: I am contributing this paper in response to the Call for Papers.

Invitation from: No response indicated

Email of Inviter: No response indicated

Criteria are met: Are met by at least one author

Presenting author will register: Yes

Abstract will be withdrawn if author cannot attend: Yes, I agree

Abstract submitted only once: Yes, I agree

Equipment Needs: No response indicated

Comments to Organizers: No response indicated

Preferred Presentation Method: Oral Preferred

Should this Paper be Considered for a SCI-MIX? No response indicated

Student Type Graduate Student

Title: Activities of Au and Au_2 cation-exchanged zeolite for methane C-H bond activation: a DFT study

Abstract Body: The methane C-H activation, the initial step for many industrially important chemical processes, on gold and gold embedded in two different types of zeolites, Faujasite and ZSM-5 was studied for the first time with a newly developed functional, M06L. A cooperative effect of gold coupled with the nanopore of zeolite plays an important role for dictating methane activation. One of most convincing results was that the Au/ZSM-5 systems yield an unexpectedly low barrier (13.6 kcal/mole) as compared to bare gold systems (21.3 kcal/mole). As for FAU and Au_2-FAU complexes, the activity was not as good as the corresponding Au-ZSM-5 and Au_2-ZSM-5 systems. Our findings are very important for the search for a catalyst which is able to activate the C−H bond in alkanes.

PrePrint: No response indicated

Print document.

Preview

241st ACS National Meeting, Anaheim, CA

Document ID: 19325

Program Area: INOR: Division of Inorganic Chemistry

Symposium Title: (INOR013) Inorganic Catalysts

INSTITUTIONS

1. Laboratory for Computational and Applied Chemistry, Faculty of Science and Center of Nanotechnology, Kasetsart University Research and Development Institute, Kasetsart University, Department of Chemistry, Bangkok, 10900, Thailand

2. NANOTEC Center of Excellence, National Nanotechnology Center, Kasetsart University, Bangkok, 10900, Thailand

3. Center for Advanced Studies in Nanotechnology and Its Applications in Chemical, Kasetsart University, Bangkok, 10900, Thailand

---

AUTHORS

1. Phornphimon Maitarad[1,2] , Dr., PhD

2. Pimpa Hormnirun[1,2,3] , Dr., PhD

3. Pipat Khongpracha[1,2,3] , Dr., PhD

4. Jumras Limtrakul[1,2,3] , Prof.Dr., PhD, Kasetsart University, Department of Chemistry, Laboratory for Computational and Applied Chemistry, Department of Chemistry, Faculty of Science and Center of Nanotechnology, Kasetsart University Research and Development Institute,, Bangkok, 10900, 10900, Thailand , +66 2562 5555 ext 2169, jumras.l@ku.ac.th

---

Reason for Abstract Submission: I am contributing this paper in response to the Call for Papers.

Invitation from: No response indicated

Email of Inviter: No response indicated

Criteria are met: Are met by at least one author

Presenting author will register: Yes

Abstract will be withdrawn if author cannot attend: Yes, I agree

Abstract submitted only once: Yes, I agree

Equipment Needs: No response indicated

Comments to Organizers: No response indicated

Preferred Presentation Method: Oral Preferred

Should this Paper be Considered for a SCI-MIX? No response indicated

Student Type No response indicated

Title: Structure Activity Relationship and the Electronic Property of Bis(phenoxyimine) Ligated Zirconium Catalysts for Ethylene Polymerization: A Combined CoMFA and DFT study

Abstract Body: Comparative Molecular Field Analysis (CoMFA) and Natural Bond Orbital (NBO) analysis were applied on 16 Zr phenoxy-imine (FI) post-metallocene catalysts to explore the structural requirements for catalytic activity of ethylene polymerization. The obtained CoMFA model exhibited good r^2_{cv} = 0.664 and r^2 = 0.963, and can well predict the test set. CoMFA steric-electrostatic maps and the NBO electronic distributions, as given by the second order perturbation $E^{(2)}$, can guide us to a new design for new potent catalysts. Firstly, the **R$_1$** substitution of the catalyst favors the less electron-donating group, next, the **R$_2$** substitution of the catalyst must be in the form of big bulky groups with high electron distributions and, finally, the hydrogen atom is suitable for **R$_3$** substitution. In summary, our obtained results not only can be used to rationally guide the design of new potent FI catalysts, but can also significantly save on the experimental synthesis.

PrePrint: No response indicated

[Print document.](#)

Preview

Draft Preview of Document 19372

THIS COPY IS A DRAFT ONLY. YOUR FINAL PRINTOUT WILL BE AVAILABLE AT TIME OF SUBMISSION

Print document.

241st ACS National Meeting, Anaheim, CA

Document ID: 19372

Program Area: INOR: Division of Inorganic Chemistry

Symposium Title: (INOR013) Inorganic Catalysts

INSTITUTIONS

1. Laboratory for Computational and Applied Chemistry, Faculty of Science and Center of Nanotechnology, Kasetsart University Research and Development Institute, Kasetsart University, Department of Chemistry, Jatujak, Bangkok, 10900, Thailand

2. NANOTEC Center of Excellence, National Nanotechnology Center, Kasetsart University, Jatujak, Bangkok, 10900, Thailand

3. Center for Advanced Studies in Nanotechnology and Its Applications in Chemical, Food and Agricultural Industries, Kasetsart University, Jatujak, Bangkok, 10900, Thailand

AUTHORS

1. Thana Maihom[1,2,3], Kasetsart University, Department of Chemistry, Laboratory for Computational and Applied Chemistry, Faculty of Science and Center of Nanotechnology, Kasetsart University Research and Development Institute, Kasetsart University, Jatujak, Bangkok, 10900, Thailand , +66 2562 5555 ext 2169, jumras.l@ku.ac.th

2. Jumras Limtrakul[1,2,3], Prof. Dr., PhD, Kasetsart University, Department of Chemistry, Laboratory for Computational and Applied Chemistry, Faculty of Science and Center of Nanotechnology, Kasetsart University Research and Development Institute, Kasetsart University, Jatujak, Bangkok, 10900, Thailand , +66 2562 5555 ext 2169, jumras.l@ku.ac.th

Reason for Abstract Submission: I am contributing this paper in response to the Call for Papers.

Invitation from: No response indicated

Email of Inviter: No response indicated

Criteria are met: Are met by at least one author

Presenting author will register: Yes

Abstract will be withdrawn if author cannot attend: Yes, I agree

Abstract submitted only once: Yes, I agree

Equipment Needs: No response indicated

Comments to Organizers: No response indicated

Preferred Presentation Method: Oral Preferred

Should this Paper be Considered for a SCI-MIX? No response indicated

Student Type Graduate Student

Title: Formaldehyde Encapsulated in Lithium-Decorated Metal-Organic Frameworks: A DFT Study

Abstract Body: Stability of the monomeric formaldehyde encapsulated on lithium-decorated metal-organic frameworks 5 (Li-MOF-5) has been investigated by means of the density functional method, M06-L/6-31+G (d,p).The reaction kinetics and thermodynamics equilibrium between the formaldehyde and its trimerization product, 1,3,5-trioxane are considered to assess the efficacy of Li-MOF-5 for formaldehyde preservation. The trimerization of formaldehyde takes place in a single reaction step. The calculated activation energy for the reaction on Li-MOF-5 is 33.7 kcal/mol, which is 16.4 kcal/mol higher than in the gas phase system. In addition, the calculated reaction energy with respect to the adsorption complex is endothermic by 5.9 kcal/mol and the reaction Gibbs free energy (ΔG) also becomes positive (11.0 kcal/mol). These results revealed that the formaldehyde trimerization on Li-MOF-5 is favorably a reversible reaction, suggesting that the Li-decorated MOF-5 is a good candidate material for preserving the monomeric formaldehyde.

PrePrint: No response indicated

Print document.

INOR   **Michelle Millar, Nora Radu**   **Tuesday, March 29, 2011**

781 - Theoretical study of the oxidative dehydrogenation of ethylbenzene to styrene over Fe-ZSM-5

Dr. Supawadee Namuangruk PhD, *Dr. Pipat Khongpracha PhD, Prof. Dr. Jumras Limtrakul PhD. National science and technology development agency, National Nanotechnology Center, klongluang, Phatumthani, Thailand; Department of chemistry, Kasetsart University, Laboratory for Computational and Applied Chemistry, Jatujak, Bangkok, Thailand; National nanotecnology center, Kasetsart University, NANOTEC Center of Excellent, Jatujak, Bangkok, Thailand*

The reaction mechanisms of the catalytic reaction cycle for the oxidative dehydrogenation of ethylbenzene over Fe-ZSM-5 have been investigated by the ONIOM(M06/6-31G**:UFF) method. The complete reaction cycle consists of three sub-reactions: (i) nitrous oxide decomposition, (ii) oxidative dehydrogenation of ethylbenzene, and (iii) dehydration for active site regeneration. The calculated energy barriers of the rate-limiting steps for the reactions (i), (ii) and (iii) are 47.72, 21.19, and 35.67 kcal/mol indicating that the nitrous oxide decomposition is the controlling reaction in the whole reaction cycle. For the oxidative dehydrogenation of ethylbenzene yielding styrene (ii), we proposed newly two consecutive reaction pathways, Paths A and B. For the Path A, the mechanism is proceeded by consecutive cleavages of the primary and secondary C-H bonds, respectively, while the C-H bond cleavages order for the Path B is reversed. The first C-H bond cleavage of ethylbenzene for each path is found to be rate-limiting step where the calculated activation barrier is 21.19 kcal/mol for Path A which is higher than that for Path B (13.89 kcal/mol). The reaction rate constants calculated from the activation barriers of the rate-limiting steps are 9.45 x 10^{11} and 4.63 x 10^{12} s^{-1} at 273.15 K for Paths A and B, respectively. We predicted that styrene formation from oxidative dehydrogenation of ethylbenzene is carried out via a consecutive reaction starting from the secondary C-H bond cleavage followed by the primary C-H bond cleavages, respectively.

Monday, March 28, 2011 08:00 PM
Sci-Mix (08:00 PM - 10:00 PM)
Location: Anaheim Convention Center
Room: Hall B

Tuesday, March 29, 2011 07:00 PM
Inorganic Catalysts (07:00 PM - 10:00 PM)
Location: Anaheim Convention Center
Room: Hall B

Close Window

American Chemical Society National meeting & Exposition" ครั้งที่ 242

ณ ประเทศสหรัฐอเมริกา

ระหว่างวันที่ 28 สิงหาคม -1 กันยายน 2554

จำนวน 10 เรื่อง

Reaction Mechanism of Isomerization of 1-Butene to Isobutene over Multipore H-ITQ-22 Zeolite: A DFT Study

*Bundet Boekfa[1,2,4], Piti Treesukol[1,2,4] and Jumras Limtrakul[2,3,4]**

[1]Chemistry Department, Faculty of Liberal Arts and Science, Kasetsart University Kamphaeng Saen Campus, Nakhon Pathom 73140, Thailand
[2]Center for Advanced Studies in Nanotechnology and Its Applications in Chemical, Food and Agricultural Industries, Kasetsart University, Bangkok 10900, Thailand
[3]Laboratory for Computational and Applied Chemistry, Department of Chemistry, Faculty of Science and Center of Nanotechnology, Kasetsart University Research and Development Institute, Kasetsart University, Bangkok 10900, Thailand
[4]NANOTEC Center of Excellence, National Nanotechnology Center, Kasetsart University, Bangkok 10900, Thailand
[*]Corresponding author: Tel.: +662 562 5555 ext 2169, Fax: +662 562 5555 ext 2176, E-mail address: jumras.l@ku.ac.th

Introduction

Zeolites are widely used for their range of applications in petroleum refineries and petrochemical industries[1-4]. With their size- and shape-selectivity and their ability, zeolites are the catalysts of choice for petrochemical catalysts such as hydrocarbon cracking, isomerization and oligomerization[1-3,5]. ITQ-22 (IWR) is a new synthetic multipore zeolite[6] with a pore structure that comprises 8-, 10- and 12-membered-ring pores of 4.52 x 3.32, 5.86 x 4.98 and 6.66 x 6.66 Å, respectively. This zeolite has proved to be an outstanding catalyst for isomerization-disproportionation of m-xylene, and alkylation of benzene with isopropanol and propylene[6].

1-butene isomerization over acidic catalysts is an important reaction for the production of isobutene, a raw material for methyl *tert*-butyl ether (MTBE) and ethyl *tert*-butyl ether (ETBE) production[7-12]. Many zeolites such as Ferrierite, ZSM-5 and Theta-1 zeolite[8,11] have been already used for those reactions. Corma et al. proposed the mechanism for this reaction on Theta-1 zeolite as a monomolecular mechanism[13]. Their activation energy is calculated to be 33-34 kcal/mol, which compares well with the experimental value of 30 kcal/mol. Tuma et al. used the hybrid MP2:DFT to study adsorption of the 1-butene, isobutene, *tert*-butyl cation and their alkoxide species in H-zeolite[14-15]. These studies lead us to understand the reaction in the specific pore of zeolite.

The zeolite framework effect or confinement effect, which is mainly composed of dispersive van der Waals interactions, has been proposed by Derouane[16] to explain the interactions between the zeolite framework and the adsorbed molecule. The conventional DFT functions are not able to describe the van der Waals effect from the zeolite framework. Recently, we have studied a number of adsorptions and reactions in the zeolite framework by using the recently developed M06-functionals including dispersion energy[17-24]. We found that these functionals can be used to describe the confinement effect of the zeolite framework. Combined with a second-order Møller-Plesset perturbation theory (MP2), the ONIOM (MP2:M06-2X) can successfully elucidate the adsorption and reaction mechanism of aliphatic, aromatic and heterocyclic compounds[20].

In this study, we examine the framework effects of this new multipore zeolite, H-ITQ-22, for the 1-butene isomerization into isobutene on the H-ITQ-22 zeolite by means of the well calibrated scheme of ONIOM (MP2:M06-2X). This study will provide the detailed understanding for the adsorption and reaction mechanism of butane isomerization in this new zeolite framework.
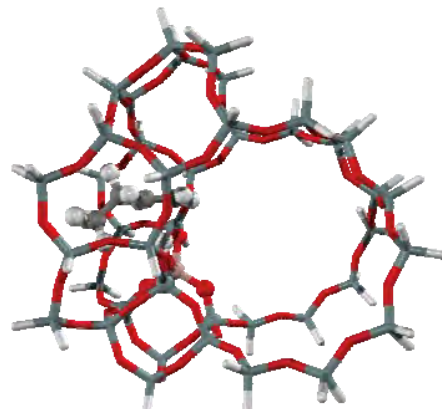

Figure 1. Presentation of 1-butene on H-ITQ-22 models 5T:42T ONIOM model. Atoms treated with the MP2 level of theory are shown in balls, whereas the areas treated with the M06-2X functional are shown in wireframes.

Methodology

The adsorption and reaction of 1-butene on H-ITQ-22 zeolite have been studied with an ONIOM model[25]. An Al atom is selected to substitute the Si atom at the T1 position. The active 5T (T means tetrahedral of Si or Al atoms) represents the Brønsted acid site assigned to be the inner layer, where the extended 42T model is the outer layer. The 5T inner layer of the ONIOM model is calculated with the MP2/6-31G(d,p) level of theory while the 42T outer layer is performed with the M06-2X/6-31G(d,p) level of theory[20]. The ONIOM 5T:42T is shown in Fig. 1. Only the active region, $AlSi_4O_4H$ and the probe molecule are allowed to relax while the rest is kept fixed with the crystallographic structure[6]. All calculations were performed using the Gaussian 03 program[26] incorporated with the Minnesota Density Functionals module 3.1 by Zhao and Truhlar[17-18].

Results and Discussion

Butane and 1-butene adsorptions onto the Brønsted acid site of H-ITQ-22. The ONIOM model for the H-ITQ-22 zeolite is illustrated in Fig. 1. The 42T quantum cluster is modeled to cover the intersection cavity (10T and 12T) where the guest molecule prefers to locate. The inner-layer 5T cluster, representing the Brønsted acid site, is calculated with the MP2 calculation while the outer-layer 42T cluster, representing the framework of zeolite, is calculated with the M06-2X functional. The acidic O1-Hz distance is calculated to be 0.97 Å. The Al ⋯ Hz bond distance is about 2.37 Å, which agrees well with the experiment data (2.38-2.48 Å)[27].

The optimized structures of butane and 1-butene on H-ITQ-22 zeolite are shown in Figures 2a and 2b, respectively. The butane molecule adsorbs in the 10T pore of H-ITQ-22 via interactions between the alkyl group and the Brønsted acid site of zeolite. The acidic O1-Hz bond distance is almost the same as in the isolated zeolite (0.97 Å). The distance between the carbon atom of butane and the Brønsted acid site (C2 ⋯ Hz) distance is 2.79 Å. The adsorption energy of butane on H-ITQ-22 is calculated to be -11.8 kcal/mol. This energy compares well with the experimental data of -11.9 kcal/mol for butane on H-MOR zeolite[28] and -12.6 kcal/mol for butane H-ZSM-5 zeolite[29].

(a) Butane,
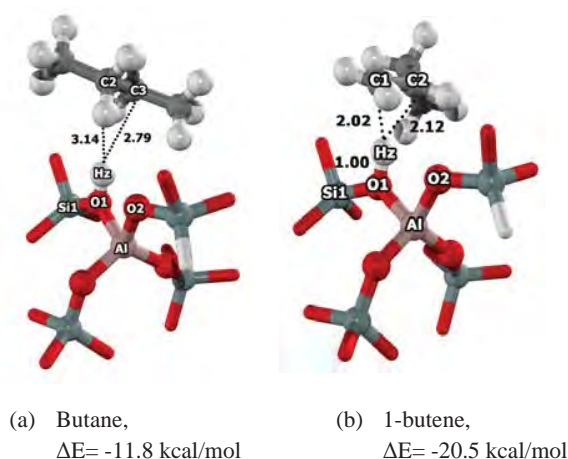   ΔE= -11.8 kcal/mol

(b) 1-butene,
     ΔE= -20.5 kcal/mol

Figure 2. Optimized structure of butane (a) and 1-butene (b) on H-ITQ-22 zeolite. Distances are in Ås.

The 1-butene molecule prefers to adsorb on the Brønsted acid site via the π-bond interaction of the double bond carbons. The acidic O1-Hz bond distance is increased to 1.00 Å. The distances between the double bond carbon and the Brønsted acid site (C1 - - Hz and C2 - - Hz) are 2.02 and 2.12 Å, respectively. The calculated adsorption energy is -20.6 kcal/mol. Only the adsorption of ethene on H-FAU from the experiment is reported to be -9.1 kcal/mol by Cant and Hall[30]. With the greater acidity of H-ITQ-22 and the larger probe molecule, our calculated adsorption energy of 1-butene on H-ITQ-22 is in the range of experimental data.

1-butene Isomerization to Isobutene on H-ITQ-22 The isomerization reaction of 1-butene to isobutene on H-ITQ-22 is proposed as a stepwise mechanism via 4 steps: 1) the secondary alkoxide intermediate formation via the protonation of 1-butene, 2) the cyclic transition state via the methyl shift and the primary alkoxide intermediate formation, 3) the *tert*-carbenium cation formation via the proton shift and 4) the protonation back to zeolite and desorption of isobutene. Fig. 3 shows the energies profile for the 1-butene isomerization reaction.

The 1-butene molecule is adsorbed in the intersection pore at the 10T position of ITQ-22 [AD, Figure 2b] with an adsorption energy of -20.5 kcal/mol. The first transition state [TS1, Figure 4a] is the secondary alkoxide intermediate formation. The Brønsted acid O1-Hz bond is broken and the strong covalent bond O2-C2 is formed. This step requires an activation energy of about 17.1 kcal/mol. The intermediate [IN1, Figure 4b] strongly interacts with zeolite with a
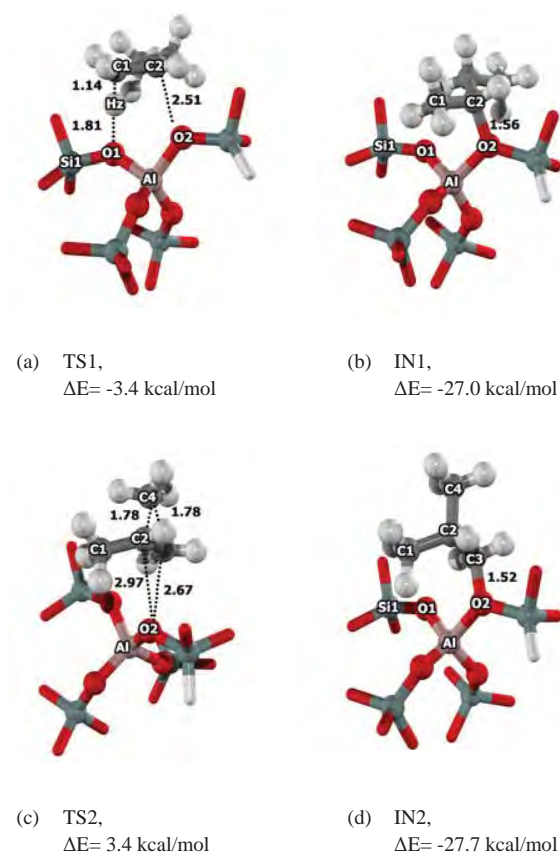

(a) TS1,
     ΔE= -3.4 kcal/mol

(b) IN1,
     ΔE= -27.0 kcal/mol

(c) TS2,
     ΔE= 3.4 kcal/mol

(d) IN2,
     ΔE= -27.7 kcal/mol

Figure 4. Optimized structure of 1-butene isomerization to isobutene on H-ITQ-22 zeolite: a) the transition structure (TS1), b) the secondary alkoxide intermediate (IN1), c) the transition structure (TS2), d) the primary alkoxide intermediate (IN2). Distances are in Ås.

relative energy of -27.0 kcal/mol. The second transition state [TS2, Figure 4c] is the cyclic transition state via the methyl shift. The C4 atom breaks the bond with the C3 atom and forms a bond with the C2 atom. This corresponds with the breaking of the O2-C2 bond and the forming of the O2-C3 bond. The activation energy is calculated to be 30.4 kcal/mol. The primary alkoxide intermediate [IN2, Figure 4d] is the product with a relative energy of -27.7 kcal/mol.

The third transition state [TS3, Figure 5a] is the proton transfer from C2 to C3 with an activation energy of 38.2 kcal/mol. This step is the rate determining step of the 1-butene isomerization reaction
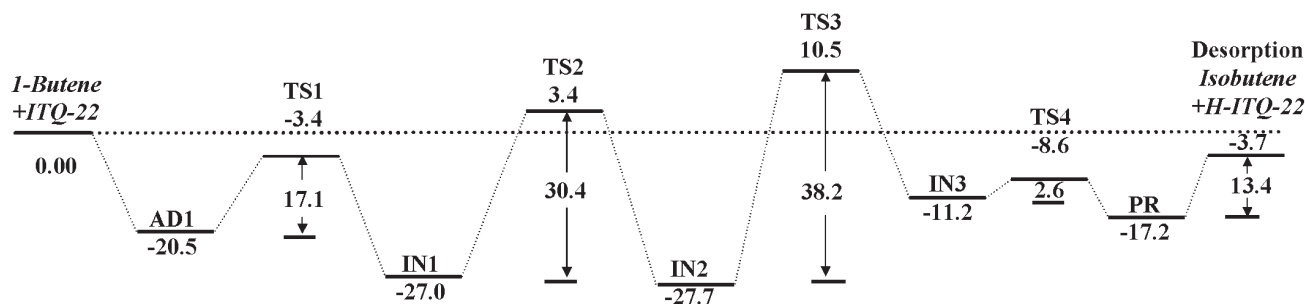

Figure 3. Potential energy diagram of the 1-butene to isobutene on the 5T:42T ONIOM (MP2:M06-2X) method (kcal/mol).

and gives the *tert*-butyl carbenium ion product [IN3, Figure 5b]. The *tert*-butyl carbenium is not stable and can move easily to isobutene via the forth transition state [TS4, Figure 5c]. The activation energy is only 2.6 kcal/mol. The isobutene product is adsorbed on H-ITQ-22 via a π-bonding interaction with a relative energy -17.2 kcal/mol [PR, Figure 5d]. The desorption energy of isobutene on H-ITQ-22 is 13.4 kcal/mol. The 1-butene isomerization to isobutene is an exothermic reaction with a heat of reaction (ΔH) of 4.1 kcal/mol.
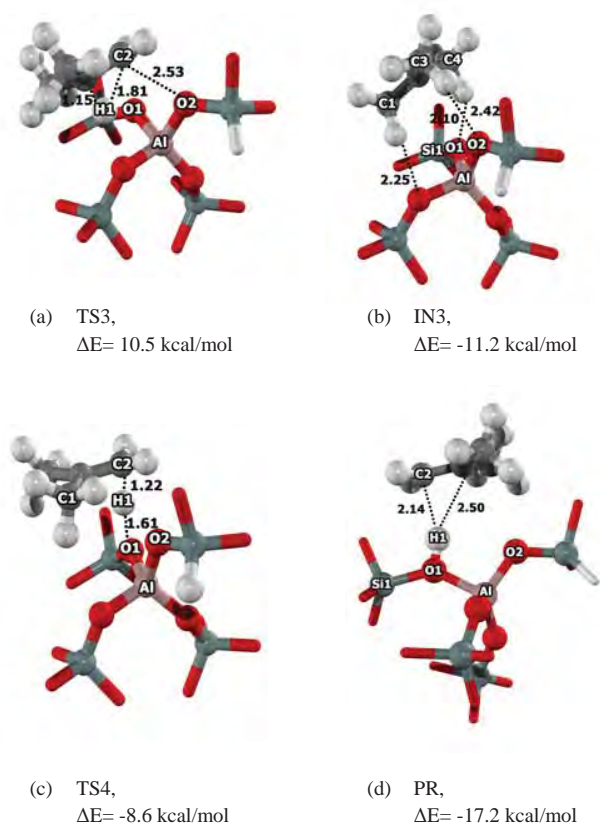

(a) TS3,
ΔE= 10.5 kcal/mol

(b) IN3,
ΔE= -11.2 kcal/mol

(c) TS4,
ΔE= -8.6 kcal/mol

(d) PR,
ΔE= -17.2 kcal/mol

Figure 5. Optimized structure of 1-butene isomerization to isobutene on H-ITQ-22 zeolite: a) the transition structure (TS3), b) the *tert*-butyl carbenium cation (IN3), c) the transition structure (TS4), d) the product isobutene adsorption (PR). Distances are in Ås.

Energetic Analysis between quantum cluster MP2 and ONIOM (MP2:M06-2X) The energies profile for 1-butene isomerization to isobutene on H-ITQ-22 is shown in Figure 3 and the energies are shown in Table 1. The adsorption energies are calculated to be -20.5 and -11.2 kcal/mol for 5T:42T and 5T, respectively. The framework increases the adsorption energy by about 45%. The reaction mechanism of 1-butene to isobutene is proposed to be step four of the mechanisms. Without the framework effect, the activation energies are calculated to be 25.4, 51.3, 46.3 and 0.6 kcal/mol on the 5T cluster with the MP2 calculation. The activation energies are decreased to be 17.1, 30.4, 38.2 and 2.6 kcal/mol with the 5T:42T ONIOM (MP2:M06-2X). The framework stabilizes the transition structure by as much as 30-40 % and the values are in the range of the experimental data. We suggest that the ONIOM (MP2:M06-2X)

is practical for the study of the framework effect on the adsorption and reaction mechanism in the ITQ-22 zeolite.

Table 1. The Contribution Analysis on the 1-butene isomerization on 5T:42T of ITQ-22 calculated with the ONIOM (MP2:M06-2X). Intrinsic activation energies are in parenthesis. Energies are in kcal/mol.

Model	5T:42T	5T // 5T:42T
Method	ONIOM (MP2:M06-2X)	MP2//ONIOM (MP2:M06-2X)
AD	-20.5	-11.2
TS1	-3.4 (17.1)	14.2 (25.4)
IN1	-27.0	-24.7
TS2	3.4 (30.4)	26.6 (51.3)
IN2	-27.7	-24.9
TS3	10.5 (38.2)	21.4 (46.3)
IN3	-11.2	4.6
TS4	-8.6 (2.6)	5.2(0.6)
PR	-17.2	7.9

Conclusions

The adsorption and isomerization reaction of 1-butene on H-ITQ-22 were theoretically studied using the ONIOM (MP2:M06-2X) approach. The adsorption energy of 1-butene on H-ITQ-22 is calculated to be -20.5 kcal/mol, which is in the range of experimental data. The reaction mechanism of 1-butene isomerization is proposed to be in four steps: 1) the secondary alkoxide intermediate formation via the protonation of 1-butene, 2) the cyclic transition state via the methyl shift and the primary alkoxide intermediate formation, 3) the *tert*-carbenium cation formation via the proton shift and 4) the protonation back to zeolite and desorption of isobutene. The activation energies are calculated to be 17.1, 30.4, 38.2 and 2.6 kcal/mol, respectively. The rate determining step is the *tert*-carbenium cation formation. This multi-pore H-ITQ-22 zeolite is suggested as one of the candidate materials for selective isomerization of 1-butene to isobutene and should be of particular interest to the petrochemical industry.

References
(1) Bhan, A.; Iglesia, E. *Acc. Chem. Res.* **2008**, *41*, 559.
(2) Corma, A. *J. Catal.* **2003**, *216*, 298.
(3) Smit, B.; Maesen, T. L. M. *Nature (London, U. K.)* **2008**, *451*, 671.
(4) Venuto, P. B. *Microporous Mater.* **1994**, *2*, 297.
(5) Yaluris, G.; Rekoske, J. E.; Aparicio, L. M.; Madon, R. J.; Dumesic, J. A. *J. Catal.* **1995**, *153*, 65.
(6) Corma, A.; Rey, F.; Valencia, S.; Jorda, J. L.; Rius, J. *Nat. Mater.* **2003**, *2*, 493.
(7) Andy, P.; Gnep, N. S.; Guisnet, M.; Benazzi, E.; Travers, C. *J. Catal.* **1998**, *173*, 322.
(8) Guisnet, M.; Andy, P.; Gnep, N. S.; Benazzi, E.; Travers, C. *J. Catal.* **1996**, *158*, 551.

(9) Houžvička, J.; Hansildaar, S.; Ponec, V. *J. Catal.* **1997**, *167*, 273.

(10) Jousse, F.; Leherte, L.; Vercauteren, D. P. *Mol. Simul.* **1996**, *17*, 175.

(11) Meriaudeau, P.; Bacaud, R.; Ngoc Hung, L.; Vu, A. T. *J. Mol. Catal. A: Chem.* **1996**, *110*.

(12) Mériaudeau, P.; Tuan, V. A.; Le, N. H.; Szabo, G. *J. Catal.* **1997**, *169*, 397.

(13) Boronat, M.; Viruela, P.; Corma, A. *Phys. Chem. Chem. Phys.* **2001**, *3*, 3235.

(14) Tuma, C.; Kerber, T.; Sauer, J. *Angew. Chem.-Int. Edit.* **2010**, *49*, 4678.

(15) Tuma, C.; Sauer, J. *Phys. Chem. Chem. Phys.* **2006**, *8*, 3955.

(16) Derouane, E. G.; Chang, C. D. *Microporous Mesoporous Mater.* **2000**, *35-36*, 425.

(17) Zhao, Y.; Truhlar, D. G. *J. Phys. Chem. C* **2008**, *112*, 6860.

(18) Zhao, Y.; Truhlar, D. G. *Acc. Chem. Res.* **2008**, *41*, 157.

(19) Bobuatong, K.; Probst, M.; Limtrakul, J. *J. Phys. Chem. C* **2010**, *114*, 21611.

(20) Boekfa, B.; Choomwattana, S.; Khongpracha, P.; Limtrakul, J. *Langmuir* **2009**, *25*, 12990.

(21) Boekfa, B.; Pantu, P.; Probst, M.; Limtrakul, J. *J. Phys. Chem. C* **2010**, *114*, 15061.

(22) Maihom, T.; Boekfa, B.; Sirijaraensre, J.; Nanok, T.; Probst, M.; Limtrakul, J. *J. Phys. Chem. C* **2009**, *113*, 6654.

(23) Pantu, P.; Boekfa, B.; Limtrakul, J. *J. Mol. Catal. A: Chem.* **2007**, *277*, 171.

(24) Wannakao, S.; Boekfa, B.; Khongpracha, P.; Probst, M.; Limtrakul, J. *ChemPhysChem* **2010**, *11*, 3432.

(25) Dapprich, S.; Komiromi, I.; Byun, K. S.; Morokuma, K.; Frisch, M. J. *THEOCHEM* **1999**, *461-462*, 1.

(26) Frisch, M. J.; Trucks, G. W.; Schlegel, H. B.; Scuseria, G. E.; Robb, M. A.; Cheeseman, J. R.; Montgomery, J. A., Jr.; Vreven, T.; Kudin, K. N.; Burant, J. C.; Millam, J. M.; Iyengar, S. S.; Tomasi, J.; Barone, V.; Mennucci, B.; Cossi, M.; Scalmani, G.; Rega, N.; Petersson, G. A.; Nakatsuji, H.; Hada, M.; Ehara, M.; Toyota, K.; Fukuda, R.; Hasegawa, J.; Ishida, M.; Nakajima, T.; Honda, Y.; Kitao, O.; Nakai, H.; Klene, M.; Li, X.; Knox, J. E.; Hratchian, H. P.; Cross, J. B.; Adamo, C.; Jaramillo, J.; Gomperts, R.; Stratmann, R. E.; Yazyev, O.; Austin, A. J.; Cammi, R.; Pomelli, C.; Ochterski, J. W.; Ayala, P. Y.; Morokuma, K.; Voth, G. A.; Salvador, P.; Dannenberg, J. J.; Zakrzewski, V. G.; Dapprich, S.; Daniels, A. D.; Strain, M. C.; Farkas, O.; Malick, D. K.; Rabuck, A. D.; Raghavachari, K.; Foresman, J. B.; Ortiz, J. V.; Cui, Q.; Baboul, A. G.; Clifford, S.; Cioslowski, J.; Stefanov, B. B.; Liu, G.; Liashenko, A.; Piskorz, P.; Komaromi, I.; Martin, R. L.; Fox, D. J.; Keith, T.; Al-Laham, M. A.; Peng, C. Y.; Nanayakkara, A.; Challacombe, M.; Gill, P. M. W.; Johnson, B.; Chen, W.; Wong, M. W.; Gonzalez, C.; Pople, J. A. *Gaussian 03, revision B.05;* *Gaussian, Inc.: Pittsburgh, PA*, 2003.

(27) Klinowski, J. *Chem. Rev.* **1991**, *91*, 1459.

(28) Eder, F.; Stockenhuber, M.; Lercher, J. A. *J. Phys. Chem. B* **1997**, *101*, 5414.

(29) Yoda, E.; Kondo, J. N.; Domen, K. *J. Phys. Chem. B* **2005**, *109*, 1464.

(30) Cant, N. W.; Hall, W. K. *J. Catal.* **1972**, *25*, 161.

Decomposition of Nitrous oxide on Au-Embedded Graphene

Anawat Thivasasith[1,2,3], Pipat Khongpracha[1,2,3], Chompunuch Warakulwit[1,2,3] and Jumras Limtrakul[1,2,3]*

[1]Laboratory for Computational and Applied Chemistry, Department of Chemistry, Faculty of Science and Center of Nanotechnology, Kasetsart University Research and Development Institute, Kasetsart University, Bangkok 10900, Thailand
[2]Center for Advanced Studies in Nanotechnology and Its Applications in Chemical, Food and Agricultural Industries, Kasetsart University, Bangkok 10900, Thailand
[3]NANOTEC Center of Excellence, National Nanotechnology Center, Kasetsart University, Bangkok 10900, Thailand

*Corresponding author: Tel. +66 2562 5555 ext 2169, Fax: +66 2562 5555 ext 2176,
E-mail address: jumras.l@ku.ac.th

Introduction

Metal nanostructures deposited on an exfoliated or a single graphene sheet have been the subject of numerous investigations due to their considerable promise in the various applications including catalysis[1], electrocatalyst and fuel cell[2], biosensors[3], and surface enhanced Raman scattering (SERs)[4]. Apart from metal nanostructures deposited onto a graphene sheet, recently the metal embedded graphene has attracted attention from both experimental[5] and theoretical[6] points of view due to its interesting electronic (and also magnetic) structures[6] and high thermal stability[5] opening up tremendous opportunities in advancing catalysis based on graphene[2]. A graphene sheet with a single-vacancy defect or the missing lattice atom, the simplest defect in any material[7], is good substrate material for metal embedded graphene. Many transition metal atoms can form strong covalent bonds with high binding energies ranging between 2-8 eV with an under-coordinate atom at a vacancy[6] indicating possible use in catalysis[7]. The catalytic activity of metal embedded graphene including Au-, Fe-, and Cu-embedded graphene was studied by using the CO oxidation as a benchmark probe[2]. To the best of our knowledge, the catalytic activity of the metal-embedded graphene for the decomposition of nitrous oxide (N_2O), an attractive subject from the environmental point of view, has not been investigated. Then, in this work, we aim to investigate the catalytic activity of a metal-embedded (Au) graphene, for the nitrous decomposition. This is because, in many cases, molecular oxygen can be adsorbed preferentially on small Au clusters[8] and N_2O can also act as an oxygen donor.

Model and Methods

The spin-unrestricted density functional theory (DFT) calculations were carried out using the DMol^3 package. All results were obtained by the generalized gradient approximation with the Perdew-Burke-Ernzerhof (PBE) functional. DFT semicore pseudopotentials (DSPPs) and a double numerical basis set including a d-polarization function (DND) were selected. Within the DSPP scheme implemented in DMol^3, all-electron calculations were performed for C and O atoms, and relativistic effects were included for Au. The real-space global orbital cutoff radius was set to 6 Å. A hexagonal graphene supercell (4×4 graphene unit cells) containing 32 atoms was set up to represent the system. One carbon atom was substituted by an Au atom. The minimum distance between the graphene sheet and its mirror images is greater than 20 Å, which is sufficiently large to avoid interactions between them. In the geometric optimization and the transition state (TS) searching steps, the Brillouin zone integration was performed with the Monkhorst-Pack 3×3×1 k-point sampling. The minimum-energy pathway for elementary reaction steps was computed using the nudged elastic band (NEB) method[9]. For the density-of-states (DOS) calculations, the 6×6×1 k-point sampling was used to achieve high accuracy. Charge distribution in each system was calculated with the Hirshfeld charge analysis method[10]. The adsorption energy E_{ad} between the adsorbate and Au/graphene is defined as;

$$E_{ad} = E_{cpx} - (E_{Au/graphene} + E_{adsorbate})$$

where the subscripts cpx, Au/graphene, and adsorbate denote the total energies of the adsorption complex and the corresponding substances.

Results and Discussion

In this work, DFT calculations were performed to investigate the reaction mechanisms of the decomposition of the nitrous oxide molecule on the Au-embedded graphene models. The bond length between the Au atom and each of the three neighboring carbon atoms is 2.30 Å, and the height of the Au atom above the graphene base plane is 1.67 Å both of which are in good agreement with those of previous calculations based on the plane-wave basis[2,3]. Moreover by means of the Hirshfeld charge population analysis, there is about a 0.40e electron transfer (Q) from Au to the graphene sheet.

The spin density mainly accumulates on the Au atom and those three neighboring carbon atoms (Figure 1b). To gain a deeper insight into the electron structure of Au-embedded graphene, the spin-polarized local density of states are projected on Au-5d and Au-6s orbitals and the neighboring C-2p orbital is plotted, as shown in Figure 1c. Because of the formation of C-Au bonds and electron transfer from Au to C, Au-5d, Au-6s, and C-2p orbitals are partially filled. As a result, the high density of spin-polarized states around E_F is localized on C-2p, Au-5d and Au-6s orbitals. This confirmed that the region at the gold atom is an active site for the incoming nitrous oxide molecule.

The nitrous decomposition on the Au-embedded graphene was proposed to occur via the concerted mechanism. The reaction intermediates related to this mechanism are shown in Figure 2a. At the initial step (IS), the N_2O molecule approaches the Au- embedded graphene in a tilted direction (the Au-O-N angle = 131.6°) and transfers an O atom to the Au-embedded graphene. At the transition state (TS) the O atom is pointing to the Au atom and the bond distance of O–Au is 2.12 Å. In comparison to the isolated N_2O molecules, the O–N2 lengthens from 1.20 to 1.62 Å and N1–N2 shortens from 1.14 to 1.13 Å. The N1–N2–O is changed from a linear to a bent alignment on account of the changing of the electronic hybridization of the central atom in the N_2O molecule. Finally, the product (PRO) that the bond between O and Au is formed (1.96 Å).

The adsorption of N_2O with Au-embedded graphene, Figure 2a shows the most stable configuration of N_2O on the Au-embedded graphene system with $E_{ad}(N_2O)$ = -4.26 kcal/mol. Meanwhile, there is about a 0.02e electron transfer from N_2O to the Au-embedded defect graphene, which occupies in Au-5d orbitals. In this case, the electrons not only accumulate on the Au atom but also on C-Au bond. The O atom of N_2O approaches the Au-embedded graphene and reaches TS. The activation energy barrier E_a is estimated to be 26.26 kcal/mol (Figure 3). At this configuration, there is about a 0.04e electrontransfer from Au-5d and Au-6s to N_2O (spin-polarized states are localized around E_F, figure 2b) which are occupied in N_2O-$2\pi^*$ orbitals and subsequently lead to the elongation of the O-N2 bond length from 1.13 to 1.62 Å (Figure 2a-TS). After the TS, the

intermediate complex (INT) is formed. At this point, there is about a 0.06 electron transfers from the Au-embedded graphene to O of N_2O and this leads to the complete cleavage of the O–N2 bond from 1.13 to 3.30 Å. The process is found to be an endothermic process with respect to the initial state. Finally, the N_2 molecule is desorbed from the complex with the required energy of 0.24 kcal/mol.

In the previous studies, the N_2O decomposition on the defect carbon nanotube had a reaction barrier of 40.3 kcal/mol[11] and 30.0 kcal/mol on the defect graphene at room temperature. In this work, a much lower activation energy barrier for the nitrous decomposition catalyzed by Au-embedded graphene of 26.3 kcal/mol is found. Due to the low activation barrier involved, the reaction is likely to proceed rapidly at room temperature. Moreover, the catalytic activity of this graphene-based catalyst may be tuned or enhanced by the curvature of a sheet due to its flexible character. Another important property of Au-embedded graphene is its plane structure with high surface area, which ensures its good catalytic efficiency and activity in reaction progresses.
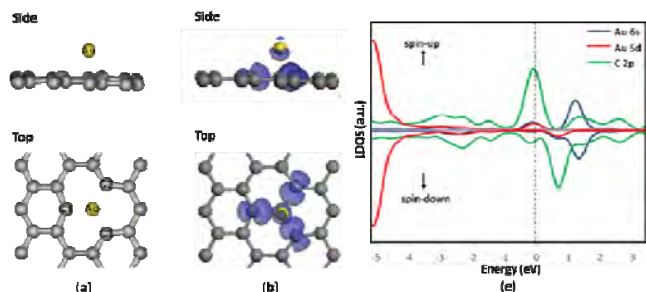

Figure 1. Electronic and geometric structure of Au-embedded graphene. (a) Side and top view of the geometric and (b) spin-density isosurface. (c) Spin-polarized local density of states projected on 5d (red curve) and 6s (blue curve) orbitals of Au as well as 2p (green curve) orbitals of neighboring carbon atoms.
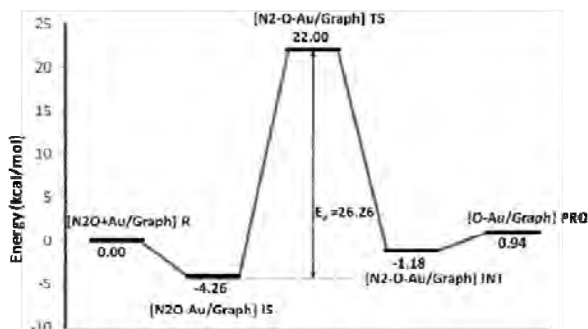

Figure 3. Schematic energy profiles corresponding to local configurations along the minimum-energy pathway via the $N_2O \rightarrow$ N_2+O route.
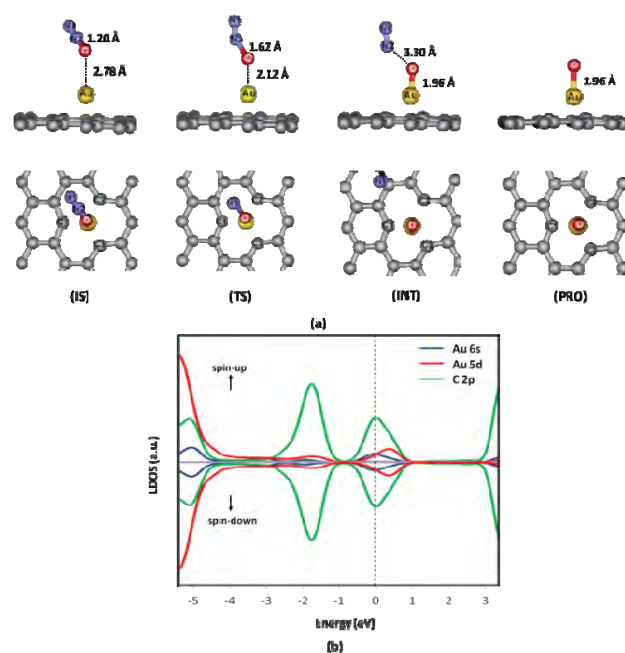

Figure 2. Local configuration of the adsorbates on the Au-embedded defect graphene at various intermediate states, (a) including the initial state (IS), transition state (TS), intermediate state (INT), and product state (PRO) along the minimum-energy pathway via the $N_2O \rightarrow$ N_2+O route. (b) Spin-polarized local density of state of transition state projected on 5d (red curve) and 6s (blue curve) orbitals of Au as well as 2p (green curve) orbitals of neighboring carbon atoms.

Conclusions

The nitrous decomposition on Au-embedded graphene is predicted to occur at room temperature. The high catalytic activity of Au-embedded graphene may be attributed to the partially occupied s and d orbital localized in the vicinity of the Fermi level because of the interactions between the Au atom and the C neighboring atom of graphene. However, we can expect that the metal atom is not limited to Au. Other transition-metal- embedded graphene is expected to have high catalytic activity, such as Ag, Cu-embedded graphene. The proposed method transforms the inert graphene to a highly active material for catalysis. This opens a new avenue to fabricate low cost and highly efficient catalysts based on carbon.

References

(1) Li, Y.; Fan, X.; Qi, J.; Ji, J.; Wang, S.; Zhang, G.; Zhang, F., *Mater. Res. Bull.* **2009**, *45* (10), 1413-1418.

(2) Muszynski, R.; Seger, B.; Kamat, P. V., *J. Phys. Chem. C* **2008**, *112* (14), 5263-5266.

(3) Hong, W.; Bai, H.; Xu, Y.; Yao, Z.; Gu, Z.; Shi, G., *J. Phys. Chem. C* **2010***, 114* (4), 1822-1826.

(4) Goncalves, G.; Marques, P. A. A. P.; Granadeiro, C. M.; Nogueira, H. I. S.; Singh, M. K.; Gracio, J., *Chem. Mater.* **2009**, *21* (20), 4796-4802.

(5) Gan, Y.; Sun, L.; Banhart, F., *Small* **2008**, *4* (5), 587-591.

(6) Krasheninnikov, A. V.; Lehtinen, P. O.; Foster, A. S.; Pyykk; ouml; P.; Nieminen, R. M., *Phys. Rev. Lett.* **2009**, *102* (12), 126807.

(7) Banhart, F.; Kotakoski, J.; Krasheninnikov, A. V., *ACS Nano* **2011,** *5* (1), 26-41.

(8) Tsunoyama, H.; Sakurai, H.; Tsukuda, T., *Chem. Phys. Letters* **2006**, *429* (4-6), 528-532.

(9) Lu, Y.-H.; Zhou, M.; Zhang, C.; Feng, Y.-P., *J. Phys. Chem. C* **2009**, *113* (47), 20156-20160.

(10) Song, E. H.; Wen, Z.; Jiang, Q., *J. Phys. Chem. C* **2011**, *115* (9), 3678-3683.

(11) Namuangruk, S.; Khongpracha, P.; Tantirungrotechai, Y.; Limtrakul, J., *J. Mol. Graph. Model.* **2007**, *26* (1), 179-186.

DENSITY FUNCTIONAL THEORY STUDY ON CATALYTIC CRACKING OF *n*-HEXANE ON HETEROPOLY ACID COMPARISON WITH FAU ZEOLITE

Saowapak Choomwattana[1,2,3], Thana Maihom[1,2,3], and Jumras Limtrakul [1,2,3]*

[1]Laboratory for Computational and Applied Chemistry, Department of Chemistry, Faculty of Science and Center of Nanotechnology, Kasetsart University Research and Development Institute, Kasetsart University, Bangkok, Thailand
[2]NANOTEC Center of Excellence, National Nanotechnology Center, Kasetsart University, Bangkok, Thailand
[3]Center for Advanced Studies in Nanotechnology and Its Applications in Chemical, Food and Agricultural Industries, Kasetsart University, Bangkok, Thailand
*Corresponding author's e-mail address: jumras.l@ku.ac.th

Introduction

In petroleum refining and petrochemical conversion, acid-catalyzed reactions of alkanes, including cracking, dehydrogenation, isomerization, and disproportionation is of significant importance. One reaction among those most thoroughly investigated is the cracking reaction. This one has the possibility for comparing experimental results with theory and the promising insight into the molecular mechanism of more complicated reactions. The key components of industrial petroleum cracking catalysts are solid proton-donor acids, including zeolites. Numerous researches concerning solid catalysts have been conducted due to their catalytic activity for the low-temperature reaction. What lies beneath the catalyst effectiveness is the strength of the acid. It influences both pathways and the nature of reacting species in the cracking reaction.

Both zeolites and heteropoly acids (HPA) are well known superacids. Without a doubt, zeolite is capable of cracking hydrocarbons. For instance, monomolecular cracking reactions over ZSM-5, Beta and Faujasite zeolites occur at the temperature of 623-773 K.[1] HPA is, on the other hand, less well known for the application in hydrocarbon cracking reactions due to its poor stability and lack of monodispersity. An example of this is the experimental work on the stability and catalytic property of phosphotungstic acid (HPW) on the *n*-hexane cracking reaction.[2] It was reported that, in a fixed bed reactor and the nitrogen-hexane mixture feed at atmospheric pressure, the catalyst was active at 473 K for only 8 minutes before it died completely. The drawbacks are possibly surmountable as many attempts, such as applying catalyst support and stabilizer,[3-5] have been made to improve the catalyst.

Regarding the molecular point of view, bimolecular and monomolecular mechanisms were proposed to explain the catalytic cracking of hydrocarbons,[6-8] while the classical bimolecular mechanism, consisting of hydride transfer, isomerization and β-scission, was suggested for the condition of high partial pressure of hydrocarbons and low reaction temperature. Monomolecular cracking is believed to be dominant in the cracking reaction of hydrocarbons under low pressure and high temperature reaction.[6,7] The key reacting species of the latter mechanism is a high-energy nonclassical two-electron three-center carbonium ion which is formed by the direct protonation of Brønsted acid to the C−C bond.[6,7] Subsequently, the carbonium ion collapses, leading to the scission of the C−C bond to produce alkane and alkene products. In our calculation, we reported in 2010 that the protonation step is found to be the rate-determining step.[9] Therefore, only the information of this step could lead to a reasonable prediction for the catalyst effectiveness.

Attempts have been made to develop the computational methodology that can precisely predict the physical and chemical properties of the catalyst itself and the catalyzed reactions. The new meta-hybrid density functional M06 series[10,11] have been recently developed for the accurate computation of the covalent and non-covalent binding energies of adsorbates with the zeolite acid site. The results were comparable to MP2 calculations at a high basis set but at much more affordable computer times. M06-L is the most accurate functional for transition metals and is especially efficient for calculations on large systems.[12] Therefore, it is practical for presenting systems.

In this work, the density functional theory, M06-L including dispersion energy, has been employed to determine transition states and the corresponding energy barriers of the reactions related to the first step of cracking *n*-hexane catalyzed by a protonated zeolite (H-FAU) and a heteropoly acid (HPA). Hexane is chosen as a reactant in this work because it is widely used experimentally as a benchmark in cracking reactions to study the catalyst acidity.[13,14] The direct comparison of the protolytic cracking of *n*-hexane on zeolite and heteropoly acid has been performed for the first time to provide insight into understanding these two catalysts for industrially important cracking reactions.
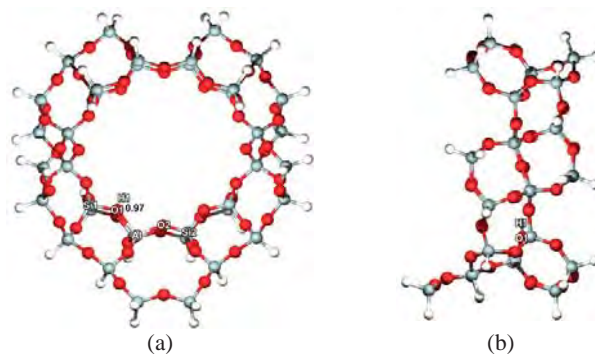

Figure 1. 38T cluster model of H-FAU zeolite: (a) front view with the acidic bond distance and (b) side view.

Figure 2. Cluster model of α-Keggin HPW heteropoly acid: (a) atomistic graphics with the acidic bond distance and (b) an orange tetrahedron representing the phosphate anionic core of the HPW.

Models and Method

Nanocluster models of zeolite (H-FAU) and Heteropoly Acid (α-Keggin HPW) were generated from their lattice structures.[15,16] The 38T cluster model of H-FAU, illustrated in Figure 1 covers the 12-membered-ring window connecting two supercages of faujasite. It is symmetrically extended from the 12T of the 12-membered-ring to include 38 tetrahedral atoms. Silicon at the T2 position was replaced by aluminum to model a Brønsted acid site. For the phosphotungstic acid, the cluster model (see Figure 2a) whose molecular formula is $H_3PW_{12}O_{40}$, can be considered as a $W_{12}O_{36}$ cage (which is composed of 12 edge-sharing WO_6 metal-oxygen octahedra) enveloping a

phosphate (PO_4^{3-}) anion (Figure 2b). Similar to zeolites, the acidic proton, for the charge neutralization, of HPW heteropoly acid resides on framework oxygen atoms. We adopted the model from the work of Yang and co-workers[17] which proposed a rational model based on experimental works.[18]

For the zeolite system, only the 5T active region of "SiOHAl(OSi)$_2$OSi" and the reacting molecule are allowed to relax during geometry optimizations, while the rest of the structure is kept fixed at the crystallographic coordinates. For the HPW system, all atoms are allowed to relax during the optimizations. M06-L density functional was used in all calculations. The basis set of 6-31G(d,p) was employed for Al, Si, O, P and H atoms, while the W atom was described by the Effective Core Potentials (ECP) of Stuttgart RSC 1997 ECP.[19] All calculations were performed with the Gaussian 03 code[20] modified to incorporate the Minnesota Density Functionals module 3.1 by Zhao and Truhlar.

Results and Discussion

Bare Catalysts. H-FAU and HPW share a common character, Brønsted acid that is accessible, thus being proficient in acid catalysis. From a review of Mizuno and Misono,[21] it was stated that heteropoly acids such as HPW in the solid state are pure Brønsted acids and stronger acids than the conventional solid acids such as SiO_2-Al_2O_3, H_3PO_4/SiO_2, and HX and HY zeolites. By definition, one can analyze the Brønsted acidity from deprotonation energy calculated with the following equation:

Deprotonation energy $=$ E(H-Catalyst) $-$ E(H$^+$) $-$ E(Catalyst)

From our calculation, we found the same trend as the deprotonation energy of H-FAU and HPW; 310.9 and 263.1 kcal/mol, respectively. Even so, the O–H acidic bond in both catalysts is the same (0.97 Å, shown in Figures 1 and 2). The finding can be construed as the confinement effect of the zeolitic framework influences a stronger attraction of proton or other adsorbates to the framework oxygen, O1, thus requiring more energy to deprotonate the catalyst.
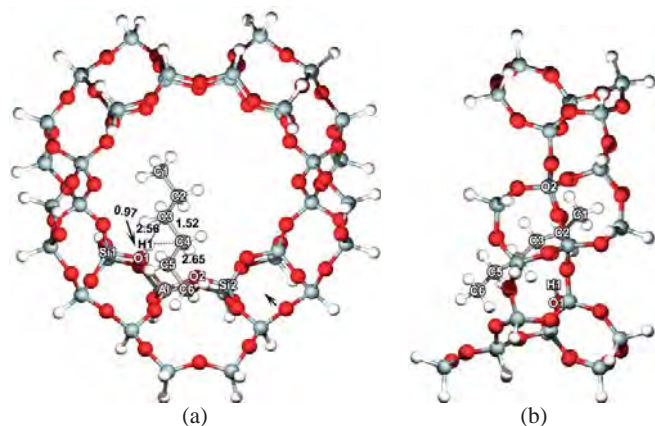

Figure 3. Optimized structures of the adsorption state of *n*-hexane protolytic cracking over H-FAU: (a) front view and (b) side view.

_n_-Hexane adsorption. Upon the adsorption (see Figures 3 and 4), there is no significant change in the bond lengths of the O1–H1 acidic bond and the cracking of the C3–C4 bond, when comparing to the isolated components. Nevertheless, the intermolecular distances between the alkane and the catalytic acid of the catalysts are different.

The zeolite proton resides in 'the valley' of the oxygen framework. On the other hand, the curvature of the HPW active site is upward. The proton of HPW is therefore more accessible to the adsorbate. Consequently, the average intermolecular distance between *n*-hexane and the proton is 2.62 Å for H-FAU and 2.42 Å for HPW.
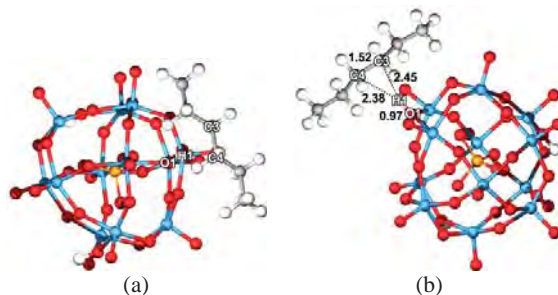

Figure 4. Optimized structures of adsorption state involved in the protolytic cracking of *n*-hexane over HPW: These views are meant to imitate the view of *n*-hexane in Figures 3 (a) and (b), respectively.

Once the intermolecular distance is larger, the adsorption energy is generally expected to be less. In this present work, there is a contrary. The corresponding adsorption energies for H-FAU and HPW systems are −11.7 and −6.8 kcal/mol, respectively. The calculated adsorption energy of the H-FAU system agrees well with an experimental measurement of −12.7 kcal/mol.[21] The tendency contradiction between the intermolecular distance and the adsorption energy can be explained with the confinement effect of the zeolite pore that plays a dominant role in the adsorption. This is another proof of the major contribution of the confinement effect in the zeolite catalysis.

Transition State of Protolytic Cracking of *n*-Hexane. The adsorbed *n*-hexane molecule is protonated by the acidic proton at the central C−C bond to form the adsorbed 3-C-hexonium intermediate. Selected geometrical parameters for the reaction step and optimized structures are shown in Figures 5 and 6 for reactions in H-FAU and HPW, respectively.
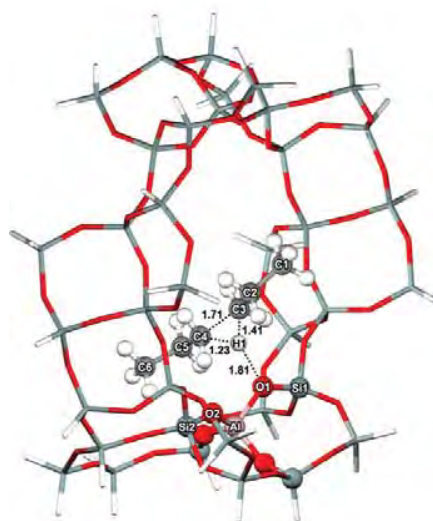

Figure 5. Optimized structure of the transition state of *n*-hexane protolytic cracking over H-FAU.

At the transition state, the H1 proton is protonated to the C3–C4 bond of *n*-hexane. The interaction that holds the transition complex of the proton-accepting reacting species and the proton-donating catalyst together can be considered as electrostatic.[23-25] In H-FAU, the Brønsted O1–H1 bond distance is elongated from 0.98 to 1.81 Å while the C3–C4 bond distance is increased to 1.71 Å. The C3–H1 and C4–H1 distances are 1.41 and 1.23 Å, respectively. The geometry of the transition state structure in HPW is similar to that in H-FAU with slight differences in the HPW system, i.e. a shorter Brønsted O1–H1 bond distance (1.61 Å) and proton transfer distances (C3–H1 = 1.41 Å and C4–H1 = 1.28 Å). The existence of true transition states has been confirmed by frequency calculations resulting in one imaginary frequency related to the movement of the acidic proton of zeolite (H1) to the *n*-hexane C3–C4 bond and the breaking of the C3–C4 bond.
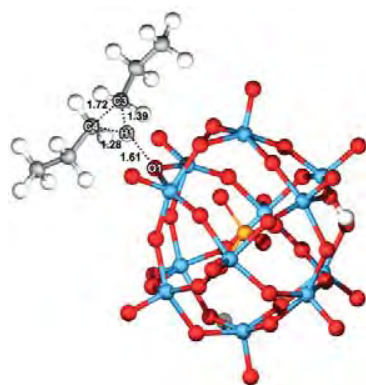

Figure 6. Optimized structure of *n*-hexane protolytic cracking over HPW.

The adsorption energies of *n*-hexane are predicted to be −11.7 and −6.8 kcal/mol for H-FAU and HPW, respectively, the former value is in good agreement with experimental measurements. This indicates that the models employed for zeolite as well as for HPW can be well represented by the M06-L functional. The cracking reaction is assumed to proceed via the first step of the C–C activation and is found to be the rate-determining step with activation energies of 44.7 and 41.4 kcal/mol for H-FAU and HPA, respectively. It is noted that the relative energy of the transition state is 33.0 kcal/mol for H-FAU and 34.6 kcal/mol for HPW. The apparent activation energy is only 1.63 kcal/ml different. The consequence is that the stability of the adsorption is the key factor to determine the height of the activation barrier.
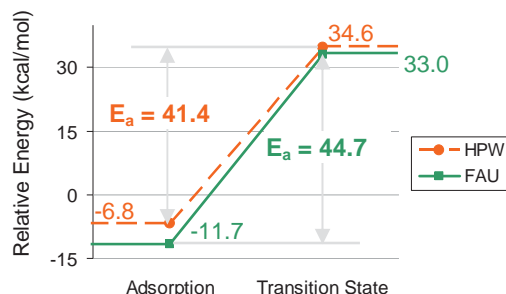

Figure 7. Energy profile for *n*-hexane protolytic cracking catalyzed by H-FAU zeolite (solid line) and HPW heteropoly acid (dashed line) comparing to the isolated systems.

With the comparable catalytic efficiency presented in the present study, HPW could be used instead of H-FAU. However, heteropoly acids lack the confinement effect that is provided by the zeolite pore. This weakness can be overcome by applying the acids into other porous materials. Nowadays, there is a number of publications reporting about the hybrid materials of heteropoly compounds (in either protonated or anionic form) and metal-organic frameworks (MOFs)[26-28] Utilizing the molecular design approach, one can vary the type of heteropoly acid and the composition combination of the MOFs to achieve the materials with a desired catalytic property of the acid and the tailored environment (i.e. size and shape of the pore and functionality) of the framework.

Conclusions

The key step of the *n*-hexane cracking reaction over two different types of solid acid catalyst has been investigated by utilizing the 38T H-FAU and α-Keggin HPW cluster models calculated at the M06-L/6-31G(d,p) level of theory. These calculations give adsorption energies which represent the experimental data well. The key transition state of the protolytic cracking, which is the rate-determining step of the overall cracking reaction, was optimized and analyzed. The different activities of the Brønsted acid catalysts can be explained by the different adsorption energies which are mainly due to the presence of the confinement effect of the zeolite pore that facilitates the adsorption but raise the activation barrier at the same time. The present study shows the advantages and disadvantages of both catalysts. While the zeolite provides confinement effect and shape selectivity, it lacks variety, thus being difficult to modify to suit any new applications. Alternatively, heteropoly acid has no confinement effect and such a specific selectivity, but it is tunable by varying the elemental composition and the geometry. Not only for a better stability and dispersion, but for the combination of heteropoly acid into hybrid materials is promising for breakthrough applications.

References
(1) Kotrel, S.; Rosynek, M. P.; Lunsford J. H. *J. Phys. Chem. B* **1999**, *103(5)*, 818–824.
(2) Jalil, A.; Faiz, M.; Tabet, N.; Hamdan, N. M.; Hussain, Z. *J. Catal.* **2003**, *217(2)*, 292–297.
(3) Bhorodwaj, S. K.; Dutta D. K. *App Clay Sci.*, **2011**, doi:10.1016/j.clay.2011.01.019.
(4) Fiuza, R. A.; Santos, I. V.; Fiuza, R. P.; José, N. M.; Boaventura, J. S.; *Macromol*. *Symp.* **2011**, *299-300(1)*, 234–240.
(5) Betz, D.; Altmann, P.; Cokoja, M.; Herrmann, W. A.;Kuhn, F.E. *Coord. Chem. Rev.* **2011**, doi:10.1016/j.ccr.2010.12.004.

(6) Haag, W. O.; Dessau, R. M. *Proc. 8th Intl. Cong. Catal. Berlin (Dechema, Frankfurt-am-Main),* **1984**, 2, pp 305−316.

(7) Kotrel, S.; Knözinger, H.; Gates, B. C. *Micropor. Mesopor. Mater.* **2000**, *35−36*, 11-20.

(8) Corma, A.; Orchilles, A. V. *Micropor. Mesopor. Mater.* **2000**, *35−36*, 21-30.

(9) Maihom, T.; Pantu, P.; Tachakritikul, C.; Probst, M. and Limtrakul J. *J. Phys. Chem. C* **2010**, *114(17)*, 7850–7856.

(10) Zhao, Y. and Truhlar, D. G. *J. Phys. Chem. C* **2008**, *112*, 6860–6868.

(11) Zhao, Y. and Truhlar, D. G. *Acc. Chem. Res.* **2008**, *41(2)*, 157–167.

(12) Kumsapaya, C.; Bobuatong, K.; Khongpracha, P.; Tantirungrotechai, Y.; Limtrakul, J. *J. Phys. Chem. C* **2009**, *113(36)*, 16128–16137.

(13) Bourdillon, G.; Gueguen, C.; Guisnet, M. *Appl. Catal.* **1990**, *61(1)*, 123-139.

(14) Lercher, J. A.; Jentys, A. ; Brait, A. *Mol. Sieves Sci. Technol.* **2008**, *6*, 153-212.

(15) Alberti, A.; Davoli, P.; Vezzalini, G. Z. Z. *Kristallogr.* **1986**, *175*, 249–256.

(16) Soares-Santos P. C. R.; Cunha-Silva, L.; Sousa, F. L.; Mafra, L.; Rocha, J.; Cavaleiro, A. M. V.; Trindade, T.; Paz, F. A. A.; Klinowski, J. ; Nogueira, H. I. S. *J. Molec. Struct.* **2008**, *888(1-3)*, 99-106.

(17) Yang, J.; Janik, M. J.; Ma, D.; Zheng, A.; Zhang, M.; Neurock, M.; Davis, R. J.; Ye, C. and Deng, F. *J. Am. Chem. Soc.,* **2005**, *127*(51), pp 18274-18280.

(18) Ueda, T; Tatsumi, T; Eguchi, T.; Nakamura, N. *J. Phys. Chem. B* **2001**, *105(23)*, 5391–5396.

(19) Dolg, M.; Stoll, H.; Preuss, H.; Pitzer, R. M. *J. Phys. Chem.* **1993**, *97*, 5852–5859.

(20) *Gaussian 03, revision B.05*; Gaussian, Inc.: Pittsburgh, PA, **2003**.

(21) Mizuno, N.; Misono, M.*Chem. Rev.* **1998**, *98 (1)*, 199–218.

(22) Eder, F.; Stockenhuber, M.; Lercher, J. A. *J. Phys. Chem. B* **1997***, 101(27)*, 5414–5419.

(23) Galadima, A.; Anderson, J. A.; Wells, R. P. K. *Sci. World J.* **2009**, *4(3)*, 15-22.

(24) Bharad, J. V.; Madje, B. R.; Ubale, M. B. *Int. J. ChemTech Res.* **2010***, 2(1)*, 346-353.

(25) Vollmer, J. M.; Truong, T. N. J. *Phys. Chem. B* **2000**, *104(26)*, 6308–6312.

(26) Dang, D.-B.; Bai, Y.; He, C.; Wang, J.; Duan, C.-Y.; Niu, J.-Y. *Inorg. Chem.* **2010**, *49(4)*, 1280–1282.

(27) Ma, F.-J.; Liu, S.-X.; Liang, D.-D.; Ren, G.-J.; Zhang, C.-D.; Wei, F.; Su, Z.-M. *Eur. J. Inorg. Chem.* **2010**, *24*, 3756–3761.

(28) Juan-Alcaniz, J.; Ramos-Fernandez, E. V.; Lafont, U.; Gascon, J.; Kapteijn, F. *J. Catal.,***2010**, *269(1)*, 229-241.

Synthesis of Precisely Size-Controlled Gold Nanoparticles and Their Infusion into Mesoporous Silica SBA-15 by Compressed Carbon Dioxide Solution Technique

Sarawoot Impeng[1,3,4], Amporn Sane[2,3,4], Chompunuch Warakulwit[1,3,4], Panvika Pannopard[1,3,4], Boonruen Sunpetch[1,3,4], Pipat Khongpracha[1,3,4], Jumras Limtrakul[1,3,4]*

[1]Department of Chemistry, Faculty of Science and Center of Nanotechnology, Kasetsart University Research and Development Institute, Kasetsart University, Bangkok 10900, Thailand
[2]Department of Packaging and Materials Technology, Faculty of Agro-Industry, Kasetsart University, Bangkok 10900, Thailand
[3]NANOTEC Center of Excellence, National Nanotechnology Center, Kasetsart University, Bangkok 10900, Thailand
[4]Center for Advanced Studies in Nanotechnology and Its Applications in Chemical, Food and Agricultural Industries, Kasetsart University, Bangkok 10900, Thailand
*Corresponding author's e-mail address: jumras.l@ku.ac.th

Introduction

Gold nanoparticles (AuNPs) especially with a diameter less than 5 nm have attracted great interest from scientific and industrial standpoints due to their excellent catalytic activity in various important chemical reactions including many oxidation and hydrogenation reactions at low temperatures. AuNPs supported on metal oxide were used as high active and durable catalysts for CO oxidation,[1] alcohols oxidation,[2] water-gas shift reaction,[3] C-C bond formation,[4] and so on. In particular, low temperature CO oxidation catalyzed by AuNPs deposited on reducible metal oxides[5] (TiO_2, CeO_2, Fe_2O_3, and Co_3O_4) and nonreducible metal oxides[1f,6] (Al_2O_3 and SiO_2) has been widely investigated. These studies reported that the catalytic activity depended on the size of AuNPs as well as the nature of supports. In many cases using the reducible supports for gold nanoparticles, the support or the Au-support interface was reported to play an important role on their catalytic activity leading such supported gold nanoparticles to be active catalysts.[1c] Particularly, AuNPs with a size smaller than 5 nm supported on nonreducible metal oxides were reported to be active. It is suggested that the catalytic activity of such gold nanoparticles is derived from the change of electronic structure or the higher density of reactive defective sites of the nanoparticles.[1f] For those reducible supports, however, the catalytic activity still depends on the size of AuNPs.[7]

Mesoporous silica materials have been considered as ideal catalyst supports because of their well-defined pore size as well as their high thermal and chemical stability. SBA-15 has been synthesized with a tunable structure, large pore diameter in the range of 2–30 nm and a wall thickness of 3.1–6.4 nm. This allows facile diffusion of the molecules into the porous structure of the silica, even for bulky molecules, making them desirable for depositing small metal nanoparticles inside. As the surface of mesoporous silica is highly negative charged; it is difficult to prepare AuNPs supported on SBA-15 with $AuCl_4^-$ being used as a precursor via direct deposition-precipitation and the impregnation technique.[2b] To overcome this limitation, the surface of mesoporous silica was modified with functional groups such as $-SH$[1f,8] and $-NH_2$.[9] Nevertheless, this method produced AuNPs with a broad size distribution as well as poorly controllable size and shape. Alternatively, AuNPs supported on a pure surface of mesoporous silica can be achieved by replacing the $AuCl_4^-$ precursor with $[Au(en)_2]^{3+}$ a cation precursor[1e] or using the colloidal deposition method.[2b,10] Employing colloidal AuNPs is of specific interest since the size distribution and shape of the nanoparticles can be effectively controlled as well as their catalytic activity that depends on the type

of protecting ligands. Tsukuda *et al.* reported that AuNPs stabilized by poly(vinylpyrrolidone) (PVP) provided weak interaction between the nanoparticles and the protecting polymer such that part of the nanoparticle surface was exposed and readily accessible for catalytic conversion.[11]

Recently, Liu *et al.* successfully deposited AuNPs (with a diameter of ~1 nm) stabilized by triphenylphosphine into pure mesoporous silica (SBA-15, HMS, MCF) dispersed and stirred in an organic medium.[2b] However, low loading of AuNPs (less than 1 wt %) was still obtained because of high viscosity and surface tension of the dispersion medium. Thus, it remains a challenge for developing a new technique to infuse AuNPs into pure mesoporous silica SBA-15. A supercritical fluid could be an excellent medium for the infusion of AuNPs due to its tunable solvent strength, high diffusivity, as well as low viscosity and surface tension. Especially, supercritical carbon dioxide ($scCO_2$) has been considered as an attractive solvent due to it being inexpensive, non-toxic, and non-flammable with a low critical temperature (31 °C) and moderate critical pressure (73.8 bar).[12] In addition, the solvent power of $scCO_2$ can be improved by adding an organic cosolvent. Gupta and co-workers reported the success of infusion of Au nanocrystals (2.2 ± 0.3 nm) protected with dodecanethiol into mesoporous SBA-15 with high Au loadings of up to 2.5 wt % by using a mixture of toluene and $scCO_2$ (1:3 v/v) at a temperature and pressure of 35 °C and 241 bar, respectivly.[13] Nevertheless, the disadvantage of using gold nanostructures protected by thiols is their low catalytic activity due to the strong interaction between thiol and the gold surface. Then, the usage for catalytic application is still limited. Thus far, the infusion of AuNPs with supercritical fluids for catalytic application has still been limited. Therefore, the aim of this work was to study the feasibility of the compressed CO_2 solution technique to infuse PVP-stabilized AuNPs into pure mesoporous SBA-15 in order to obtain the gold-supported mesoporous silica as a high active catalyst.

Experimental Section

Materials. Pluronic P123 triblock copolymer ($EO_{20}PO_{70}EO_{20}$), sodium borohydride ($NaBH_4$), and hydrogen tetrachloroaurate(III) trihydrate ($HAuCl_4.3H_2O$) were purchased from Sigma-Aldrich. Poly(vinylpyrrolidone) (PVP, MW = 40 000) was obtained from Fluka. Sodium silicate solution ($Na_2Si_3O_7$, 32 wt % SiO_2) was supplied by PQ Chemicals (Thailand). Analytical grade hydrochloric acid (HCl, 36.5–38.0 %) and absolute ethanol (98 %) were provided by J.T. Baker and Carlo Erba, respectively. CO_2 (purity >99.98%) was purchased from Chattakorn Lab Center (Thailand). All chemicals were used as received. Water was distilled and deionized before using in our experiments.

Synthesis of SBA-15. Mesoporous silica SBA-15 was synthesized by adapting the previously published method.[14] In a typical experiment, 0.845 g of Pluronic 123 was dissolved in 60 mL of deionized distilled water (DI water). During stirring of the solution, 3.125 g of sodium silicate solution was gradually added, followed by rapidly adding 5.4 mL of HCl to the Pluronic 123 solution. The mixture was continuously stirred and heated at 40 °C for 24 h. The mixture was autoclaved at 100 °C for 24 h and then filtered to collect as a white powder product. The product was neutralized by washing with DI water and then dried in a hot air oven at 140 °C for 3 h. Finally, the product was calcined at 550 °C for 6 h in order to obtain SBA-15.

Preparation of PVP-stabilized Au nanoparticles. The colloidal of PVP-stabilized Au (Au:PVP) nanoparticles were prepared by following the previous work reported by Tsunoyama *et al.*[4b,15] Typically, an aqueous mixture containing $HAuCl_4$ (1 mM, 50 mL) and PVP (5.56 g) was gently stirred for 30 min at 0 °C. Then, an aqueous solution of $NaBH_4$ (0.1 M, 5 mL) was rapidly added to the

mixture under vigorous stirring. At this step, the color of this solution immediately changed from pale yellow to dark brown, indicating the formation of the desired Au nanoparticles. The aqueous suspension of Au:PVP nanoparticles was kept at 0 °C under continuous stirring for 1 h. The colloidal suspension was centrifuged at 4000 rpm using a membrane tube with a 10 kDa molecular weight cut-off (MWCO) to separate and remove the inorganic impurities left in the mixture. The obtained dark brown product of Au:PVP nanoparticles was freeze-dried under vacuum conditions for 2 days.

Infusion of Au nanoparticles into SBA-15. The synthesized Au:PVP nanoparticles were infused into SBA-15 using a compressed solution containing $scCO_2$ and ethanol. Typically, the prepared SBA-15 (250 mg) was added into a variable-volume view cell. Au:PVP nanoparticles (5–10 mg) previously dispersed in ethanol (1–5 g) was then loaded into the cell. Next, $scCO_2$ (5–12 g) was loaded into the cell and the mixture was pressurized to 241 bar and heated at 35 °C. The obtained mixture was continuously stirred using a magnetic stirring bar for 3 h. Next, the mixture was depressurized and cooled down to ambient conditions. The resulting sample was dried in air to remove ethanol, and then calcined at 370 °C for 2 h to remove the PVP protecting-ligand from the AuNPs. The weight ratios of Au:PVP nanoparticles to SBA-15 used in this study were 1:25 and 1:50, while those of ethanol to $scCO_2$ were varied between 1:12 and 1:1.

Characterization. The powder sample of AuNPs-loaded SBA-15 was dispersed in ethanol and sonicated for 2 min. Then, the suspension was dropped onto a carbon-coated copper grid and dried at ambient conditions before being characterized by a transmission electron microscope (TEM, JEOL JEM-2010) with an accelerating voltage of 200 kV. Wide angle X-ray diffraction (XRD) data were collected via a PhiLips X'Pert Pro diffractometer with Cu Kα radiation (λ=0.1543 nm) operating with an accelerating voltage of 40 kV and current of 30 mA. Low angle XRD patterns were also collected using a Rigaku-TTRAX III diffractometer with Cu Kα radiation operating with 50 kV and 300 mA. N_2 adsorption-desorption isotherms were measured in a Micrometrics ASAP 2020 instrument at 77 K. All powder samples were degassed at 150 °C overnight before the measurements. The specific surface area was calculated using the Brunauer-Emmett-Teller (BET) method.[16] The total pore volume was estimated from the amount adsorbed at a relative pressure of about of 0.99, whereas the pore size distribution was determined from the adsorption branches of the isotherms by using the Barrett-Joyner-Halenda (BJH) method.[17] Thermogravimetric analysis (TGA) was performed using a Perkin Elmer TGA7 by heating from 30 to 370 °C with a rate of 10 °C/min and then maintained at 370 °C for 2 h under N_2 gas atmosphere.

Results and Discussion

Synthesis of SBA-15. Mesoporous silica SBA-15 produced in this work was characterized by N_2 adsorption-desorption isotherms, TEM, and low angle XRD. Figure 1a shows N_2 adsorption-desorption isotherms of the synthesized SBA-15, revealing a typical type IV with an H1 hysteresis loop. In addition, the shape of isotherms exhibits the hysteresis loop with very sharp adsorption-desorption branches, indicating uniform pore size distribution of SBA-15.[18] In the hysteresis loop, N_2 adsorption quantity rapidly increased from 300 to 500 cm^3g^{-1} at a relative pressure (P/P_0) of ~0.7 due to capillary condensation.[14a]

The BET specific surface area and total pore volume of the synthesized SBA-15 are 727 m^2g^{-1} and 0.83 cm^3g^{-1}, respectively. The pore size distribution was determined from the adsorption branches of the isotherms by using the BJH method, it is 7.6 nm (see Figure 1b). These results agree well with that obtained in the previous report of SBA-15.[14]
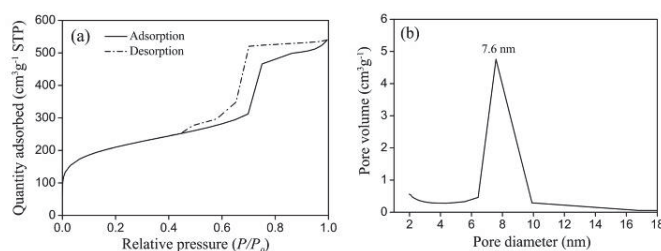

Figure 1. N_2 adsorption-desorption isotherms (a) and pore size distribution curve (b) of SBA-15

TEM analysis results illustrate that the synthesized SBA-15 has a well-ordered mesoporous channel (Figure 2a) and hexagonal honeycomb structures (Figure 2b) with the mean pore size and wall thickness of approximately 7–8 and 4–5 nm, respectively. Low angle XRD pattern of the SBA-15 exhibited three characteristic peaks at 2θ values of 0.87, 1.49, and 1.74° (see Figure 3) which were respectively indexed to (100), (110), and (200) reflections of the two-dimensional hexagonal ($p6mm$) mesostructure,[14a] in accordance with the TEM results (Figure 2). The d-spacing estimated from the first peak (d_{100}) was 10.1 nm. The unit cell parameter (a_0) corresponding to the distance between two pore centers calculated using $a_0 = 2d_{100}/\sqrt{3}$ was equal to 11.7 nm. Furthermore, the wall thickness estimated from the difference of the a_0 value and the pore size determined by N_2 adsorption-desorption isotherm analysis, was approximately 4.1 nm, relatively close to that determined from TEM images.
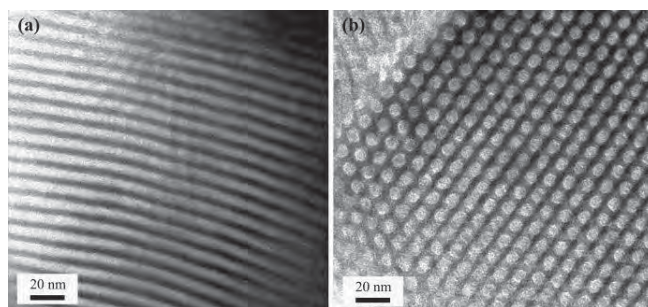

Figure 2. TEM images of pure SBA-15: (a) viewing normal to the pore axis; (b) viewing along the pore axis.
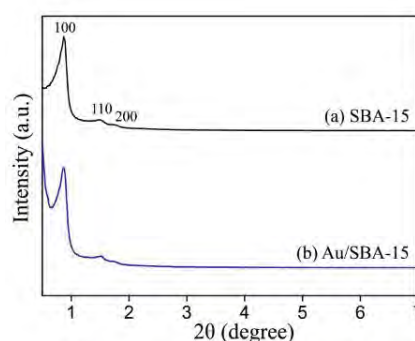

Figure 3. Low angle XRD patterns of: (a) SBA-15; (b) Au/SBA-15 composite (1:25 Au:PVP nanoparticles to SBA-15; 1:1 ethanol to $scCO_2$).

Preparation of Au:PVP nanoparticles. The synthesized Au:PVP nanoparticles were characterized by TEM and TGA analyses. Figure 4 shows a TEM image and the related particle size distribution of Au:PVP nanoparticles. The obtained nanoparticles were spherical and uniform with a narrow size distribution. The size of nanoparticles ranged from 1.0 to 4.0 nm with an average diameter of 2.3 ± 0.6 nm. The size of Au:PVP nanoparticles synthesized in this study was slightly larger than that previously reported by Tsunoyama *et al.* (1.3 ± 0.3 nm).[4b,15] TGA analysis of Au:PVP nanoparticles was also performed to determine a suitable calcination temperature for removing the PVP protecting-ligand without inducing aggregation of AuNPs after infusion into the SBA-15. TGA curves of Au:PVP nanoparticles are shown in Figure 5. It is shown that all of the PVP, the stabilizing polymer (67% in weight loss was found), was completely removed at the temperature of 370 °C indicating this temperature is suitable for calcination of the Au:PVP/SBA-15 composite.
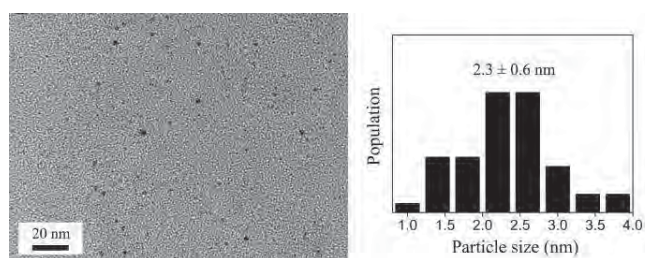

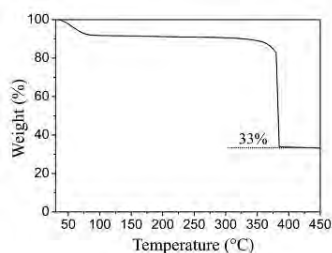**Figure 4.** TEM image and size distribution of Au:PVP nanoparticles.

Figure 5. TGA curve of Au:PVP nanoparticles.

Infusion of Au:PVP nanoparticles into SBA-15. Our preliminary study has shown that Au:PVP nanoparticles were not well-dispersed in scCO$_2$, owing to the non-polar nature of scCO$_2$. In general, the polarity of scCO$_2$ can be increased by mixing with a polar solvent. Therefore, ethanol was added to scCO$_2$ to improve the dispersibility of Au:PVP nanoparticles. Infusion of Au:PVP nanoparticles into mesoporous SBA-15 was carried out at a temperature of 35 °C and a pressure of 241 bar because the mixture of ethanol and scCO$_2$ formed a homogeneous solution at this condition. Using a mixture of ethanol and scCO$_2$ (1:12 w/w), infusion of Au:PVP nanoparticles in SBA-15 was carried out with the Au:PVP nanoparticles to SBA-15 weight ratios of 1:25 and 1:50. After calcination of Au:PVP/SBA-15 composites at 370 °C for 2 h, the resulting Au/SBA-15 composites were characterized by TEM, low- and wide angle XRD, and N$_2$ adsorption-desorption isotherms. TEM results illustrated the trend of increasing the amount of Au loading in SBA-15 when the Au:PVP nanoparticles to SBA-15 weight ratio changed from 1:50 to 1:25, as shown in Figure 6. Furthermore, Au loading content seemed to depend on the concentration of ethanol present in the infusion medium. Increasing the ethanol concentration by changing the ethanol to scCO$_2$ weight

ratio from 1:12 to 1:1 increased the Au loading content (compare between Figures 6b and 7a) when the Au:PVP nanoparticles to SBA-15 weight ratio remained constant at 1:25. Low angle XRD patterns of Au/SBA-15 composites exhibited similar characteristic peaks as pure SBA-15, as shown in Figure 3. Therefore, both low angle XRD and TEM results indicated that the infusion process used in this work did not damage the mesostructure of the SBA-15.
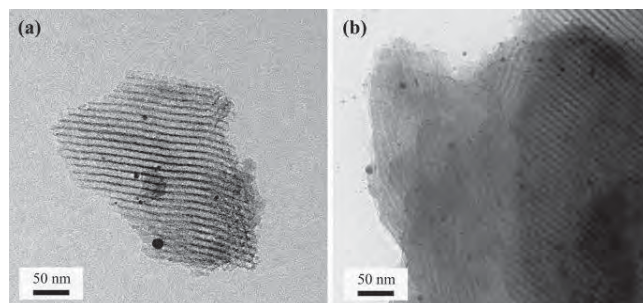

Figure 6. TEM images of Au/SBA-15 composites prepared by infusion of Au:PVP nanoparticles into SBA-15 using 1:12 ethanol to scCO$_2$ mixture with Au:PVP nanoparticles to SBA-15 weight ratios of: (a) 1:50; (b) 1:25 after calcination at a temperature of 370 °C.
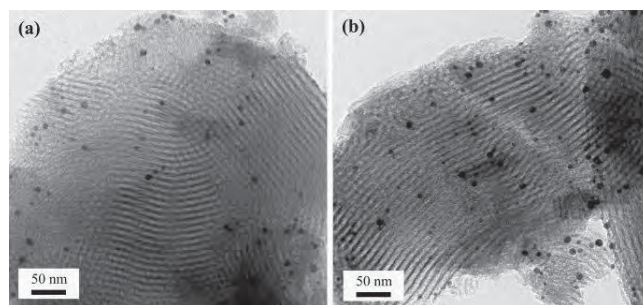

Figure 7. TEM images of Au/SBA-15 composites prepared by infusion of Au:PVP nanoparticles into SBA-15 using 1:1 ethanol to scCO$_2$ mixture and 1:25 Au:PVP nanoparticles to SBA-15, followed by calcination at temperatures of: (a) 370 °C; (b) 500 °C.

In addition, XRD analysis of the Au/SBA-15 composites showed only a broad peak at 2θ of ~23° due to the amorphous nature of SiO$_2$, similar to that of pure SBA-15 (Figure 8). Rombi and co-workers reported that XRD patterns of Au/SBA-15 composites after calcinations at 560 °C in flowing air for 6 h showed intense peaks at $2\theta = 38.2$, 44.7, and 64.6°, corresponding to the (111), (200), and (220) crystal planes of the face-centered cubic structure of Au; however, after calcinations at 300 °C, only a small broad peak still appeared around $2\theta = 38°$.[1f] In our work, there were no characteristic peaks corresponding to the presence of Au. This could be due to the lower crystallinity of AuNPs and different calcination conditions (i.e., temperature, time, flowing gas) used for Au/SBA-15 composites.

It has been recognized that the location of metal nanoparticles, on the surface or in the channels of a mesoporous support, is important for the catalytic activities and applications.[19] In this work, AuNPs seemed to appear both on the surface and in the channels of SBA-15 (Figures 6b and 7a). It was found that, unlike AuNPs located in the channels of mesoporous SBA-15, those located on the surface of the mesoporous structures tended to aggregate or sinter when increasing the calcination temperature from 370 and 500 °C. In addition, the size of AuNPs located on the surface of mesoporous

SBA-15 somewhat increased with increasing calcination temperature, while that of AuNPs located inside the channel of SBA-15 remained unchanged (compared between Figures 7a and b). It can be deduced that most of AuNPs located inside the channel of SBA-15. Furthermore, N_2 adsorption-desorption isotherms of the Au/SBA-15 composite (1:25 Au:PVP nanoparticles to SBA-15; 1:1 ethanol to $scCO_2$) were similar to those of the SBA-15. The BET specific surface area of this composite is 622 m^2g^{-1} while the reduction of the pore size distribution and total pore volume was not observed in the Au/SBA-15 composite. This result consequently confirmed again that the infusion of AuNPs into SBA-15 by using the compressed carbon dioxide solution approach is successful.
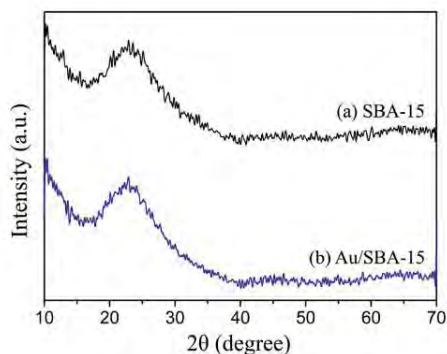

Figure 8. XRD patterns of: (a) SBA-15; (b) Au/SBA-15 composite (1:25 Au:PVP nanoparticles to SBA-15; 1:1 ethanol to $scCO_2$).

Conclusions

We have demonstrated that compressed carbon dioxide solution technique can be used to infuse the AuNPs (2.3 ± 0.6 nm) into mesoporous SBA-15 at moderate experimental conditions (35 °C, 241 bar). The success of infusion of AuNPs into SBA-15 was confirmed by TEM and N_2 adsorption-desorption isotherms. Our infusion method could be a promising environmentally friendly technique for fabricating the composites of metal nanostructures/mesoporous materials. In addition, loading content of AuNPs in SBA-15 as well as their catalytic activity are currently under investigation.

References

(1) (a) Haruta, M.; Yamada, N.; Kobayashi, T.; Iijima, S. *J. Catal.* **1989,** *115,* 301. (b) Haruta, M.; Tsubota, S.; Kobayashi, T.; Kageyama, H.; Genet, M. J.; Delmon, B. *J. Catal.* **1993,** *144,* 175. (c) Haruta, M. *Chem. Rec.* **2003,** *3,* 75. (d) Comotti, M.; Li, W. C.; Spliethoff, B.; Schüth, F. *J. Am. Chem. Soc.* **2006,** *128,* 917. (e) Zhu, H.; Ma, Z.; Clark, J. C.; Pan, Z.; Overbury, S. H.; Dai, S. *App. Catal., A* **2007,** *326,* 89. (f) Rombi, E.; Cutrufello, M. G.; Cannas, C.; Casu, M.; Gazzoli, D.; Occhiuzzi, M.;

Monaci, R.; Ferino, I. *Phys. Chem. Chem. Phys.* **2009,** *11,* 593. (g) Widmann, D.; Liu, Y.; Schuth, F.; Behm, R. J. *J. Catal.* **2010,** *276,* 292.

(2) (a) Hutchings, G. J.; Carrettin, S.; Landon, P.; Edwards, J. K.; Enache, D.; Knight, D. W.; Xu, Y. J.; Carley, A. F. *Top. Catal.* **2006,** *38,* 223. (b) Liu, Y.; Tsunoyama, H.; Akita, T.; Tsukuda, T. *J. Phys. Chem. C* **2009,** *113,* 13457. (c) Liu, Y.; Tsunoyama, H.; Akita, T.; Tsukuda, T. *Chem. Lett.* **2010,** *39,* 159. (d) Su, F. Z.; Liu, Y. M.; Wang, L. C.; Cao, Y.; He, H. Y.; Fan, K. N. *Angew. Chemie. Int. Ed.* **2008,** *47,* 334.

(3) (a) Fu, Q.; Deng, W.; Saltsburg, H.; Flytzani-Stephanopoulos, M. *App. Catal., B* **2005,** 56, 57. (b) Silberova, B. A. A.; Mul, G.; Makkee, M.; Moulijn, J. A. *J. Catal.* **2006,** *243,* 171.

(4) (a) Carretin, S.; Guzman, J.; Corma, A. *Angew. Chem., Int. Ed.* **2005,** *44,* 2242. (b) Tsunoyama, H.; Sakurai, H.; Ichikuni, N.; Negishi, Y.; Tsukuda, T. *Langmuir* **2004,** *20,* 11293.

(5) (a) Grunwaldt, J. D.; Baiker, A. *J. Phys. Chem. B* **1999,** *103,* 1002. (b) Liu, H.; Kozlov, A. I.; Kozlova, A. P.; Shido, T.; Iwasawa, Y. *Phys. Chem. Chem. Phys.* **1999,** *1,* 2851. (c) Okumura, M.; Tsubota, S.; Haruta, M. *J. Mol. Catal. A* **2003,** *199,* 73. (d) Delannoy, L.; El Hassan, N.; Musi, A.; To, N. N. L.; Krafft, J. M.; Louis, C. *J. Phys. Chem. B* **2006,** *110,* 22471. (e) Kotobuki, M.; Leppelt, R.; Hansgen, D. A.; Widmann, D.; Behm, R. J. *J. Catal.* **2009,** *264,* 67. (f) Carrettin, S.; Concepción, P.; Corma, A.; López Nieto, J. M.; Puntes, V. F. *Angew. Chemie., Int. Ed.* **2004,** *43,* 2538. (g) Widmann, D.; Leppelt, R.; Behm, R. J. *J. Catal.* **2007,** *251,* 437.

(6) Chiang, C. W.; Wang, A.; Wan, B. Z.; Mou, C. Y. *J. Phys. Chem. B* **2005,** *109,* 18042.

(7) Haruta, M. *Gold Bull.* **2004,** *37,* 27.

(8) (a) Guari, Y.; Thieuleux, C.; Mehdi, A.; Reyé, C.; Corriu, R. J. P.; Gomez-Gallardo, S.; Philippot, K.; Chaudret, B. *Chem. Mater.* **2003,** *15,* 2017. (b) Petkov, N.; Stock, N.; Bein, T. *J. Phys. Chem. B* **2005,** *109,* 10737.

(9) (a) Yen, C. W.; Lin, M. L.; Wang, A.; Chen, S. A.; Chen, J. M.; Mou, C. Y. *J. Phys. Chem. C* **2009,** *113,* 17831. (b) Gu, J.; Fan, W.; Shimojima, A.; Okubo, T. *J. Solid State Chem.* **2008,** *181,* 957. (c) Bore, M. T.; Pham, H. N.; Switzer, E. E.; Ward, T. L.; Fukuoka, A.; Datye, A. K. *J. Phys. Chem. B* **2005,** *109,* 2873.

(10) (a) Zhu, J.; Kónya, Z.; Puntes, V. F.; Kiricsi, I.; Miao, C. X.; Ager, J. W.; Alivisatos, A. P.; Somorjai, G. A. *Langmuir* **2003,** *19,* 4396. (b) Zheng, N.; Stucky, G. D. *J. Am. Chem. Soc.* **2006,** *128,* 14278. (c) Turner, M.; Golovko, V. B.; Vaughan, O. P. H.; Abdulkin, P.; Berenguer-Murcia, A.; Tikhov, M. S.; Johnson, B. F. G.; Lambert, R. M. *Nature* **2008,** *454,* 981.

(11) Tsukuda, T.; Tsunoyama, H.; Sakurai, H. *Chem. Asian J.* **2011,** *6,* 736.

(12) Sane, A.; Limtrakul, J. *J. Supercrit.Fluids* **2009,** *51,* 230.

(13) Gupta, G.; Shah, P. S.; Zhang, X.; Saunders, A. E.; Korgel, B. A.; Johnston, K. P. *Chem. Mater.* **2005,** *17,* 6728.

(14) (a) Zhao, D.; Feng, J.; Huo, Q.; Melosh, N.; Fredrickson, G. H.; Chmelka, B. F.; Stucky, G. D. *Science* **1998,** *279,* 548. (b) Chareonpanich, M.; Nanta-ngern, A.; Limtrakul, J. *Mater. Lett.* **2007,** *61,* 5153.

(15) Tsunoyama, H.; Sakurai, H.; Negishi, Y.; Tsukuda, T. *J. Am. Chem. Soc.* **2005,** *127,* 9374.

(16) Brunauer, S.; Emmett, P. H.; Teller, E. *J. Am. Chem. Soc.* **1938,** *60,* 309.

(17) Barrett, E. P.; Joyner, L. G.; Halenda, P. P. *J. Am. Chem. Soc.* **1951,** *73,* 373.

(18) Tanev, P. T.; Pinnavaia, T. J. *Chem. Mater.* **1996,** *8,* 2068.

(19) Rioux, R. M.; Song, H.; Hoefelmeyer, J. D.; Yang, P.; Somorjai, G. A. *J. Phys. Chem. B* **2005,** *109,* 2192.

Oxidation of Carbon Monoxide by Nitrous Oxide Decomposition on Fe-embedded graphene

Sippakorn Wannakao[1,2,3], Thana Maihom[1,2,3],
Pipat Khongpracha[1,2,3],
*Bundet Boekfa[2,3,4], and Jumras Limtrakul[1,2,3]**

[1]Laboratory for Computational and Applied Chemistry, Department of Chemistry, Faculty of Science and Center of Nanotechnology, Kasetsart University Research and Development Institute, Kasetsart University, Bangkok 10900, Thailand
[2]Center for Advanced Studies in Nanotechnology and Its Applications in Chemical, Food and Agricultural Industries, Kasetsart University, Bangkok 10900, Thailand
[3]NANOTEC Center of Excellence, National Nanotechnology Center, Kasetsart University, Bangkok 10900, Thailand
[4]Chemistry Department, Faculty of Liberal Arts and Science, Kasetsart University Kamphaeng Saen Campus, Nakhon Pathom 73140, Thailand
*Corresponding author's e-mail address: jumras.l@ku.ac.th

Introduction

The production of poisonous carbon monoxide (CO) from the combustion of fuel, vehicles, and industrial processes, is considered to be one of the big current environmental issues to be solved.

Many experimental and theoretical studies[1-19], mostly based on transition metals have been made to study the reaction between CO and O_2. Among the automobile emitted gases, nitrous oxide (N_2O) is very harmful for the environment since it has been found to contribute to the greenhouse gas concern (ca. 300 times more warming potential than CO_2) and has also caused ozone depletion. Even though it is not as active as oxygen, the N_2O can be used as one of the oxidizing agents for many reactions. Therefore, the study of the CO oxidation with the N_2O decomposition by one catalyst seems to be the most promising ways of reducing two harmful automobile gases at the same time.

Graphene, is a one layer sheet of carbon atoms which has unique properties and is considered as the new generation of electronic materials.[20-21] With its large surface area, graphene can be used as a support for the heterogeneous catalysis. Many metals have been loaded to the graphene sheet and used to catalyze the CO oxidation with O_2, for example, Au, Fe, and Cu.[22-24] Among those, Fe-embedded graphene (Fe-Graphene) is a low cost catalyst that can enable reaction under a low temperature condition. Moreover, the Fe has been recognized as one of the active species for the decomposition of N_2O.

In this work, we employed the periodic density functional theory calculation for studying the oxidation of CO by using N_2O decomposition on Fe-Graphene as an oxidizing catalyst. To the best of our knowledge, the Fe-Graphene for N_2O decomposition has never been studied before. This work shows the possibility for utilizing the Fe-Graphene as a bi-functional catalyst for reducing both environmentally harmful gases. This is very important for developing an automobile catalytic converter that can clean up more than one gas by one process.

Methodology

The spin unrestricted density functional theory with the generalized gradient approximation (GGA) with the Perdew-Burke-Ernzerhof (PBE) functional[25] that is implemented in the DMol3 code[26-27] was used in this study. The double numerical basis set including the d-polarization functional and the DFT semicore pseudopotentials (DSPPs) were employed. By the DSPP scheme, all electron calculations were performed for the C, N and O atoms, and relativistic effect was included for the Fe.

We selected the 4x4 supercell of graphene which was found in literature[22,24] to be sufficient for studying the reaction as a model for this study. The Fe atom was placed at the single vacant site that was introduced in the middle of the model (see Figure 1) due to the high Fe diffusion barrier of the defect compared to the perfect graphene.[23] In order to avoid the interaction of the mirror image, the distance between the sheets was set at 20 Å. The Brillouin zone intregation was calculated with 3 x 3 x 1 k-point sampling for the geometry optimizations. The global orbital cutoff with fine quality was selected. The population analysis was perform by the Hirshfeld charge analysis method[28]. Transition structures were confirmed by one imaginary frequency that corresponded with the reaction coordinate.
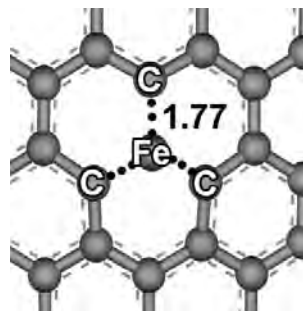

Figure 1. The embedded Fe atom on the single vacant site of the graphene

Results and Discussion

The Fe atom was located on the single vacant site of the graphene with the optimized distance between the Fe atom and the adjacent C atoms being 1.77 Å. The charge of the Fe atom was +0.254e according to the Hirshfeld population analysis. This indicates the charge transfer from the Fe atom to the graphene vacant site.
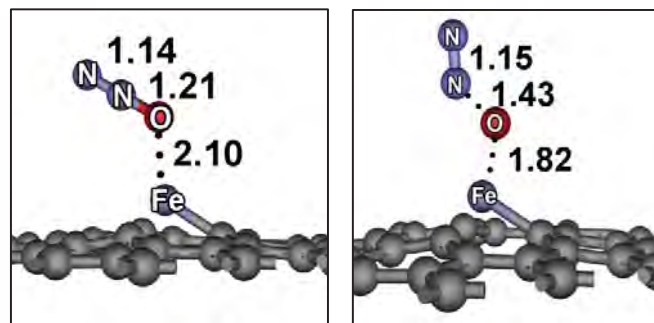

Figure 2. The adsorption structure of N_2O (Left) and the transition structure of the N_2O decomposition step (right)

The structure of the N_2O adsorption and the transition state of the N_2O decomposition are showed in Figure 2 above. The N_2O adsorbed on the Fe site by the interaction between the lone pair electron of N_2O oxygen atom and the Fe atom with the Fe–O distance of 2.10 Å and the corresponding adsorption energy was −10.0 kcal/mol. The distance between the O and N atom was elongated to

1.21 Å from 1.19 Å of the gas phase N_2O. The charge of the Fe atom was reduced to +0.139e that corresponded with the reducing of the negative charge of the O atom from −0.119e to −0.029e and the summarized charge of N_2O was +0.321e. These indicate the charge transfer from the N_2O molecule to the Fe active site. After the N_2O adsorption, the reaction proceeded via the transition structure (TS1), which the N−O bond breaking to give the oxygen atom attached to the Fe site and the N_2 molecule. The O−Fe and O−N distance were 1.82 Å and 1.43 Å, respectively. This step required the activation energy of 8.0 kcal/mol. The Fe atom gained a more positive charge (+0.156e) that is consistent with the more negative O atom (−0.129e) and the summarized charge of the N_2O molecule (−0.075e). This charge transfer might occur by the oxygen transfer from N_2O to the Fe active site. After that, the N_2 molecule can easily desorbe by the low desorption energy of 1.7 kcal/mol with the Fe−O intermediate remaining stable with the relative energy of −37.2 kcal/mol. The Fe−O distance was 1.62 Å and the charge of the Fe and O atom were +0.201e and −0.252e respectively. This specie can be the oxidizing site for the CO oxidation.
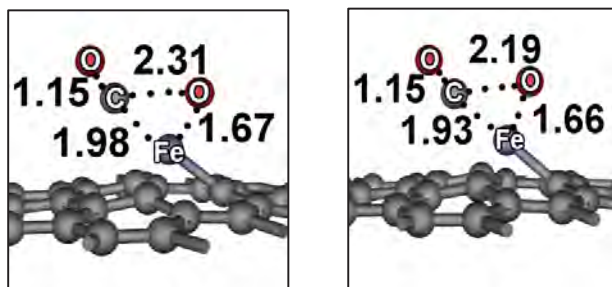

Figure 3. The adsorption structure of CO (Left) to the Fe−O site and the transition structure of the CO_2 formation step (right)

The CO molecule adsorbed on the Fe−O site with the C atom of the CO bound to the Fe atom with adsorption energy of −10.5 kcal/mol. The Fe−C distance was 1.98 Å while the Fe−O elongated to 1.67 Å. The C atom and the active O atom were ready to react with the distance between C and O of 2.31 Å. The charge of the CO molecule was +0.099e which was obtained from +0.159e of the C atom and −0.060e of the O atom while the Fe atomic charge was +0.125e. This shows that the charge was moving from the O atom of the CO through the C atom to the Fe active site (see Figure 3). The CO_2 formation can easily occur by the very low activation energy of 4.0 kcal/mol. The reacting C and O atoms moved close to 2.19 Å. The CO_2 desorption energy was 9.6 kcal/mol. The transformation of the N_2O and CO to the highly stable product (CO_2 and N_2) was exothermic by -80.2 kcal/mol. The decomposition of N_2O molecule was considered to be a rate limiting step due to its higher energy barrier during the reaction pathway that was mentioned above. The energy barrier was lower than that of the O_2 activation on the Fe-Graphene from the ref 23. Moreover, the transition structure of the CO_2 formation that we found in this work was more favorable than that cited in literature (4.0 kcal vs 25.6 kcal/mol).

From these results, one can imply that the Fe-Graphene exhibits properties of a bi-functional catalyst that can be used for reducing the N_2O and oxidizing the CO by a single step. By the low activation energy, Fe-Graphene might convert these harmful vehicle gases at the ambient condition.

Conclusions

The oxidation of carbon monoxide using the nitrous oxide as an oxidizing agent on Fe-Graphene was studied by mean of density functional theory with the PBE functional. Graphene can induce the positive charge of the Fe atom and make it ready to react with the N_2O molecule. The charge transfer between the Fe atom and N_2O molecule was found to be important for the N_2O decomposition step. The activation of N_2O (activation energy was 8.0 kcal/mol) was more favorable than the activation of O_2 that was previously studied. After the N_2O decomposition, the CO molecule easily reacts to the Fe−O intermediate obtaining the low activation energy of 4.0 kcal/mol. From this study, we suggest the Fe-Graphene as one candidate for reducing the toxic gases from vehicles at ambient conditions.

References
(1) Ackermann, M. D.; Pedersen, T. M.; Hendriksen, B. L. M.; Robach, O.; Bobaru, S. C.; Popa, I.; Quiros, C.; Kim, H.; Hammer, B.; Ferrer, S.; Frenken, J. W. M. *Phys. Rev. Lett.* **2005**, *95*, 255505.
(2) Alavi, A.; Hu, P.; Deutsch, T.; Silvestrelli, P. L.; Hutter, J. *Phys. Rev. Lett.* **1998**, *80*, 3650.
(3) Bleakley, K.; Hu, P. *J. Am. Chem. Soc.* **1999**, *121*, 7644.
(4) Chen, M. S.; Cai, Y.; Yan, Z.; Gath, K. K.; Axnanda, S.; Goodman, D. W. *Surf. Sci.* **2007**, *601*, 5326.
(5) Eichler, A. *Surf. Sci.* **2002**, *498*, 314.
(6) Eichler, A.; Hafner, J. *Surf. Sci.* **1999**, *435*, 58.
(7) Kandoi, S.; Gokhale, A. A.; Grabow, L. C.; Dumesic, J. A.; Mavrikakis, M. *Catal. Lett.* **2004**, *93*, 93.
(8) Kimble, M. L.; Castleman Jr, A. W.; Mitrić, R.; Bürgel, C.; Bonacic-Koutecky, V. *J. Am. Chem. Soc.* **2004**, *126*, 2526.
(9) Krenn, G.; Bako, I.; Schennach, R. *J. Chem. Phys.* **2006**, *124*, 144703.
(10) Liu, D. J. *J. Phys. Chem. C* **2007**, *111*, 14698.
(11) Liu, W.; Zhu, Y. F.; Lian, J. S.; Jiang, Q. *J. Phys. Chem. C* **2007**, *111*, 1005.
(12) Nakai, I.; Kondoh, H.; Amemiya, K.; Nagasaka, M.; Nambu, A.; Shimada, T.; Ohta, T. *J. Chem. Phys.* **2004**, *121*, 5035.
(13) Nakai, I.; Kondoh, H.; Shimada, T.; Resta, A.; Andersen, J. N.; Ohta, T. *J. Chem. Phys.* **2006**, *124*, 224712.
(14) Oh, S. H.; Hoflund, G. B. *J. Catal.* **2007**, *245*, 35.
(15) Salo, P.; Honkala, K.; Alatalo, M.; Laasonen, K. *Surf. Sci.* **2002**, *516*, 247.
(16) Sljivancanin, Z.; Hammer, B. *Phys. Rev. B* **2010**, *81*, 121413.
(17) Stampfl, C.; Scheffler, M. *Surf. Sci.* **1999**, *433*, 119.
(18) Zhang, C. J.; Baxter, R. J.; Hu, P.; Alavi, A.; Lee, M. H. *J. Chem. Phys.* **2001**, *115*, 5272.
(19) Zhang, C. J.; Hu, P. *J. Am. Chem. Soc.* **2001**, *123*, 1166.
(20) Geim, A. K.; Novoselov, K. S. *Nat. Mater.* **2007**, *6*, 183.
(21) Novoselov, K. S.; Geim, A. K.; Morozov, S. V.; Jiang, D.; Zhang, Y.; Dubonos, S. V.; Grigorieva, I. V.; Firsov, A. A. *Science* **2004**, *306*, 666.
(22) Song, E. H.; Wen, Z.; Jiang, Q. *J. Phys. Chem. C* **2011**, *115*, 3678.
(23) Li, Y.; Zhou, Z.; Yu, G.; Chen, W.; Chen, Z. *J. Phys. Chem. C* **2010**, *114*, 6250.
(24) Lu, Y. H.; Zhou, M.; Zhang, C.; Feng, Y. P. *J. Phys. Chem. C* **2009**, *113*, 20156.
(25) Delley, B. *Phys. Rev. Lett.* **1996**, *77*, 3865.
(26) Delley, B. *J. Chem. Phys.* **1990**, *92*, 508.
(27) Delley, B. *J. Chem. Phys.* **2000**, *113*, 7756.
(28) Hirshfeld, F. L. *Theor. Chim. Acta* **1977**, *44*, 129.

Precisely Size-controlled Metal Nanoparticles (Au, Pd and Pt) Inserted into Metal-Organic Frameworks (MOFs): Synthesis and Catalytic Properties

Sudarat Yadnum[1,2,3], Pipat Khongpracha[1,2,3], Chompunuch Warakulwit[1,2,3] and Jumras Limtrakul[1,2,3]*

[1]Laboratory for Computational and Applied Chemistry, Department of Chemistry, Faculty of Science and Center of Nanotechnology, Kasetsart University Research and Development Institute, Kasetsart University, Bangkok 10900, Thailand
[2]Center for Advanced Studies in Nanotechnology and Its Applications in Chemical, Food and Agricultural Industries, Kasetsart University, Bangkok 10900, Thailand
[3]NANOTEC Center of Excellence, National Nanotechnology Center, Kasetsart University, Bangkok 10900, Thailand
[*]Corresponding author: Tel.: +662 562 5555 ext 2169, Fax: +662 562 5555 ext 2176, E-mail address: jumras.l@ku.ac.th

Introduction

Metal organic frameworks (MOFs) have attracted much attention in the past decade due to their high porosity and high specific surface area making them suitable for many applications, including gas storage, separations, and catalysis[1-7]. For the latter, the unique structure of MOFs, resulted from the combination of the long-range order of a solid-state template material with a tunable dimensionality and chemical tailoring of the inner surface of the channels and cavities, makes them promising candidates for embedding and supporting functional nanomaterials. A number of functional nanoparticles for embedding, e.g. Cu, Ru, Pd, Au, Ag and Pt metal nanoparticles, into the cavities of MOFs, are relevant for many applications, especially for heterogeneous catalysis, have been achieved by using various preparation methods. These methods include gas-phase infiltration, solid grinding (SG), and solution impregnation[8-15]. In many cases, the resulting metal@MOFs catalysts exhibited unique catalytic activity[16].

Among MOFs that have been previously reported, the MIL-101, a zeolite-type MOF, has been known to possess a large surface area (Brunauer-Emmett-Teller (BET) surface area of ca. 3000 m^2 g^{-1}), large pore size (of ca. 29-34 Å), and good chemical resistance to water and organic solvents. These properties are desirable for depositing small metal nanoparticles by using a colloidal deposition preparation method[17,18]. The MIL-101 supported gold nanoparticles (Au/MIL-101) was recently synthesized for catalytic application for aerobic oxidation of alcohols. The prepared Au/MIL-101 exhibited extremely high catalytic activities in the liquid-phase aerobic oxidation of a wide range of alcohols under ambient conditions in the absence of water or base[16]. The electron donation of the aryl rings of organic linker molecules composed in the MIL-101 to the surface of gold nanoparticles through the π-bond interactions is suggested to facilitate the formation of anionic Au leading to the favorable activation of O_2 on the Au surfaces[19-24]. This study raises the question of how the electron donation of the aryl rings to the surface of other metal nanoparticles, such as Pd and Pt, could affect the reaction catalyzed by those metal nanoparticles The insight into the combined role between an intrinsic catalytic activity of precisely size-controlled metal nanoparticles (Au, Pd and Pt) and the electron donation effect gained from the organic linker of MOFs on the activity and selectivity of the reaction remains a great challenge.

In this research, we aim to synthesize the noble metal nanoparticles of gold, palladium, and platinum encapsulated into the MIL-101, in order to be heterogeneous catalysts for oxidation of alcohols, by using colloidal deposition of the metal nanoparticles stabilized by poly(N-vinyl-2-pyrrolidone) (PVP). This method was used for preparing the Au/MIL-101 in the previous work[16]. The catalytic activity and selectivity of the obtained metal/MIL-101 hybrid materials in the aerobic oxidation of alcohols will be further investigated.

Experimental Method

Raw chemicals. Chromium nitrate ($Cr(NO_3)_3.9H_2O$, Sigma-Aldrich, 99%), Terephthalic acid ($C_8H_6O_4$, Sigma-Aldrich, 98%), Polyvinylpyrrolidole (K-30, wt~40,000, Fluka), Sodium borohydride ($NaBH_4$, Sigma-Aldrich, 99%), Potassium tetrachloro palatinate (II) (K_2PtCl_4, Sigma-Aldrich, 99.9%), Gold (III) chloride trihydrate ($HAuCl_4.3H_2O$, Sigma-Aldrich, 99.9%), Palladium (II) chloride ($PdCl_2$, Sigma-Aldrich, 99.9%), Hydrofluoric acid (HF, 48%), Ethyl alcohol (C_2H_5OH, 98%) were used. The deionized water was made in our laboratory.

Catalyst Preparation

Synthesis of MIL-101. The MIL-101 was prepared by using the previously published hydrothermal reaction method [25]. Briefly, $Cr(NO_3)_3·9H_2O$ (5 mmol), HF (5 mmol), terephthalic acid (5 mmol), and DI water (24 mL) were mixed and reacted at 220 ℃ for 8 h in an autoclave under vacuum. After that, the reaction mixture was allowed to cool down slowly to room temperature for 12 h. Next, in order to remove the residual carboxylic acid left in the form of large white crystals, the mixture was then filtered through a large-pore filter, a nylon membrane filter with pore diameter of 41 μm (Spectra/Mesh Nylon Macroporous filters). The MIL-101 product remained in the filtrate part. Later, the MIL-101 product was separated from the filtrate, which contained the unreacted terephthalic acid, by using a small-pore paper filter (Whatman, No. 1). The solid that remains on the filter paper was then washed by a solution of 95 % v/v ethanol in water and further taken out from the filter paper. The sample powder of MIL-101 was obtained after soaking the washed solid in a solution of 95 % v/v ethanol in water at 80 ℃ for 24 h and followed drying at 150 ℃ under vacuum overnight.

Preparation of Au:PVP, Pd:PVP and Pt:PVP nanoparticles. The metal colloids stabilized by PVP were synthesized by following Tsunoyama's method[26]. Typically, hydrogen tetrachloroaurate tetrahydrate ($HAuCl_4.3H_2O$), tetrachloropalladate ($PdCl_4$) and potassium tetrachloroplatinate (K_2PtCl_4) were used as metal sources. Poly(N-vinyl-2-pyrrolidone) (PVP) with an average molecular weight of ca. 40 kDa was used as a stabilizer. Sodium borohydride ($NaBH_4$) was used as a reducing agent. 555.5 mg (0.0139 mmol) of PVP was added into the aqueous solution of each metal source (1 mM, 50 mL). The resulting mixture was placed in an ice bath at 0 ℃ and stirred for 30 min. Then, an aqueous solution of $NaBH_4$ (100 mM, 5 mL) was rapidly added into the mixture under vigorous stirring. After the addition of the $NaBH_4$ aqueous solution, the mixture was further stirred for 1h. For the case of Au:PVP, after addition of the $NaBH_4$ aqueous solution, the color of the reaction mixture immediately turned from pale yellow to dark brown, indicating the formation of small Au nanoclusters (NCs). For the Pd:PVP case and Pt:PVP, there is no change in color of the reaction mixtures observed. The resulting mixtures of metal:PVP were used as starting materials for the next colloidal deposition step.

Synthesis of metal/MIL-101 by colloidal deposition of the metal nanoparticles stabilized by PVP. Typically, in order to support the metal nanoparticles onto the MIL-101, 0.5 g of the synthesized MIL-101 powder was added to 4 mL of DI water and then dispersed in the water by sonicating in an ultrasonic bath for 20s. As-prepared mixtures of metal:PVP were sonicated for 20s before using. Two mixtures were then mixed and stirred in an ice

bath at 0 ºC for 4 h. The metal/MIL-101 was obtained after filtration of the finally obtained mixture by using a normal paper filter (Whatman, No. 1). The metal/MIL-101 sample was washed with DI water and then dried under N_2 gas.

Characterization Powder X-ray diffraction (XRD) patterns of the samples were obtained by a Rigaku diffractometer (TTRAX III) using Cu Kα radiation (for the low angle XRD pattern) operating at an accelerating voltage of 50 kV and a current of 300 mA and a Philips diffractometer (X'Pert Pro) with Cu-Kα radiation (for the high angle XRD pattern) operating at an accelerating voltage of 40 kV and a current of 30 mA. The BET surface area, pore size and pore volume measurements were performed by using the N_2 adsorption/desorption isotherms characterization measured at 77 K on a Micromeritics ASAP 2010 instrument. The size and morphology of MIL-101 and metal/MIL-101 were investigated by using a transmission electron microscope (TEM) and scanning electron microscope (SEM).

Results and Discussion

Characterization of MIL-101. Low angle powder X-ray diffraction pattern recorded from 2 to 7 degrees of 2θ by using the step-size of 0.01 degrees and the scan speed of 0.5 degrees/minute are shown in Figure 1a. The high angle XRD pattern recorded from 5 to 50 degrees using the step-size of 0.01 degrees and the scan speed of 0.5 degrees/minute are shown in Figure 1b. The diffraction peak positions and relative diffraction intensities of MIL-101 as synthesized were found to correspond with those obtained in the previous literature[25] reported for MIL-101, confirming the obtaining of MIL-101.
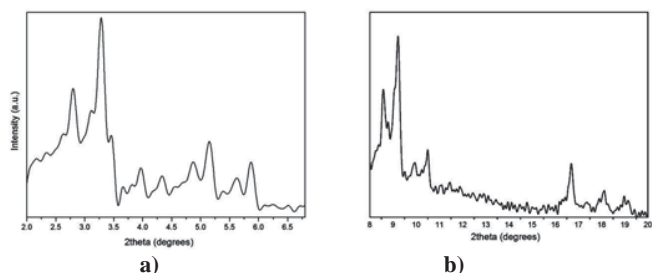

Figure 1. (a) Low angle and (b) high angle XRD patterns of the synthesized MIL-101 sample.

The morphology of MIL-101 was studied by using scanning electron microscopy (SEM). The SEM images with low and high magnifications of the synthesized MIL-101 are shown in Figures 2a and 2b, respectively. It can be seen that the obtained powder of MIL-101 was composed of cubo-octahedral crystals with quite uniform size in the range of 1-2 μm in diameter (see Figure 2). This result agrees well with that obtained in the previous report of MIL-101[25].
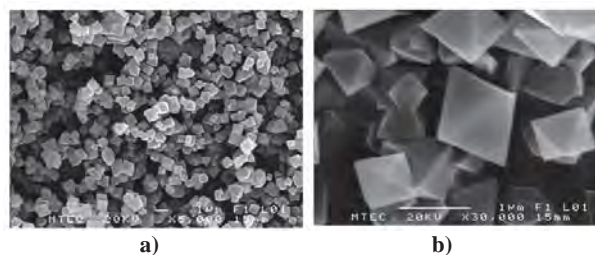

Figure 2. (a) Low magnification and (b) high magnification SEM images of the as-synthesized MIL-101.

For the TEM investigation of MIL-101 sample, the dry powder of as-synthesized MIL-101 was dispersed in absolute ethanol for a few minutes by using an ultrasonic bath and then deposited on a carbon-coated Cu TEM grid. Then the grid was let in air until dry. TEM images of MIL-101 confirm the nearly perfect cubo-octahedral crystal structure of the synthesized MIL-101 (see Figure 3).
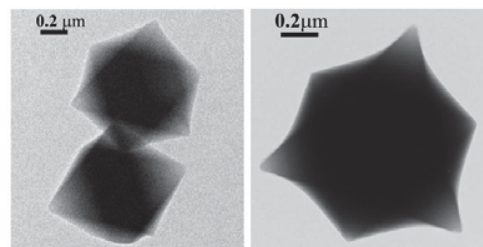

Figure 3. TEM images of the as-synthesized MIL-101 showing the nearly perfect cubo-octahedral crystal structure.

The BET surface area, pore size and pore volume of the MIL-101 samples were determined by using the N_2 adsorption/desorption measurement. Before the measurement, the sample was degassed under vacuum overnight at 100 ºC. The BET surface area (S_{BET}), pore size and pore volume (V_{pore}) of the obtained MIL-101 were 3,384 m^2/g, 25.428 Å and 1.611 cm^3/g, respectively. These values indicate that the synthesized MIL-101 has a high specific surface area and pore volume that could facilitate the inclusion of metal nanoparticles into the structure of MIL-101. Furthermore, the obtained BET surface area is in good agreement with the previously reported value of MIL-101[25].

Characterization of metal/MIL-101. Due to the small size (sub-ten nanometer) of the metal nanoparticles synthesized by using PVP as a stabilizer in which the XRD pattern of metal nanoparticles was not expected to be observed in the metal/MIL-101 sample, the XRD pattern of the metal/MIL-101 was not recorded. The SEM and TEM images of the synthesized Au/MIL-101, Pd/MIL-101 and Pt/MIL-101 are shown in Figures 4, 5 and 6, respectively. It can be seen from the SEM image (see Figures 4a, 5a and 6a) that the cubo-octahedral crystal structure of the MIL-101 still remained after addition of the metal:PVP nanoparticles followed by calcination at 200°C. This indicates that the colloidal deposition method used for supporting the metal nanoparticles onto the MIL-101 structure did not destroy the structure of MIL-101.
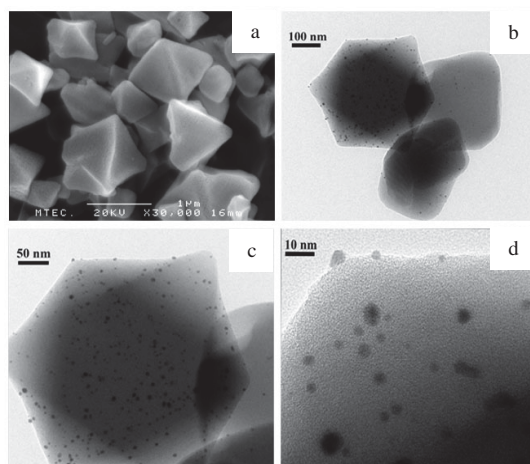
Figure 4. (a) SEM and (b-d) TEM images of the synthesized Au/MIL-101.
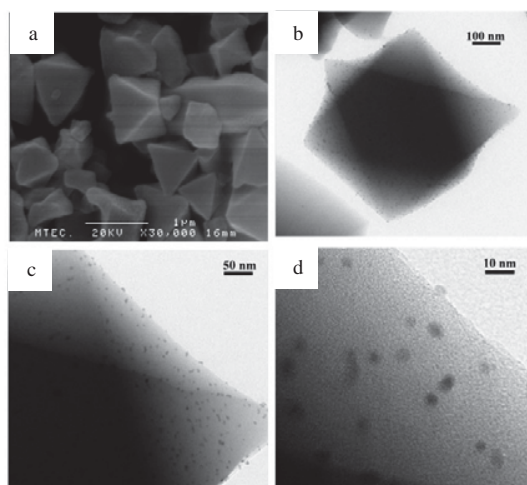

Figure 5. (a) SEM and (b-d) TEM images of the synthesized Pd/MIL-101.

From the TEM images of the metal/MIL-101 (Figures 4b-4d, 5b-5d and 6b-6d), it is found that the Au, Pd and Pt nanoparticles with average diameters of 2.59 ± 1.27, 2.80 ± 0.67 and 1.62 ± 0.41 nm, respectively (which are in good agreement with the MIL-101 pore size of about 2.9-3.4 Å[25]) were successfully supported onto the MIL-101 structure by using the simple colloidal deposition method used in this work. The high magnification TEM images of the metal/MIL-101 (Figures 4d, 5d and 6d) show that all the Au and Pd nanoparticles and some Pt nanoparticles were highly dispersed in the structure of MIL-101 support whereas a part of the Pt nanoparticles tended to form an aggregate structure during the preparation. Due to the MIL-101 pore size of about 2.9-3.4 Å, which is much smaller than the size of the aggregate structure found (the diameter is in the order of tens of nanometers), it is suggested that the Pt nanoparticles with aggregate structure were located onto the external surface of MIL-101 whereas the highly dispersed part was located in the porous channels of MIL-101. This aggregate structure further implies the weak interaction between the MIL-101 surface and Pt:PVP nanoparticles during the colloidal deposition.
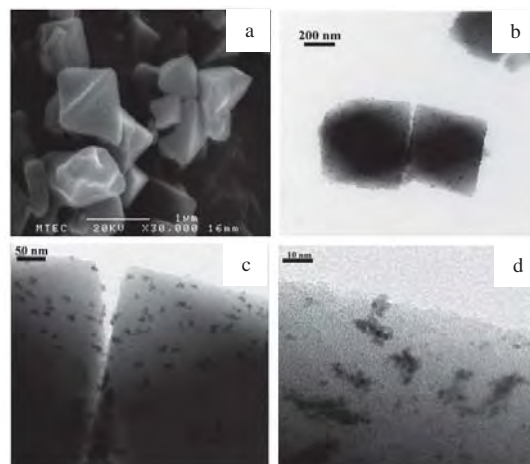

Figure 6. (a) SEM and (b-d) TEM images of the synthesized Pt/MIL-101

Conclusions

In this work, we prepared precisely size-controlled metal nanoparticles (Au, Pd and Pt) embedded into metal-organic frameworks (MIL-101) by using the simple colloidal deposition followed by calcination. The XRD, SEM, TEM and N_2 adsorption/desorption characterization of the as-synthesized MIL-101 confirmed the characteristic of MIL-101 showing the successful synthesis achieved by using the hydrothermal method. The SEM and TEM characterizations of the prepared Au/MIL-101, Pd/MIL-101, Pt/MIL-101 sample show that preparation method used allows preservation of the MIL-101 structure. The high magnification image TEM images of the prepared Au/MIL-101, Pd/MIL-101, Pt/MIL-101 sample show that Au, Pd and Pt nanoparticles with average diameters of 2.59 ± 1.27, 2.80 ± 0.67 and 1.62 ± 0.41 nm, respectively were successfully supported both in the porous channels and onto the external surface of MIL-101. Observation of a part of Pt nanoparticles with the aggregate structure leads us to suggest that the Pt:PVP nanoparticles had weaker interaction to the MIL-101 surface than other metal nanoparticles, Au:PVP and Pd:PVP nanoparticles. This implies the difference on intrinsic properties of metal nanoparticles which could further lead to the difference in catalytic activity and selectivity for oxidation of alcohols.

References

(1) Mueller, U.; Schubert, M.; Teich, F.; Puetter, H.; Schierle-Arndt, K.; Pastre, J. *J. Mater. Chem* **2006**, *16*, 626.

(2) Kitagawa, S.; Kitaura, R.; Noro, S.-i. *Angew. Chem., Int. Ed* **2004**, *43*, 2334.

(3) Lee, J.; Farha, O. K.; Roberts, J.; Scheidt, K. A.; Nguyen, S. T.; Hupp, J. T. *Chem. Soc. Rev* **2009**, *38*, 1450.

(4) Zhao, X.; Xiao, B.; Fletcher, A. J.; Thomas, K. M.; Bradshaw, D.; Rosseinsky, M. J. *Science* **2004**, *306*, 1012.

(5) Dincă, M.; Long, J. R. *Angew. Chem., Int. Ed* **2008**, *47*, 6766.

(6) Yaghi, O. M.; O'Keeffe, M.; Ockwig, N. W.; Chae, H. K.; Eddaoudi, M.; Kim, J. *Nature* **2003**, *423*, 705.

(7) Furukawa, H.; Ko, N.; Go, Y. B.; Aratani, N.; Choi, S. B.; Choi, E.; Yazaydin, A. O.; Snurr, R. Q.; O'Keeffe, M.; Kim, J.; Yaghi, O. M. *Science*, **2010**, *329*, 424.

(8) Schroder, F.; Esken, D.; Cokoja, M.; van den Berg, M. W. E.; Lebedev, O. I.; Van Tendeloo, G.; Walaszek, B.; Buntkowsky, G.; Limbach, H.-H.; Chaudret, B.; Fischer, R. A. *J. Am. Chem. Soc.* **2008**, *130*, 6119.

(9) Mueller, M.; Hermes, S.; Kähler, K.; van den Berg, M. W. E.; Muhler, M.; Fischer, R. A. *Chem. Mater.* **2008**, *20*, 4576.

(10) Hermes, S.; Schröter, M.-K.; Schmid, R.; Khodeir, L.; Muhler, M.; Tissler, A.; Fischer, R. W.; Fischer, R. A. *Angew. Chem., Int. Ed.* **2005**, *44*, 6237.

(11) Houk, R. J. T.; Jacobs, B. W.; Gabaly, F. E.; Chang, N. N.; Talin, A. A.; Graham, D. D.; House, S. D.; Robertson, I. M.; Allendorf, M. D. *Nano Lett.* **2009**, *9*, 3413.

(12) El-Shall, M. S.; Abdelsayed, V.; Khder, A. E. R. S.; Hassan, H. M. A.; El-Kaderi, H. M.; Reich, T. E. *J. Mater. Chem* **2009**, *19*, 7625.

(13) Kleist, W.; Maciejewski, M.; Baiker, A. *Thermochim Acta*, **2010**, *499*, 71.

(14) Ishida, T.; Nagaoka, M.; Akita, T.; Haruta, M. *Chem.–Eur. J.* **2008**, *14*, 8456.

(15) Jiang, H.-L.; Liu, B.; Akita, T.; Haruta, M.; Sakurai, H.; Xu, Q. *J. Am. Chem. Soc.* **2009**, *131*, 11302.

(16) Liu, H.; Liu, Y.; Li, Y.; Tang, Z.; Jiang, H. *J. Phys. Chem. C*, **2010**, *114*, 13362.

(17) Pan, Y.; Yuan, B.; Li, Y.; He, D. *Chem. Commun*, **2010**, *46*, 2280.

(18) Yuan, D.; Zhao, D.; Sun, D.; Zhou, H.-C. *Angew. Chem., Int. Ed.*, **2010**, *49*, 5357.

(19) Salisbury, B. E.; Wallace, W. T.; Whetten, R. L. *Chemical Physics* **2000**, *262*, 131.

(20) Okumura, M.; Kitagawa, Y.; Haruta, M.; Yamaguchi, K. *Chem. Phys. Lett.* **2001**, *346*, 163.

(21) Stolcic, D.; Fischer, M.; Ganteför, G.; Kim, Y. D.; Sun, Q.; Jena, P. *J. Am. Chem. Soc.* **2003**, *125*, 2848.

(22) Stiehl, J. D.; Kim, T. S.; McClure, S. M.; Mullins, C. B. *J. Am. Chem. Soc.* **2004**, *126*, 1606.

(23) Barton, D. G.; Podkolzin, S. G. *J. Phys. Chem. B* **2004**, *109*, 2262.

(24) Chowdhury, B.; Bravo-Suarez, J. J.; Mimura, N.; Lu; Bando, K. K.; Tsubota, S.; Haruta, M. *J. Phys. Chem. B* **2006**, *110*, 22995.

(25) Férey, G.; Mellot-Draznieks, C.; Serre, C.; Millange, F.; Dutour, J.; Surblé, S.; Margiolaki, I. *Science* **2005**, *309*, 2040.

(26) Tsunoyama, H.; Sakurai, H.; Negishi, Y.; Tsukuda, T. *J. Am. Chem. Soc.* **2005**, *127*, 9374.

Shape-selective Hydrocarbon Cracking of *n*-hexane on MCM-22 zeolite

Supakit Tiewcharoen[1,2], Bundet Boekfa[1,2,4], Piti Treesukol[1,2], Thana Maihom[2,3,4] and Jumras Limtrakul[2,3,4]*

[1]Chemistry Department, Faculty of Liberal Arts and Science, Kasetsart University Kamphaeng Saen Campus, Nakhon Pathom 73140, Thailand
[2]Center for Advanced Studies in Nanotechnology and Its Applications in Chemical,Food and Agricultural Industries, Kasetsart University, Bangkok 10900, Thailand
[3]Laboratory for Computational and Applied Chemistry, Department of Chemistry, Faculty of Science and Center of Nanotechnology, Kasetsart University Research and Development Institute, Kasetsart University, Bangkok 10900, Thailand
[4]NANOTEC Center of Excellence, National Nanotechnology Center, Kasetsart University,Bangkok 10900, Thailand
[*]Corresponding author: Tel.: +662 562 5555 ext 2169, Fax: +662 562 5555 ext 2176, E-mail address: jumras.l@ku.ac.th

Introduction

Zeolites are widely used as heterogeneous catalysts for petroleum refineries and the petrochemical industry. With its size and shape-selectivity, many petrochemical processes take advantage of this material as catalysts, for instance in hydrocarbon cracking, isomerization and oligomerization, etc. The hydrocarbon cracking is an important reaction to break down the large-hydrocarbon crude oil into light-hydrocarbons fuel[1-2].

The hydrocarbon cracking reaction on zeolites have been studied both experimentally[3-5] and theoretically[6-14]. The mechanism is proposed via both a monomoleculear mechanism and a bimolecular mechanism. With the low pressure of hydrocarbons and high reaction temperature, the mechanism is believed to be a monomolecular mechanism[3-4]. This mechanism proceeds through carbonium ion intermediate and gives alkane and alkene products. Maihom et al.[14] studied the *n*-hexane cracking on H-FAU and H-ZSM-5 with the M06-2X functional. The reaction mechanism was proposed to be two steps: 1) protonation to form a hexonium intermediate and 2) decomposition to propane and propene products. They found that the first step was the rate determining step with activation energies of 45.7 and 45.8 kcal/mol for H-FAU and H-ZSM-5, respectively. This study provided us the understanding of the mechanism occurring in the large- and medium- pore zeolites.

MCM-22 (MWW framework) is an outstanding large pore zeolite[15-16]. It contains two different pore sizes, two-dimensional sinusoidal 10T (1.4 Å x 5.1 Å) channels and large cylindrical supercages 12T (7.1 Å x 18.2 Å). Katada et al.[17] studied the cracking of *n*-hexane and octane on several zeolites, such as H-MOR, H-MCM-22, H-ZSM-5. The adsorption energies were measured to be 7.6, 14.6, and 11.0 kcal/mol for H-FAU, H-ZSM-5 and H-MCM-22 zeolite, respectively. For the cracking reaction of *n*-hexane, the activation energies were reported to be 41.1, 36.5 and 30.4 kcal/mol, respectively. These results illustrated the performance of H-MCM-22 zeolite on the hydrocarbon cracking reaction.

In this study, we performed the quantum chemical calculation to study the *n*-hexane cracking on H-MCM-22 zeolite. We employed the ONIOM methodology[18] which is capable of predicting the adsorption and reaction mechanism in the zeolite framework[19-23]. The single point energy at the large quantum cluster with M06-2X function[19-25] was carried out to improve the energy. Our calculations are in good agreement with the previous experimental data which provide the detailed understanding on the mechanism.
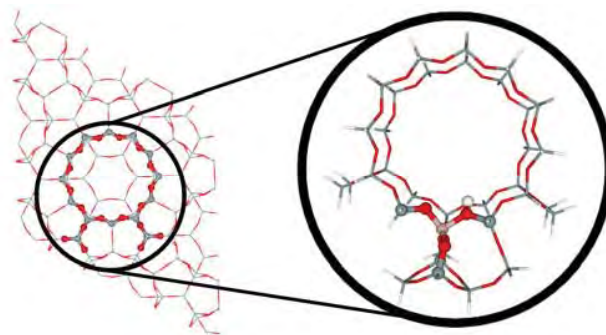

Figure 1. Presentation of H-MCM-22 models 5T:34T ONIOM model. Atoms treated with the M06-2X level of theory are shown in balls, whereas the areas treated with the HF functional are shown in wireframes.

Methodology

The geometry of the H-MCM-22 zeolite was obtained from the crystallographic structure[16]. The Al atom substituted for the Si atom at the T1 position. The 34T quantum cluster was utilized to represent the 10T sinusoidal and 12T channels of the supercage of H-MCM-22, as shown in Fig. 1. For computational cost efficiency, the ONIOM scheme was applied on the 34T model of H-MCM-22 zeolite[20]. The 5T quantum region of the Brønsted acid site was assigned to be the inner layer while the 34T model was the outer layer. The geometries were optimized at the ONIOM model 5T:34T with the M06-2X/6-31G(d,p):HF/3-21G level of theory. To improve the energy, the single point at the high level M06-2X/6-31G(d,p) was performed. Only the active region ($AlSi_4O_4H$) and the probe molecule were allowed to relax while the rest was kept fixed with the crystallographic coordinate. All calculations were performed using the Gaussian 03 program[26] incorporated with the Minnesota Density Functionals module 3.1 by Zhao and Truhlar[25,27].

Results and Discussion

Molecular cluster and Adsorption of *n*-hexane with H-MCM-22. The 34T quantum cluster of H-MCM-22 zeolite, shown in Figure 1, is modeled to cover the intersection region between the 10T sinusoidal and 12T channels of the supercage where the adsorbates prefer to locate. The Brønsted acid site in H-MCM-22 is modeled to be the inner layer 5T quantum cluster while the extended framework is represented by the lager 34T cluster. The Brønsted acid O1-Hz bond length is 0.97 Å. The Al ⋯ Hz distance is 2.44 Å, which compared well with the experimental data (2.38-2.48 Å)[28].

The *n*-hexane adsorbed on H-MCM-22 at the intersection region between the 10T sinusoidal and 12T channels of the supercage of MCM-22 [AD, Figure 2a]. In this study, the adsorption through the central C-C bond of *n*-hexane is focused because the main propane and propene products are produced from central C-C bond breaking. The O1-Hz bond is not significantly changed due to weak interaction. The distances between *n*-hexane and the proton of Brønsted acid are 2.75 and 2.82 Å for Hz ⋯ C3 and Hz ⋯ C4, respectively. The calculated adsorption energy of -11.1 kcal/mol with the M06-2X//ONIOM(M06-2X:HF) method agrees well with experiment report of -11.0 kcal/mol[17].
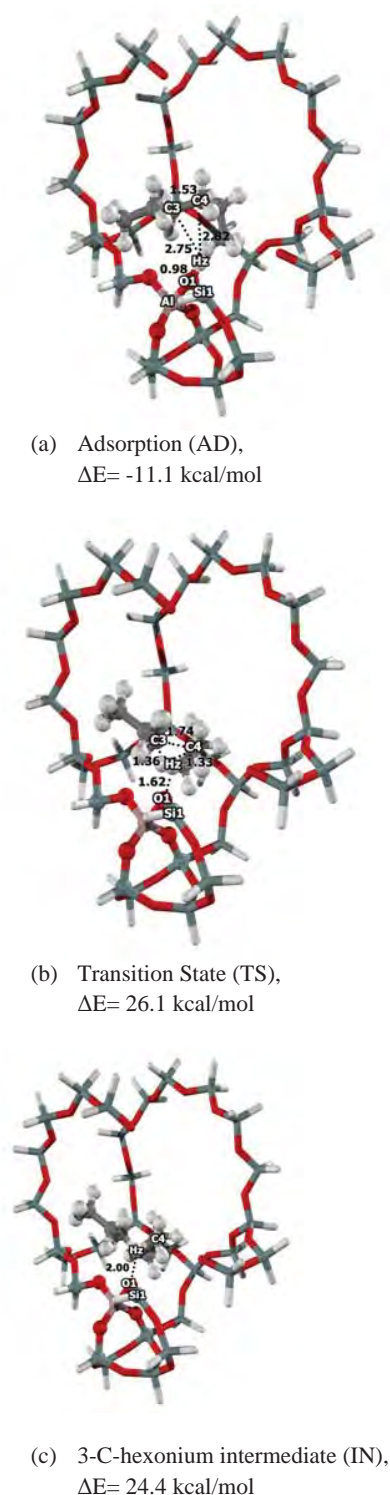
(a) Adsorption (AD),
ΔE= -11.1 kcal/mol

(b) Transition State (TS),
ΔE= 26.1 kcal/mol

(c) 3-C-hexonium intermediate (IN),
ΔE= 24.4 kcal/mol

Figure 2. Optimized structure of Adsorption (a), Transition State (b) and 3-C-hexonium intermeidate (c) of *n*-hexane on H-MCM-22 zeolite. Distances are in Ås.

The Cracking Reaction of *n*-hexane with H-MCM-22. The cracking reaction of n-hexane is studied in the H-MCM-22 zeolite. Based on the previous calculation, the reaction mechanism is proposed through the two steps: (1) Protonation of n-hexane and (2) Decomposition of the Hexonium intermediate to produce propane and propene products. This study is focused on the protonation of n-Haxane which is the rate determination step of reaction.

The *n*-hexane molecule is adsorbed in the intersection region of H-MCM-22 with an adsorption energy -11.1 kcal/mol [AD, Figure 2a]. The transition state is the protonation of acidic proton to the central C-C bond of *n*-hexane to form the adsorbed 3-C-hexonium intermediate. At the transition state [TS, Figure 2b], the H1 migrates to the C3-C4 bond of *n*-hexane. The O1-Hz bond distance increases from 0.98 Å to 1.62 Å and the C3-C4 bond increases from 1.53 Å to 1.74 Å. The distances Hz-C3 and Hz-C4 are 1.36 and 1.33 Å. The transition state structure has been confirmed by a single imaginary frequency at 828.5i cm⁻¹. The calculated activation energy is 37.2 kcal/mol. This activation energy is lower than the previous calculations on H-ZSM-5 and H-FAU which are 45.8 and 45.7 kcal/mol, respectively. The lower activation energy for *n*-hexane cracking on H-MCM-22 agrees well with experimental data [17].

The product of this step is the 3-C-hexonium intermediate [IN, Figure 2c]. The O1-Hz distance is 1.90 Å while the Hz-C1 and Hz-C2 distances are 1.23 and 1.27 Å, respectively. The 3-C-hexonium interacts with the zeolite surface with the relative energy of 24.4 kcal/mol. The reaction is an endothermic reaction with the reaction energy of 24.4 kcal/mol. This energy is lower than the previous calculation, 33.6 and 26.9 kcal/mol for H-FAU and H-ZSM-5, respectively. This was due to the lower activation energy of the transition state in H-MCM-22.

For the bare 5T quantum cluster, the calculated adsorption energy of *n*-hexane on H-MCM-22 is -6.0 kcal/mol. The calculated activation energy for *n*-hexane cracking is 50.9 kcal/mol. The zeolite framework stabilizes the adsorption complex and the transition state structure by about 54 % for its adsorption energy and 37% for its activation energy. Our results show that H-MCM-22 can stabilize the adsorption structure and transition complexes that give lower activation energy for *n*-hexane cracking.
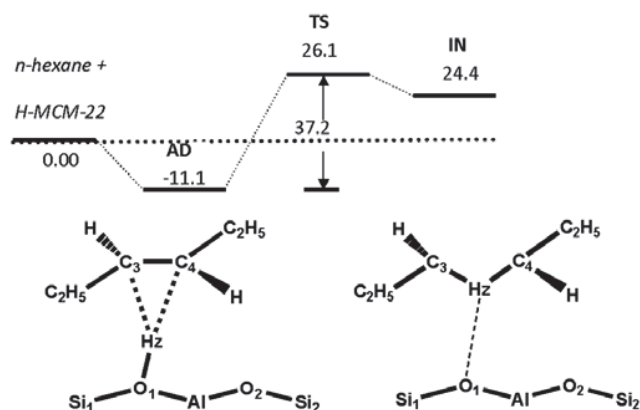

Figure 3. Potential energy diagram of the *n*-hexane to 3-c-hexonium intermediate on the 34T// ONIOM (5T:34T) with M06-2X//ONIOM (M06-2X:HF) method (kcal/mol).

Conclusion

The hydrocarbon cracking of *n*-hexane over H-MCM-22 zeolite has been calculated via the ONIOM (5T:34T) M06-2X/6-31G(d,p):HF/3-21G method. To improve the energy, the single point calculation at the large quantum 34T with M06-2X/6-31G(d,p) level of theory has been performed. The adsorption energy of *n*-hexane on the H-MCM-22 is predicted to be -11.1 kcal/mol, which lies between those of the H-FAU (−10.8 kcal/mol) and the ZSM-5 complexes (−18.2 kcal/mol), all of which are in good agreement with experimental data. The reaction mechanism of *n*-hexane to propane and propene is proposed via the 3-C-hexonium. Only the rate-determining step of the 3-C-hexonium formation is calculated. The calculated actual activation energy of *n*-hexane on H-MCM-22 is 37.2 kcal/mol, which is lower than the previous calculations on H-FAU and H-ZSM-5 of 45.7 and 45.8 kcal/mol, respectively. Thus, the results obtained with this hybrid-meta functional, parametrized to include the London dispersion energy, suggest that the H-MCM-22 zeolite is one of the promising candidate catalysts for hydrocarbon cracking.

References

(1) Weitkamp, J. *Solid State Ionics* **2000**, *131*, 175.
(2) Stöcker, M. *Microporous Mesoporous Mater.* **2005**, *82*, 257.
(3) Kotrel, S.; Rosynek, M. P.; Lunsford, J. H. *J. Phys. Chem. B* **1999**, *103*, 818.
(4) Kotrel, S.; Knozinger, H.; Gates, B. C. *Microp. Macrop. Mat.* **2000**, *35-36*, 11.
(5) Corma, A.; Orchilles, A. V. *Microporous Mesoporous Mater.* **2000**, *3536*, 21.
(6) Collins, S. J.; Omalley, P. J. *J. Catal.* **1995**, *153*, 94.
(7) Collins, S. J.; O'Malley, P. J. *Chem. Phys. Lett.* **1995**, *246*, 555.
(8) Kazansky, V. B.; Frash, M. V.; van Santen, R. A. *Catal. Lett.* **1994**, *28*, 211.
(9) Blaszkowski, S. R.; Nascimento, M. A. C.; Van Santen, R. A. *J. Phys. Chem.* **1996**, *100*, 3463.
(10) Frash, M. V.; Van Santen, R. A. *Top. Catal.* **1999**, *9*, 191.
(11) Zheng, X.; Blowers, P. *J. Phys. Chem. A* **2005**, *109*, 10734.
(12) Boronat, M.; Viruela, P.; Corma, A. *J. Phys. Chem. B* **2000**, *104*, 1944.
(13) Boronat, M.; Corma, A. *Appl Catal A Gen* **2008**, *336*, 2.
(14) Maihom, T.; Pantu, P.; Tachakritikul, C.; Probst, M.; Limtrakul, J. *J. Phys. Chem. C* **2010**, *114*, 7850.
(15) Corma, A.; Corell, C.; Llopis, F.; Martínez, A.; Pérez-Pariente, J. *Applied Catalysis A, General* **1994**, *115*, 121.
(16) Leonowicz, M. E.; Lawton, J. A.; Lawton, S. L.; Rubin, M. K. *Science* **1994**, *264*, 1910.
(17) Katada, N.; Suzuki, K.; Noda, T.; Miyatani, W.; Taniguchi, F.; Niwa, M. *Appl Catal A Gen* **2010**, *373*, 208.
(18) Dapprich, S.; Komiromi, I.; Byun, K. S.; Morokuma, K.; Frisch, M. J. *THEOCHEM* **1999**, *461-462*, 1.
(19) Boekfa, B.; Choomwattana, S.; Khongpracha, P.; Limtrakul, J. *Langmuir* **2009**, *25*, 12990.
(20) Boekfa, B.; Pantu, P.; Probst, M.; Limtrakul, J. *J. Phys. Chem. C* **2010**, *114*, 15061.
(21) Maihom, T.; Boekfa, B.; Sirijaraensre, J.; Nanok, T.; Probst, M.; Limtrakul, J. *J. Phys. Chem. C* **2009**, *113*, 6654.
(22) Namuangruk, S.; Khongpracha, P.; Pantu, P.; Limtrakul, J. *J. Phys. Chem. B* **2006**, *110*, 25950.
(23) Pantu, P.; Boekfa, B.; Limtrakul, J. *J. Mol. Catal. A: Chem.* **2007**, *277*, 171.
(24) Zhao, Y.; Truhlar, D. G. *Theor. Chem. Acc.* **2008**, *120*, 215.
(25) Zhao, Y.; Truhlar, D. G. *Acc. Chem. Res.* **2008**, *41*, 157.
(26) Frisch, M. J.; Trucks, G. W.; Schlegel, H. B.; Scuseria, G. E.; Robb, M. A.; Cheeseman, J. R.; Montgomery, J. A., Jr.; Vreven, T.; Kudin, K. N.; Burant, J. C.; Millam, J. M.; Iyengar, S. S.; Tomasi, J.; Barone, V.; Mennucci, B.; Cossi, M.; Scalmani, G.; Rega, N.; Petersson, G. A.; Nakatsuji, H.; Hada, M.; Ehara, M.; Toyota, K.; Fukuda, R.; Hasegawa, J.; Ishida, M.; Nakajima, T.; Honda, Y.; Kitao, O.; Nakai, H.; Klene, M.; Li, X.; Knox, J. E.; Hratchian, H. P.; Cross, J. B.; Adamo, C.; Jaramillo, J.; Gomperts, R.; Stratmann, R. E.; Yazyev, O.; Austin, A. J.; Cammi, R.; Pomelli, C.; Ochterski, J. W.; Ayala, P. Y.; Morokuma, K.; Voth, G. A.; Salvador, P.; Dannenberg, J. J.; Zakrzewski, V. G.; Dapprich, S.; Daniels, A. D.; Strain, M. C.; Farkas, O.; Malick, D. K.; Rabuck, A. D.; Raghavachari, K.; Foresman, J. B.; Ortiz, J. V.; Cui, Q.; Baboul, A. G.; Clifford, S.; Cioslowski, J.; Stefanov, B. B.; Liu, G.; Liashenko, A.; Piskorz, P.; Komaromi, I.; Martin, R. L.; Fox, D. J.; Keith, T.; Al-Laham, M. A.; Peng, C. Y.; Nanayakkara, A.; Challacombe, M.; Gill, P. M. W.; Johnson, B.; Chen, W.; Wong, M. W.; Gonzalez, C.; Pople, J. A. *Gaussian 03, revision B.05; Gaussian, Inc.: Pittsburgh, PA*, 2003.
(27) Zhao, Y.; Truhlar, D. G. *J. Phys. Chem. C* **2008**, *112*, 6860.
(28) Klinowski, J. *Chem. Rev.* **1991**, *91*, 1459.

ACTIVITY OF GOLD-SUPPORTED MFI ZEOLITES FOR NITROUS OXIDE DECOMPOSITION: A DENSITY FUNCTIONAL STUDY

Thana Maihom[1,2,3], Pipat Khongpracha[1,2,3] and Jumras Limtrakul[1,2,3]*

[1]Laboratory for Computational and Applied Chemistry, Department of Chemistry, Faculty of Science and Center of Nanotechnology, Kasetsart University Research and Development Institute, Kasetsart University, Bangkok 10900, Thailand
[2]Center for Advanced Studies in Nanotechnology and Its Applications in Chemical, Food and Agricultural Industries, Kasetsart University, Bangkok 10900, Thailand
[3]NANOTEC Center of Excellence, National Nanotechnology Center, Kasetsart University, Bangkok 10900, Thailand
*Corresponding author's e-mail address: jumras.l@ku.ac.th

Introduction

Nitrous oxide (N_2O), from industrial and motor vehicle exhausts, is well known as an environmental pollutant because it is a strong greenhouse effect gas and also plays an important role in the destruction of the stratospheric ozone layer. With increasing concern over environmental problems, the development of methods for reducing N_2O has become not only extremely important but also attractive. The catalytic decomposition is one of the most promising ways to remove the N_2O. Among a variety of tested catalysts, metals such as Fe, Co, Cu and Ag containing zeolite structures included MFI, MOR, FER, and Y show promising activity features for N_2O decomposition.[1-11]

Gold (Au) containing zeolites is one of the catalysts that has been verified for catalyzing the decomposition of N_2O. Previously, the experimental studies found that the Au/MFI can catalyze the decomposition of N_2O to N_2 even in the presence of O_2.[12] Additionally, Au-zeolites also showed high activity for various reactions such as direct NO decomposition, CO activation and the water gas shift (WGS) reaction at low temperature.[13-17]

The different oxidation states of Au species have been proposed and investigated as catalytic active sites in the literature. Ichikawa et al.[18] have concluded that Au^+ was the dominant active site for the Au/NaY, Au/Na-MOR, and Au/Na-MFI zeolites where the reaction could take place. Sachtler et al.[19] analyzed the Au/MFI zeolite by using FTIR, XRD, HRAEM and CO-TPR and found that the Au^+ and Au^{3+} were the dominant golds present; however, the Au^+ was irreversibly transformed to Au^0 at 500°C. In addition, Fierro-Gonzalez and Gates[20] have synthesized and characterized mononuclear Au^+ and Au^{3+} complexes in NaY zeolite and also tested the activity for the NO reduction with CO. In that report, they found the Au^{3+} complex was more active than the Au^+ complex. That finding emphasizes that the oxidation state of Au in zeolite seriously influences catalytic activity.

To the best of our knowledge, the decomposition of N_2O on different species of Au in zeolite has not been theoretically studied and compared previously. In this work, we report the theoretical investigation on the activity of the Au cation and Au atom supported MFI zeolite for the decomposition of N_2O by using the M06-L method. The reaction mechanism and relative energies and structures of intermediates and transition states are discussed.

Models and Method

The MFI zeolites were represented by the 12T cluster model that was generated from its lattice structures.[21] The 12T cluster model of MFI, illustrated in Figure 1, covers the 10-membered-ring window at the interconnection between the straight channel and the zigzag channel. One aluminium atom was substituted for a silicon atom at the T12 site to generate the Brønsted acid site. In the model of Au/MFI, the Brønsted site of zeolite is exchanged by Au cation (Figure 1a). For the Au/H-MFI model, an Au atom was placed next to the Brønsted site of zeolite (Figure 1b).

The M06-L density functional[22-23] was used in all calculations. The series of this method has been shown to be very useful for studying adsorption and reaction mechanisms in the zeolites.[24-30] The basis set of 6-31G(d,p) was employed for the N_2O molecule and all zeolitic atoms, while the Au atom was described by the Effective Core Potentials (ECP) of Stuttgart RSC 1997 ECP.[31] During geometry optimizations, only the 5T active region and the adsorbates were allowed to relax while the rest of the structure is kept fixed at the crystallographic coordinates. The total spin singlet state was employed for all calculations of the reaction coordinates. Transition states were confirmed to have one imaginary frequency corresponding to the reaction coordinate. All calculations were performed with the Gaussian 03 code[32] modified to incorporate the Minnesota Density Functionals module 3.1 by Zhao and Truhlar.
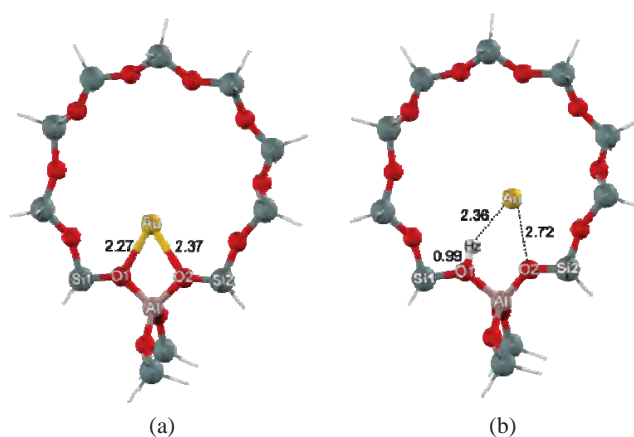

(a)   (b)

Figure 1. Optimized geometric parameters of the Au supported MFI models: (a) Au/MFI zeolite (b) Au/H-MFI zeolite.

Results and Discussion

Structures of Au/MFI and Au/H-MFI. Optimized structures of Au/MFI and Au/H-MFI zeolites are illustrated in Figures 1a and 1b, respectively. In the Au/MFI zeolite, the Au cation (Au^+) is coordinated with the two oxygen bridging atoms of zeolite having the bond distances of 2.27 and 2.37 Å for Au⋯O1 and Au⋯O2, respectively. The Al⋯Au distance is predicted to be 3.10 Å. The Mulliken population analysis for the partial atomic charge on the Au is calculated to be +0.189e. As for the Au/H-MFI zeolite, the Au atom interacts with a Brønsted proton (Hz) and the oxygen bridging (O2) of the zeolite. The acidic bond (O1–Hz) of zeolite is calculated to be 0.99 Å. The calculated distances of Au⋯Hz and Au⋯O2 are 2.36 and 2.72 Å, respectively. The electron transfer from the Hz and O2 to the Au atom cause the Mulliken charge on the Au atom to be negative (–0.366e).

Adsorption of N_2O on Au/MFI and Au/H-MFI. The optimized adsorption structures of N_2O on the Au cation of the Au/MFI zeolite is shown in Figures 2a. It can be seen that the N_2O molecule interacts with the Au^+ by its lone pair electron. The oxygen–nitrogen (O–N1) bond of N_2O is elongated from 1.19 to 1.26 Å. The distance between the nitrous oxide oxygen (O) and the Au^+ of

zeolite is 2.31 Å and the corresponding adsorption energy (ΔE) for this complex is –15.9 kcal/mol, which agrees well with the previous calculation.[33] The positive charge on Au is reduced from +0.189e to +0.102e by reason of the electrons transferred from O to Au.

Figure 3a depicts the adsorption structure of N_2O interacted with the Au atom of the Au/H-MFI zeolite. The N_2O is weakly adsorbed on zeolite through interactions between the π-bond of N_2O and Au atom. The adsorption interactions are weak so that the structures of the Au/H-MFI zeolite and the adsorbed N_2O are not significantly altered. The bond distances of O1–Hz, Au⋯Hz, Au⋯O2 of zeolite and the O–N1 bond of N_2O differ slightly from the corresponding isolated molecules. The internuclear distances of Au⋯O and Au⋯N1 between the adsorbed N_2O and the Au active site are comparable. The negative charge of the Au atom is increased from –0.366e to – 0.423e. The calculated adsorption energy (ΔE) is –5.5 kcal/mol which is almost three times lower than that derived from the Au/MFI complex (ΔE = –15.9 kcal mol).

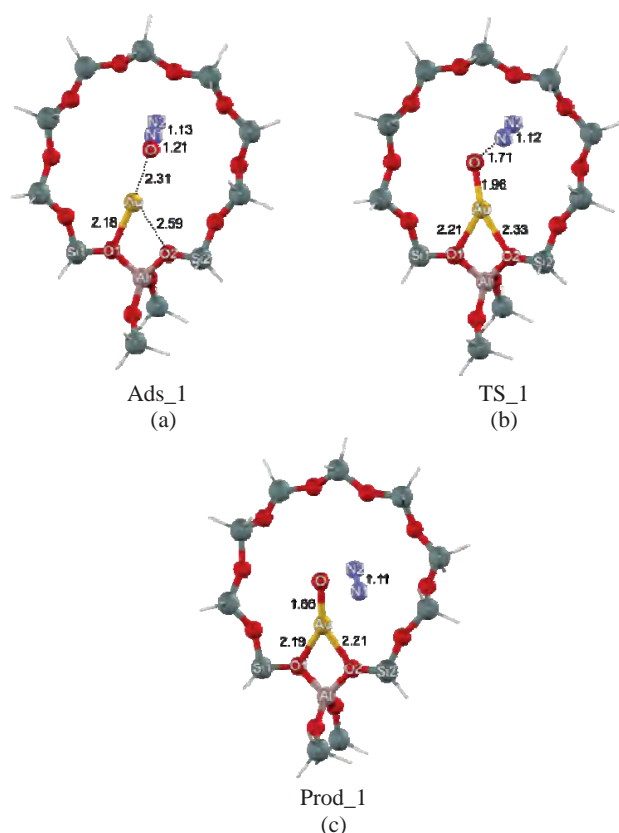Ads_1
(a)

TS_1
(b)

Prod_1
(c)

Figure 2. Optimized structures of adsorption (Ads_1), transition state (TS_1) and product (Prod_1) involved in the decomposition of N_2O over Au/MFI zeolite.

Reaction Mechanism of N_2O Decomposition on Au/MFI and Au/H-MFI zeolites. The decomposition of N_2O on Au/MFI is depicted in Figure 2. This reaction is initiated by the adsorption of nitrous oxide on the active Au cation site of MFI zeolite (Ads_1). Here, its adsorption energy is –15.9 kcal/mol. The adsorbed N_2O is decomposed via the transition state of the N–O bond breaking (TS_1). In this transition state, TS_1, the N–O bond of N_2O is cleaved and the Au⋯O distance is contracted leading to form a new bond (Figure 2b). The activation energy for this transition state is

41.9 kcal/mol. The transition state proceeds then by the deposition of an oxygen species on the Au center and the formation of a nitrogen molecule (Prod_1). In it, the Au⋯O distance is reduced to 1.86 Å. The adsorption energy of this complex with respect to the isolated reactants is 16.2 kcal/mol, significantly less than the adsorption energy of nitrous oxide.
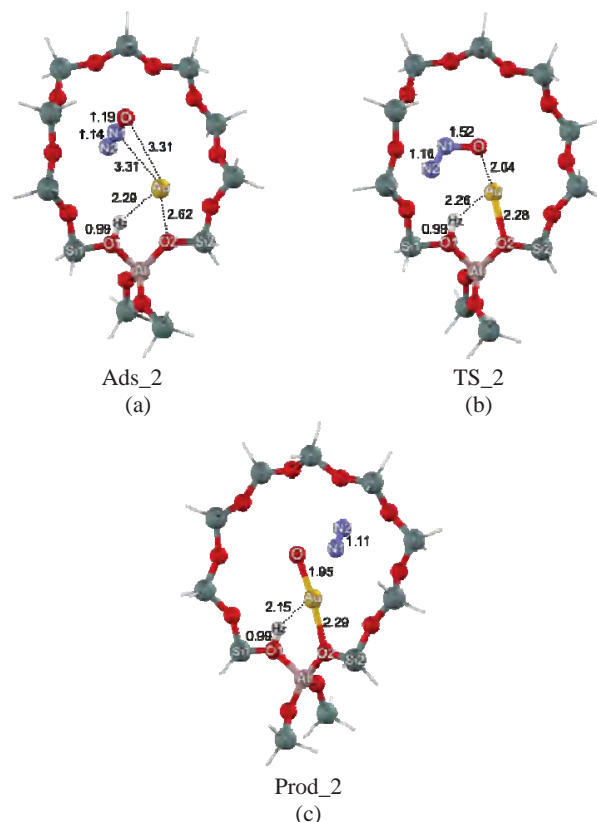

Ads_2
(a)

TS_2
(b)

Prod_2
(c)

Figure 3. Optimized structures of adsorption (Ads_2), transition state (TS_2) and product (Prod_2) involved in the decomposition of N_2O over Au/H-MFI zeolite.

The equivalent decomposition of nitrous oxide on Au/H-MFI zeolite is shown in Figure 3. This reaction proceeds as the decomposition on Au/MFI discussed above. Ads_2 shows the N_2O adsorption complex whose adsorption energy is evaluated to be –5.5 kcal/mol. Then, the N–O bond of the adsorbed nitrous oxide is cleaved and the Au–O bond is formed (TS_2). Again, the surface oxygen species is generated on the active Au center and a nitrogen molecule also formed in the zeolite framework. The activation energy is 15.2 kcal/mol, which is significantly lower than the N_2O decomposition on Au/MFI reported earlier. The surface Au–O bond distance in the surface oxygen species is 1.95 Å (Prod_2). The calculated adsorption energy of this complex is –15.8 kcal/mol, which is more stable than N_2O adsorption.

The activation energy for the decomposition of N_2O on Au/H-MFI zeolite is found to be lower than on Au/MFI zeolite (cf. Figure 4). With respect to the adsorption complex, the decomposition product on Au/H-MFI is also more stable than the Au/MFI. This shows that the Au/H-MFI zeolite is kinetically and thermodynamically favored for the N_2O decomposition over Au/MFI zeolite.
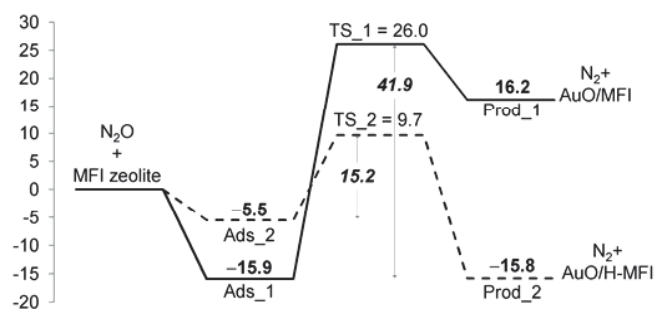
Figure 4. Energy profile for the N$_2$O decomposition for both zeolites: Au/MFI zeolite (solid line) and Au/H-MFI (dashed line) zeolite (energies are in kcal/mol).

Conclusion

The density functional calculations, M06-L including dispersion energy, has been employed for investigating the N$_2$O decomposition reaction over Au/MFI and Au/H-MFI zeolites. The reaction is proposed to proceed in a single step of the N$_2$O N–O bond breaking to give the surface oxygen deposited on the Au active site and the nitrogen molecule. The calculated activation barriers (E$_a$) for N2O decomposition are observed to be E$_a$ = 41.9 and E$_a$ =15.2 kcal/mol for the reaction over Au/HMFI and Au/H-MFI zeolites, respectively. The latter E$_a$ is much lower than that of the former as a result of more negative charges of the gold atom found in the Au/H-MFI as compared to the Au/ZSM-5 adduct. The formation of the N$_2$O decomposition product on Au/H-MFI (–15.8 kcal/mol) is also more stable in energy than on Au/MFI (16.2 kcal/mol). On the basis of these results, it can be concluded that the Au/H-MFI zeolite is more active for N$_2$O decomposition than Au/MFI zeolite.

References

(1) Shelef, M.; *Chem. Rev.* **1995**, *95*, 209.
(2) Gomez, S.A.; Campero, A.; Martínez-Hernández, A.; Fuentes, G.A.; *Appl. Catal. A* **2000**, *197*, 157.
(3) Yahiro, H.; Iwamoto, M. *Appl. Catal. A* **2001**, *222*, 163.
(4) Parez-Ramirez, J.; Kapteijn, F.; Mul, G.; Moulijin, J.A. *Chem. Commmun.* **2001**, 693.
(5) Heyden, A.; Peters, B.; Bell, A.T.; Keil, F.J. *J. Phys. Chem. B* **2005**, *109*, 1857.
(6) Schidder, M.; Kumar, M.S.; Klementiev, K.; Pohl, M.M.; Brückner, A.; Grünert, W. *J. Catal.* **2005**, *231*, 314.
(7) Devades, M.; Kröcher, O.; Elsener, M.; Wokiaun, A.; Söges, N.; Pfeifer, M.; Demel, Y.; Mussmann, L. *Appl. Catal. B Environ.* **2006**, *67*, 187.
(8) Chupin, C.; van Veen, A.C.; Konduru, M.; Despres, J.; Mirodals, C. *J. Catal.* **2006**, *241*, 103.

(9) Pantu, P.; Boekfa, B.; Sunpetch, B.; Limtrakul, J. Chem. Eng. Comm. **2008**, *195*, 1477.
(10) Shibata, J.; Takada, Y.; Shichi, A.; Satokawa, S.; Satsuma, A.; Hattori, T. *Appl. Catal. B Environ.* **2004**, *54*, 137.
(11) Shibata, J.; Shimizu, K.; Takada, Y.; Shichi, A.; Yoshida, H.; Satokawa, S.; Satsuma, A.; Hattori, T. *J. Catal.* **2004**, 227, 367.
(12) Gao, Z.; Sun, Q.; Chen, H.; Wang X.; Sachtler, W.M.H. *Catal. Lett.* **2001**, *72*, 1.
(13) Qiu, S.; Ohnishi, R.; Ichikawa, M. *J. Chem. Soc., Chem. Commun.* **1992**, 1425–1427.
(14) Fierro-Gonzalez, J. C.; Gates, B. C. *J. Phys. Chem. B* **2004**, *108*, 16999–17002.
(15) Salama, T. M.; Shido, T.; Ohnishi, R.; Ichikawa, M. *J. Chem. Soc., Chem. Commun.* **1994**, 2749–2750.
(16) Mohamed, M. M.; Salama, T. M.; Ichikawa, M. *J. Colloid Interface Sci.* **2000**, *224*, 366–371.
(17) Mohamed, M. M.; Ichikawa, M. *J. Colloid Interface Sci.* **2000**, *232*,381–388.
(18) Mohamed, M. M.; Salama, T. M.; Ichikawa, M. *J Colloid Interface Sci* **2000**, *224*, 366.
(19) Qiu, S.; Ohnishi, R.; Ichikawa, M. *J Phys Chem Lett* **1994**, *98*, 2719.
(20) Fierro-Gonzalez, J.C.; Gates, B.C. *J. Phys. Chem. B* 2004, *108*, 16999.
(21) van Koningsveld, H.; van Bekkum, H.; Jansen, J. C. *Acta. Crystallogr. B* **1987**, *43*, 127.
(22) Zhao, Y.; Truhlar, D. G. *J. Phys. Chem. C* **2008**, 112, 6860.
(23) Zhao, Y.; Truhlar, D. G. *Acc. Chem. Res.* **2008**, 41, 157.
(24) Maihom, T.; Boekfa, B.; Sirijaraensre, J.; Nanok, T.; Probst, M.; Limtrakul, J. *J. Phys. Chem. C* **2009**, 113, 6654.
(25) Boekfa, B.; Choomwattana, S.; Khongpracha, P.; Limtrakul, J. *Langmuir* **2009**, 25(22), 12990.
(26) Kumsapaya, C.; Bobuatong, K.; Khongpracha, P.; Tantirungrotechai, Y.; Limtrakul, J. *J. Phys. Chem. C* **2009**, 113, 16128.
(27) Maihom, T.; Pantu, P.; Tachakritikul, C.; Probst, M.; Limtrakul, J. *J. Phys. Chem. C* **2010**, 114, 7850.
(28) Boekfa, B.; Pantu, P.; Probst, M.; Limtrakul, J. *J. Phys. Chem. C* **2010**, 114, 15061.
(29) Wannakao, S.; Boekfa, B.; Khongpracha, P.; Probst, M.; Limtrakul, J. *ChemPhysChem* **2010**, 11, 3432.
(30) Bobuatong, K.; Probst, M.; Limtrakul, J. *J. Phys. Chem. C* **2010**, 114, 21611.
(31) Dolg, M.; Stoll, H.; Preuss, H.; Pitzer, R. M. *J. Phys. Chem.* **1993**, *97*, 5852.
(32) *Gaussian 03, revision B.05*; Gaussian, Inc.: Pittsburgh, PA, **2003**.
(33) Sierraalta, A.; Hernandez-Andara, R.; Ehrmann, E. *J. Phys. Chem. B* **2006**, *110*, 17912.

STRUCTURES AND REACTION MECHANISMS OF BUTADIENE CYCLOADDITION OVER METAL-EXCHANGED FAUJASITE

Thittaya Yutthalekha [1,2,3], Bundet Boekfa[1,2,3,4]
and Jumras Limtrakul [1,2,3*]

[1]Laboratory for Computational and Applied Chemistry, Department of Chemistry, Faculty of Science and Center of Nanotechnology, Kasetsart University Research and Development Institute, Kasetsart University, Bangkok 10900, Thailand
[2]Center for Advanced Studies in Nanotechnology and Its Applications in Chemical, Food and Agricultural Industries, Kasetsart University, Bangkok 10900, Thailand
[3]NANOTEC Center of Excellence, National Nanotechnology Center, Kasetsart University, Bangkok 10900, Thailand
[4]Chemistry Department, Faculty of Liberal Arts and Science, Kasetsart University Kamphaeng Saen Campus, Nakhon Pathom73140, Thailand
*Corresponding author's e-mail address: jumras.l@ku.ac.th

Introduction

Butadiene cycloaddition reaction is one of the alternative routes for styrene production with the benefit of higher conversion[1] compared to the conventional route[2]. Benzene alkylation is ultimately required by both processes for dehydrogenation to styrene. The cycloaddition of butadiene to 4-vinylcyclohexene is a well-known thermally-initiated cycloaddition reaction between two butadienes in which one serves as the diene and the other serves as the dienophile. This reaction is believed to proceed via a concerted mechanism or two-step mechanism. From theoretical investigations, it has been shown that both mechanisms are similar in their energetics[3,4]. Several studies propose the use of various catalysts for the reaction, such as the promoted ZrO_2 catalyst, Pd catalysts supported on alumina, polyoxometalate and zeolite[5-10]. A previous study reported that the cycloaddition of butadiene over a Cu-exchanged zeolite produces an excellent yield of 4-vinylcyclohexene[11-14] while the Brønsted acid[13] site of zeolite and the alkaline-exchanged zeolite[15] such as NaX[11,16], yield the oligomeric compounds as major products.

Transition metals supported on zeolite have been found to be active catalysts for many processes[17-19]. Copper containing zeolites have long drawn strong attention because of their activity in the decomposition of NO. Moreover, Cu-exchanged in zeolites such as CuZSM-5, CuX, CuY and CuMCM-41 was found to activate multiple carbon–carbon bonds in alkenes (ethene, propene, butenes), ethyne, and benzene. The activation was evidenced by a measured red-shift of multiple bonds stretching by 80–130 cm^{-1} for alkenes, 168 cm^{-1} for ethyne, 16 cm^{-1} for benzene[20-22]. The charge transfer phenomenon between the alkene molecule and the cationic active site resulted in the bond weakening, an important factor for catalyzing the reaction.

Zeolites are microporous aluminosilicates with a large number of atoms in the unit cell, where the use of such sophisticated methods as periodic calculation are too computationally demanding and expensive. In theoretical studies, small clusters are usually used for representing models of catalytic zeolite. However, these cluster models do not incorporate the framework effect, which has an important role for reactions inside zeolites. More recently, the newly developed M06 functional, in which the dispersion force was taken into account, is successfully applied to study the interaction and reactions of hydrocarbon on various zeolites[23-25].

To the best of our knowledge, only a small number of theoretical studies of the mechanisms on the systems of butadiene cycloaddition over Cu-exchanged Faujasite have been reported to date. The aim of this work is to study the effects of the metal inside zeolites and possible mechanisms for the reaction.

Methods

The cluster model of Faujasite was obtained from their crystal lattice structures. To account for the framework effect of the zeolite pores, we applied the ONIOM2 approach to the 50T cluster representing the supercage of faujasite zeolite in which the reactions can occur. The 50T cluster which divides the faujasite structure into two layers is shown in Figure1. The inner layer consists of the 10T cluster and the reactive species, which were treated with the M06L functional using the 6-31G(d,p) basis set for H, C, O, Al and Si atoms, while the Stuttgart RSC 1997 effective core potential (ECP) were used for the Cu atom. The outer layer is the 40T extended structure of faujasite zeolite, treated with the UFF force field to account for the effect of the Faujasite framework on the adsorbed species inside the pore. Normal mode analyses were carried out to verify the transition states to have one imaginary frequency whose mode correspond to the reaction coordinate. The total spin was kept constant at the singlet ground states for Cu(I) whereas it was kept constant at the doublet ground states for Cu(II). NPA charges and electronic configuration were determined by Natural Bond Orbital (NBO) methods.

All calculations in this work have been performed by using the Gaussian 03 program incorporated with the Minnesota Density Functionals module 3.1 by Zhao and Truhlar[26-28].
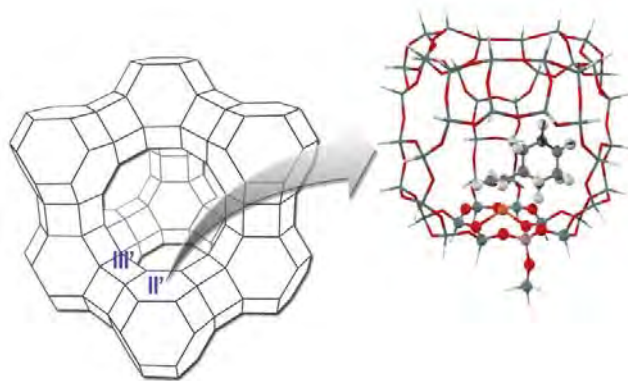

Figure1. Model of the 50T cluster, the 10T quantum cluster is drawn as the bond and stick model.

Results and Discussion

The metal exchanged zeolite Models and Adsorption Complexes. The optimized structures of Cu-exchanged Faujasite, whose metal ion acts as an active site are shown in Figure1. The metal ion lies between the three bridging oxygen atoms of the zeolite framework. The Al-Cu bond is 3.06 Å, which agrees with previous work[28].
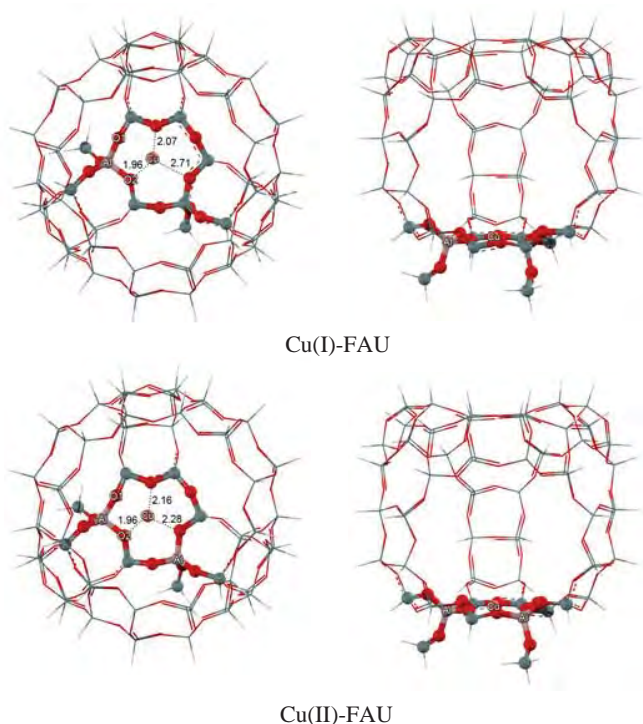
Cu(I)-FAU

Cu(II)-FAU

Figure1. Optimized structures of the Cu(I) and Cu(II) exchanged Faujasite

The optimized structures of butadiene adsorbed via the π complex on the metal ion are shown in Figure2. For the Cu(II)-FAU system, the adsorption energy is calculated to be 37.36 kcal/mol, which is much higher than the Cu(I)-FAU system of -35.82 kcal/mol. The C1=C2 bonds of adsorbed 1,3 butadiene was increased to 1.39 and 1.37 Å for Cu(I)-FAU and Cu(II)-FAU system, respectively in comparison with the isolated molecule(1.33 Å). In the coadsorption complex, the Cu(II)-FAU system yields coadsorption energy of -50.48 kcal/mol while the Cu(I)-FAU system give coadsorption energy of -42.83 kcal/mol.
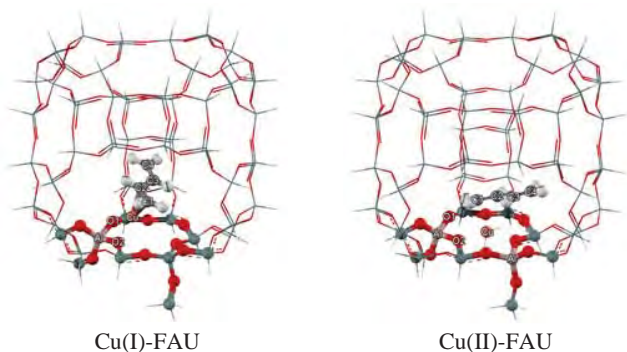

Cu(I)-FAU   Cu(II)-FAU

Figure2. Adsorption complex structures (Å) of butadiene on Metal exchanged Faujasite

The Reaction Mechanism of butadiene cycloaddition. We investigated two different mechanisms of this reaction: stepwise mechanism and concerted mechanism, which are shown in Figure3.
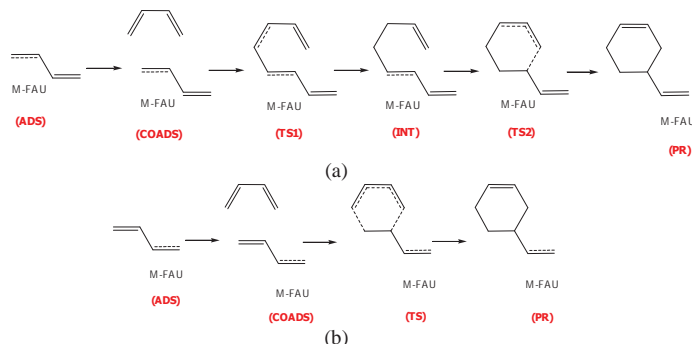

(a)

(b)

Figure3. Proposed mechanisms of butadiene cycloaddition:
    (a) Stepwise mechanism
    (b) Asynchronous concerted mechanism

The stepwise mechanism, the optimized structures are shown in Figure4 and the reaction energies are shown in Table1. This mechanism is composed of two steps. The first step, formation of the first C-C bond, is the rate determining step and followed rapidly by ring closure of the second C-C bond. The calculated activation energies are calculated to be 19.91 and 9.12 kcal/mol for Cu(I)-FAU and Cu(II)-FAU system, respectively.
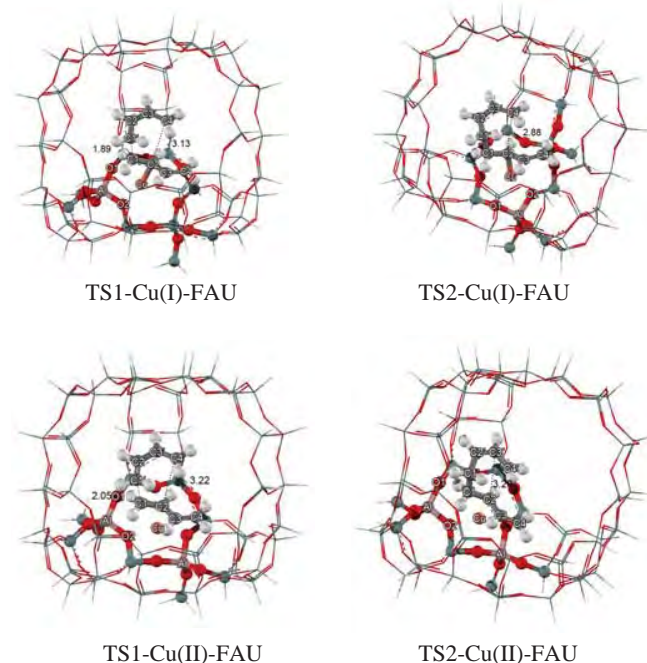

TS1-Cu(I)-FAU   TS2-Cu(I)-FAU

TS1-Cu(II)-FAU   TS2-Cu(II)-FAU

Figure4. Transition state structures (Å) of butadiene cycloaddition on Metal exchanged Faujasite.

Table1. Reaction energies (kcal/mol) of the butadiene cycloaddition on Cu-FAU zeolite calculated with 10T:50T ONIOM (M06L:UFF), Activation energies are in parenthesis

Model	Ads	Coads	TS1	INT	TS2	Pr
Cu(I)-FAU	-35.82	-42.83	-22.92 (19.91)	-24.40	-22.81 (1.59)	-84.42
Cu(II)-FAU	-37.36	-50.48	-41.35 (9.12)	-49.56	-44.97 (4.59)	-88.30

The concerted mechanism, the optimized transition state structures are shown in Figure5 and the reaction energies are shown in Table1. The lower activation energy compared with the stepwise mechanism indicating that this mechanism is more favorable than the stepwise mechanism. The geometries of the transition states are asynchronous structures in which the distances between two molecules in cyclic transition are not equal. The activation energies are predicted to be 12.36 and 6.99 kcal/mol for Cu(I)-FAU and Cu(II)-FAU system, respectively.

Table2. Reaction energies (kcal/mol) of the butadiene cycloaddition on Cu-FAU zeolite calculated with 10T:50T ONIOM (M06L:UFF), Activation energies are in parenthesis.

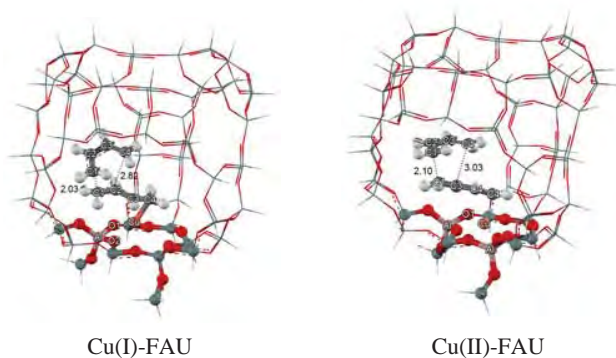| Model	Ads	Coads	TS	Pr
Cu(I)-FAU	-35.82	-42.83	-29.36 (12.36)	-84.42
Cu(II)-FAU	-37.35	-50.48	-43.48 (6.99)	-88.30

Cu(I)-FAU   Cu(II)-FAU

Figure5. Transition state structures (Å) of butadiene cycloaddition on Metal exchanged Faujasite.

The interaction between butadiene and metal exchanged-Faujasite can be examined in visual detail by using NBO analysis derived at the 10T high level of ONIOM FAU-50T model. The NBO calculations which are shown in Figure6 and Table3 evidenced that, the activation of the adsorbed butadiene molecule was revealed by the π back donation of d electrons of metal to π^* antibonding orbitals of a butadiene. As a result, butadiene acquired a negative charge, whereas the metal became more positive. Part of the charge transmitted to the molecule came from the metal itself and part from the zeolite framework which acted as an 'electron reservoir'.
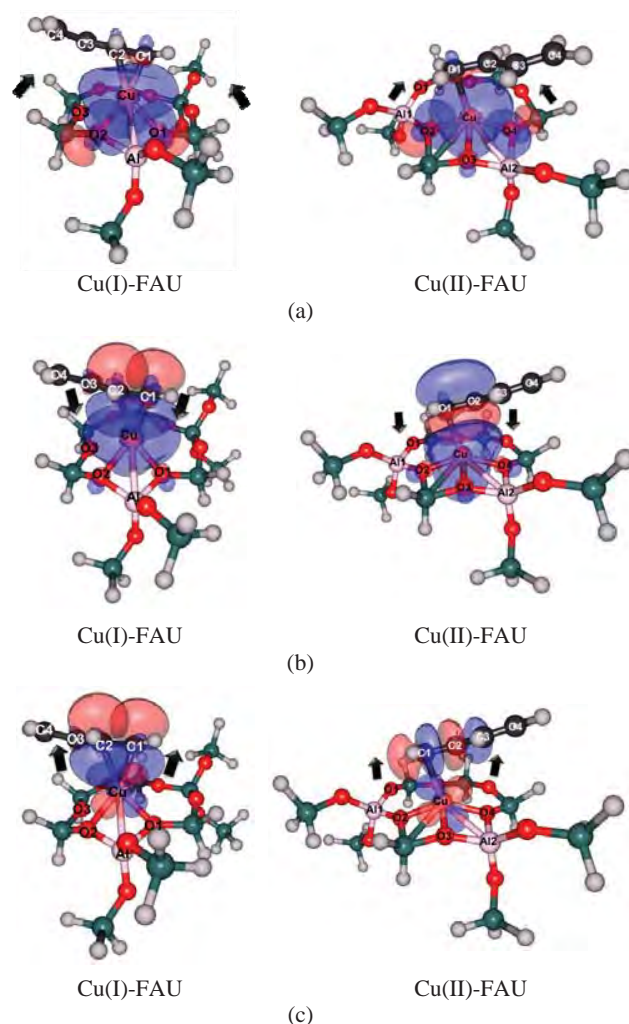

Cu(I)-FAU   Cu(II)-FAU
(a)

Cu(I)-FAU   Cu(II)-FAU
(b)

Cu(I)-FAU   Cu(II)-FAU
(c)

Figure6. The interaction between butadiene and metal exchanged-Faujasite obtained from calculation at the 10T high level of ONIOM FAU-50T:
  (a) The charge transfer of the nearest oxygen in zeolite to the metal cation.
  (b) The σ-donation from bonding π electron or p orbital (in the case of Cu(I)) of butadiene to the orbital of the metal.
  (c) The d-π^* electron back donation from d orbital of the metal to π^* orbital of butadiene

Table3. Natural population analysis (NPA) parameters of adsorptions of butadiene and concerted transition state on Metal exchanged Faujasite which were obtained from M06L/6-31G(d,p) calculations.

systems	Partial Charge					
	Cu	C1	C2	Al	O1	O2
Butadiene(BD)	-	-0.42	-0.24	-	-	-
Cu(I)-FAU	0.73	-	-	2.09	-1.32	-1.32
Cu(I)-FAU-BD	0.69	-0.56	-0.33	2.08	-1.30	-1.30
Cu(I)-FAU-TS	0.78	-0.43	-0.27	2.10	-1.32	-1.31
Cu(II)-FAU	1.08	-	-	2.09	-1.32	-1.28
Cu(II)-FAU-BD	1.06	-0.53	-0.21	2.10	-1.33	-1.24
Cu(II)-FAU-TS	0.98	-0.39	-0.21	2.11	-1.30	-1.33

Conclusions

The butadiene cycloaddition over metal-exchanged zeolite has been investigated by the ONIOM (M06L:UFF) approach. The basis set are the Stuttgart RSC 1997 effective core potential (ECP), for Cu atom, and 6-31G(d,p) for the rest. The reaction mechanism is proposed both stepwise and concerted mechanism. For the stepwise, the activation barriers are 19.1 and 1.59 kcal/mol for Cu(I)-Faujasite and 9.12 and 4.59 kcal/mol for Cu(II)-Faujasite. For concerted mechanism, the activation barriers are 12.36 and 6.99 kcal/mol for Cu(I) and Cu(II) Faujasite, respectively. The lower activation barrier on Cu(II)-Faujasite is due to the metal weakening the butadiene by electron back donation which comfirmed by the NBO analysis. This study gives better understanding of the structures and mechanistic properties at the molecular level of the metal-exchanged zeolite catalyst which are useful for further improvement of styrene production.

References

(1) Vaughan, W. E. *Journal of the American Chemical Society* **1932**, *54*, 3863.

(2) Christensen, C. H.; Johannsen, K.; Schmidt, I.; Christensen, C. H. *Journal of the American Chemical Society* **2003**, *125*, 13370.

(3) Li, Y.; Houk, K. N. *Journal of the American Chemical Society* **1993**, *115*, 7478.

(4) Von Doering, W. E.; Franck-Neumann, M.; Hasselmann, D.; Kaye, R. L. *Journal of the American Chemical Society* **1972**, *94*, 3833.

(5) Thomas, M. L.; Fraga-Dubreuil, J.; Coote, A. S.; Poliakoff, M. *Green Chemistry* **2008**, *10*, 197.

(6) Alimardanov, K. M.; Abdullayev, A. F. *Petroleum Chemistry* **1995**, *35*, 508.

(7) Neumann, R.; Dror, I. *Applied Catalysis A: General* **1998**, *172*, 67.

(8) De Bruyn, M.; Neumann, R. *Advanced Synthesis and Catalysis* **2007**, *349*, 1624.

(9) Choi, Y. S.; Park, Y. K.; Chang, J. S.; Park, S. E.; Cheetham, A. K. *Catalysis Letters* **2000**, *69*, 93.

(10) Castellan, A.; Tauszik, G. R. *Journal of Catalysis* **1977**, *50*, 172.

(11) Maxwell, I. E.; de Boer, J. J.; Downing, R. S. *Journal of Catalysis* **1980**, *61*, 493.

(12) Maxwell, I. E.; Downing, R. S.; Van Langen, S. A. J. *Journal of Catalysis* **1980**, *61*, 485.

(13) Voskoboinikov, T. V.; Coq, B.; Fajula, F.; Brown, R.; McDougall, G.; Luc Couturier, J. *Microporous and Mesoporous Materials* **1998**, *24*, 89.

(14) Kugel, V. Y.; Lakhman, L. I.; Abramova, A. V.; Matiyeva, Z. M.; Smirnov, V. K.; Irisova, K. N.; Livenbuk, M. I.; Slivinskii, Y. V. *Petroleum Chemistry* **1997**, *37*, 297.

(15) Dessau, R. M. *Journal of the Chemical Society, Chemical Communications* **1986**, 1167.

(16) Chang, J. S.; Park, S. E.; Gao, Q.; Férey, G.; Cheetham, A. K. *Chemical Communications* **2001**, 859.

(17) Dimitrov, C.; Leach, H. F. *Journal of Catalysis* **1969**, *14*, 336.

(18) Nieminen, V.; Kumar, N.; Datka, J.; Päivärinta, J.; Hotokka, M.; Laine, E.; Salmi, T.; Murzin, D. Y. *Microporous and Mesoporous Materials* **2003**, *60*, 159.

(19) Espeel, P. H.; De Peuter, G.; Tielen, M. C.; Jacobs, P. A. *Journal of Physical Chemistry* **1994**, *98*, 11588.

(20) Datka, J.; Kukulska-Zajac, E. *Journal of Physical Chemistry B* **2004**, *108*, 17760.

(21) Datka, J.; Kukulska-Zajac, E.; Kozyra, P. *Journal of Molecular Structure* **2006**, *794*, 261.

(22) Kukulska-Zajac, E.; Kozyra, P.; Datka, J. *Appl. Catal. A-Gen.* **2006**, *307*, 46.

(23) Boekfa, B.; Choomwattana, S.; Khongpracha, P.; Limtrakul, J. *Langmuir* **2009**, *25*, 12990.

(24) Kumsapaya, C.; Bobuatong, K.; Khongpracha, P.; Tantirungrotechai, Y.; Limtrakul, J. *Journal of Physical Chemistry C* **2009**, *113*, 16128.

(25) Maihom, T.; Pantu, P.; Tachakritikul, C.; Probst, M.; Limtrakul, J. *Journal of Physical Chemistry C* **2010**, *114*, 7850.

(26) Zhao, Y.; Schultz, N. E.; Truhlar, D. G. *Journal of Chemical Theory and Computation* **2006**, *2*, 364.

(27) Zhao, Y.; Truhlar, D. G. *Accounts of Chemical Research* **2008**, *41*, 157.

(28) Drake, I. J.; Zhang, Y.; Briggs, D.; Lim, B.; Chau, T.; Bell, A. T. *Journal of Physical Chemistry B* **2006**, *110*, 11654.

Catalytic Dehydrogenation of Propane over Au(I) exchanged ZSM-5: Density Functional Theory Calculations

Winyoo Sangthong[2,3,4] *and Jumras Limtrakul,*[1,2,3,4*]

[1] Laboratory for Computational and Applied Chemistry, Department of Chemistry, Faculty of Science and Center of Nanotechnology, Kasetsart University Research and Development Institute, Kasetsart University, Bangkok 10900, Thailand
[2] Center for Advanced Studies in Nanotechnology and Its Applications in Chemical, Food and Agricultural Industries, Kasetsart University, Bangkok 10900, Thailand
[3] NANOTEC Center of Excellence, National Nanotechnology Center, Kasetsart University, Bangkok 10900, Thailand
[4] Center of Nanotechnology, Kasetsart University Research and Development Institute, Kasetsart University, Bangkok, 10900, Thailand
[*]Corresponding author: Tel.: +662 562 5555 ext 2169, Fax: +662 562 5555 ext 2176, E-mail address: jumras.l@ku.ac.th

Introduction

Currently, the demand of alkenes has increased because they are important starting materials for chemical industrial procedures, especially propene[1]. Generally, propene could be obtained by dehydrogenation of propane. However, the conventional steam cracking process has the problem of a high energy-consuming process that also produces CO_2 and deactivation of the catalyst by coke production. Therefore, the research for alternative ways for the production of propene becomes imperative. One of the alternative ways is the direct catalytic non-oxidative dehydrogenation of propane over zeolitic catalysts. Transition metal supported on ZSM-5 increases the rate of non-oxidative propane conversion and the selectivity to unsaturated products[2-7]. Au^+ is found to be an active specie for dehydrogenation of propane[8]. Therefore, Au(I)-exchanged ZSM-5 could be considered as a new catalyst for propane dehydrogenation. In order to investigate this reaction mechanism, theoretical methodology can offer an understanding that has still not been studied by experimental investigations. In this work, we put forward a preliminary report of the efficiency enhancements for propane dehydrogenation by using Au(I)-ZSM-5 as a high-quality cooperative catalyst using the density functional theory with the well calibrated M06-L functional.

Methodology

The crystal lattice structure of ZSM-5 was taken from the work of van Koningsveld, et al[9]. The Al atom is selected to substitute a Si atom at the T12 position, which is the most energetically favored position[10,11]. The 34T cluster is used to represent the active site of ZSM-5 and employed throughout this study, as shown in Fig.1. It includes the 10-membered ring representing the main gateway to the intersection between the straight channel and the zigzag channel, where the reactions normally take place. The atomic coordinates are treated with the density functional theory (DFT) method using the M06-L functional. The 6-31G(d,p) basis set was used for Al, Si, O, C and H atoms and the effective core potential basis of LANL2DZ was used for the singlet state of the Au atom. Only the 5T regions [(≡SiO)₃Al(OH)Si≡] of zeolite and the reactants were allowed to relax during the geometry optimization, while the rest were fixed at the crystallographic coordinates. For metal exchanged zeolite, Au(I) was placed at the ion exchange site in the zigzag channel window. The frequency calculations were performed at the same level of theory to verify that the transition states had one imaginary frequency whose mode corresponds to a saddle point of the reaction

coordinate. Single point calculations at the M06-L/6-311+G(2df,2p) level of theory were also carried out in order to obtain more reliable results. All calculations were performed by using the Gaussian 03 code, with the M06-L functional implemented by Donald G. Truhlar and Yan Zhao[12,13].
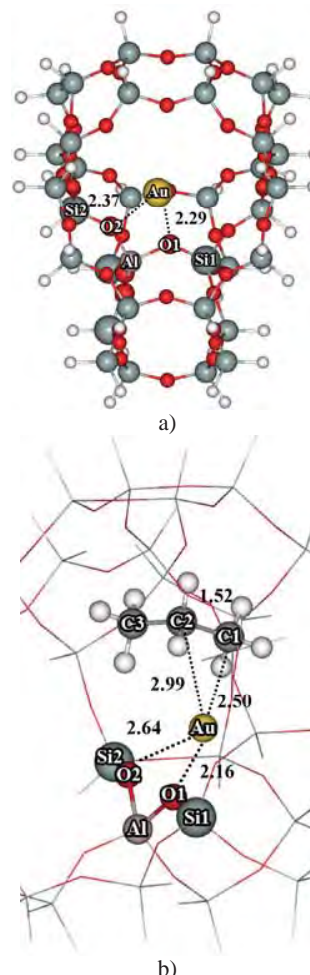

a)

b)

Figure 1. Structure of 34T cluster of Au(I)-ZSM-5 (a) and optimized adsorption structure of propane over Au(I)-ZSM-5 (b).

Results and Discussion

Structure of Au(I)-ZSM-5 and propane adsorption complex. The model of the 34T Au(I)-ZSM-5 clusters and their optimized propane adsorption complexes are illustrated in Figures 1a and 1b. In the optimization, the atoms in the 5T region in the clusters are optimized with the exception of the atoms in the extended framework. The exchanged Au cation is located over the aluminum atom and bidentated two oxygen atoms, O1 and O2, close to the aluminum atom. The bond distances of Au···O1 and Au···O2 of Au(I)-ZSM-5 are calculated to be 2.29 Å and 2.37 Å, respectively.

In order to clearly demonstrate the propane conversion process, it is important to study propane physisorption over the active site of metal exchanged ZSM-5. The selected geometrical structures of this interaction are presented in Figure 1b. For the adsorption of propane on Au(I)- ZSM-5, we found that propane adsorbed on zeolite through interactions between methyl and methylene carbon atoms and the Lewis acid site. This interaction results in a small deviation of the

structure of the Au(I)-ZSM-5 such that the Au···O1 and Au···O2 distances in Au(I)-ZSM-5 are slightly changed and the C-C bond of propane differs slightly from the isolated molecules. The binding energy is calculated to be -29.0 kcal/mol. The C1···Au and C2···Au distances are 2.50 and 2.99 Å, respectively. In this study, we focus only on the adsorption on the central C1-C2 bond of propane because we decided to choose methylene hydrogen abstraction to be the first step of the dehydrogenation reaction.
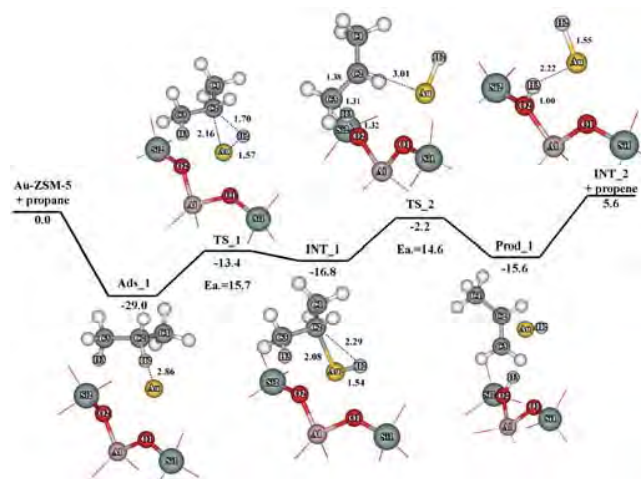

Figure 2. Energy profile for the methylene hydrogen abstraction and the formation of propene of the dehydrogenation of propane over the 34T cluster model of Au(I)-ZSM-5 calculated at M06-L/6-311+G(2df,p)//M06-L/6-31G(d,p).

Methylene hydrogen activation. The reaction starts with the C2-H2 bond of the adsorbed propane molecule as it is activated by the Au cation to form the gold-propyl hydride intermediate. The structures and energy profile of this step are shown in Figure 2. At the transition state (TS_1), the Au ion is inserted to the C2-H2 bond of propane. The C2-H2 bond distance is increased from 1.10 Å to 1.70 Å while the Au-C2 and Au-H2 distances are reduced to 2.16 Å and 1.57 Å, respectively. The activation energy of this step is 15.7 kcal/mol and has been confirmed by frequency calculations resulting in one imaginary frequency at 660.8i cm^{-1}, related to the breaking of the C2-H2 bond by the insertion of Au$^+$ yields the inserted propyl hydride intermediate (INT_1). The inserted propyl hydride intermediate stabilized on the zeolite surface with the relative energy of -16.8 kcal/mol with respect to the isolated reactants. The distances of Au-C2 and Au-H2 are 2.08 and 1.54 Å, correspondingly.

The formation of propene. The Au-propyl hydride intermediate can be converted to propene and the Au hydride intermediate through the abstraction of the hydrogen atom from the propyl hydride intermediate to the zeolite framework, to yield an adsorbed propene molecule and the Au hydride intermediate. At the transition state (TS_2), the H3 proton on the C3 atom is elongated to be transferred toward an oxygen atom (O2) of the zeolite framework and the C3-H3 bond and the Au-C2 are dissociated. Simultaneously, the C2-C3 single bond is being contracted to become the C2-C3 double bond. The C3-H3 bond is elongated to 1.31 Å and the O2-H3 distance is reduced to 1.32 Å. The Au-C2 bond is increased from 2.08 Å to 3.01 Å, and the C2-C3 bond distance is decreased from 1.51 Å to 1.38 Å. Normal mode analysis reveals one imaginary frequency at 1,281.5i cm^{-1} of the transition state that corresponds to the movement of the H3 atom between the O2 and C3 atoms. The

activation energy of this step is 14.6 kcal/mol. After the deprotonation is completed, the propene molecule and the Au hydride intermediate are produced (Prod_1). The desorption of the propene molecule requires an energy of 21.2 kcal/mol while the Au hydride intermediate remains adsorbed on the Brønsted acid site (INT_2).
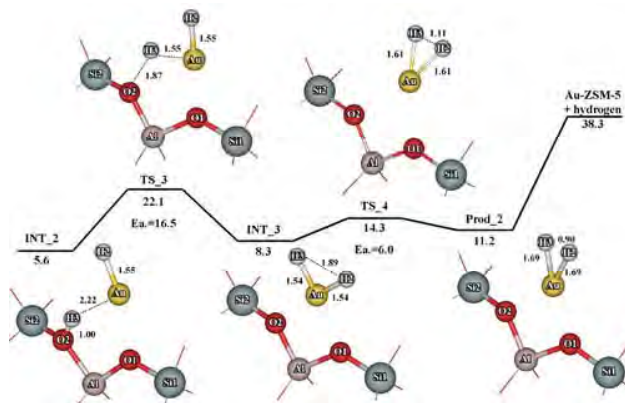

Figure 3. Energy profile for the hydrogen production and the regeneration of the active site over the 34T cluster model of Au(I)-ZSM-5 calculated at M06-L/6-311+G(2df,p)//M06-L/6-31G(d,p).

Hydrogen production and the regeneration of the active site. After the propene molecule desorbs from the surface, the Au hydride intermediate remains adsorbed on the Brønsted acid site. Finally, the active site is regenerated by the formation of the hydrogen molecule from the Au hydride intermediate (INT_2). The structures and energy profile of this reaction consist of two steps and are shown in Figure 3. First, the conversion of the Au hydride intermediate to the Au dihydride intermediate via the protonation reaction. At the transition state (TS_3), the H3 proton is transferred to the Au hydride intermediate. The Au-H3 distance is decreased to 1.55 Å and the O2-H3 bond distance is elongated to 1.87 Å. The transition structure has been confirmed by frequency calculations resulting in one imaginary frequency at 388.0 cm^{-1}, related to the O2-H3 bond breaking and the Au-H3 bond forming, simultaneously. The activation energy of this step is 16.5 kcal/mol. Dihydride groups (INT_3) on Au can form a bond to produce the hydrogen molecule. This step requires the energy of only 5.5 kcal/mol. Normal mode analysis reveals one imaginary frequency at 650.1i cm^{-1} associated with the H2-H3 bond formed in the transition state structure (TS_4). The product of this step is the hydrogen molecule chemisorbed on Au(I)-ZSM-5 (Prod_2). The distance between Au and H2 is 1.69 Å and the Au-C3 distance is 1.69 Å. Finally, the hydrogen molecule desorbed from Au with the energy of 27.1 kcal/mol.

Conclusion

Propane adsorption and its dehydrogenation reaction mechanism of the propane/Au(I)-ZSM-5 system have been investigated by DFT calculations with the M06-L functional. Propane adsorbs over Au(I)-ZSM-5 by the interaction of methyl and methylene carbon atoms and Au$^+$ with the binding energy 29.0 kcal/mol. For the reaction mechanism, the reaction begins with the methylene hydrogen abstraction yielding the Au inserted propyl methyl intermediate. The calculated activation energy is 17.8 kcal/mol. Eventually, propene can be produced by the proton transferred from the intermediate to the oxygen atom of the active site. This step requires the activation energy of 12.5 kcal/mol. The zeolitic framework plays an important role in the formation of propene from the stabilization of the

transition state. The intermediate of this step is AuH adsorbed over the Brønsted acid site. The active site is regenerated by the protonation of AuH with activation energy of 18.1 kcal/mol to form the dihydrogen intermediate. Then, the conversion of the dihydrogen intermediate to the hydrogen molecule requires the activation energy of 6.0 kcal/mol. Finally, the hydrogen molecule desorbs from Au(I)-ZSM-5 that requires the energy of 27.1 kcal/mol. This zeolite is suggested to be an interesting candidate material for dehydrogenation of propane to propene, which is more important in industrial chemical processes.

References
1) Cavani, F.; Ballarini, N.; Cericola, A. *Catal. Today.* **2007**, 127, 113.
2) Nakamura, I.; Fujimoto, K. *Catal. Today*. **1996**, 31, 335.
3) Dooley, K. M.; Price, G. L.; Kanazirev, V. I.; Hart, V. I. *Catal. Today*. **1996**, 31, 305.
4) Berndt, H.; Lietz, G.; Volter, J. *Appl. Catal*. **1996**, 146, 365.
5) Biscardi, J. A.; Iglesia, E. *J. Catal*. **1999**, 182, 117.
6) Heemsoth, J.; Tegeler, E.; Roessner, F.; Hagen, A. *MicroporousMesoporous Mater.* **2001**, 46, 185.
7) Kazansky, V.; Serykh, A. *MicroporousMesoporousMater.* **2004**, 70, 151.
8) Chowdhury, A. K.; Wilkins, C. L. *J. Am. Chem. SOC*., **1987**, 109(18), 5336.
9) van Koningsveld, H.; Tuinstra, F.; van Bekkum, H.; Jansen, J. C. *Acta Crystallogr., Sect. B*. **1989**, 45, 423.
10) Boekfa, B.; Choomwattana, S.; Khongpracha, P.; Limtrakul, J. *Langmuir.* **2009**, 25(22), 12990.
11) Maihom, T.; Boekfa, B.; Sirijaraensre, J.; Nanok, T.; Probst, M.; Limtrakul, J. *J. Phys. Chem. C* **2009**, 113, 6654.
12) Zhao, Y.; Truhlar, D. G. *J. Phys. Chem. C*. **2008**, 112, 6860.
13) Zhao, Y.; Truhlar, D. G. *Acc. Chem. Res*. **2008**, 41, 157.